Mémoire

Auteur : Groyne, Maria
Promoteur(s) : De Becker, Michael; Munhoven, Guy
Faculté : Faculté des Sciences
Diplôme : Master en sciences spatiales, à finalité approfondie
Année académique : 2022-2023
URI/URL : http://hdl.handle.net/2268.2/18644

UNIVERSITY OF LIÈGE

FACULTY OF SCIENCES

DEPARTMENT OF ASTROPHYSICS, GEOPHYSICS AND OCEANOGRAPHY

MASTER THESIS
SMEM0029-1

Astrochemical pathways for the synthesis of amino-acids in interstellar clouds

---

Maria GROYNE

A thesis conducted for the obtention of the degree of Master in Space Sciences in Research Focus

Supervisors:
Michaël DE BECKER
Guy MUNHOVEN
Liège University

Reading Committee:
Michaël DE BECKER
Guy MUNHOVEN
Michaël GILLON
Jean-Christophe MONBALIU
Liège University

Academic year **2022-2023**

Acknowledgements

Before letting you discover the work I have been carrying out with heart throughout this academic year 2022-2023, I would like to thank all the people who helped and supported me all along my journey as a student, up to this master thesis.

First and foremost, I would like to express my sincere gratitude toward my supervisor, Dr. Michaël De Becker, for suggesting this very interesting subject of master thesis, which conceals questions to be asked and elucidated. As a little young scientist dreaming of doing research, how could I have hoped for something more exciting?

Secondly, my thanks are addressed to both Dr. Michaël De Becker, and my co-supervisor, Dr. Guy Munhoven, for their huge trust and support throughout this work, as well as the interesting and enriching discussions we have been exchanging.
Beyond the present thesis, I would also like to point out the great humanity and understanding that you both have shown during all our exchanges all along my master cursus. A good work can only be done in a trustworthy environment. Let me thank you warmly.

Moreover, I would like to address a huge thank you to Dr. J-C. Monbaliu, for his constant presence throughout this year for aspects directly related to chemical principles in my work. I also thank you for allowing me to take part to some of your courses as a free student - this allowed me to expand my horizons to new chemical knowledge, in addition to my master's degree, in a very enriching environment.

Continuing on the academic community, I thank the members of the Reading Committee, namely Dr. Michaël De Becker, Dr. Guy Munhoven, Dr. Michaël Gillon and Dr. Jean-Christophe Monbaliu, for the time spent at reading this manuscript.

Apart from the university of Liège, a special attention is dedicated to Mrs. Anne-Cécile Eugène and Mr. Etienne Goffin, two modern languages teachers from my former secondary school (Séminaire de Floreffe), for their meticulous help in their reviewing of this work since the beginning of its writing.

In the following, I must thank various other people for their human contribution to my life as a student and/or during the writing of my thesis.
Dans ce contexte, je vais commencer par remercier Madame Florence Ellebout, pour son soutien exceptionnel et sa présence tout au long de mon master à l'Université de Liège.

En ce qui concerne mon cursus avant le master, je voudrais exprimer ma reconnaissance au Professeur Benoît Champagne, de l'Université de Namur, pour m'avoir soutenue durant ces années, et poussée à me dépasser. Cela m'a aidé à croire en moi, et je vous remercie pour cela. De plus, je

remercie Madame Beaudhuin, du Séminaire de Floreffe, de m'avoir formée à apprendre, d'avoir nourri cette soif de nouvelles connaissances tout en m'apprenant à travailler rigoureusement.

Je voudrais également remercier la vie universitaire d'avoir placé sur mon chemin des personnes extraordinaires telles que Romain Christiaens, Ismael Lahmaïd, Benjamin Seron et bien d'autres, sans oublier ma merveilleuse partenaire de vie, Julie Dekkers, qui m'a soutenue tout au long de cette année, attentive à chaque fois que je lui parlais en long et en large de mon travail, et toujours présente dans les pires comme dans les meilleurs moments.

Il me reste maintenant à remercier ma famille, et tout particulièrement mes parents et ma soeur, pour tout le soutien qu'ils m'ont apporté durant mes études, et ma vie en général. Vous m'avez toujours permis de me surpasser, et cela dans le meilleur cadre qu'il soit. Merci du fond du coeur. De plus, je remercie chaleureusement mon tonton, Remy Colin, pour les différents dessins présents dans ce début de mémoire, permettant de mettre en image mes passions scientifiques.

Mes derniers remerciements vont à ma plus fidèle amie, Belle. Merci de me suivre dans toutes mes aventures avec tant de patience et tendresse.

Et je finirai par *A mes plus belles étoiles, je vous envoie mon merci le plus cher,*

Thank you all! Merci à tous!
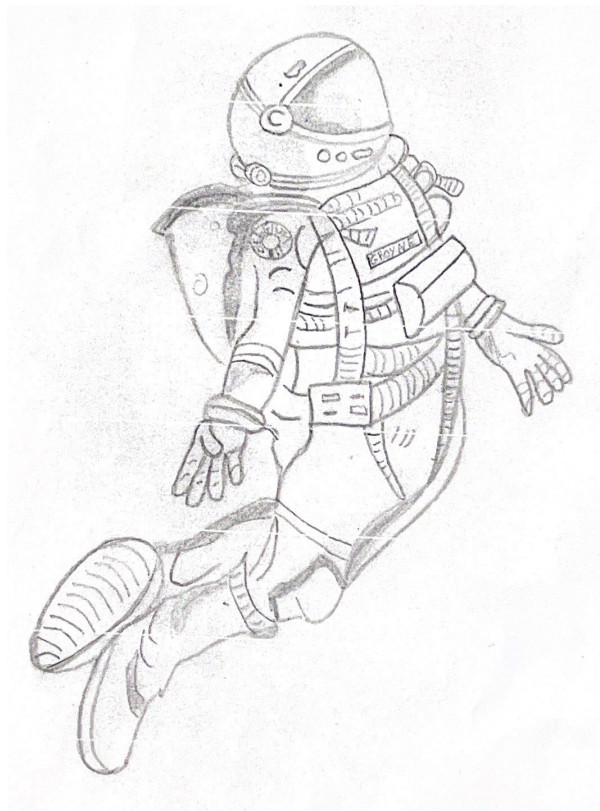
© Remy Colin
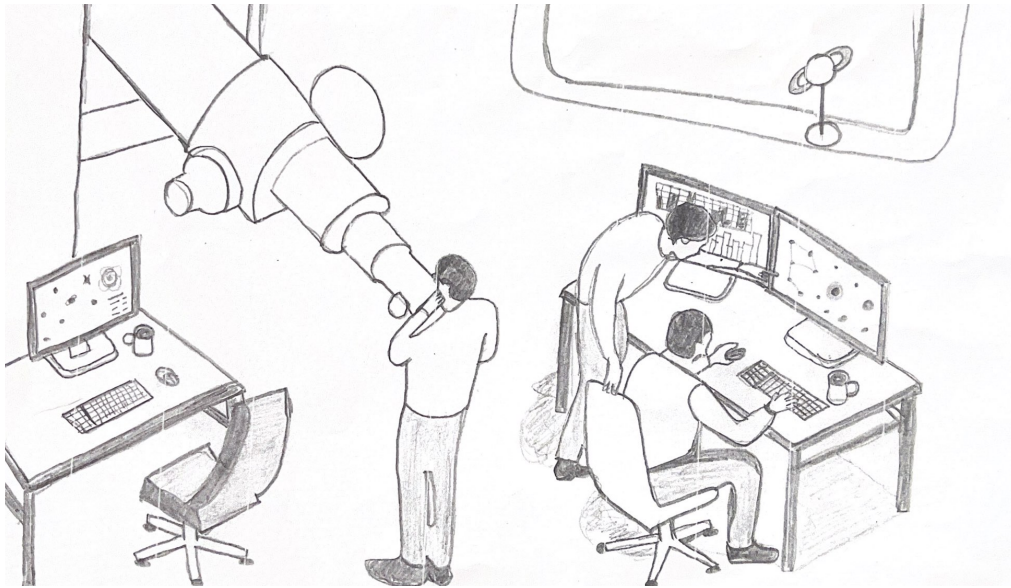
"Learn from yesterday, live for today, hope for tomorrow. The important thing is not to stop questioning."

"Never give up on what you really want to do. The person with big dreams is more powerful than one with all the facts."

Albert Einstein

Abstract

There is much evidence to support the exogeneous origin of amino acids on Earth. For instance, one may cite the identification of amino acids in meteoritic samples with isotopic ratios pointing towards a non-terrestrial origin, the enantiomeric excess found in the Murchison meteorite in the same direction as the homochirality problem found on Earth, or the detection of glycine in the coma of comet Churyumov-Gerasimenko and some of its likely precursors in the Interstellar Medium (ISM). However, if we adopt an exogeneous point of view, one can wonder if these amino acids are formed in the initial molecular cloud, during the formation of the solar system in a cold region of the protoplanetary disk, due to a modification due to a perturbation, or via processing within the parent-body.

To achieve a deeper insight into this issue, this master thesis focuses on a hypothetical formation of glycine in dense molecular clouds. After a deep bibliographic analysis of the many proposed mechanisms and a selection of the most relevant ones to be considered in Chapter 1, the gas-phase *Astrochem* code has been used. Its basic functionalities have been explained in Chapter 2. Starting from this modelling tool, the most likely precursors of glycine in a pure gas-phase context have been deeply investigated in Chapter 3 in which we have inferred the relative temporal evolution of the abundances and studied their major contributing paths. This has allowed us to deeply discuss the potential of these routes in such a medium. Moreover, we have been able to compare our results with earlier studies, in which much simpler astrochemical networks have been used. The results for the most abundant molecular species present a good match with respect to previous studies, but do not when more complex species are considered. Finally, in Chapter 4, we have focused on potential network extensions, that are based on our results and discussions in the previous chapter and on theoretical considerations.

In a nutshell, this study is offering a deep insight into the behaviour of the simplest precursors of the proposed/selected glycine formation pathways in a pure gas phase context.
Furthermore, this work is paving the way to direct long-term scientific perspectives, as discussed in Chapter 6. For instance, one may indeed cite the call for a much comprehensive and scientifically well funded astrochemical code, accompanied by a network based on rigorous kinetic parameters.

Contents

Chapter 1

Introduction and Scientific Context

Throughout this introductory chapter, the main concepts related to the core of the study will be discussed. First of all, the meaning of the so-called *astrochemistry*, its importance in different scientific contexts and the main guidelines driving the development of this research field will be addressed. This step being completed, we will review the chemical and physical concepts governing gas phase and grain surface processes as well as their crucial interplay in different astrophysical environments. A last section will be dedicated to the leading molecular species in this study, namely the amino acids, organic compounds of great biochemical interest. In that context, deep bibliographic investigation of the many proposed interstellar pathways towards their formation will be performed. This will allow us to finally deeper insights into the main practical objectives of this work.

1.1   *What lies behind the astrochemical field of research?*

First and foremost, it is paramount to clarify what we call *astrochemical science*. In fact, some confusion can be caused by an inaccurate use of this notion in different reference books or by some authors. This step is therefore crucial to ensure that we are on the same page. It can simply be defined as "*the science devoted to the study of the chemical processes at work in astrophysical environments, including the interstellar medium, comets, circumstellar and circumplanetary regions*" (De Becker, 2013).

As a result, astrochemistry can be distinguished from astrophysics, focusing on physical principles ruling the formation and evolution of astronomical objects. However, besides the clear distinction to be made between those two field of research, some interdisciplinary work is essential in astrochemistry and those two disciplines are widely complementary. Consequently, one can consider astrochemistry as the "*transition zone*" between the astrophysical and chemical research fields (see Figure 1.1).

Figure 1.1:   Visual representation of the introduced working definition of astrochemistry in terms of links with its direct parent fields, namely chemistry and astrophysics.

Similarly, one has to make a sharp distinction between chemistry and molecular spectroscopy, even if both approaches have to be investigated to improve our understanding of astrochemistry (and many

other disciplines such as terrestrial atmospheric studies, stellar atmospheric research, chemistry in general, ...). Indeed, although a confusion is regularly made in the scientific literature, there is a fundamental difference between those two terms. We can define:

Chemistry as the science dedicated to the study of the transformation of molecular species in one given astrophysical environment owning its characteristic physical parameters (e.g. a phase of the Interstellar Medium (ISM)) or, more globally, a given medium;

Molecular spectroscopy as a set of methods aimed at the qualitative and quantitative diagnosis and census of molecular species in a typical astrophysical environment (or, more globally, a given medium).

⇒ Molecular spectroscopy can be seen as a method allowing a census of the primary material available for (astro)chemical processes in one given (astrophysical) medium. There is therefore a bivocal relation between the two terms, but they have to be distinguished.

Moreover, independently to the simple detection, the study of the transformation of molecular species (definition of chemistry) over time can be monitored to some extend via molecular spectroscopy. However, timescales in astrochemistry are largely greater than the ones we consider on Earth. The experimentation is therefore unavoidably limited in terms of ability to be representative of what really happens in space, and some approximations have to be done in order to empirically simulate the conditions in astrophysical media. The modelling of molecular spectra in those typical environments is another way to proceed, frequently used for astrochemical purposes.

A direct relation can also be highlighted between astrochemistry and multiple astrobiological issues, mostly related to the general question of the origin and evolution of life. It includes the study of the origin of the terrestrial homochirality, the search for more and more complex species, etc). This will be addressed more specifically in section 1.4.

Taking into account all those examples of links between astrochemistry and various disciplines, there is no doubt that **dynamic interdisciplinary exchanges** have the capability to substantially improve our understanding of astrochemical issues. (De Becker, 2013)

From a practical point of view, the astrochemist has to tackle different challenges. First of all, contrary to standard laboratory chemistry, astrochemical processes refer to chemical processes happening under unusual conditions, totally different from what we used to face on Earth with classical chemistry issues. Indeed, if we first consider the typical highest densities that can be found in the interstellar medium, around $\sim 10^6$ molecules/cm^3 in the densest molecular clouds, this is many orders of magnitude lower than in our atmosphere ($\sim 10^{19}$ molecules/cm^3 in normal conditions of temperature and pressure at sea level). This is reminiscent of the meaningful statement by Arthur Stanley Eddington in 1926: *"It is difficult to admit the existence of molecules in interstellar space, because once a molecule is dissociated it seems to be no chance for atoms to join again"*. In other words, the first challenge the pioneers in astrochemistry have faced is to admit the existence of molecular species in the ISM. Besides, the very peculiar physical conditions (extreme cold/hot temperature conditions, strong radiation field or cosmic ray interactions, ...) prevailing in various interstellar regions constitute a second substantial challenge when dealing with astrochemical issues. As a consequence, it is very difficult to reproduce, even with the best technologies, such low densities, temperature and extreme

conditions empirically on Earth to simulate the ISM. Furthermore, as we will discuss in more details in section 1.3, the combination of the typical low densities even in the densest molecular clouds, and the cryogenic conditions in it makes the kinetic of the processes in such environments very slow. The associated timescales are therefore affected, as mentioned above.
Molecular spectroscopic investigations are not straightforward either since no separation of samples is possible to make the diagnosis and analyses of the spectra easier. (De Becker, 2013)

Following those challenges, the experimental aspects of astrochemistry are restricted to specific studies. Here is a non-exhaustive list of experiments carried out in connection to various astrochemical issues:

- The study of interstellar ice, present in molecular clouds where the temperature is very low, of the order of 10-20 K (as we will see in section 1.3). It involves the simulation of interstellar ice analogs and the fate of the captured molecules in those icy mantles facing cosmic rays or UV radiations. This requires reaching very low temperatures, high vacuum [1] and extreme conditions (high UV radiation or Cosmic Rays (CR) interactions);

- The study of extraterrestrial material such as meteorites, cometary coma and samples of asteroids;

- The simulation of the space erosion on the asteroids, or on the surfaces of some planets/moons (e.g. Titan and the possibility of formation of organic compound by impact of CR on solid acetylene present in ices on Titan's surface (Abplanalp et al., 2019));

- ...

Those experiments are completed thanks to more common techniques such as spectroscopic study (for diagnostic and kinetic studies), various chromatography techniques, mass spectrometers.
Next to the empirical studies, theoretical research is also of great interest. For instance, there exist astrochemical models based on kinetic constant and numerical methods. Astrochemists also rely on known theoretical chemistry methods, such as the post-Hartree Fock (HF) ones, Density Functional Theory (DFT), molecular dynamic simulations, ... (NASA Ames Research Center; IAS Orsay)

To summarize, astrochemical studies are achieved through observational, computational modelling works, as well as laboratory experiments.

1.2 Molecular complexity and astrophysical filiation

Since the first identification of a molecule (CH) in the ISM by Swings and Rosenfield in 1937 using optical spectroscopy, scientists have taken advantage of technological breakthroughs in terms of detection capabilities (such as the development of radio astronomy and radiotelescopes). It leads to numerous discovered molecules with increasing number of constituting atoms, those being themselves more and more diversified. Nowadays (10th of July, 2023)), the census of discovered molecules in the ISM is given in Table 1.1.

From this census, we can now admit that molecules are present in the ISM. Even if this latter is composed of more than 98% of hydrogen and helium, the remaining 2% of heavier elements allow the presence of a great variety of chemical interstellar compounds.

---

[1]As previously explained, even with the highest densities in the ISM, they are pretty small compared to what we typically find in the terrestrial atmosphere in standard temperature and pressure conditions.

Table 1.1: Temporary census of the main chemical species discovered so far in the ISM. From a general point of view, the higher the number of constituting atoms of the backbone chain, the more recent the detection. (completed from De Becker (2021-2022))

Number of atoms	Chemical species
2 atoms	AlCl, AlF, AlO, C_2, CF^+, CH, CH^+, CN, CN^-, CO, CO^+, CP, CS, FeO, H_2, HCl, HF, NH, KCl, N_2, NO, NO^+, NS, NaCl, O_2, OH, OH^+, PN, SH, SH^+, SO, SO^+, SiC, SiN, SiO, SiS, SiP, TiO, ArH^+, NS^+, VO, HeH^+, PO^+
3 atoms	AlNC, AlOH, C_3, C_2H, C_2O, C_2P, C_2S, CO_2, H_3^+, CH_2, H_2Cl^+, H_2O, H_2O^+, H_2S, HCN, HCO, HCO^+, HCS^+, HCP, HNC, HN_2^+, HNO, HOC^+, KCN, MgCN, NH_2, N_2H^+, N_2O, NaCN, OCS, SO_2, c-SiC_2, SiCN, SiNC, SiCSi, FeCN, TiO_2, CCN, S_2H, HCS, HSC, NCO, , NCS, CaNC, MgC_2, NCS, HSO
4 atoms	l-C_3H, c-C_3H, C_3N, C_3O, C_3S, C_3H^+, H_3O^+, C_2H_2, H_2CN, H_2CO, H_2CS, HCCN, HCCO, $HCNH^+$, HCNO, HOCN, $HOCO^+$, HNCO, HNCS, HSCN, NH_3, SiC_3, PH_3, H_2O_2, HMgNC, MgCCH, NCCP, CNCN, HONO, HCCS, HNCN, $HCCS^+$, H_2NC
5 atoms	C_5, CH_4, c-C_3H_2, l-C_3H_2, H_2CCN, H_2C_2O, H_2CNH, H_2COH^+, C_4H, C_4H^-, HC_3N, HCCNC, HCOOH, NH_2CN, SiC_4, SiH_4, HCOCN, HNCNH, HC_3N^-, CH_3O, $NCCNH^+$, CH_3Cl, MgC_3N, NH_2OH, HC_3O^+, HC_3S^+, H_2CCS, C_4S, HCCCO, HCOSH, HCSCN, NaCCCN, MgC_3N^+
6 atoms	c-H_2C_3O, C_2H_4, CH_3CN, CH_3NC, CH_3OH, CH_3SH, l-H_2C_4, HC_3NH^+, $HCONH_2$, C_5H, HC_2CHO, HC_4N, CH_2CNH, C_5N^-, C_5S, SiH_3CN, z-HNCHCN, MgC_4H, HC_3CO^+, CH_2CCH, H_2CCCS, HCSCCH, MgC_5N, CH_5^+, $HCCNCH^+$, CH_3CO^+, C_5O, c-C_5H, C_5H^+, HCCCCS, MgC_4H^+
7 atoms	c-C_2H_4O, CH_3C_2H, H_3CNH_2, CH_2CHCN, H_2CHCOH, C_6H, C_6H^-, HC_4CN, CH_3CHO, CH_3NCO, HC_5N^-, HC_5O, $HOCH_2CN$, HNCHCCH, HC_4NC, CH_2CHCCH, C_3HCCH, H_2C_5, MgC_5N, CH_2CCCN, NC_4NH+, MgC_5N^+
8 atoms	H_3CC_2CN, $H_2COHCOH$, CH_3OOCH, CH_3COOH, C_6H_2, CH_2CHCHO, CH_2CCHCN, C_7H, NH_2CH_2CN, $(NH_2)_2CO$, CH_3SiH_3, $(NH_2)_2CO$, CH_2CHCCH, $HCCCH_2CN$, MgC_6H, HC_5NH^+, $C_2H_3NH_2$, Z-$(CHOH)_2$ HCCCHCCC, C_7N^-, CH_3CHCO, HMgCCCN, MgC_6H^+
9 atoms	CH_3C_4H, CH_3OCH_3, CH_3CH_2CN, CH_3CONH_2, CH_3CH_2OH, C_8H, HC_6CN, C_8H^-, CH_2CHCH_3, CH_3CH_2SH, CH_3NHCHO, HC_7O, H_3C_5CN (2 isomers), HCCCHCHCN, H_2CCHC_3N, C_5H_4, $H_2CCCHCCH$, OHCHCHCHO, $CH_2CHCHNH$
10 atoms	CH_3COCH_3, CH_3CH_2CHO, CH_3C_5N, CH_3OCH_2OH, C_6H_4, HC_2CCHC_3N, HC_7NH^+, $C_2H_5NH_2$, C_2H_5NCO, t-$CH_3CHCHCN$, c-$CH_3CHCHCN$, $CH_2C(CH_3)CN$
>10 atoms	HC_8CN, CH_3C_6H, $CH_3OC_2H_5$, $HC_{10}CN$, C_6H_6, C_2H_5OCHO, C_3H_7CN, CH_3COOCH_3, $C_2H_5OCH_3$, CH_3CHCH_2O, C_6H_5CN, CH_3COCH_2OH, C_{60}, C_{60}^+, C_{70}, c-C_5H_5CN, $C_{10}H_7CN$ (2 isomers), c-C_5H_6, c C_9H_8, $NH_2CH_2CH_2OH$, CH_3C_7N, i-C_3H_7OH, n-C_3H_7OH, CH_2CCHC_4H, g-CH_2CHCH_2CN, $HC_{11}N$, C_5H_5CCH (2 isomers), C_6H_5CCH, CH_3C_7N, c-CH_2CHCH_2CN, c-$C_5H_4CCH_2$, c-C_9H_7CN, $C_{10}H^-$, $C_{10}H$, E-1-C_4H_5CN, $C_{11}H_{12}N_2O_2$
Deuterated	HD, H_2D^+, HDO, D_2O, DCN, DCO, DNC, N_2D^+, NHD_2, ND_3, HDCO, D_2CO, CH_2DCCH, CH_3CCD, D_2CS, NH_3D^+

Besides, from Table 1.1, we directly get a feeling of what means ***molecular complexity***, increasing with discoveries. This concept has to be emphasized since it drives one of the most important general question that astrochemists are striving to answer: *"To which complexity level of molecular species can a given abiotic environment lead, and over which timescale?"*. In fact, we can assume to some extent that the level of complexity reachable in one given environment translates, in a sense, the potential of this medium to be an efficient candidate to develop a form of life (since it requires a certain level of complexity in the molecular population of that environment). The issue of the origin

of terrestrial life should therefore be resolved by filling the scientific gap concerning the link between terrestrial and interstellar/extra-terrestrial molecular complexity, assuming an exogenous[2] origin of prebiotic molecules.

To define the molecular complexity in a more quantitative way, Mil'man (1989) tried to use the informative theory, as introduced by Bertz (1981, 1982, 1983). In his proposed definition, Mil'man took three main factors into account:

- a quantity defined by n, the total number of atoms, and the number of equivalent atoms;

- the functional complexity (defined by the membership of the structural atoms and their substitutes to diverse functional groups);

- the chirality complexity index taking the chirality of the system into account, also influencing the complexity. Indeed, chirality plays crucial roles in biological systems. For instance, we can cite the strereoselectivity of some biochemical reactions due to the high specificity of enzymes to their substrate. (Mil'man, 1989)

More recent studies (e.g. (Randic and Plavsic, 2002)) also addressed the question of the definition of molecular complexity, with more and more advanced considerations. In the astrochemical context, we can restrict our discussions to the definition of Mil'man.

From that definition, one may define a molecular complexity scale through a proxy being *"the amount of information that is needed to fully, and unambiguously, characterize a molecular compound."* (De Becker, 2013). Regarding this scale, astrochemical studies can be implemented through two opposite but complementary approaches:

i. **The bottom-up approach**: *From a set of given molecules in a given astronomical environment, how can we build more complex species?* Starting from a simple specie, the purpose is to find, step by step, which more complex species can be built. One therefore *climbs* the molecular complexity scale reaction by reaction.

ii. **The top-down approach**: *From which precursors a molecule of a given molecular complexity can be build?* In this first, I will mostly follow this approach, walking down our complexity ladder, starting from chemical entities of undeniable astrobiological interest: amino acids (see section 1.4).

Remark: Despite the words *step by step* could be seen as a very sequential strategy, from a given molecule, a complete astrochemical network can be drawn regarding the number of possible reactions and interplays between them, as it will be discussed further in the following sections.

A second guideline driving a lot of astrochemical studies is the astrophysical filiation or, in other words, the transformation of a given astronomical environment and consequently of its

---

[2]Actually, there are two alternative theories for the origin of prebiotic molecules on Earth. The exogenous synthesis assumes that prebiotic molecules came from space (thanks to comets or asteroids entering the atmosphere, or meteorites impacting the surface). This point of view is supported by the detection of different organic molecules in ISM with a quite appreciable complexity (e.g. Polycyclic Aromatics Hydrocarbons, ...) and the detection of species of biochemical interest (nucleobases, sugars, amino acids, ...) in some meteorites (e.g. Murchinson meteorite samples). The small enantiomeric excess in the same direction as the homochirality problem (sugars and amino acids) found in meteoritic samples (Cronin and Pizzarello, 1997) also supports this first hypothesis.

The second theory is based on endogenous considerations, with prebiotic molecules synthesized from simple abiotic molecules in the planetary atmosphere and various energy sources (such as proposed in the Urey-Miller experiment (Miller, 1953)). For the rest of our discussions, we will assume an exogenous origin of prebiotic molecules.

physical conditions due to astrophysical events. Indeed, if the physical conditions change, it results in changes of the chemical processes at place (for more details, see section 1.3). This is therefore of astrochemical relevance. Yet, from interstellar clouds (diffuse to dense) to planetary system, conditions are greatly varying, leading to two main consequences: (i) for each astrochemical study, the astrophysical environment is one of the main factors to be taken into account, (ii) astrochemical search can help understanding some astrophysical processes happening during those changes, recalling once more the interdisciplinary aspect. Moreover, although we have to keep in mind that the stellar evolution does not own to the realm of astrochemistry, but rather astrophysics, there is a direct link between them thanks to this astrophysical filiation concept. For instance, one can cite the supernova remnants and stellar outflows interacting with the interstellar matter, leading to compression and enhancement of densities in the downstream region, or simply the interaction between the radiations from the stars and the interstellar matter. Those interactions are to a large extent responsible for the differentiation of the various phases in the ISM (see the next section).

Main objectives of this thesis

This work focuses on the possibility of exogeneous formation pathways of amino-acids in dense interstellar molecular clouds, and more specifically on the simplest one, namely glycine. In that context, following a top-down approach, the first objective consists in a deep investigation and a relevant selection among the many proposed glycine interstellar formation pathways in the current scientific literature. Before entering such detailed considerations, we will review the main fundamental principles that are required to understand the *astro-chemical* processes addressed in this work.

From a practical point of view, these selected glycine formation routes are aimed at being the basic guidelines to subsequent astrochemical modelling efforts. In this scope, the basic precursors will be studied with the open source *Astrochem* code. The primary focus will be put on the interplay and on the expected relative contributions of these paths. On a more global view, a secondary objective will be dedicated to a better understanding of what is an astrochemical code, how it works and what the stability of the results is when perturbing some model parameters.

This work is intended to be the basis to open the door to more ambitious and longer-term modelling and computational works.

1.3   Gas phase versus grain surface processes & their crucial interplay

In this section, the main chemical and physico-chemical aspects ruling astrochemical processes will be reviewed. To be faithful to the importance of the interdisciplinarity in astrochemistry highlighted previously with great insistence, this work is intended to be as accessible as possible to each scientist who could read it, including astrophysicists, astrobiologists, chemists or any scientist that would be interested in this topic. I therefore encourage the reader, depending on his own affinities with some concepts, to be more attentive to the ones which seem less familiar.

1.3.1   The different phases of the Interstellar Medium

The ISM is one of the main environments of interest in astrochemistry or in astrophysics in general[3]. It is therefore suitable to take a closer look to its properties. From a global point of view,

---

[3]For instance, the ISM is the birthplace of stars, themselves constituting a significant source of energy in the Milky Way or, more globally, in galaxies. Moreover, even if the baryonic matter is nowadays mostly in the stars (or in

the ISM is located in the galactic plane where most of the matter is concentrated, and is composed of different ingredients, all gathered in Table 1.2 (Draine, 2011). The first two components are the ones studied in astrochemistry, as well as their interactions with CR and the electromagnetic radiations. There are other indirect links of astrochemical interest between those ingredients: for instance, the presence of magnetic field in context of hydrodynamic shocks can influence the compression in the post-shock region, therefore influencing the densities and the astrochemical processes at work.

Table 1.2: Basic components of the Interstellar Medium

	Components	Characteristics
Matter components	**Interstellar gas**	- major mass component of the ISM (even if small, 10-15% the total stellar mass of the galaxy) - atoms, ions, electrons and molecules in gas phase (Hydrogen being the major gas component) - nearly thermal velocity distribution
	Interstellar dust	- represents only $\sim 1\%$ of the gas component - small particles in solid phase ($< 1~\mu$m for the majority) - completely mixed with the interstellar gas (lots of interplay, see subsection 1.3.5)
	Cosmic Rays	- charged non-thermal particles (energetic ions and electrons) - galactic CR: likely accelerated in astrophysical environment (via Diffusive Shock Acceleration processes or other mechanisms)
	Dark Matter	- speculative and poorly understood component - non-gravitational interactions with baryonic matter (if present[a]) negligible: difficult to probe - seems to account for $\sim 90\%$ of the total mass of the galaxy
Energy components	Electromagnetic radiations	- different sources: Cosmic Microwaves Background, starlight, spectral lines from ions, atoms and molecules, photons of thermal & non-thermal origin, ...
	Magnetic field	- induced by electric currents in the ISM - guides charges particles (Lorentz force) - of great importance in some astrophysical processes
	Gravitational field	- induced by the matter components presented above - self-gravitating cloud in some places of the ISM

[a] The dark matter is indeed considered as part of the ISM if those interactions exist with the interstellar baryonic matter or the interstellar magnetic field.

Therefore, we will consider the **interstellar gas and dust** as our basic material of study, and their chemical fate will be studied. As mentioned in Table 1.2, those two ingredients are mixed up in the ISM and, as a consequence, the study of their chemical evolution can not be rigorously achieved by studying them separately, as we will see in subsection 1.3.5.

Moreover, the interstellar gas and dust are forming different **phases**, each of them displaying its own set of physical properties and making the ISM absolutely not homogeneous. It is convenient to adopt a conventional classification of the interstellar phases, even though it can vary a bit from one author

accretion disk around black holes), this matter was primary in the ISM at early time of the galaxy. It is also worth mentioning that the interstellar chemical content is enriched via previous stellar population.

to another. In our discussion, we will rely on a quite detailed classification, as shown in Table 1.3 (Draine, 2011).

Remark: It is worth mentioning that an additional phase can be considered, which is the stellar remnants and stellar outflows, even though it is subject to debate. Some authors are considering it as part of the ISM, while others see it as an object part of the parent star.

Note that the volume filling factor quantifies the volume of the galactic disk occupied by this phase.

Table 1.3: Phases of the Interstellar Medium, inspired from Draine (2011)

Phases	Main characteristics	Temperature (order of magnitude)	Filling factor
Coronal gas or Hot Ionized Medium (HIM)	- induced by the passage of a blast wave: shock-heated gas $\Rightarrow$ highly ionized species (e.g. O VI)	$> 10^5$ K	0.5
HII regions and Warm Ionized Medium (WIM)	- mostly made of HII [a] (+other ions) - photo-ionisation from the radiation field of hot stars (O-B stars) - densities ranging from 0.2 to $10^4/\text{cm}^3$ (HII regions denser than WIM)	$\sim 10^4$ K (O-B stars)	0.1
Warm HI region or Warm Neutral Medium (WNM)	- mostly made of HI[b] (+ some ions) - densities typically around $0.6/\text{cm}^3$ - frequently called photo-dissociation region	5000 K	0.4
Cool HI region or Cold Neutral Medium (CNM)	- same composition of WNM but denser (typically $30/\text{cm}^3$) - also called photo-dissociation region (very few remaining molecules)	100 K	0.01
Diffuse Molecular Cloud	- similar to CNM but denser ($\sim 100 /\text{cm}^3$) - densities such as H_2 significantly present (self-shielding concept[c] preventing photo-dissociation processes)	10-50 K	0.001
Dense Molecular Cloud	- phase with the lowest temperature $\longleftrightarrow$ biggest densities (10^3-$10^6/\text{cm}^3$) $\equiv$ gravitational bounding - mainly made of H_2 and CO molecules (self-shielding concept[c])	10-20 K	0.0001

[a] HII = ionized hydrogen (due to photo-ionisation)
[b] HI = neutral hydrogen
[c] This concept (as well as the photo-reactions mentioned) will be addressed in more details in 1.3.3.

As we can understand from this Table 1.3, the decreasing intensity of the stellar radiation field (and therefore the decreasing range of available λ) from HII regions to molecular gas clouds is the key factor explaining the existence and properties of those phases. It has also to be kept in mind that those phases are not statics, dynamical interactions exists between them. Moreover, a low volume filling factor in not representative of a less important phase. The best examples are the dense molecular clouds, representing a tiny fraction of the galactic disk but being of prime importance: apart from being the birthplace of star formation (astrophysical issue), the astrochemistry taking place there is very rich and deserves to be examined in details.

For this work, the molecular clouds will be of great importance.

1.3.2 Kinetic versus thermodynamical considerations

In chemistry, there exists 2 mains approaches to address and study a chemical transformation, which are:

i. **The kinetic approach**: study of the evolution of a system as a function of time. The reaction intermediates are taken into account;

ii. **The thermodynamical approach**: study of the initial and final states (state functions), leaving aside the temporal evolution of the system and the way it comes from the initial to the final states. It can also be defined as the study of the energy changes in a system as well as the related heat transfers and work on the surrounding medium. Those quantities allow to quantify chemical equilibriums and their displacements in response to changes in the system.

Those two distinct approaches are totally complementary, and both have to be studied in order to characterise (astro)chemical processes completely. Indeed, a reaction has to be thermodynamically feasible in a finite time scale [4] to be considered. It is therefore important to emphasize the main theoretical background needed to follow both strategies.

Starting with the kinetic study of a system made of a set of interconnected transformations, the first question to be addressed concerns the factor of influence of reaction kinetics. Fundamentally, it is governed by two major system parameters: the **temperature** and the **number densities** (or, equivalently, the concentrations or partial pressures) in reactants.

To understand those factors of dependency, one must rely on the so-called *collision theory* (valid for gas phase processes, under the hypothesis of perfect gas[5]), involving the concept of *effective collisions*. One may firstly wonder about the meaning of those collisions: effective collisions are collisions leading to chemical transformations. In other words, all collisions are not leading to a chemical reaction, the reactants must encounter in a given geometry and have the required kinetic energy, larger than E_a, the activation barrier (concept that will be discussed in more details later on in this subsection). In that context, the collision theory stipulates that the reaction rate is proportional to the number of effective collisions, and is expressed by equation 1.1 (valid for a bimolecular process, between reactant A and B).

$$v_A = -dn_A/dt = Z_{AB}.f \tag{1.1}$$

Where v_A corresponds to the rate of disappearance of reactant A ($cm^{-3}.s^{-1}$), n_i is the number density in i ($/cm^3$), Z_{AB} is the number of collisions per unit time and per unit volume, and f is an efficiency factor (adimensional) ranging from 0 to 1.

Yet, Z_{AB} can be expressed easily through the following expression:

$$Z_{AB} = \sigma. <v_p> .n_A.n_B$$

With σ being the cross-section of the particle considered (units of surface), $<v_p> = \sqrt{8k_BT/\pi\mu}$ is the relative mean velocity of the particles (derived from the Maxwell-Boltzmann distribution, k_B being the Boltzmann constant, T the temperature in K and μ the reduced mass).

---

[4]This time scale depends on the context, and is large for astrochemical transformations compared to our standard terrestrial chemistry.

[5]In real cases, there will therefore be deviations with respect to the tendency highlighted by this development, but that is a convenient and simple theory to introduce the factors of influence of chemical kinetics.

Concerning f, it is well represented by the Boltzmann statistics (statistical thermodynamics):

$$f \propto e^{-E_a/k_B T}$$

Where E_a corresponds to the activation barrier, expressed in joules [J]. This term will be discussed hereafter.

Substituting Z_{AB} and f in equation 1.1, we find the equation 1.2 (equality if all collision geometries lead to a reaction, provided the energy barrier is crossed):

$$v_A \propto \sigma.\sqrt{8k_B.T/\pi.\mu} \, . \, n_A.n_B.e^{-E_a/k_B.T} \tag{1.2}$$

From equation 1.2 we clearly see the influence of the densities in reactants: the reaction rate increases if those number densities increase. This could have been predicted since an increase of the number density in reactants leads to an increase of the number of collisions. In addition, one can define the rate coefficient k, or equivalently the kinetic *constant* (positive quantity which varies with the temperature) of the reaction by the equation 1.3:

$$k = \sigma.\sqrt{8k_B.T/\pi.\mu} \, . \, e^{-E_a/k_B.T} \tag{1.3}$$

Via the expression of the rate coefficient, the influence of temperature on the kinetic of a reaction is clearly highlighted:

$$v_A \propto k \propto \sqrt{T}.e^{-E_a/k_B.T}$$

With the pre-exponential term $\sqrt{T}$ being related to the properties of the gas ($< v_p >$), and the exponential factor $e^{-E_a/k_B T}$ to the activation barrier.

As a consequence, if the temperature increases, it leads to an increase of the rate coefficient and therefore of the reaction rate. In other words, the reaction rate increases with the temperature[6]. This temperature dependency is described in the rate coefficient/kinetic constant.
Let us note that the units of k depend on the order of the reaction, as we will discuss later.

However, it is worth mentioning that this conclusion is not valid for enzymatic kinetics, since those biological catalysts are active in a limited range of temperatures (and physico-chemical conditions in general). Those expressions are only relevant in that range of temperatures. Moreover, the enzymatic kinetics relies on other considerations (e.g. Michaelis-Menten equations) that the one used in classical kinetics. For the rest of the discussion, the enzymatic class of reactions will be set aside as we will consider chemical reaction relevant in typical abiotic astrochemical context. Nevertheless, it was important to emphasize this point for the sake of clarity and scientific accuracy.

> *Remark:* there exists a more advanced theoretical approach to express the temperature dependency of k. This approach, proposed by Erying in 1935, is based on the *transition state theory*. It is therefore not based on the gas kinetic theory and on the perfect gas approximation for which impenetrable spheres are assumed, but rather on potential energy surfaces and the search for characterizing the so-called *activated complex*.

To go deeper into the kinetic considerations, one must take notice that the influences of the abundance of reactants and the temperature do not manifest themselves in the same way in all chemical processes. This point deserves some comments:

---

[6]Neglecting the influence of T on E_a. This temperature dependency will be discussed further in chapter 2.

- **The reaction order** *and its impact on the way the number density in reactants manifests its kinetic effect:* the order of a reaction is defined as the molecularity (number of reactants) of the corresponding elementary process[7]. To understand the dependency of a chemical transformation to its reaction order, let us have a look at Table 1.4 presenting the rate equations (to be solved to get densities as a function of time) corresponding to different orders.

  From this table, the rate equations highlight the impact of the reaction order: the number of reactant(s) involved in the equation, and therefore the units of k are changing depending on the order of reaction.

Table 1.4: Equation rates for uni-, bi-, & t(h)er-molecular elementary processes

Order	Rate equation	Comments
First order	$A \rightarrow C$ $v_A = -dn_A/dt = k.n_A$	units of k: $[\text{s}^{-1}]$
Second order	$A + B \rightarrow C$ $v_A = -dn_A/dt = k.n_A.n_B$	units of k: $[\text{s}^{-1}.cm^3]$
Third order	$A + B + M \rightarrow C + M$ $v_A = -dn_A/dt = k.n_A.n_B.n_M$	- the third body M only has an energetic role - the probability that 3 bodies encounter in the ISM is *negligible*

  Moreover, as mentioned in Table 1.4, the probability of effective collision of 3 bodies is quite negligible in the Interstellar Medium, regarding the typical densities. However, this order will have a great significance for dust grain processes, as we will see in subsection 1.3.4.

- **The activation barrier** *and its influence on the kinetic constant*: the activation barrier is a concept in kinetic referring to the energy that has to be provided to a system to enable a given chemical transformation. This activation barrier, noted E_a, can be defined through energy diagrams: as we can see on Figure 1.2 showing a theoretical energy diagram of a hypothetical elementary process, E_a is basically the energy difference between the transition state (or activated complex) and the reactant. It must be clearly distinguished from the energy difference between the product and the reactant, owing to the realm of thermodynamic considerations. We will come back to this quantity when addressing the thermodynamics aspects.

  From equation 1.3, one easily realizes the intuitive influence of E_a on k, and therefore on the reaction rate proportional to this rate coefficient: if the activation barrier increases, the term $e^{-E_a/k_B T}$ will decrease, leading to a decrease of k and consequently of the reaction rate. Let us notice that the E_a is impacted by the temperature and pressure of the considered reaction medium, which is translated in the temperature effect on the partition functions and on the various contributions to the energies of the reactants, transition states, and products.

  It is worth mentioning that the reaction coordinates are not a temporal variable. It roughly represents the evolution of the system parameters as the inter-nuclear distance and the torsion angle. Moreover, it is worth recalling that the use of a catalyst decreases E_a and therefore facilitates (decrease of k, see equation 1.3) the chemical transformation.

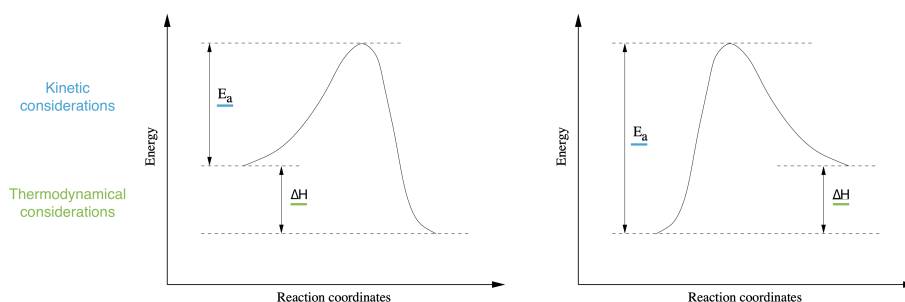[7]An elementary process $\equiv$ process for which there is no known reaction intermediate.

Figure 1.2: "Energy diagrams of hypothetical one-step chemical processes. ΔH is the difference between the energy content of products and reactants, and E_a is the activation energy barrier. Left side: exothermic process. Right side: endothermic process.", modified from De Becker (2021-2022)

- For reaction happening not in gas-phase, **the inter-molecular interactions with the solvent or surrounding medium**

- **The physical state of the reactants** (*Is it a homogeneous or a heterogeneous process? And, in which phase?*), and **the effective surface area** (for solid phase processes principally, or interface reactions)

It goes without saying that this list is non-exhaustive. Other factors can influence the temperature and number densities dependencies of the kinetics of a process but the factors listed above are the most relevant ones in an astrochemical context and we will focus on them in the following discussions.

In relation with the previous subsection, the densities and temperatures are therefore of great importance for kinetic aspects in (astro)chemistry. Regarding the differences in temperature and densities in the different phases, it is of prime importance to take the phase of the ISM concerned by each study into account. Indeed, the astrochemical processes ruling the evolution of the chemical population are impacted in terms of kinetic depending on the physical parameters of the phase of interest.

If one considers the low densities prevailing in the ISM (compared to what we find on Earth) as well as the low temperatures (especially in molecular clouds), astrochemical processes are very *slow*. In fact, the astrochemical time-scale is quite large compared to the dynamical time-scale of the medium, and the equilibrium can not be reached for those numerous cases. This will be further discussed at the end of this point.

As for the thermodynamic approach, one should firstly remember the first and second laws of thermodynamics. I refer the reader to the Appendix A if a brief reminder of those fundamentals is needed. For a shorter recalling, we know that the second law allows to answer the question of the spontaneity evolution direction of a given system without any external work input. There are basically two main spontaneity criteria:

i. **A probabilistic criterion ($\Delta S > 0$)**: for an irreversible transformation, the evolution of a given system will always tend towards the maximal entropy, S;

ii. **An energetic criterion ($\Delta H < 0$)**: a system tends to evolve naturally towards its minimal energy. It therefore suggests an energy release and a decrease of enthalpy (H)

However, those two criteria can not explain the spontaneity of a given reaction on their own. There exist spontaneous transformations with a $\Delta S < 0$ or a $\Delta H > 0$. In fact, if we combine the probabilistic and energetic criteria, the variation in **(Gibbs) free energy** allows us to define a requirement for a spontaneous chemical process (also called an exergonic reaction): at a constant level of pressure and temperature (and composition), a given process is spontaneous if it is characterised by a decrease in free energy, G. For a process at thermodynamic equilibrium, the ΔG is equal to zero. Mathematically, at $\Delta P = \Delta T = 0$, the 2nd principle of thermodynamic is given in equation 1.4

$$\Delta G = \Delta H - T.\Delta S < 0 \tag{1.4}$$

From equation 1.4, several conclusions can be drawn. Firstly, a process characterized by the favorable energetic criterion ($\Delta H < 0$) as well as the favorable probabilistic criterion ($\Delta S > 0$) will always be spontaneous, no matter the temperature (*but, one has to keep the kinetic considerations in mind! A thermodynamically spontaneous process does not mean a fast process! If the temperature is too low, a process can be spontaneous but the reactants may not have enough energy to overcome the energy barrier, coming from kinetic considerations (see equation 1.3)! The same conclusion is valid for a spontaneous process if the number densities are too low, leading to a very slow process.*). On the contrary, transformations displaying both the unfavorable criteria ($\Delta S < 0$ and $\Delta H > 0$) will always be impossible (there is no temperature at which a negative or zero ΔG can be reached). Furthermore, for cases with only one of both favourable criteria, namely $\Delta S > 0$ **or** $\Delta H < 0$, the feasibility of the reaction depends on the temperature. *From kinetic considerations, we know that an increase of temperature leads to an increase of the rate constant and therefore of the reaction rate. However, it is worth mentioning that an increase of temperature does not always mean a thermodynamically more spontaneous process, as for the case with $\Delta H < 0$ and $\Delta S < 0$ (over a given temperature, the process is not anymore spontaneous). Once more, we understand the crucial complementarity of kinetic and thermodynamic considerations: a fast process has to be thermodynamically feasible and, inversely, a thermodynamically spontaneous process has to be feasible in a reasonable time scale, as discussed above. Therefore, for a complete chemical study of a process, both the kinetic and thermodynamic aspects have to be investigated.* To summarize this spontaneity concept, Figure 1.3 gathers the considerations for different combinations of ΔH and ΔS. It important to keep in mind that this figure are based on the assumption that ΔH and ΔS do not vary with T in the temperature interval that is considered. For those reasons, considerations in Figure 1.3 are valid for a limited range of temperatures (for instance, to be rigorous, ΔH varies with T according to Kirchhoff's law; a similar law exists for ΔS.).

Moreover, one may discuss in more details the concepts of chemical equilibrium versus thermodynamic equilibrium. A chemical system is said to be at *chemical* equilibrium when a sufficient time has elapsed such that its composition does not vary anymore. In this state, direct and inverse reactions are occurring at the same rate, and the composition of the system does not change with time. The resulting so-called equilibrium constant K is usually defined as in equation 1.5, only valid for system at chemical equilibrium (the relation in parenthesis highlights the link of K with the rate coefficients, k_1 and k_2 respectively standing for the direct and inverse rate coefficient of an hypothetical bimolecular reversible process).

$$K = \prod_{i=1}^{n} (n_i)^{\nu_i} (= k_1/k_2) \tag{1.5}$$

where ν_i is a stoichiometric coefficient negative for reactants, positive for products (and null for eventual catalysts).

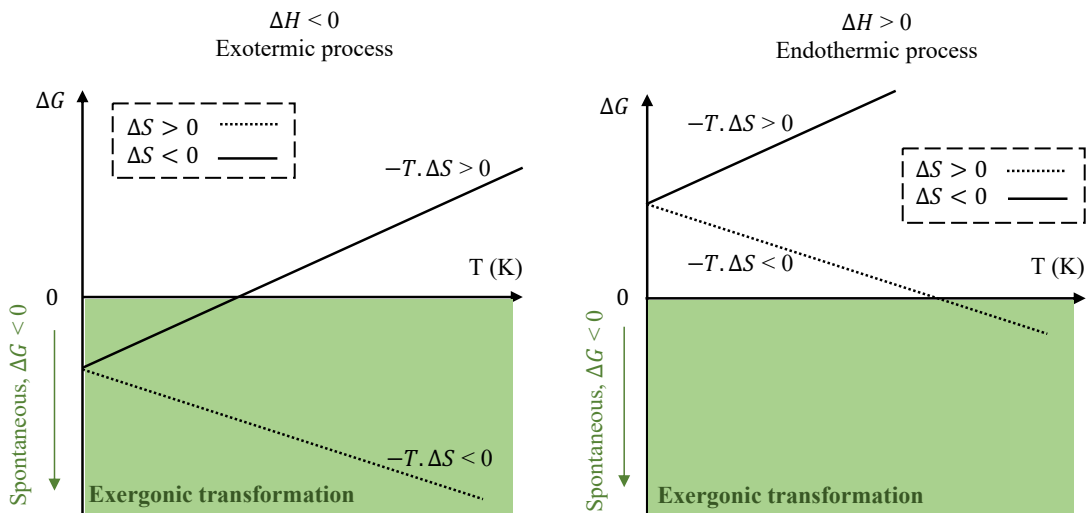Figure 1.3: ΔG of an exothermic (left) and an endothermic (right) hypothetical transformations with respect to the temperature T . In both cases, the ΔG for a positive (hashed line) and negative variation of entropy ΔS are represented (inspired from Wouters (2015)).

This positive constant is lower than unity for non-spontaneous/endergonic reactions and greater than unity for spontaneous/exergonic ones. In addition, a value of 1 characterizes a chemical system not only at chemical equilibrium, but also at thermodynamical equilibrium (isoenergetic/thermoneutral processes), with ΔG being equal to zero as mentioned before.

The resulting relation between the thermodynamic quantity ΔG (in its intensive units) and the equilibrium constant K is given in equation 1.6.

$$\Delta G = -R.T.lnK \quad ; \quad K = e^{\left(\frac{-\Delta G}{R.T}\right)} \tag{1.6}$$

In that context, the general concept of chemical equilibrium can be considered as time-scale dependent. Indeed, a chemical equilibrium can be reached only if the time needed to reach it is smaller than the dynamical time scale. In other words, a system is said to be **out-of equilibrium** if the elapsed time is not sufficient for the chemical equilibrium to be reached (out-of-equilibrium conditions that will be discussed in Chapter 3), or if the physical conditions of the system change before the time interval needed to reach chemical equilibrium.

Consequently, regarding the rather long time-scale associated with several processes is astrochemistry (as discussed before), astrochemical modelling of a system made of interconnected reactions will mainly deal with out-of-equilibrium processes, with a negligible minority of processes at chemical equilibrium. To generalize the task, the astrochemists assume that all processes are out-of-equilibrium, dealing therefore only with time-dependant inference of the abundances, without relying on equilibrium constant and equilibrium displacement (contrary to what can be usually assumed for terrestrial issues). However, it is important to stress out that it does not mean that the thermodynamical aspects are meaningless in the case of astrochemical issues, it would simply mean that the equilibrium constants are not valid and a full time-dependant kinetic treatment has to be implemented for the modelling of the abundances. Besides, the thermodynamic quantities characterizing the spontaneity of the studied processes are still of great interest, and the thermodynamic aspects can not be neglected for a rigorous work.

1.3.3 Gas-phase processes

So far, we have considered hypothetical reactions but, more specifically, the following question can be asked: *What are the main gas-phase reactions occurring in the ISM?* Actually, there are different kinds of chemical transformations, involving various kinds of reaction partners and showing different relevance depending on the interstellar phase considered. An overview of the different reactions and their own characteristics is given in Table 1.5 (De Becker, 2013).

Before dealing with the details of this table, let us define (De Becker, 2013) some quantities:

- For the photo-chemical processes:

  - α^{PD} is the reaction rate coefficient of photo-dissociation in the absence of dust grain extinction;
  - α^{PI} is the reaction rate coefficient of photo-ionisation in the absence of dust grain extinction;
  - $\sigma^{diss}(\nu)$ is the photo-dissociation cross-section at frequency ν;
  - $\sigma^{ion}(\nu)$ is the photo-ionisation cross-section at frequency ν;
  - ν_{diss} is the the photon frequency limit for the dissociation (knowing that the mean bonding energy between 2 atoms ranges from ~ 5 to 10 eV, corresponding therefore to FUV photons);
  - $\nu_{H,ion}$ is the photon frequency limit for the ionisation of the hydrogen atom (corresponding to an energy of 13.6 eV);
  - J_{IS} is the mean intensity of the interstellar radiation field. The order of magnitude given in table corresponds to a $J_{IS} \approx 10^8$ FUV photons/cm^2.s.sr;
  - γ is a factor that depends on the species;
  - A_v is the dust extinction factor in magnitude units for a given frequency ν.

  α^{PD}, α^{PI} and γ are estimated from radiative transfer studies and are tabulated in the very useful *UMIST database for astrochemistry*[8] (Woodall et al., 2007).

- For processes involving atoms, molecules and/or ions & reactions induced by electrons or (secondary) CR, knowing that the relations given for the kinetic constants are empirical relations:

  Warning: α', β' and γ' are different parameters from the ones used in the photo-chemical context. This point is highlighted with the *prime* mark. Those three factors are typical for a given temperature interval.

  - α' depends on the species and the temperature interval considered;
  - β' depends on the species and the temperature interval considered. For perfect gas, $\beta' = 0.5$ (reducing the relation to the Arrhenius law [9]) but deviations with respect to this value are observed for real cases (Van Der Walls interactions);
  - γ' is equal to $\dfrac{E_a}{k_B}$.

---

[8]http://udfa.ajmarkwick.net

[9]This law is an empirical law studying the temperature dependency of the kinetic constant k under the perfect gas hypothesis. Atoms are therefore considered as impenetrable spheres.

Table 1.5: Overview of the different gas-phase processes occurring in various interstellar phases. (De Becker, 2013)

Type of reaction	Process Name	Order of magnitude for k + comments	Relevance in various astrochemical contexts
Photo-chemical reactions	**Photo-dissociation** (PD) $AB + h\nu \rightarrow A + B$	$k_{PD} = \alpha^{PD} e^{-\gamma A_v}(\beta_{ss})$; $\alpha^{PD} = \int_{\nu_{diss}}^{\nu_{H,ion}} 4\pi J_{IS}\sigma^{diss}(\nu)d\nu$ *(if no attenuation)* ; $\alpha_{PD} \approx 10^{-9} - 10^{-10}$ s^{-1}	- HI region & WNM/CNM (far enough from O-B stars so that ionizing UV photons absorbed in the WIM, HII or hot coronal gas, see below)
	Photo-ionisation (PI) $A + h\nu \rightarrow A^+ + e^-$	$k_{PI} = \alpha^{PI} e^{-\gamma A_v}$; $\alpha^{PI} = \int_{\nu_{H,ion}}^{\infty} 4\pi J_{IS}\sigma^{ion}(\nu)d\nu$ *(if no attenuation)* ; $\alpha_{PI} \approx 3.10^{-10} - 10^{-12}$ s^{-1}	- HII region, WIM & coronal hot gas where E$_{photon}$ high enough (E$_{PI} > E_{PD}$)
Reactions between atoms, molecules and/or ions	**Neutral-neutral reaction** $A + B \rightarrow C + D$	$k = \alpha'\left(\frac{T}{300}\right)^{\beta'} e^{-\gamma/T}$ E_a generally large *(bond breaking)*, $\alpha \sim 10^{-12} - 10^{-14}$, $\beta' \sim 0 - 3$	- more generally in warm regions (post-shocks, photo-dissociation regions, ...) regarding the high typical value of E_a to overcome
	Ion-neutral reaction $A^+ + B \rightarrow C^+ + D$	Stronger interaction (polarization-induced) between reactants than for NN $\rightarrow k_{ion-N} \sim 10^{-10}$ up to 10^{-9} cm^3 s^{-1}	- anywhere ions can be met regarding the lower value of k with respect to neutral processes
	Charge transfer reaction $A^+ + B \rightarrow B^+ + A$	No bond breaking, $k_{ion-N} \sim 10^{-9} cm^3 s^{-1}$	- where ions are present ; - of prime interest for the ionization balance in the ISM
	Radiative association $A + B \rightleftarrows AB^* \rightarrow AB + h\nu$	No fragment, excess of energy of the product evacuated through radiation, kinetics governed by the AB* life time $k_{rad.\ assoc} \sim 10^{-20} - 10^{-16}$ cm^3 s^{-1} for small molecules	- for larger molecules, more vibrational energy levels $\rightarrow$ larger AB* life time: more significant where larger (PAH, etc) molecules are present
	Associative detachment $A^- + B \rightarrow AB + e^-$	The e$^-$ takes the energy excess, $k \sim 10^{-9}$ cm^3 s^{-1}	- very few anions in the ISM (very short-lived species) ; - CN$^-$ detected
	Association by collision $A + B + M \rightarrow AB + M$	M takes the energy excess	- The probability of a three body encounter is quite small (see. subsection 1.3.4) regarding the interstellar typical densities ; - where T high enough such as M has a large kinetic energy
	Dissociation by collision $AB + M \rightarrow A + B + M$	/	
Reaction induced by electrons or CR	**Dissociative electronic recombination** $A^+ + e^- \rightarrow A^* \rightarrow C + D$	$k_{elec.\ recomb} = \alpha'\left(\frac{T}{300}\right)^{\beta'}$ (barrierless) and $k \sim 10^{-7}$ s^{-1}	- e$^-$ from ionisation do not disappear from ISM ; - Principal termination process of cationic chains $\Rightarrow$ where cations are present
	Reaction induced by CR or secondary CR *a. Dissociation*	globally between $\sim 10^{-17}$ s^{-1} for CR and 10^{-10} -10^{-9} cm^{3}s^{-1} for secondary CR ex: $H_2 + CR \rightarrow H^+ + H + e^-$; $He^+ + CO \rightarrow C^+ + O + He$	- source of cations in dense clouds interior (where self-shielding prevents from UV photons)
	b. Ionisation	ex: $H_2 + CR \rightarrow H_2^+ + e^-$; $CO + CR \rightarrow CO^+ + e^-$	
	c. Indirect UV photons source $\rightarrow$ indirect photo-reaction	ex: $CO + CR \rightarrow C + O$; $C + CR \rightarrow C^+ + e^-$	- only source of UV photon in dense clouds (! the dust extinction contribution , cf. reddening law!)

16

From this table, several comments can be made. Firstly, in the ISM, the **photo-chemistry** is active only in regions where the photons with the required energy are able to penetrate, as we have already understood from Table 1.3. Moreover, the dust grain influence deserves some more discussion. One remarkable propriety of interstellar dust grains is their extinction capability (through absorption and scattering of the incoming photons) observed from the mid infrared ($\lambda \sim 30\mu m$) to the so-called *vacuum ultraviolet* ($\lambda \sim 0.1\mu m$). The important characteristic of this extinction process is its reddening effect on interstellar spectra when dust grains are present in the line of sight. In other words, this attenuation of the radiation field is achieved through a *reddening law*, leading to a greater extinction of UV photons than in the IR domain. Since photo-dissociation and photo-ionisation are dealing with FUV photon or even more energetic photons, this process is of prime importance. As a consequence of this decreasing effect of the dust contribution to the number of available photons with the required energy, the distribution of FUV photons decreases when we go deeper and deeper in a given cloud (the optical depth increases towards the center of the cloud, the FUV photons encouter more and more dust particles), therefore explaining the decreasing exponential given in Table 1.5.

In addition, another important process in the context of photo-dissociation needs to be discussed. This process is *self-shielding*, already mentioned in Table 1.3. Indeed, we noticed in this table that, in diffuse and dense molecular clouds, the self-shielding mechanism prevents the photo-dissociation processes to occur. Actually, in dense regions of the ISM, in addition to the reddening extinction due to dust, the radiation field is attenuated by the abundant molecular species at the cloud surface through photo-dissociation[10]. Therefore, depending on the depth considered and the distribution of molecules in a given cloud, the photo-dissociation rate of that population of molecules varies. For instance, for a given hypothetical homogeneous dense molecular cloud, the molecular population lying in a rather thin shell at the surface of the cloud will absorb the photons with the required energy (E_{PD}, characteristic of each bound in a molecule), shielding therefore the interior of the cloud from those photons. For cases where a self-shielding process is significant, a related multiplicative factor ($\beta_{ss} < 1$) is added to k_{PD} expression (if no self-shielding, β_{ss} is equal to 1).

Regarding **reactions between chemical entities**, one can firstly discuss the systematic presence of a **fragment** D. In fact, in the ISM, one generally deals with small molecules. The molecule resulting from the reaction of A with B will consequently have a too high internal energy. In fact, contrary to conditions that can be met on Earth, no exchange with the solvent or stabilizing interactions are possible to allow the existence of such a product, and the molecule resulting from the reaction of A with B will evacuate this energy excess through the loss of the D fragment. For instance, one can cite the following example to illustrate this point with a real case: $O + H_2 \rightarrow OH + H$, the product H being the fragment lost from the short-lived H_2O entity. H_2 is therefore not synthesized that way in the ISM! For more complex species, the simple addition of reactants is possible if the temperature is high enough to store the excess of energy in the ro-vibrationnal levels: $A + B \rightarrow C$.

Moreover, **neutral-neutral** (NN) reactions generally take place where the temperature allows to overcome the γ' factor or, equivalently, the energetic activation barrier. However, this type of reaction can also occur in a cold medium, but only if this E_a is very small, or even null. In that context, reactions involving atoms (low E_a) or between free radicals (barrierless[11]) are good candidates, leading to reactions with $k = \alpha' \left(\dfrac{T}{300} \right)^{\beta'} \sim 10^{-12}$ s^{-1}, with the γ' equal to zero.

Concerning the case of **ion-neutral** transformations, the processes are faster than for NN reactions. In fact, in the case of neutral-neutral, the only attractive interaction favouring the encounter of the

---

[10]The ionizing radiation having already been absorbed closer to the star...

[11]As we can easily understand, a barrierless process is to some extent *temperature independant*. Indeed, no energy barrier has to be surpassed to access the product, no activated complex (transition state) comes into play. However, such reaction are diffusion limited, this dissuion being dependant on the densities and temperature.

reactants are Van Der Waals forces, decreasing quite fast with the distance ($\propto 1/r^6$) and therefore effective at very short interatomic distances. On the contrary, when an ion is considered, a polarization induced interaction comes into play, with a less steep dependency on the distance ($\propto 1/r^4$). As a result, in the case of ion-molecule reactions, the interaction driving the attraction between reactants and favouring their encounter has an effect on longer distances. Consequently, a given ion-neutral activation barrier is greatly reduced with respect to the corresponding neutral process. It therefore explains why the kinetic constant for such processes is greater than for NN processes, with values of the order of $\sim 10^{-9} - 10^{-10}$ cm^3 s^{-1}. Moreover, this low E_a has the consequence to provide to the ion-neutral gas-phase processes the propriety to be nearly temperature in-dependant (low temperature needed to overcome the E_a), allowing it to take place anywhere ions are present. Let us note that for molecular species displaying permanent dipole, the k for ion-molecule processes can take even greater values, such as 10^{-7} cm^{3}s^{-1}, these processes being barrierless. This point demonstrates the importance of the presence of ionic species in the ISM: a small abundance of ions can have a great impact on astrochemical kinetics regarding the typical k, 2 to 4 (or even more if one considers molecular species displaying a permanent dipole) orders of magnitude greater than for NN processes.

A final comment can be made about **CR induced reactions** in molecular clouds. Indeed, it is firstly important to stress out the fact that this type of reaction is of prime importance for the astrochemistry of dense molecular clouds where the probability of encounter with a photon is almost null. In fact, it constitutes a source of dissociation and ionization, as well as an indirect UV photons source, where direct stellar light is not available. Moreover, in the dense cloud, the probability of a atom/molecule colliding with a CR is much higher than in the more diffuse ones.

One may also wonder about the physical explanation behind such difference between the kinetic constant associated with a reaction implying a primary CR or a secondary CR. CR species have been defined in Table 1.2. Concerning secondary CR (He$^+$), they are produced by the following reaction:

$$\text{He} + \text{CR} \rightarrow \text{He}^+ + \text{e}^-$$
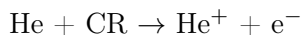
Actually, the difference between the respective kinetic constants comes from the inverse proportionality between the geometrical cross-section of a particle (included in the α' parameter) and its energy. This dependency can be explained on the basis geometrical considerations: the cross-section $\sigma(E)$ is different for different impact parameters. From a classical point of view and considering particles as rigid spheres, the cross section of a collision phenomenon is given by πd^2 where d corresponds to the sum of the two nuclear diameters. After the collisions, the change of direction undergone by the particles depends on the impact parameter b, related to the angular momentum L and the momentum p of the particles ($L = p.b$). On the other hand, from a quantum point of view, we know that for an angular momentum $L = \sqrt{l(l+1)}$ (with l being the second quantum number), the associated cross section for a frontal[12] collision ($l = 0$) corresponds to:

$$\sigma_{l,\lambda} = (2l + 1)\frac{\lambda^2}{4\pi} = \pi\lambdabar^2 = \frac{h^2}{8\pi mE} \Rightarrow \sigma(E) \propto \frac{1}{\sqrt{E}}$$

the second line of the equation being found using the De Broglie relations ($\lambda = h/p$ or $\lambdabar = \hbar/p = \lambda/2\pi$ and, for non relativistic bodies or, neglecting the relativistic effect brought by CR, $p^2/2m = E$) (Kippenhahn and Weigert, 1994). The indirect proportionality relation is clearly highlighted. Since a

---

[12]We know that all chemical reactions are not frontal and more complex trajectories have to be taken into account for complex reactions such as in organic chemistry and the Bürgi -Dunitz angle for the nucleophile attack on a carbonyle or trigonal unsaturated center. However, in first approximation, this assumption is valid for such a simple reaction with a CR and will not have any consequence on the rest of the discussion.

secondary CR has a lower energy than a primary one due to an energy loss in the inelastic collision process producing it, the cross section and therefore the kinetic constant is much higher for process involving secondary CR. It is worth mentioning that if the CR had a higher cross-section, it would not be able to reach the interior of the dense molecular cloud (it would indeed interact with many particles before reaching it). This large mean free path is of crucial importance. Regarding the high abundance of He in the Universe, this process provides cations in a non negligible amount in dense molecular clouds, where stellar light can not ionize, or even dissociate molecules. The cationic processes displaying higher k values than NN processes, it demonstrates the prime interest of this process in such interstellar regions.

Finally, the indirect photon source can be further discussed. As a result of an ionizing interaction of a molecule with a CR, the resulting free electron may excite a particle present in the medium and lead to the emission of an UV photon and a resulting photo-reaction (ex: indirect photo-dissociation of CO). It therefore constitutes the only source of UV photons in dense clouds' interiors as well as a source of neutral C from its main reservoir, CO.

1.3.4   Grain surface processes

As already seen in Table 1.2, dust grains constitute a minor (only $\sim 1\%$ of the gas component) but very important component of the ISM. Their presence has been demonstrated through several pieces of evidence. First of all, an indirect clue comes from the depletion in gas phase of the component contained in those grains. Actually, if one takes the relative abundances of the elements measured in the solar photosphere as a reference - all chemical species have to be in gas phase since dust grain can not survive the temperature of such environments - the abundance of some elements in interstellar gas[13] seems depleted by comparison to that reference (Draine, 2011). The depleted elements are therefore expected[14] to be trapped in the interstellar dust grains, as quantified in Table 1.6. The tendency of those elements to such condensation processes leading to the formation of refractory (i.e. heat-stable & heat-resistant, pressure and chemical decomposition) grains can be explained by their respective *condensation temperature* ($T_{cond,k}$, defined as the temperature below which 50% of atoms of element k are in solid phase), the most depleted elements displaying the highest $T_{cond,k}$, as illustrated in Figure 1.4(Draine, 2011).

Other evidence of the presence of interstellar dust grains can be found in the observations of their interactions with electromagnetic radiation. For instance, on can cite their wavelength-dependent attenuation, as already introduced in subsection 1.3.3 when addressing the extinction capability (through absorption and scattering of the incoming photons) of dust grain and its reddening effect on spectra. It is also worth mentioning that, coupled to this depletion, the corresponding extinction curve made it possible to put constraints on dust grains composition, size and variety. Moreover, the electromagnetic energy absorbed by dust is re-emitted in the thermal infrared (detectable from sub-mm to $\sim 2\mu m$). In addition, the dust grain existence in the ISM is supported by many other clues - the solid-state absorption light in the IR detected in stellar spectrum seen through dense molecular clouds, the identification of presolar grains preserved in comets and asteroids, the scattered light in reflection nebula - and is now well accepted in the scientific community (Draine, 2011).

---

[13]Measured in diffuse interstellar cloud to avoid as much as possible the presence of icy mantle, subject that will be discussed afterwards.

[14]Actually, one can not directly analyse dust grain components regarding the too high complexity of the resulting expected spectra (spectral features are broad and therefore difficult to attribute conclusively to a spectral line, and the UV-visible absorption is mostly a continuum) (Draine, 2011). Moreover, detection using radio- or microwave-telescopes (arguably the most widely used detection technique nowadays) are using the rotational transition and are therefore unable to detect molecules trapped in solid phase. As a consequence, the solid phase can not be studied in detail.

Table 1.6: Photospheric solar abundances (ppm) of selected elements relative to H abundance, taken from Asplund et al. (2009) (it therefore corresponds to the respective number of those elements relative to 10^6 H atoms, and is considered as the reference), and their respective abundances (relative to 10^6 H atoms) in interstellar gas (Jenkins, 2009) & interstellar dust (inferred from the difference between the total expected abundance (reference) and the gas-phase abundance). Their corresponding percentage in both phases compared to the total expected abundance in the ISM is also given.

	Reference value	Abundance in interstellar gas	Percentage lying in interstellar gas	Abundance in interstellar dust	Percentage lying in interstellar dust
O [a]	537	372	69.3%	165	30.7%
C	295	93[b]	31.5%	202	68.5%
N	74	62[c]	83.8%	12	16.2%
Mg	43.7	3.6	8.2%	40.1	91.8%
Si	35.5	3.0	8.45%	32.5	91.55%
Fe	34.7	0.36	1.04%	34.34	98.96%
Ni	1.74	0.015	0.86%	1.725	99.14%

[a] The percentage of O trapped in dust grains is strongly varying with the line of sight studied (subject not well understood yet, under study), contrary to other elements where the variations are of the order of 10%. (Draine, 2011)

[b] Compared to the values reported in Jenkins (2009), the gas-phase abundance of C has been reduced by a factor 2, as suggested by Sofia and Parvathi (2010).

[c] This value can be discussed, but the important point is the fact that nitrogen shows a low level of depletion almost everywhere (by looking towards any line of sight). For instance, if one compares the abundance in gas phase in the diffuse H_2 region to the one in ionized region around O-B star (WIM), we found that 100% of nitrogen is in gas phase, with no contribution in the solid (dust) phase. (Jenkins, 2009)
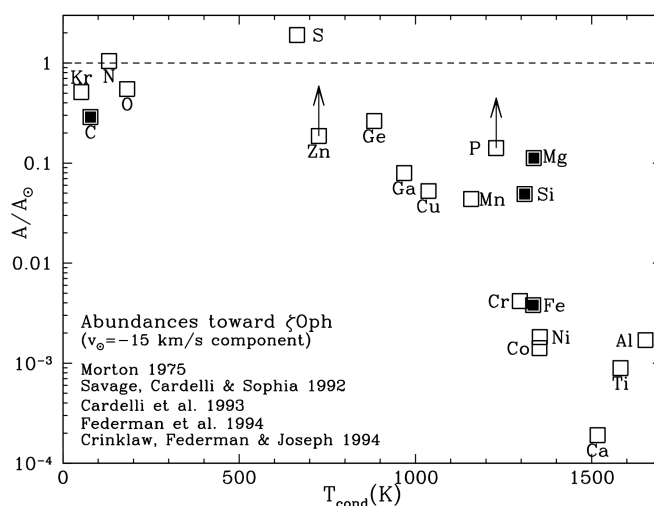
Figure 1.4: Gas-phase abundances (relative to solar) in the diffuse cloud toward ξ Ophiuchi plotted versus condensation temperature (T_{cond}), from Draine (2011) and references therein. The dashed horizontal line represents the solar abundance.

More specifically, concerning their composition, the major mass fraction of dust grains is constrained to the following materials: silicates (pyroxene or olivine composition), oxides of silicon, magnesium & iron, carbon solids (such as graphite, diamond, fullerenes but also amorphous carbon), hydrocarbons (including PAHs), carbides (e.g. silicon carbides) and metallic Fe. Other minor mass contributions from elements such as titanium and chrome are also considered. Regarding their size, interstellar grains are of the order of a few Å to $\sim 0.1 \mu m$ and often up to millimeter. (Draine, 2011)

Furthermore, besides the fact that the elements trapped in the bulk body of these dust grains are not available to participate in gas-phase chemistry, a remarkable characteristic of interstellar dust grains is the hetero-catalytic property of their surface.

To understand such a kinetically favorable property, one has to come back to the termolecular processes (third order reaction), introduced in Table 1.4. Basically, the third body takes away the excess of energy. Indeed, as discussed in the previous subsection (1.3.3), the interstellar chemistry deals mainly with small molecules. As a consequence, the association of a molecule A with a molecule B leads to a direct product AB displaying an excess of internal energy, making it unstable and leading to a fragment loss. However, the presence of a third body allows the direct product AB to be stabilized by taking away its excess of energy. In such context, a simple addition without any fragment loss can be considered, which is of great interest for climbing up the molecular complexity scale.

As a first approximation, grain surfaces are generally considered as passive accreting surfaces which only play an energetic role, with no active contribution to the interstellar chemistry. However, as you may intuitively understand from the nano-size of the interstellar grains, these can be considered as nanoparticles or, for the bigger ones, an assembly of such particles (Jones, 2016). Moreover, as it just has been suggested, PAHs are possible components of interstellar dust grains. Some authors are considering such molecular species as nanoparticles (e.g. see in Tielens (2008)). An understanding of the physico-chemistry behind such particles is therefore critical to approach a more realistic view the astrochemistry taking place on dust grains surfaces in the ISM. It is indeed possible that nascent nanoparticles (mostly a-C(:H) nanoparticles, with the possibility of hetero-atom doping) are efficient catalysts (enhanced surface activity) for small molecules and radicals formation in some parts of the ISM (Jones, 2016). The possibility of a surface made of functionalized a-C:H nanoparticules is also worth being accounted for (Jones, 2016).
Even if this long-held assumption of passive dust surfaces is quite naive, we will mostly restrict our discussion to those considerations. Actually, as we will see in chapter 2, section 2.2, the astrochemical kinetic numerical model we will use (and more generally in the scientific literature) only takes simple grain-surface processes into account, treating the dust surfaces as passive surfaces that provide reaction sites for transformation between adsorbed species, or between an adsorbed and incident gas-phase species. More specifically, in this context, two different grain surface mechanisms will be looked upon: (i) the Langmuir–Hinshelwood mechanism and (ii) the Eley–Rideal mechanism.

Firstly considering the Langmuir–Hinshelwood mechanism (see left scheme on Figure 1.5), it can be sub-sequenced into four main steps, as described in Table 1.7 (with the kinetic considerations relative to each step being highlighted) (De Becker, 2013). As for the gas-phase considerations, let us define some quantities before addressing kinetic details contained in this Table:

- k_I is the accretion rate coefficient;

    n_d is the number density of interstellar dust grains;

    σ_d is the cross-section of the grains (collision theory: a high cross-section leads to a higher probability of encounter with the reactant, therefore an accreting particle in this context);

v is the mean speed of the accreting particles;

S is a sticking efficiency factor (1 if each collision leads to an adsorption). It depends on the dust grain and gas temperature.

- $\tau_{II,th}$ is the thermal migration time-scale;

ν_m is defined as the vibrational frequency of the adsorbate for the vibrational mode parallel to the dust surface;

E_m is the energetic barrier that particles have to overcome to migrate - $\sim 1/3$ of the binding energy of the particle to its adsoprtion site (~ 0.01 eV for physisorption sites, and a few eV for chemisorption sites);

T_d is the dust grain temperature. In molecular clouds, the equilibrium (thermal equilibrium with the gas phase) temperature is typically $\sim$ 10-20 K for classical macroscopic dust grain, larger than 0.01 μm of radii (for smaller grains, quantum effects prevents from the establishment of an equilibrium temperature and the problem is more complex) (Draine, 2011);

k_{osc} is the strength constant of the oscillator in the Hooke law. In the harmonic oscillator model, it therefore corresponds to the strength constant of the chemical bond/physical interaction;

μ is the reduced mass of the system 'adsorbate-adoprtion site'.

- p_{III} is the probability of reaction on an adsorption site before evaporation (for a reaction with an activation barrier; therefore not between radicals, which is done on much shorter time-scale since the probability of penetration of the activation of the reaction is equal to 1, the reaction barrier being nul);

θ_r is the surface coverage of potential reactants;

p_{E_a} is the probability of the penetration of the activation barrier E_a of the chemical transformation.

- $\tau_{II,th}$ is the thermal desorption time-scale or, in other word, the thermal residence time-scale;

ν_0 is defined as the vibrational frequency of the adsorbate (stretching mode);

E_b binding energy of the particle to its adsorption site.

Furthermore, mass and temperature influences stemming from this Table need to be further discussed. Actually, in the Langmuir–Hinshelwood mechanism, once adsorbed (I) on a chemi- or physi-sorption site, an adsorbate may migrate (II) to another binding site. As translated by the expression ruling the thermal migration time-scale ($\tau_{II,th}$) and the Hooke law aimed to express the vibrational frequency, heavier species are less mobile ($\tau_{II,th}$ higher because of a lower ν_m, inducing a higher ν_m^{-1}) than lighter adsorbates. Consequently, efficient dust-grain reaction following this mechanism generally implies the migration of at least one light adsorbate (H, D, C, N or even O). It therefore explains why such a mechanism leads to highly hydrogenated species. It also means that a higher mass species would stay longer at a given adsorption site, and should therefore be potentially visited by lighter ones several times. We will come back to that point when addressing the reaction (III). Concerning the temperature dependency of the thermal migration, as one can intuitively forecast, a higher temperature will favour the penetration of the migration activation barrier E_m of a given adsorption site. In a very cold environment, this mobility process is mostly inhibited from chemisorption sites, enabling migration only from physisorption sites. An accumulation of chemical species on chemisorption sites can therefore be expected. In such a context, the tunnelling quantum effect (Trixler, 2013) to keep a non-zero mobility is sometimes invoked, but is difficult to be included in astrochemical kinetic models.
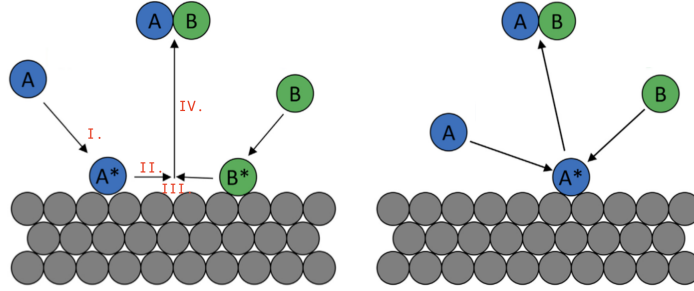
Figure 1.5: Schematic representation of (left) the Langmuir–Hinshelwood mechanism and (right) the Eley–Rideal mechanism. * represents a given adsorption site on the surface, modified from Becker (2018).

Table 1.7: Description and basic kinetic considerations of the four major steps of the Langmuir–Hinshelwood mechanism. (De Becker, 2013)

	Description of the step	Kinetic considerations
I. Accretion	Migration of atoms and molecules from gas phase to the grain surface and adoption onto this surface [a]	$k_I = n_d \sigma_d v S$
II. Migration	Migration/diffusion over the grain surface of the bounded adsorbates ; mobility through 2 processes: (i) thermal hopping migration and (ii) quantum effect (tunneling, low T)	$\tau_{II,th} = \nu_m^{-1} e^{\left(\frac{E_m}{k_B T_d}\right)}$ with[b] $\nu = \frac{1}{2\pi}\sqrt{\frac{k_{osc}}{\mu}}$
III. Reaction	Encounter of adsorbates leading to a chemical reaction (the grain taking away the excess of energy)	$p_{III} = \tau_{III,th} \theta_r p_{E_a}$
IV. Desorption	Ejection of the reaction product[c]	$\tau_{III,th} = \nu_0^{-1} e^{\left(\frac{E_b}{k_B T_d}\right)}$

[a] There are two kinds of adsorption processes: the physisorption (via van der Waals interactions) and the chemisorption (interaction acting on shorter length-scale, with the creation of a chemical bound that therefore leads to interaction energy up to about one order of magnitude greater than in case of physisorption processes) .

[b] Following the harmonic oscillator model and therefore the well-known Hooke law.

[c] More rigorously, a desorption process is possible for all adsorbates, therefore including reactants and products. Note that a chemical species may not undergo the third step (or even the second one) before desorption (IV).
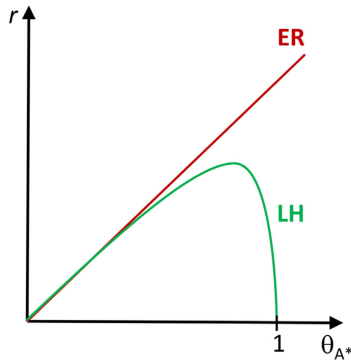
Figure 1.6: "Schematic representation of the reaction rate r for the Eley–Rideal (ER) and the Langmuir–Hinshelwood (LH) mechanisms as a function of surface coverage θ_{A*} of A", from Becker (2018).

Regarding the reaction (III), if a chemical entity keeps staying on the dust grain surface without being ejected in the gas phase (depending on the temperature, see IV), it may undergo successive chemical transformations, therefore allowing it to climb in the complexity scale. This point should be emphasized in comparison to the gas phase astrochemistry where the probability of again encountering a reaction partner for another given product is greatly weaker. Actually, depending on the ratio $\frac{\tau_{IV,th}}{\tau_{II,th}}$, one given adsorption site can be visited several times.

Addressing now the last step of this Langmuir–Hinshelwood mechanism, the ejection (IV) process of a given adsorbate depends on its mass and on the grain temperature, as described by the $\tau_{IV,th}$ formula. Those dependencies are similar to the ones associated to the thermal migration time-scale ($\tau_{II,th}$), using the appropriate vibrational frequency and the energy barrier ($E_b > E_m$). Several factors can favour a longer residence time (higher probability to undergo a reaction), such as a higher mass, a low temperature medium and a high binding energy. Therefore, regarding $\tau_{II,th}$ and $\tau_{IV,th}$, if the temperature is high enough to allow the migration but too weak to trigger a desorption, the grain-surface chemistry is efficient. It is also good to note that several desorption mechanisms exist: UV photon action (in diffuse ISM, Photodissociation Regions, ...), X-ray photon, CR interaction, hydrodynamic shock (transformation of mechanical energy into heat, leading to desorption and erosion through CR bombardment).

On the other hand, in the Eley–Rideal mechanism (see right part of Figure 1.5), only two steps are considered: an accretion-reaction step (accreting species directly interacting with the previously adsorbed chemical entity, without any consideration of migration process) , and a desorption step. It is therefore reducde to an effective collision of a given gas phase species with a partner stuck on a given grain surface (De Becker, 2013). This mechanism is the dominating simple grain-surface heterogeneous catalysis process for cases in high accretion regimes where the surface coverage is high, as shown in Figure 1.6.

Before entering into other solid-phase chemical concepts, it is worth mentioning that such simple grain-surface mechanisms are needed to explain the abundance of molecular hydrogen in the ISM. This can only be understood if this heterogeneous catalytic process is the H_2 main formation route, as discussed in Draine (2011). Moreover, a comparable process can be extrapolated to large PAHs, where similar catalytic processes are expected. This possibility has been investigated, for instance, in Bohme (1992); Campisi and Candian (2020).

In addition, another important astrochemical property of dust grain has to be discussed, which is the very rich chemistry expected in their icy mantle. This bulk-ice chemistry is needed to explain the interstellar abundance of some molecules including HCN, SO, OCS, ... as discussed in Kalvans and Shmeld (2010). Actually, in the densest dark molecular clouds[15], or as a result of the substantial increase in density and of particles speed v (Virial theorem) at the beginning of the gravitational collapse of a molecular cloud[16], the accretion of chemical species on the grains' surface is favoured (see equation of k_I in Table 1.7). It leads to the formation of layers of adsorbed chemical species, and the formation of an icy mantle. Concerning the tendency to desorption processes of those adsorbed species, and therefore the *"life-time"* of such an icy mantle, the desorption is unfavoured by the low temperature and the poor interaction with UV photons in the dense clouds' interior (see equation of τ_{IV} in Table 1.7). The innermost part of the clouds is therefore the most likely place where icy mantle can form quantitatively, as long as the temperature doesn't go beyond the sublimation threshold. From the moment the collapsing cloud formed a protoplanetary disk about the protostar,

---

[15]Where the high abundance of dust grain has been demonstrated many times, such in Pagani et al. (2010).
[16]First step of stellar system formation according to the classical scheme.

such low temperatures (along with the lack of UV photons) are met close to the midplane of the disk, far enough from the protostar. The minimum distance is called the snow line. It is also worth noting that many authors are considering only one layer of the accreted species. However, the chemistry of a given layer does not end with the formation of the next accreted layer. Therefore, thick icy mantles of a few hundred monolayers can be considered, but very few models are able to take such a complex system into account (Kalvans and Shmeld, 2010). Those mantles contain several simple interstellar molecules, such as H_2O (the most abundant one), CO, CO_2 and smaller amounts of CH_3OH, H_2CO, NH_3, CH_4 or other complex organic compounds (e.g. Oberg et al. (2011) and references therein). The chemistry in such icy mantles can be quite rich, as widely proposed in the scientific literature. For instance, theoretical studies demonstrates the relevance of a catalytic role played by the water-ices thanks to the presence of an icy *matrix* made, among others, of water molecules. Indeed, it favours the proton transfer through proton relay mechanisms, where a H_2O molecule of the icy surface is simultaneously a proton donor and acceptor (Rimola et al., 2010; Zamirri et al., 2019). Mechanisms similar to what can be considered in an aqueous solvent can therefore be imagined, increasing the number of routes towards more complex molecules (see section 1.4, subsection 1.4.2 for more details).

1.3.5 Interplay between gas and solid phase processes

As seen in the previous subsections, the temperature greatly influences the astrochemistry at play in the ISM, made of an indivisible mix of gas and solid phases. Regarding the temperature dependency of those processes (as summarized in Tables 1.5 1.7), the temperature of the considered astrophysical environment is of prime importance. As previously mentioned, the phase of the ISM that will be studied in the scope of this work is the dense molecular clouds. In that context, the interior of the cloud is not permeated by a strong FUV radiation field, thanks to the abundance of dust grains and the self-shielding process (as mentioned in subsection 1.3.3), itself correlated to the presence of abundant molecular species (absorbing, in the outer parts of the cloud, the photons with the required energy). However, the presence of UV photons in the interior of the cloud can not be ruled out completely. In fact, as mentioned in Table 1.5 (subsection 1.3.3), an indirect source of UV photons is given by the interaction of CR with the chemical species constituting the cloud.

An overview of the astrochemistry taking place in such dense molecular clouds is given in Figure 1.7. The left part of the Figure represents the astrochemically relevant material gathered in a molecular cloud. On the other hand, in the second, right part of the Figure 1.7, one divides the astrochemistry at work in such an environment into 2 major parts: (i) the gas phase processes, including cationic chains (successive cationic processes), neutral[17] ones as well as CR induced reactions, and (ii) surface processes, generally considered on dust grains surfaces, but the possibility of a transformation similarly catalyzed on large extended PAHs can also be envisaged.

Those two main chemical transformation pathways are interconnected. For instance, the accretion process allows for the connection from gas to solid phase, a loss (gain) source in terms of available compounds for the gas (solid) phase astrochemistry. Inversely, the desorption process makes the interplay from solid to gas phases, allowing therefore the chemical species processed/trapped on dust grains surfaces or in icy matrices to be (re-)injected into the gas phase, where they can undergo gas-phase chemical transformations. This interplay is crucial for the astrochemistry taking place in such dense molecular clouds.

---

[17]Indeed, even if neutral-neutral reactions display kinetic constants that are quite small compared to cationic processes, one can not neglect them. Actually, the number densities of neutral species being greatly larger than those of cationic entities, both cationic and neutral processes have to be taken into account.
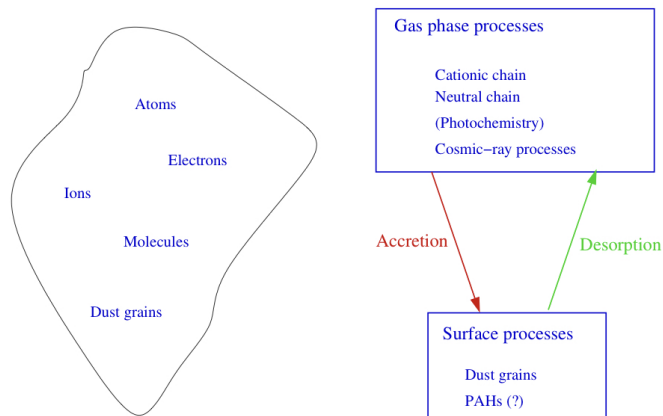
Figure 1.7: Schematic overview of the astrochemical processes happening in a given molecular cloud, from De Becker (2021-2022). Let us notice that, if the icy mantle is consequent, bulk mantle chemistry may also take place.

1.4 Amino acids

The molecular species on which this work will be focused are **amino acids**, and more specifically their formation in the Interstellar Medium. Therefore, to come back to section 1.2, this research will be mainly driven by the molecular complexity guideline.

As you may think, there is indeed a *parent* aspect to the formation of amino acids in the ISM linked to the astrophysical filiation, namely the general issue of the origin of amino-acids on Earth (assuming an exogenous origin, as previously mentioned). However, that is not the guideline of the study which focuses on the formation of this type of molecular species in the ISM rather than its potential link with a planetary system.

This section is aimed at making a overview on amino acids in general, firstly insisting on what we currently know about terrestrial amino acids and their importance in our biochemistry. In this context, their main structure will be discussed, as well as the water-demanding 3D functional structure of their corresponding macromolecule (proteins). This step being completed, the issue of the formation of amino acids in the ISM will be introduced. A subsequent deep bibliographic investigation of the many proposed interstellar pathways towards their formation (top-down approach) will be performed.

1.4.1 Amino acids in general

Amino-acids are the primary building blocks of proteins, essential macromolecules in living organisms. Actually, next to the other main families of macromolecules of great biochemical interest, which are sugars (carbohydrates), nucleic acids and lipids, proteins play a crucial biological role. Representing more than 50% of the cellular dry mass, one can cite for instance the following functions:

- *their structural role*: structural proteins (e.g. collagen, keratin, ...) aimed at giving the tissues and cells their shape, as well as their resistance against physical/mechanical constraints;

- *their immune (advocacy) role*: immunoglobulins, also called antibodies, corresponding to proteins aimed at recognizing antigens in order to inform the immune system that a foreign body has to be eliminated;

- *their transport role*: one can think for instance about the hemoglobin, allowing the oxygen transport for vertebrate living bodies;

- *their contractile and motor role:* actin and myosin are contractile proteins able to activate the movement of the muscles;

- *their hormonal role*: for instance, insulin is an hormone secreted by the pancreas that contributes to the regulation of blood glucose (for vertebrate living bodies);

- *their enzymatic role*: an enzyme is a natural catalyst (accelerating therefore biochemical transformations and ensuring an efficient metabolism) with a great specificity to its substrate. For instance, digestive enzymes (such as pancreatic amylase, protease or lipase) fragment their substrates into increasingly small molecules;

- *their function in the communication between cells* (receptive proteins)*, ...*

Concerning their structure, proteins are arranged under 3 to 4 structural organisational levels. These are:

I. *The primary structure*: basically defined as the amino-acid (monomer) sequence, linked by covalent bonds. Those chemical bounds are called peptide bonds, and are formed through consecutive condensation reactions and the loss of a water molecule, leading to the formation of a linear polymer called peptide. [18] ;

II. *The secondary structure*: peculiar stable arrangement of amino-acids to form structures such as α-helix, β-sheet, β-turns, ...

III. *The tertiary structure*: this third level of structural organisation concerns the 3D conformation that peptides adopt in water (solvent of terrestrial life). This 3D structure confers to the peptide chain its protein function. Actually, amino-acids are differentiated by their residues (as we will see here-after). These can be hydrophobic or hydrophilic. Depending on the residues constituting the sequence of amino-acids, the protein will fold such a way that the hydrophobic residues face the interior of the 3D conformation, letting the hydrophilic residues face the exterior and therefore being in contact with the aqueous solvent;

IV. *The quaternary structure*: In the case of peptides for which the secondary and tertiary structure is not sufficient to confer its function, an assembly of peptide chains (subunits) linked through weak bonds (such as ion interactions, hydrogen bonds, van der Waals forces and/or hydrophobic interactions) makes the protein functional (e.g. hemoglobin is a tetramer made of four peptide chains).

From I to IV, the level of molecular complexity is increasing towards the functional protein. Without its 3D conformation, a given protein is said to be inactive and can not carry out its function. It therefore demonstrates the crucial interest of the aqueous medium for terrestrial life. Indeed, the tertiary structure is related to the aqueous solvent constituting living bodies and leading to the folding of the protein, itself dictated by the hydrophilic and hydrophobic nature of amino-acids.

Now that we understand well the importance of proteins for terrestrial life, we can focus on their monomers for the rest of the discussion (i.e. the building blocks of the primary structure). This is

---

[18]It is worth mentioning that, *in vivo* (in cells of terrestrial living bodies), this sequence is synthesized via the so-called transcription and translation processes

indeed the likely species of prebiotic interest that could have been eventually brought to the Earth through an exogenous mechanism. It will be our working hypothesis[19], the first proteins being arguably built *in situ* on Earth thanks to the higher densities and the presence of *liquid* water.

On a molecular scale, the skeleton of an amino acids is basically characterized by an amine and a carboxylic acid functional group, separated by (at least) one carbon (one for α-amino-acids, the most-common type, α standing for the amine group position with respect to the carboxylic group) and its possible substituent(s), as seen on Figure 1.8, left.
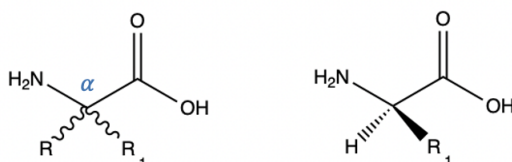
Figure 1.8: (left) General structure of α-amino-acids; (right) general structure of natural amino acids (in their common L-form).

From this general scheme, two main classes of amino-acids can be defined:

- the α-H-amino-acids: the carbon at α position with respect to the carboxylic acid is bond to (at least[20]) one hydrogen atom (see R position on the left part of Figure 1.8). Natural amino-acids (20) are part of this class of compounds[21];

- the α-methyl-amino-acids: in this case, the proton of the "standard" α-H-amino-acids is substituted by a methyl group.

Other classes of amino-acids exist, and are defined thanks to the amine group position with respect to the carboxylic group. One can cite for instance the β-amino-acids, with the amine on the carbon at the β position with respect to the carboxylic acid group, γ-amino-acids, diamino-acids (at least one carboxylic acid and two amine groups), ...

We can now focus on natural amino-acids (used to form the proteins composing living terrestrial bodies) and their so-called residues introduced beforehand. As just explained, all natural amino-acids are part of the α-H-amino-acids. What differ between them is therefore the R_1 substitute, called the amino-acid residue (see Figure 1.8, right part). This residue is characteristic of each natural amino-acid, and the physico-chemical properties (such as their acidity, their hydrophilic/hydrophobic nature, ...) differentiating each natural amino-acids are linked to those residues. As a consequence, their prime importance in our biochemistry can not be neglected.

It is also worth mentioning that the active amino-acids involved in our biochemistry are L-amino acids (even if D-forms are also used, especially in peptidoglycans, but greatly are rarer) leading to the homochirality problem (together with the large access of D-sugars). For the rest of the discussion, we will neglect this problematic. Moreover, we will focus on the glycine, which is both the simplest amino acid and the only achiral one (R and R_1 in Figure 1.8 are H atoms).

---

[19]In other words, regarding the need of liquid water to fold a protein, it should be totally irrelevant to search for active proteins in the ISM. Moreover, the low densities in the ISM would simply not allow the building of such bio-polymer, even without considering the third level of structure. The molecular complexities reached (or at least, detected) in such medium are greatly lower, as stated in Table 1.1.

[20]For glycine, both atoms linked to that carbon are H atoms. This is the simplest (natural) amino-acid.

[21]Not all α-H-amino-acids are natural, but all natural amino-acids belong to this class!

1.4.2 Amino acids in an astrophysical context

The detection in the ISM of organic molecules with increasing complexities (Polycyclic Aromatic Hydrocarbons, nitriles, formaldehyde, ...), with some of them of undeniable prebiotic interest (such as glycoaldehyde, the simplest sugar ($C_2H_4O_2$), as reported in Hollis et al. (2000)), has motivated intense investigations about the potential presence of interstellar glycine. However, even if Kuan et al. (2003) claimed to have detected such species in the hot molecular cores[22] Sgr B2(N-LMH), Orion KL, and W51 e1/e2 thanks to observations of 27 lines in 19 different spectral bands, no detection has been achieved and firmly confirmed yet. Actually, the approach followed by Kuan et al. (2003) as well as the assignments of the spectral footprints to the different glycine lines have been called into question by many authors, such as in Snyder et al. (2005). Indeed, they suggested other organic candidates to explain the observed spectral lines, and they came to the conclusion that key lines required to identify interstellar glycine have then not been found yet.

Furthermore, glycine has been found in various meteorites[23], such as claimed in Kwenvolden et al. (1970) where they analyzed fragments of Murchison (CC) meteorite, selected with caution: massive stones, with the minimum crack number [24] and therefore the least expected terrestrial contamination in the interior, and displaying the fainter exterior contamination and changes of terrestrial origin (terrestrial atmosphere leads to oxydation of material of extraterrestrial origin). Ion exchange chromatography, gas chromatography and mass spectrometer analysis suggest the presence of natural amino-acids (glycine, alanine, glutamic acid, valine and proline, the chiral ones displaying a small enantiomeric excess in the same direction as the homochirality problem, supporting therefore the exogeneous origin of amino acid). Moreover, nonprotein amino-acids (2-methylalanine or sarcosine, a N-methyl derived of glycine, β-alanine, ...) have also been found in those samples (Kwenvolden et al., 1970, 1971), as well as diamino-acids or other more exotic classes of amino-acids (Lawless et al., 1971; Meierhenrich et al., 2004; Koga and Naraoka, 2017). Besides the Murchinson meteorites, other carbonaceous chondrites' fragments have been studied and similar amino-acids species have been identified (e.g. see Cronin and Moore (1971); Lawless et al. (1971) for the analysis of the Murray meteorite, Glavin et al. (2006) for a study of Antarctic CM2 meteorites, ...).

Some clues are indicate that those amino acid compounds are likely from extra-terrestrial origin. Firstly, one can use the typical distribution of amino-acids retrieved on human hands. For instance, as serine is one of the most abundant amino-acids in finger-print, and is not firmly detected in Kwenvolden et al. (1970) (only the ion chromatography chromatogram suggests its presence, and in low abundance compared to the glycine abundance), they used this observation to support an extra-terrestrial origin, or, at least, an origin which is not directly linked to humans. Secondly, in Lawless (1973), they discussed the fact that the abundance of amino-acids decreases with increasing number of constituting atoms, which points towards an extra-terrestrial origin (chemistry at low densities and

---

[22]Early phase of massive star formation where the collapse of the molecular cloud has already started (class 0 object), leading to an increase of the temperature of the central part (> 100 K, sublimation temperature of most molecules trapped in the icy mantle of interstellar dust grains) and of the density ($> 10^7$ cm-3). As a result, such hot molecular cores are formed. The astrochemistry taking place in it is quite complex regarding the release of the molecular species from icy mantles.

[23]To ensure that we are all on the same plan, let us clarify the meaning of such small bodies. A meteorite is a chunk of interplanetary material, the most likely parent body being an asteroid encountering the Earth's orbit (or, potentially, a comet), which survives the atmospheric entry as well as the journey to the Earth's surface, and impacting it. In the context of the search of prebiotic molecular species, the carbonaceous chondrites (CCs) meteorites are of great interest regarding their abundance in C-compounds (up to 5%) and water (up to 20%).

[24]The impact of the extra-terrestrial body with the Earth's surface leads to cracking of the body, or even to its fragmentation. Actually, even if frictions lead to a decrease of the speed, a meteorite impacts the Earth with a high speed (on average 15 to 20 km/s, following the Lunar and Planetary Institute), braking its structure.

low temperature, via abiotic processes). In addition, one can also rely on isotopic ratios to support the exogeneous synthesis of the amino-acids contained in those chondrite meteorites. Actually, if an enrichment in the heavier isotopes (such as D, ^{15}N, ^{13}C) is observed in relation with cosmic standards (cosmic average D/H ratio: $\sim 10^{-5}$), it indicates a low temperature chemistry (isotopic fractionation due to the difference in zero-point energy, relevant at low temperatures). This is typical of a dense molecular phase of the ISM (or the colder region of the protostellar disk) and not found in terrestrial conditions. Another source of enrichment in isotopes ^{13}C, as well as in $^{17/18}$O in dense molecular clouds with respect to cosmic values is based on the self-shielding capabilities of abundant molecular species such as CO, the second most abundant molecule in the Universe. In fact, this second isotopic fractionation relies on a mass-independent process, based on the densities of the isotopologues of CO, namely $^{12}C^{16}O$ (the most abundant one) and $^{13}C^{17}O/^{13}C^{17}O/^{13}C^{16}O/^{12}C^{17}O/^{12}C^{18}O$ (less abundant since they are formed by, at least, a less abundant isotope), and therefore relies on their shelf-shielding capabilities (see subsection 1.3.3). The photodissociation of minor isotopologues being still efficient deeper in the cloud (their column densities being lower than the one of the major isotopologue, $^{12}C^{16}O$), the retrieval of isotopes ^{13}C, ^{17}O and ^{18}O is favored where the self-shielding of $^{12}C^{16}O$ is very efficient, preventing its dissociation in the interior of the dense molecular cloud. To go further, more complex considerations have to be taken into account when deeper studying the isotropic fractionation which can be measured in meteoritic samples (Aléon et al., 2010; Roueff et al., 2015; Colzi et al., 2020).

However, it is worth mentioning that one can not completely reject the possibility of a chemical alteration of the pristine material due to the abundance of water in such CCs meteorites (Le Guillou et al., 2014)[25] or via catalytic processes on clay minerals (Garvie and Buseck, 2007) in the parent body, as well as the thermal processing due to the journey through the Earth's atmosphere and impact with the Earth's surface. Knowing that thermal processing leads to some alteration of isotopic ratios compared to the pristine ones (from the formation of the molecular species of interest), the use of such isotopic ratio methods has to be implemented with caution: if amino-acids have been formed in astrophysical environments (and before the formation of the parent body of the future meteorite), captured in a parent body (asteroid, comet) and brought to the Earth thanks to the in-fall of a meteorite. If one assumes that it has not been destroyed through a chemical processing, its isotopic ratios will not show typical values reminiscent of a low temperature chemistry but will rather present an altered one, especially if it has faced significant thermal processing. The isotopic ratio values have therefore to be regarded with caution, analyzing those likely processing undergone by the molecular species in meteorites. However, the study of Busemann et al. (2006) reached the conclusion that meteorites seem to be able to preserve pristine isotopic ratios of organic material, sometimes exceeding the isotopic anomalies found in interplanetary dust particles (pristine dust collected in the Earth's stratosphere, the most likely parent bodies being comets). Therefore, the thermal processing seems not strong enough to lead to a sharp attenuation of the isotopic anomalies, which can consequently be comfortably used to support the exogeneous synthesis of amino acids in typically cold environments (molecular clouds or outer part of the protoplanetary disk) (Busemann et al., 2006).

Moreover, the Hayabusa 2 mission, successfully launched in December 2014 by the JAXA space agency (Japan Aerospace Exploration Agency (JAXA)), has yielded quite promising results. Actually, this mission was dedicated to the study (orbiter, lander, rovers and *in situ* sampling) of asteroid (162173) Ryugu, a C type asteroid[26]. This type represents the most pristine class of

---

[25]However, concerning the case of Murchison meteorite, the water is depleted in deuterium compared to the detected amino acids. It therefore points to the idea of a synthesis before the formation of the parent body or, at least, not through a water-assisted synthesis on the parent body (Lerner et al., 1995, 1997).

[26]Regarding the high content in organic matter and the top spinning shape of Ryugu, some authors are claiming that

objects from the formation of the solar system, and is therefore of great interest in the context of the study of the primitive composition of our solar system. This was the second space mission that returned samples on Earth from *in situ* visit of an asteroid, with more than 5 g collected. These samples were composed of surface and sub-surface grains[27]. Their subsequent analysis highlighted the rubble pile structure of this object (likely formed through fragmentation of the parent body due to a given violent collision and re-agglomeration due to gravity) as well as its high porosity (footprint of the past presence of ice, as discussed in Nakamura et al. (2023), arguably indicating a parent body formation in the outer part of the nascent solar system). Regarding its mineralogy, it has been found to be highly consistent with CC meteorites (as Murchison Meteorite), especially with the Ivuna-type carbonaceous (CI) chondrite (Nakamura et al., 2023). This is therefore in favour to the hypothesis of C-type asteroids as parent bodies of such carbonaceous undifferentiated meteorites. The chemical composition is principally reminiscent of a cold formation medium (Nakamura et al., 2023), and presents some phyllosilicates and carbonates, formed by aqueous alteration reactions at low temperatures. Concerning more specifically its organic content, it displays a quite high interest in the context of prebiotic chemistry. Indeed, as reported in Naraoka et al. (2023), among the rich variety of organic compounds, glycine and other natural and unnatural amino acids have been detected in the collected samples. However, as highlighted by Potiszil et al. (2023), aqueous alteration is expected to have an impact on the amino acids content of a given body, principally through Strecker synthesis. It however not implies that no amino acids where present before the collapse of the molecular cloud, or during the transformation from the primordial solar nebula to the protoplanetary disk. This is still a possibility, and the considerations in Potiszil et al. (2023) only mean that there is an expected increase of amino acids' content when a (parent) body experiences an aqueous alteration.

Beside these important identifications in asteroidal and meteoritic samples analyzed on Earth, another promising result comes from the Rosetta/Philae space mission[28]. Actually, the analysis through ROSINA[29] mass spectrometer measurements of the coma of Comet 67P/Churyumov-Gerasimenko allowed for the unambiguous detection of volatile glycine (with a distributed density profile at a distance of 14 to 26 km from the cometary nucleus) accompanied by methylamine and ethylamine (possible precursor molecules), as reported in Altwegg et al. (2016). It confirms results from the Stardust mission[30] for comet Wild-2 (data from 2004) and the analyses of the cloud of gas and dust surrounding the icy nucleus of that cometary body. In fact, even if those analyses have been firmly attributed to glycine of extra-terrestrial origin (and not a contamination from terrestrial molecules) thanks to a rigorous analysis of the isotopic ratio (Elsila et al., 2009), they were ques-

---

object is more rigorously an death comet that progressively lost its icy components, as discussed in Miura et al. (2022). In fact, the distinction between a dead cometary nucleus and an asteroid is sometime rather difficult to establish. Such alternative origin hypothesis for Ryugu can be defined by the Comet Asteroid Transition objects (CATs).

[27]The sub-surface samples have been collected after impact on the asteroid surface, allowing a cratering process and the unveiling of part of the asteroid material not recently exposed to space-weathering and interplanetary conditions.

[28]Rosetta mission, an ESA space probe, lasted for about 12.5 years (2004-2016). This spacecraft was equipped with the Philiae lander module. The main goal of the mission was to perform a detailed study of comet 67P/Churyumov-Gerasimenko, even if interesting fly-byes have been accomplished (Earth, Mars and 2 asteroids) during the $\sim$ 7.9 billions of km of journey towards the cometary target. The probe started observing Comet 67P/Churyumov-Gerasimenko during the approach of the latter, on the 20th of January 2014, and lasted until the end of September 2016. This was the first spacecraft aimed at orbiting and landing (November 12, 2014) a probe on a comet, which is quite challenging regarding the weak and unhomogeneous gravity at the surface of such bodies. Unfortunately, the landing of Philae failed. Despite the non-possibility of landing, interesting information could still be collected from this space mission. For more details, I refer the interested reader to the ESA's webpage (ESA).

[29]Rosetta Orbiter Spectrometer for Ion and Neutral Analysis, on board of the Rosetta probe.

[30]A completed NASA space mission (fly-by spacecraft) started in 1999 and was aimed at collecting interplanetary dust particles and drop them into the terrestrial atmosphere for their detailed analysis. For more details, the interested reader is referred to the (NASA) website.
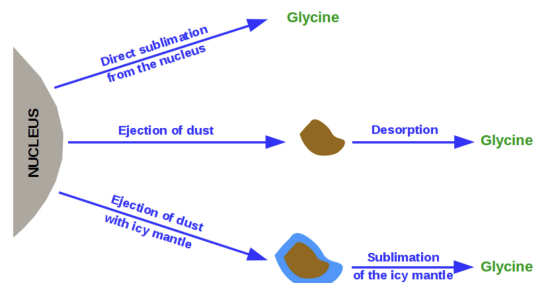
Figure 1.9: Three cases of glycine release in the coma of Comet 67P/Churyumov-Gerasimenko. Panel a: glycine sublimated directly and only from the nucleus of the comet. Panel b: firstly, dust particles are ejected from the comet, including solid-state glycine (adsorbed glycine on grain surface). In a second time, this adsorbed glycine undergoes a desorption process, leading to its ejection into the gas phase. Panel c: firstly, dust with icy mantle is ejected from the nucleus, where glycine is embedded in ice. Secondly, through diffusion in the ice and sublimation of the ice mantle, cometary glycine is released in the coma, from De Becker (2021-2022), inspired from Hadraoui et al. (2019).

tioned (see for instance Sandford et al. (2006)) because of possible chemical transformations during the collection process of samples (the detected glycine molecules were possibly formed during that process, with isotopes initially present in the comet). The results from the Rosetta/Philae mission (Altwegg et al., 2016) are therefore crucial to confirm the unambiguous likely presence of glycine of extra-terrestrial and non-anthropogenic origin in the coma of comets. The question that still needs to be answered now concerns the exact location of the synthesis of such extra-terrestrial glycine molecules. *Are they formed in the initial molecular cloud, during the formation of the solar system in a cold region of the protoplanetary disk, due to a modification via the interaction with stellar outflow, or via processing within the parent-body (as discussed before for the meteoritic samples)?* Moreover, *by which mechanism has the extra-terrestrial glycine detected in the coma of Comet 67P/Churyumov-Gerasimenko been released?* In that context, Hadraoui et al. (2019) discussed three different scenarios about the way this glycine has been released in the cometary atmosphere, as illustrated in Figure 1.9.

According to their numerical model of the distribution of glycine in the coma of Comet 67P/Churyumov-Gerasimenko, the third scenario, in which the detected glycine was embedded in a water ice mantle around the dust grains, seems to well match the observed distribution (Hadraoui et al., 2019). Further investigations are needed to better constrain the model and therefore be able to conclude on this plausible interpretation of glycine release in a cometary atmosphere with more confidence.

Henceforth, in order to deeply understand in which conditions the detected glycine in cometary coma, and meteoritic & asteroidal samples have been synthesized, and to determine if a likely exogenous formation pathway before the formation of their respective parent body can be envisaged, a detailed study of the potential glycine formation routes in the ISM has to be undertaken.

In the scientific literature, many different formation pathways have been suggested and investigated through theoretical studies or laboratory simulations. A complete discussion of all of them would quickly become a simple enumeration of all proposed pathways. Therefore, a rigorous upstream bibliographic investigation must be undertaken, and we will restrict our discussions to glycine formations routes that seem the most promising based on the available literature investigating it. For instance, both Bernstein et al. (2002); Munoz Caro et al. (2002) carried out empirical simulations of the amino

acids formation through ultraviolet photolyses of analogue of icy mantles containing simple abundant interstellar species (likely precursors, such as methanol[31], HCN, NH_3, CO and CO_2, ...).

Concerning the generally suggested abiotic mechanisms towards interstellar glycine formation, they are generally divided into two main categories in the scientific literature: (i) mechanisms involving reactions activated by water ice mantle of interstellar dust grains, and (ii) mechanisms involving gas phase processes. In other words, those formations routes are generally studied in a specific phase, and the interplay between them is generally not accounted for.

Starting with studies suggesting mechanisms invoking **chemical transformations in the icy mantle** of interstellar dust grains, one can firstly mention a **Strecker-like mechanism**. As we have seen in subsection 1.3.4, beside the catalytic properties of their surface (leading to the formation of water, ammonia and many highly hydrogenated molecular species), interstellar dust grains can harbor an icy mantle surrounding their refractory core in dense molecular clouds (or close to the middle plane of a protoplanetary disk at a distance allowing such icy mantles, this distance being generally defined as the snow line). Indeed, due to the high abundance of dust grains, and the low temperature prevailing in such regions, volatile species can freeze out (accretion and long residence time being favoured, see Table 1.7 for the dependency on n_d and T_d) onto the surface, and thus leading to the formation of an icy mantle around the core of the grain.

Furthermore, as we know from organic chemistry, a Strecker reaction is defined as an abiotic pathway of amino acid synthesis implying the reaction of an aldehyde/ketone with an amine and a CN-bearing specie in water (under acidic conditions). However, the difference with this well-known standard organic chemistry is found in the environment of reaction: in the ISM, no aqueous solvent can be considered, but one can envisage a Strecker-like mechanism activated by solid water matrices around the interstellar grains (rather than an activation under acidic conditions). For the case of glycine formation, one considers the most simple precursors to this mechanism: formaldehyde, ammonia, hydrogen cyanide and water, embedded in the icy mantle. Depending on the relative abundance of NH_3 and HCN, the mechanism starts with the nucleophilic attack by the ammonia or by the cyanide molecule on the formaldehyde, leading to routes a (equations 1.7 to 1.9) and b (equations 1.10 to 1.12) respectively.

Formation route a

$$H_2C{=}O + NH_3 \rightleftharpoons NH_2CH_2OH \qquad (1.7)$$

$$NH_2CH_2OH \rightleftharpoons HN{=}CH_2 + H_2O$$

$$HN{=}CH_2 + HCN \rightleftharpoons H_2NCH_2CN \qquad (1.8)$$

$$H_2NCH_2CN + H_2O \rightleftharpoons H_2NCH_2COOH + NH_3 \qquad (1.9)$$

Formation route b

$$H_2C{=}O + HCN \rightleftharpoons H_2C(OH)CN \qquad (1.10)$$

$$H_2C(OH)CN + NH_3 \overset{b.1}{\rightleftharpoons} NH_2CH_2OH \qquad (1.11)$$
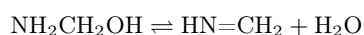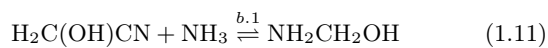
then eq. 1.7 (second step) to 1.9

$$or \quad \overset{b.2}{\rightleftharpoons} H_2NCH_2CN \qquad (1.12)$$
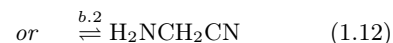
then eq. 1.9

Formation route a is based on the classical scheme of the Strecker synthesis. Indeed, ammonia seems to be the best nucleophile compared to hydrogen cyanide, based on the electronegativity of nitrogen (3.4) with respect to carbon (2.2). If we describe briefly this first scheme, equation 1.7 is in fact a condensation of the formaldehyde with the ammonia, leading to the formation of an imine molecule ($HN{=}CH_2$). It is followed by the formation of a α-aminonitrile (H_2NCH_2CN) via a nucleophilic

---

[31]Which is decomposed into formaldehyde by UV photolysis (Bernstein et al., 2002).

attack of the cyanide on the formed imine (equation 1.8), itself followed by the hydrolysis of this α-aminonitrile (equation 1.9) to form the final glycine (H_2NCH_2COOH).

In a context where the abundance of ammonia is negligible compared to hydrogen cyanide, and thanks to isomerization of HCN/HNC (Woon, 2000) as it will be further discussed in Chapter 3, *formation route b* may become considerable. In such a mechanism, the starting point is a nucleophilic attack of the cyanide on the formaldehyde (equation 1.10), forming a cyanohydrin ($H_2C(OH)CN$). This step being completed, the nucleophilic attack of this glyconitrile by ammonia and the departure of a leaving group lead to two sub-routes: *sub-route b.1* and *sub-route b.2*. Indeed, if this reaction happens in a terrestrial lab, in water and at room temperature, one can rely on the pKa (acidity constant) value of the corresponding acid of the likely leaving group (here, -OH and -CN) to determine which leaving group is the best (lowest pKa, therefore -CN in this case, corresponding therefore to the sub-route b.1). However, such values are tabulated in water at room temperature. Since conditions are drastically different in a molecular cloud (cryogenic, 10-20 K, no liquid water), the acidity constants have to be reviewed. Indeed, as we have seen in subsection 1.3.2, equilibrium constants are temperature-dependant. We also have to keep in mind that such ices display different intermolecular interactions than in an aqueous solvent, where the well-known solvation process is a key point. One can therefore not put aside the possibility of the -OH leaving group for the nucleophilic attack of NH_3 (sub-route b.2). After the respective nucleophilic attack, both sub-routes b.1 and b.2 return to equations from formation route a, discussed just before. It is also good to notice that after step 1.10, the simultaneous presence of water and cyanohydrin will lead to a by-product, a hydroxy acid ($H_2C(OH)COOH$), by hydrolysis of the cyano group of the cyanohydrin. In other words, in absence of ammonia, formation route b will lead to the formation of hydroxy acid rather than amino-acid. It demonstrates the prime importance of both ammonia and hydrogen cyanine for this Stecker-like mechanism to lead to glycine formation. All these considerations about routes a and b gathered in Figure 1.10.

At first glance, this Strecker-type reaction seems a very promising candidate for the glycine formation in the ISM. Indeed, interstellar $H_2C=O$ (Snyder and Buhl, 1969), NH_3 (Cheung et al., 1968) and HCN (Ziurys and Turner, 1986) have been identified in the ISM, those being the most simple precursors starting from the carbonyle compound. Moreover, the amino acetonitrile (H_2NCH_2CN) intermediate compound has been firmly detected in molecular clouds, as reported in Belloche et al. (2008). Therefore, even if glycine has not yet been identified in the ISM, a simple hydrolysis of H_2NCH_2CN would lead to a glycine molecule. It is therefore justified to expect its presence in the ISM, especially in icy mantles, where the encounter with a water molecule is highly likely. Let us note that this suggests the presence of H_2NCH_2CN in such ices, explaining therefore why most of the authors are simulating this whole Strecker-like-synthesis in water-ice matrices. It is however worth keeping in mind the crucial interaction between gas and solid-phase, and we can not exclude that a part of the mechanism takes place in gas-phase. Furthermore, as mentioned in subsection 1.3.4, some catalytic effects can be attributed to the water molecules present in water ice mantles (e.g Woon (2002a); Courmier et al. (2005); Koch et al. (2007, 2008) where such catalytic effects are studied for different precursors/intermediates of the Strecker-like mechanism). In Rimola et al. (2010), they report a quantum kinetic and thermodynamic study (at DFT B3LYP level) of the Strecker-like mechanism via the classical route a (equations 1.7 to 1.9). They adopted a cluster approach consisting in a H_2O cluster model made of 18 water molecules simulating the ice surface. This work highlighted that, if all reaction steps occur at the modelled water ice surface, these are all thermodynamically favourable (negative variation in Gibbs free energy). Moreover, all reactions steps are catalyzed (decrease of the activation energy barrier compared to pure gas-phase reaction) by four water molecules forming the icy matrix, as one can visualize for instance in Figure 1.11 for the condensation reaction of the formaldehyde with the ammonia (equation 1.7). Those four H_2O molecules allow the proton transfers ($\sim H^+$ mentioned in Figure 1.10) to be kinetically more efficient by acting as proton donors and
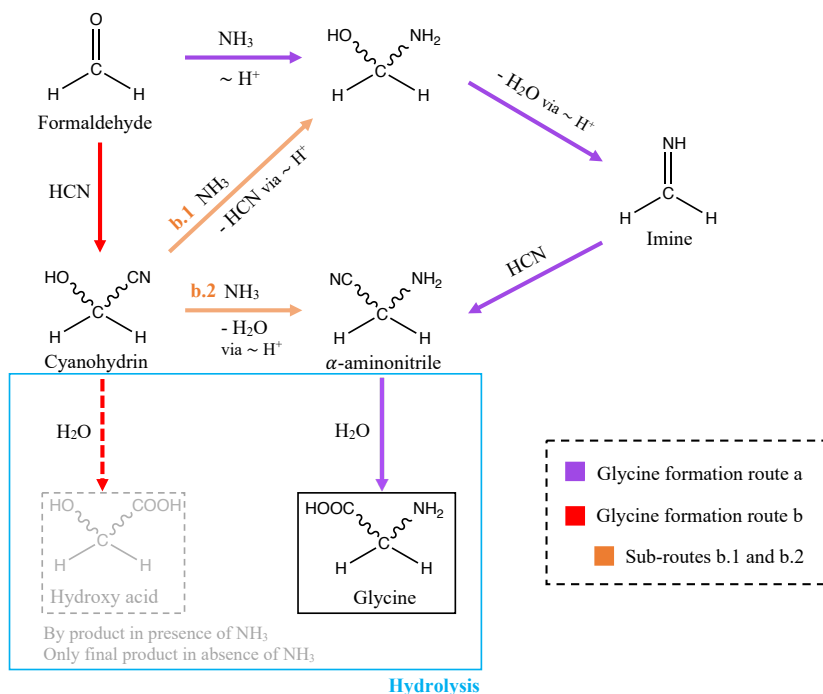
Figure 1.10: Overview of the two glycine formation pathways via Strecker-like mechanism. Purple arrows stand for formation route a; red and orange arrows represent route b, the orange one indicating sub-routes b.1 and b.2. In absence of ammonia, only the reaction pathway represented in red will be undergone, with no amino acid formation. NB: $\sim H^+$ corresponds to a prototropy, an intramolecular rearrangement implying a displacement of an hydrogen atom. Inspired from De Becker (2021-2022).

acceptors simultaneously. This is called a *proton-relay* mechanism. Rimola et al. (2010) also studied the reaction steps in ice cavities, simulated assuming a dielectric continuum. The E_as are significantly lower than those occurring at the ice surface, simulated by the water cluster discussed here-above.

However, this candidate is not as promising as it seems. The main flaw of this Strecker-like mechanism lies actually in its kinetics. Indeed, even if the catalytic role played by the water ice lowers the activation barriers, these are still too high to be efficient at the typical temperatures of molecular clouds, especially for the hydrolysis of the amino acetonitrile to form the glycine molecule, namely the last step of the mechanism. Moreover, the reaction barrier to form the imine from H_2NCH_2OH seems to be quite high for such cryogenic temperatures. However, as we will see when addressing the Woon's mechanism, the imine can be easily formed through a simple radical pathway. We will discuss it in details later in this section.

Remark: It is however good to note that Gibbs free energy and energy barrier values have not only been calculated for cryogenic temperatures (10 K), but also for 100 and 200 K, the range of temperatures corresponding to hot cores (Rimola et al., 2010). The results indicate that an increase in temperature disfavors all the reactions considered in this mechanism by slightly increasing the energy barriers (by a value up to 2 kcal.mol^{-1}). This could be attributed to unfavourable entropic conditions (Rimola et al., 2010), which can be, for instance, explained by the fact that the proton-relay mechanism requires a specific orientation of the molecules involved in the transition states. An increase in temperature will disfavour it.
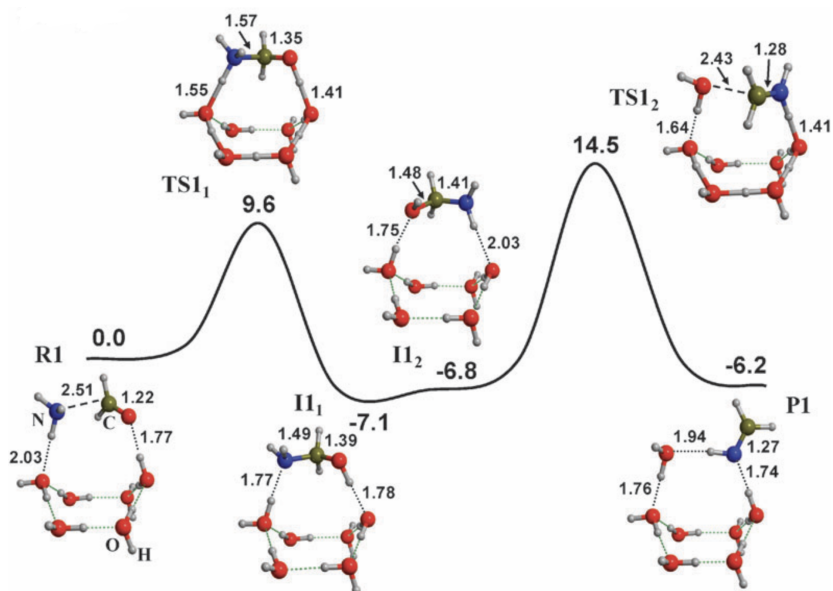
Figure 1.11: ZPE-corrected B3LYP/6-31+G(d,p) potential energy profile for the first reaction of route a, described by equation 1.7 (relative energy values quantifies the energy with respect to the energy of the reactants (R1), in kcal.mol^{-1}). Note that the bond distances are in Å, and that only the optimized part of the H_2O-ice model is shown for the sake of clarity, from Rimola et al. (2010). Similar diagram corresponding to the two other reactions steps towards glycine (equations 1.8 and 1.9) are presented in the referred paper.

Based on some conclusions from Rimola et al. (2010), Kayanuma et al. (2017) investigated an alternative reaction to the equation 1.9. This implies a **Büchener-Bergs** reaction, defined as a reaction between the amino acetonitrile (H_2NCH_2CN) and a carbon dioxyde (CO_2) molecule, leading to the formation of a hydratoin (2,4-imidazolidinedione, identified in meteorites but not in the ISM). The hydrolysis of this latter then leads to glycine formation. Those reactions are also considered at ice surface, water molecules playing a similar catalytic role than discussed in Rimola et al. (2010). However, even if those reactions are both thermodynamically favourable, the highest energy barrier (hydrolysis) is still too high (110 kJ.mol^{-1}) to occur at cryogenic temperatures, typical of molecular clouds. Nevertheless, this is possible if an external energy source can be invoked, such as heating by radioactive nuclei, by shock during the planet formation stage or heating of the meteoric parent body (Kayanuma et al., 2017).

For the above proposed mechanisms, the external processing of the water ice has been neglected. However, as discussed in the aforementioned study performed by Bernstein et al. (2002), observations indicate a very interesting chemistry occurring in interstellar icy mantle analogues (H_2O-ice containing small amounts of CH_3OH, NH_3 and HCN) at 15 K and 10^{-8} torr under UV photolysis conditions. They detected several amino acids precursors such as N-formyl glycine, which yields to glycine after hydrolysis. They concluded that the UV-photons interactions with the icy mantle of interstellar dust grains could have played a key role in the origin of glycine in meteoritic samples (Bernstein et al., 2002). Furthermore, although the densest molecular clouds are mostly impermeable to interstellar UV radiations due to self-shielding mechanisms, UV-photons can be induced by CR, as explained in subsection 1.3.3, Table 1.5 and the related discussion. Such UV-photon incidence induces generally homolytic dissociations of chemical bonds. In the context of UV radiation of interstellar ices, the impacted chemical bonds belong to surface species, which leads to the formation of radicals. Regarding

the generally considered composition of interstellar icy mantles, the most abundant radicals should come from the photolysis of water molecules, the latter leading to H and OH radicals. Higher energy UV photons (if present, which is not so likely[32]) may lead to cations production. Moreover, CRs are also efficient cations suppliers, besides their homolytic cleavage capability. The H_3O^+/H^+ ions should therefore be abundant. As a result, taking the effect of CR induced UV-photons and CR themselves (significant energy input in the icy mantles) into account, the surface chemistry of interstellar ices (and potentially the subsurface chemistry, where surface species can be brought through diffusion effects, or simply by adsorption of a new layer on top of it) is activated by **protonated and radical** species. Indeed, as discussed for instance in Walch et al. (2001), the replacement of the formaldehyde in equation 1.7 by the corresponding protonated specie CH_2OH^+ *activates* the reaction (as usually observed in organic chemistry experiments via acidic H^+ activation of carbonyle groups, for instance). This activation actually decrease the LUMO of the carbonyl group-bearing species, leading to an easier nucleophilic attack. The product of this first step is therefore an iminium cation, or, in other words, an activated imine. The subsequent substitution of the imine in equation 1.8 by an iminium cation, studied in Walch and Bakes (2001), and the izomerization of HCN/HNC then leads to $NH_2CH_2CNH^+$, itself hydrolysed in glycine. This proton-activated Strecker-type mechanism (protonated version of route a) displays barrierless and low barrier steps, which is therefore plausibly achieved in the cold conditions of dense interstellar clouds.

This external ice processing has also been studied in Woon (2002b) for instance, where the author based his quantum chemical simulations on Bernstein et al. (2002)'s observations in order to evaluate the viability of various glycine formation routes in UV irradiated dilute H_2O-ice containing CH_3OH and HCN (no ammonia compared to the Bernstein's experiment). Actually, as it has been highlighted later in a subsequent study performed by Elsila et al. (2007), the major glycine formation route in irradiated ices is achieved in absence of ammonia, even if minor pathways involve it. Alternatively to Walch and Bakes (2001), Woon (2002b) investigated radical pathways rather than protonated ones. He concluded that the recombination of COOH and H_2CNH_2 radicals directly leads to glycine (alanine and serine being possibly formed via additional steps, therefore explaining Bernstein's results). The complete corresponding glycine formation pathway is described in Figure 1.12. As we can see on this figure, the H_2CNH_2 radical formation is passing by an imine. The Woon mechanism displays therefore a clear interesting interconnection with the classical Strecker-like route.

Woon (2002b) also highlighted the fact that much more energy is available in irradiated ices than in icy mantles completely isolated from any UV radiations. Indeed, photolysis products (generally radicals) seem to display a significant excess of internal energy (distributed between rovibrational energy levels and translational kinetic energy), which can enable the crossing of the activation barrier of potential subsequent reactions (this is also valid for cationic species from CR interaction). In addition, the recombination of radicals (barrierless) releases energy. In ice at a cryogenic temperature of 10-20 K, typical of dense molecular clouds, most radicals (except H) are however not able to diffuse in the ice to react with another radical. Heavier radicals therefore only react with H and nearby radicals, which drastically limits the number of potential reaction partners.

The viability of Woon's mechanism has been confirmed through the empirical and theoretical study performed by Holtom et al. (2005), in which they showed that the CR bombardment of interstellar ice analogues containing CO_2/NH_2CH_3 leads to the synthesis of glycine, as well as its isomer $CH_3NHCOOH$. On the other hand, Elsila et al. (2007) performed isotopic labelling experiments on

---

[32]Generally, the high energy UV-photons are absorbed by the HIM and WIM interstellar phase, see Table 1.3. Moreover, the UV-photon induced by CR reactions are most likely of moderate energy, regarding their collisional production mechanism (see discussion related to Table 1.5.

a) COOH radical formation

b) H₂C-NH₂ radical formation

c) COOH & H₂C-NH₂ radical recombination (barrierless)
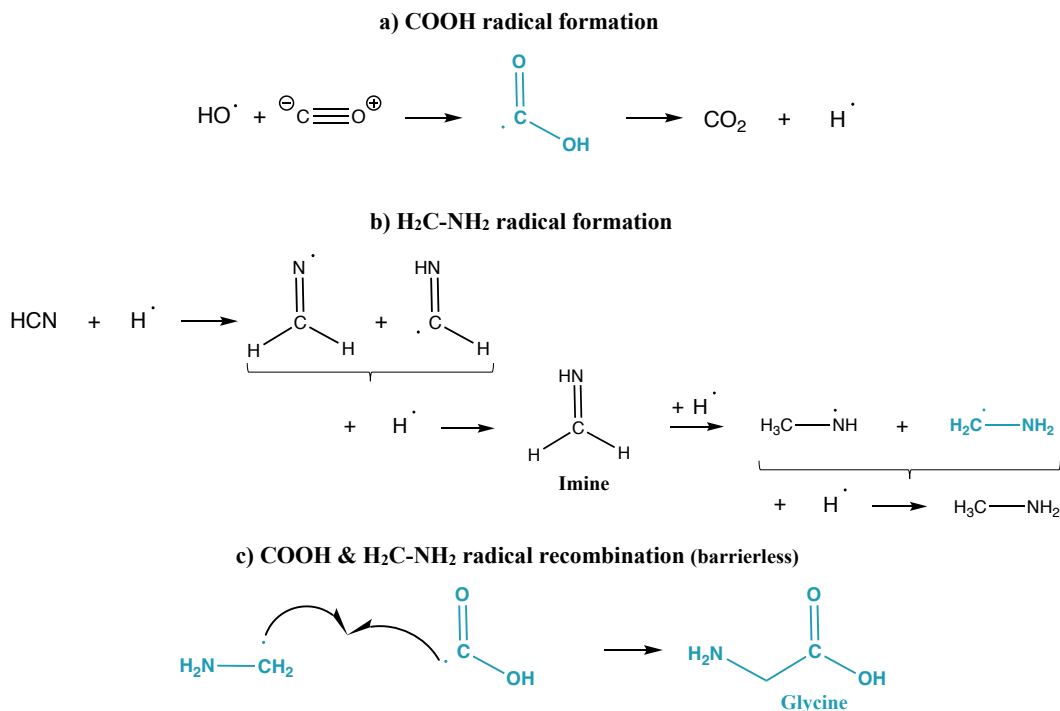
Figure 1.12: Radical glycine formation pathway investigated in Woon (2002b). Note: all radical recombinations are barrierless.

irradiated interstellar ice in order to extend the work of Bernstein et al. (2002) and be able to trace the origin of the constituent atoms in the observed products. In that context, they investigated two main formation routes proposed in the scientific literature and discussed above: a Strecker-type mechanism and a radical-radical pathway such as proposed in Woon (2002b). Their results were consistent with Woon's mechanism concerning the origin of the nitrogen and the central carbon (α-carbon, as illustrated in Figure 1.8) of the glycine, while the origin of the carbon of the carboxylic acid group does not match with this formation route. Indeed, the main formation pathway invokes HCN as the supplier for the three atoms constituting the glycine backbone: nitrogen, α-carbon and acidic carbon from the COOH group. Minor glycine synthesis routes imply NH_3 and/or CH_3OH as providers of nitrogen and α-carbon respectively. They therefore conclude that a modified Woon's radical-radical mechanism could match their results. This modified mechanism would imply the formation of the acidic carbon through a nitrile precursor (amino acetonitrile, reminiscent of the last step of the Strecker-type synthesis) rather than a carboxylic acid one (Elsila et al., 2007).

In a more recent work, Rimola et al. (2012) investigated another mechanism also invoking low energy barrier and barrierless reactions but, in this case, taking advantage of both the proton and radical activations of the kinetic of chemical processes. In that context, H_2O being the most abundant molecule in the icy mantle of interstellar grains, Rimola et al. (2012) used the $OH\bullet/H_3O^+$ ion-radical pair as defects in a 8-H_2O cluster. Compared to the non-cation-catalyzed mechanisms discussed beforehand (Rimola et al., 2010; Kayanuma et al., 2017) where water molecules play a proton relay role, in this case the surface H_3O^+ cations and $OH\bullet$ radicals further favour the reaction through more efficient proton-transfer mechanisms, as illustrated for example in Figure 1.13.
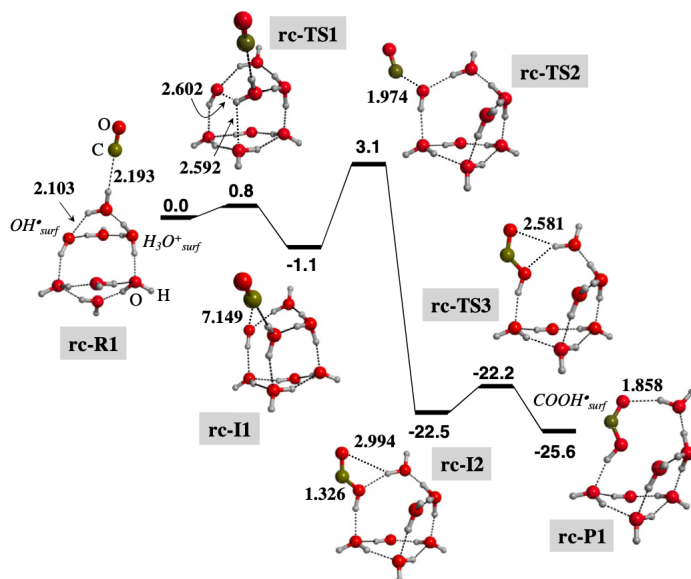
Figure 1.13: "Electronic potential energy profile for the formation of the COOH radical via coupling of the OH radical surface defect with an incoming CO molecule on the radical cationic (rc) cluster. The zero energy reference stands for for rc-R1", from Rimola et al. (2012).

The complete reaction pathway studied in Rimola et al. (2012) is described in Figure 1.14. The presence of $H_2C=NH_2^+$ can be explained by the formation of a $H_2C=NH$ molecule through H• on HCN, as invoked by Woon (2002b) and illustrated in Figure 1.12, followed by a proton transfer from the H_3O^+ ionic defect of the water-ice surface.

All reactions are thermodynamically favourable. It is also worth mentioning that the rate constants for each reaction step have been calculated at different temperatures. The results seem to indicate that those reactions are kinetically feasible on astronomical time-scale at a temperature range of 100-200 K, typical of hot cores or shocked regions rather than quiet cold dense molecular clouds.
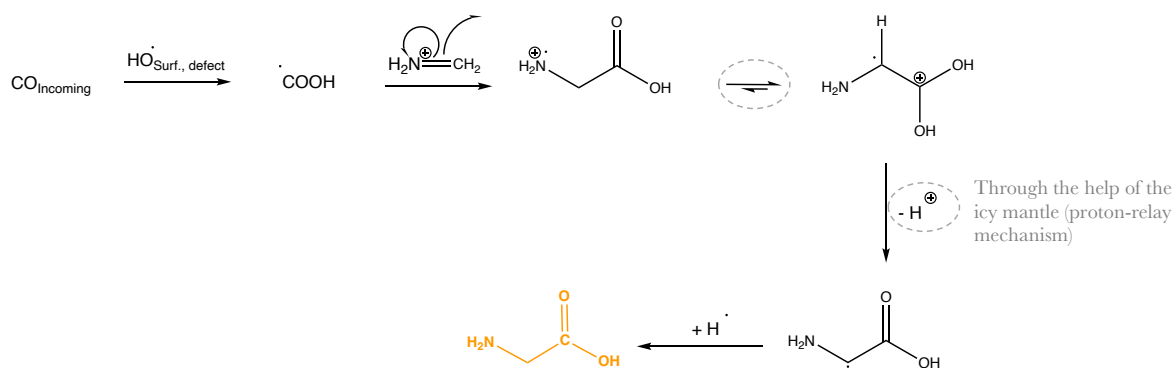
Figure 1.14: Overview of the glycine formation pathway (only the most efficient studied pathway is shown) studied in Rimola et al. (2012). It is interesting to note that if the last H• addition is replaced by other radical species (such as $H_3C•$), this simple mechanism can lead to the formation of other amino acids (serine if $H_3C•$).

The here-above discussed mechanisms represent only a part of the numerous pathways that have already been proposed in the literature in the context of the solid-phase astrochemistry of interstellar molecular clouds, and several alternatives may exist. In that context, Garrod (2013) built a astrochemical network to simulate coupled gas-phase, grain-surface and bulk-ice chemistry in hot cores. This chemical network[33] is based on previous networks (Garrod et al., 2008, itself extended from Garrod and Herbst (2006), and Belloche et al. (2009) where Garrod is the second author) and has been further extended thanks to the addition of various relevant reactions (formations and destruction processes)[34] implying glycine and related species including its amino aldehyde glycinal (H_2NCH_2CHO), propionic acid (CH_3CH_2COOH) and propanal/propanoic aldehyde (CH_3CH_2CHO), as well as their precursors. Most of these additional mechanisms mostly follow radical-radical synthesis pathways (where radicals meet through thermal diffusion), including, for instance, the formation route proposed in Woon (2002b). A gas-phase glycine synthesis route (proposed in Blagojevic et al. (2003)) has also been included in the network, but has shown insignificant contribution to the glycine formation. In relation to this new chemical network accounting for glycine, the author coded a new three-phase (gas-phase, grain-surface and bulk-ice chemistry) astrochemical kinetic model, MAGICKAL (which is unfortunately not open source[35]). This model has been applied on warm-up (8 to 400 K) hot-core models starting from a free-fall collapse of a molecular cloud. The results highlighted different interesting points. We will come back to them in due time, but the most important conclusions are summarized below:

- Four final radical-radical process leading to glycine have been implemented in the network (see equations 1.13 - 1.16) , and it is found that glycine is formed within and upon icy mantles of dust grain through the 3 last ones of these radical-radical recombinations, between ~ 40 K [36] and 120 K. Regarding the final total contribution in the gas-phase after sublimation (at the evaporation temperature), none of those three formation routes showed a strong dominance.

$$H\bullet + \bullet NHCH_2COOH \rightleftharpoons H_2NCH_2COOH \tag{1.13}$$

$$\bullet NH_2 + \bullet CH_2COOH \rightleftharpoons H_2NCH_2COOH \tag{1.14}$$

$$NH_2CH_2 \bullet + \bullet COOH \rightleftharpoons H_2NCH_2COOH \tag{1.15}$$

$$NH_2CH_2CO \bullet + \bullet OH \rightleftharpoons H_2NCH_2COOH \tag{1.16}$$
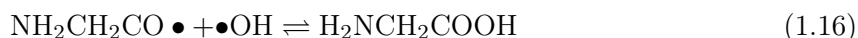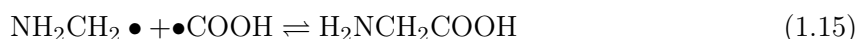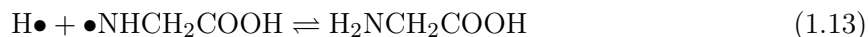
- Glycine displays a rather high evaporation temperature, ~ 200K [37];

---

[33]A chemical network in astrochemistry can be defined as various sets of formation and destruction routes of various interconnected chemical species. In order to kinetically simulate the astrochemistry at work in a given astrophysical environment, astrochemical models have been built, based on such chemical networks. In that context, one includes all parameters characterizing the rate constant of the reaction, given its reaction type (as we have seen in Tables 1.5 and 1.7, the parameter defining the kinetic constant depends on the reaction type).

[34]Examples of the relevant added reactions can be found in Table 2 and 3 of Garrod (2013).

[35]https://garrodgroup.as.virginia.edu/resources

[36]This lower temperature limit is above the characteristic temperature of dark molecular clouds, the environment we aim to study. However, the encounter between reactants within the icy-mantle is here accounted through thermal diffusion. To better understand the chemistry in such icy matrix at cryogenic temperature, typical of dense molecular clouds, a statistical approach is more suitable. We will discuss further this point latter on.

[37]A subsequent work (Ioppolo et al., 2021) reported a value of the same order of magnitude, 245K. The difference can be attributed to the pressure considered for the reaction medium for instance.

- Depending on the temperature, and on the warming time-scale of the physical model, one could still find slight differences in the degree of influence of each final glycine formation route. In the context of this outcome from Garrod (2013), Sato et al. (2018) discussed glycine formation pathways ending by 1.14, 1.15 and 1.16 in more details (quantum investigation), in the respective range of temperature where their contribution dominates (for the model warming up at intermediate speed in Garrod (2013)). Those three complete formation routes are represented in Figure 1.15. The results show that the highest activation barrier amounts to 7.75 kJ/mol for both routes 1a and 1b (the concerned reaction step being in their common path), against 33.41 kJ/mol for the route 2.

Before addressing the gas-phase glycine astrochemistry, one can also mention the important outcomes from the very recent laboratory and kinetic modelling study performed by Ioppolo et al. (2021) (Garrod being in the team of authors, allowing the support of their three-phase astrochemical model MAGICKAL). In contrast to the previous considerations, Ioppolo et al. (2021) considered the glycine formation in dark cloud accounting for a non-diffusive mechanism within the icy matrices, in a much earlier star-formation stage than previously assumed (see the bottom of Figure 1.16). Indeed, as we have seen, many authors investigated glycine formation at higher temperature conditions, such as for instance in Garrod (2013) where the glycine formation has been simulated in a hot core (collapsing molecular cloud, with a temperature increasing from 8 to 400K).

The reaction scheme studied in Ioppolo et al. (2021), which can be visualized in Figure 1.16, is based on the results from their own experimental work, the study performed in Qasim et al. (2020) and the review made by Linnartz et al. (2015). They demonstrate that glycine can be formed in such dense cloud physical conditions (at a temperature around 15 K) through a primeval formation pathway that does not require any energetic irradiation such as stellar UV photons, CR and CR induced UV photons. Astrochemical models obtained with MAGICKAL (were the chemical network from Garrod (2013) has been extended) and microscopic kinetic Monte Carlo simulations (keeping track of the position of the adsorbed species [38]) have supported this result. Actually, as we can see in Figure 1.16, the reaction network considered is composed of atoms as well as of radicals. However, Ioppolo et al. (2021) have argued that the radicals of interest can indeed be formed in another way. For instance, during the formation of a water ice layer, atom addition leads to the formation of OH radicals. Then, they assumed that all radicals are formed through H- and OH- induced addition/abstraction via stable species deposited at the surface of the ice.

Focusing now on formation pathways involving **gas phase processes**, one can basically consider all reactions presented before, but this time in gas phase[39]. The energetic barrier should be impacted since one can no longer consider any catalytic or stabilizing effect. Indeed, such energetic barriers are generally inferred through quantum chemical calculation, via the Transition State (TS) theory. In computations aimed at modelling solid-phase chemistry, several techniques can be used to simulate the ice-effect on the approach of the reaction partners, such as an H_2O matrix as in Rimola et al. (2010, 2012) for reactions occurring at the surface, or the consideration of a dielectric constant

---

[38]This could be of great interest in dark cloud conditions since the mobility of the chemical species, except for the hydrogen, is inhibited. The astrochemistry taking place there is therefore ruled by the probability that two possible reactant partners lie close to each other rather than by a diffusive mechanism. Note that this non-diffusive statistical mechanism has been taken into account in the astrochemical model code through the application of the non-diffusive treatment introduced in Garrod and Pauly (2011) and applied to all reactions

[39]It would be relevant to bring some adaptations to the mechanisms, regarding the beforehand discussed loss of fragments arising in gas phase for small species. However, in publications where the gas phase has been considered, the exactly same pathway is investigated, for the sake of comparison. We will discuss this point in Chapter 3.
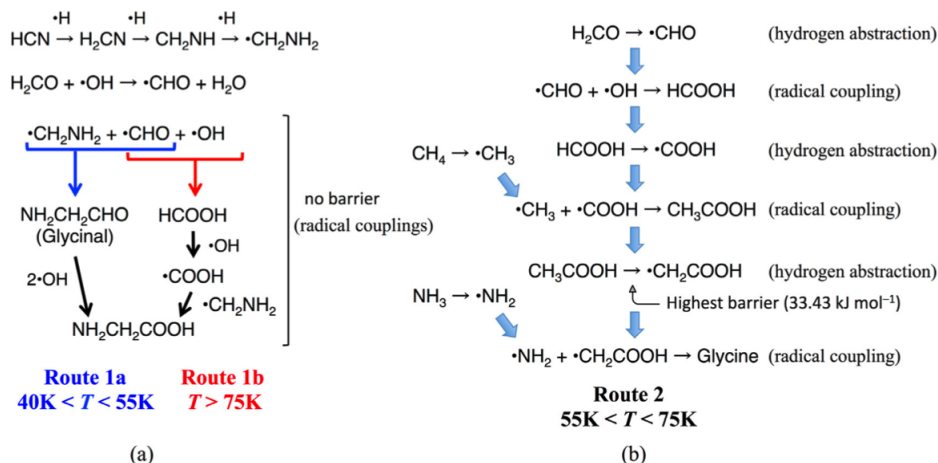
Figure 1.15: Overview of the three glycine formation pathways studied in Sato et al. (2018). The left panel (a) represents route 1a (40 K < T < 55 K), the final radical-radical reaction corresponding to reaction 1.16, and route 1b (T > 75 K), ended by reaction 1.15; The right panel (b) corresponds to route 2 (55 K < T < 75 K), the final step being reaction 1.14, Figure taken from Sato et al. (2018)
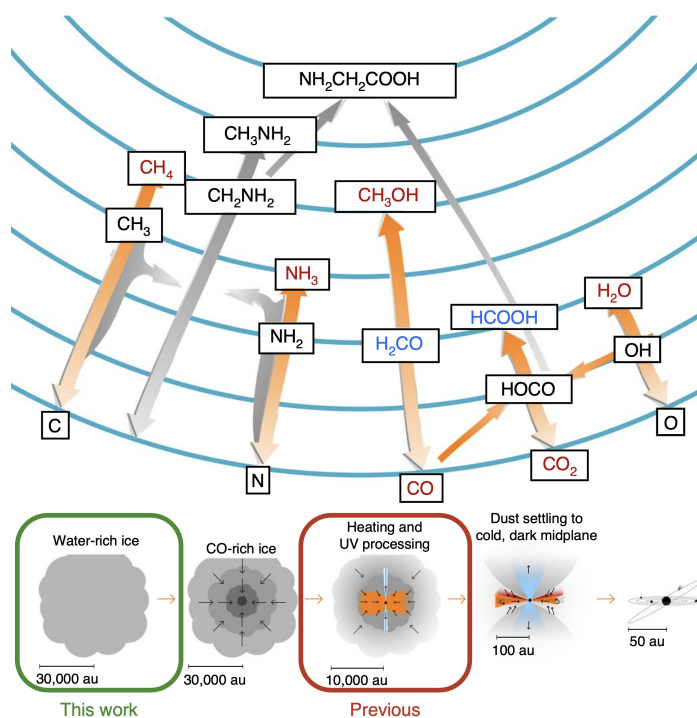
Figure 1.16: Overview of the surface glycine formation route in a water-rich ice during early stages of low-mass stellar formation. "Each blue ring represents an additional hydrogenation step. Hydrogenation–addition reactions are depicted with upward arrows, whereas downward arrows indicate hydrogenation–abstraction reactions. Horizontal (or diagonal) arrows are radical–radical recombination reactions. Orange arrows depict non-energetic surface reaction routes tested under laboratory conditions. Grey arrows are reactions investigated by the authors. (...) Species that are unambiguously detected in ices in prestellar cores are depicted in red; tentatively detected species are in blue. The remaining species involved in this reaction scheme are in black.", from Ioppolo et al. (2021)

of the reaction medium [40] to broadly simulate the intermolecular interactions in the bulk-ice, leading to long-range electrostatic effects. In the case of gas-phase reactions, simulations are done in vacuum conditions regarding the low densities in the ISM, even in the densest clouds. This has a direct impact on the reactants approach, and consequently on the TS and activation energies. Additionally, contrary to solid-phase, the efficiency of radical coupling is limited since there is a significant possibility for the formed glycine to lose a fragment due to the absence of a third body taking back the excess of energy. However, glycine is quite complex compared to simple species such as water, ammonia, CH, CH_2, ... the excess of energy may therefore eventually be spread over its ro-vibrational energy levels. Yet, it is unlikely that the vibrational energy levels (not accounting for the zero-point levels) are active at cryogenic temperatures prevailing in dense molecular clouds (statistical thermodynamics computations can be performed to check it), but rather in hot cores conditions.

For instance, in Rimola et al. (2010) and Rimola et al. (2012), all the calculations have also been performed in vacuum (simulating gas phase) for, respectively, each step of the classical Strecker-like synthesis and for the alternative route taking advantage of ionic-radical defects in the ice. The energetic barriers are generally higher than in solid-phase, with some steps that seem prohibitive at 10-20 K for the neutral path. Woon (2002b) also studied all his proposed reaction steps in both phases.

Additionally, in the study performed by Walch et al. (2001) and already discussed beforehand for their investigation of the iminium cation formation from the protonated classical Strecker-like mechanism in water ice mantle, they also studied a gas-phase **cationic** version of this transformation. In that context, they replaced the ammonia in equation 1.7 by a NH_3^+ cation, leading to the formation of CH_2NH^+ (Figure 1.17). In the subsequent study performed by Walch and Bakes (2001), they however did not calculate the barriers for the next step of this cation activated mechanism, which corresponds to the reaction of CH_2NH^+ with HCN in gas phase. Let us note that no loss of fragment is considered.
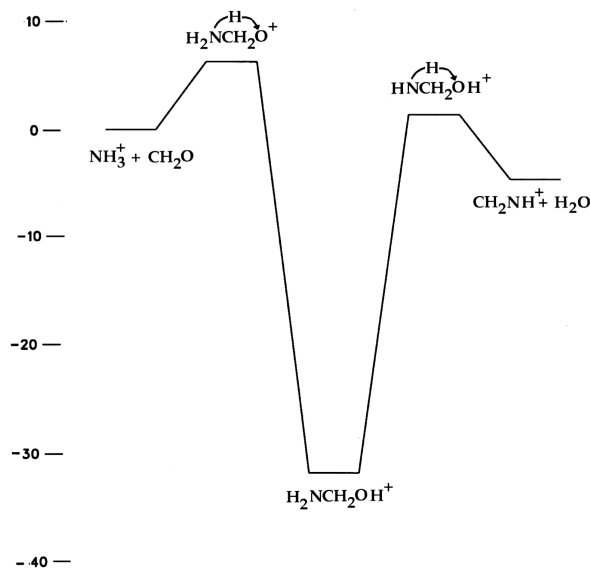
Figure 1.17: Energy diagram for the gas-phase reaction H_2CO + NH_3^+ (numbers correspond to relatives energies compared to the reactants, in kcal/mol), from Walch et al. (2001)

[40]Generally considered as the one of liquid water, the dielectric constant of water-ice being poorly constrained and H_2O represents the main constituent of such interstellar ices.

It is important to stress out the fundamental difference between the protonated (proposed in the water ice phase) and the cationic (investigated in the gas phase) alternative to the classical Strecker-type pathway. Even if the effect on the activation barrier is a lowering, the physico-chemical explanation behind the respective decrease of the activation energy is totally different. For the cationic activation of the pathway, one relies on the difference in the physical interactions between reactants, as discussed in section 1.3.3. Actually, the cationic version of a given mechanism deals with polarization induced interaction, acting at longer distance than the simple Van Der Waals interactions characterizing neutral-neutral processes. On the other hand, in the case of the protonated mechanism, the lowering of the reaction barrier is explained by a decrease of the LUMO, favoring the nucleophilic attack.

Notwithstanding, it is important to stay critical with the schemes dressed in the literature described before, with a distinction between proposed grain surface and gas-phase mechanisms. Indeed, one can not reject interconnections between them. As a matter of example, a given glycine precursor may be formed via a first gas-phase mechanism, adsorbed onto the dust-grain surface, diffuse into the bulk of the ice to be then embedded in a solid-phase process, leading or not to glycine. Those considerations are taken into account in the previously well-discussed paper by Garrod (2013), with their MAGICKAL code of three-phase astrochemical models. However, this could be further improved by a more complete chemical network, adding more gas-phase pathways and subsequent adsorption of the related intermediate species, as well as by accounting for a non-diffusive mechanism in temperature range where it is justified. Unfortunately, even if such an even more improved model is realistically implementable, it needs good constraints on all the parameters characterising the rate coefficient of each reaction, which is not the case for all processes. Further quantum computations are therefore needed to determine/better constrain these un-/not-well known coefficients, which is time-consuming. Moreover, as mentioned before, the MAGICKAL code is proprietary. Actually, few astrochemical models are available; we can mention the gas-phase *Astrochem* model Maret and Bergin (2015) and the three-phase model called *Chempl* Du et al. (2021). The latter is, however, a very recent source code, with several difficulties of practical implementation (for a complete use of its native functionalities).

Finally, before addressing the objectives of the present work, one has to keep in mind that the above proposed mechanisms do not represent an exhaustive list. Other mechanisms have been proposed in the literature, but trying to take all of them into account would quickly become a nightmare to handle with. It was therefore necessary to apply selection criteria, and the presented mechanisms have been narrowed down after a thorough analysis of their scientific relevance. The prime criterion that has been applied is the level of scientific knowledge known about (quantum calculations, kinetic simulations, ...). In addition, we have also considered the number of studies referencing it with a minimum number of drawbacks (kinetic or thermodynamical) as a relevant selection criterion. Table 1.8 summarizes the selected pathways to be further investigated in this present work as well as in subsequent studies, along with the associated scientific papers.

Table 1.8: Selected glycine interstellar formation routes along with their reference publication

Type of mechanism	• *Comments*	• *Paper*	Type of study	Phase considered
Strecker-like (Figure 1.10)	Study of the classical route a	Rimola et al. (2010)	Quantum Computations	Icy-mantle: - surface: H_2O cluster model - bulk-ice: dielectric constant + gas-phase
	Alternative to the last step (Buchener-Berg)	Kayanuma et al. (2017)	Quantum Computations	Ice surface: H_2O molecules (1, 2 or 3) as catalysts + gas-phase
	Activated routes: - first step (towards imine): activation via protonated (ice) or cationic (gas) specie	Walch et al. (2001)	Quantum Computations	Icy-mantle(bulk): dielectric constant +Gas-phase
	- second step (toward amino aceto-nitrile): proton-activation	Walch and Bakes (2001)	Quantum Computations	Icy-mantle (bulk): dielectric constant
Radical-radical (or implying radicals)	From COOH and H_2CNH_2 radicals	Woon (2002b); (Figure 1.12)	Quantum Computations	Icy-mantle: dielectric constant +gas-phase
		Holtom et al. (2005)	empirical support	irradiated ice
	Modified Woon's pathway	Elsila et al. (2007)	Empirical	Irradiated ice analogue
	Study of 4 final radical-radical routes	Garrod (2013) (eq. 1.13 to 1.16);	Astrochemical Kinetic Modelling	Coupled gas-phase, ice surface and bulk-ice
	Study of divers simple processes (atoms, radicals)	Ioppolo et al. (2021) (Figure 1.16)	Astrochemical Kinetic Modelling	Garrod's model (statistical approach)
Cationic & radical	$OH\bullet/H_3O^+$ ion-radical pair (defect, ice processing)	Rimola et al. (2012) (Figure 1.14)	Quantum Computations	Icy-mantle: H_2O cluster model (with defects) +gas-phase

Insight into the main objectives of the following chapters

Henceforth, one may come back to the main objectives of the following chapters. The interstellar glycine formation paths of interest being selected, these will be our starting point for the rest of the study. With the aim to better understand the interplay between these routes and assess the potential dominance of one/some of them, astrochemical modelling efforts are required.

In this scope, current astrochemical models are associated to a set of species characterized by a quite low molecular complexity. Therefore, no available network includes the proposed formation/destruction routes of glycine. Moreover, as previously stated, the available and usable Astrochemical models developed in the literature exclusively consider the gas-phase. We will therefore study the temporal evolution of the abundance of the basic low complexity precursors of the selected paths in different modelled interstellar clouds using the playable *pure* gas-phase *Astrochem* code. The latter includes very interesting and useful functionalities such as the possibility of retrieving the main contributing paths for the studied species. The modelled astrophysical conditions will be considered as the interior of dense molecular clouds, consisting in a unique cell characterized by a temporally constant mean density, temperature, CR-ionisation rate and visual extinction of the radiation field. The primary focus will be devoted to the interplay and expected relative contributions of these paths. In that way we expect to be able to discuss future potential network extensions, towards incrisingly advanced glycine precursors. The main results of these investigations should constitute an interesting source of knowledge since few scientific papers have used such modelling tools to thoroughly analyze the astrochemistry taking place in these interstellar media[41].

Furthermore, a secondary objective of the following discussions is linked to a better understanding of what is an astrochemical code, how it works and what the stability of the results is when perturbing some model parameters. Indeed, this secondary source of discussions and reflections should be very interesting for future improvements of the currently available astrochemical code. Without completely understanding the modelling tools used in scientific simulations, we will not be able to discuss the validity of their results rigorously, and will even less be able to improve them.

The achievement of these main objectives is expected to be the starting point towards more ambitious and longer-term works, such as the elaboration of a more comprehensive, multiple-phase astrochemical code, including rigorous kinetic parameters and accounting for a well-funded interplay between the phases.

For a more global view of the main objectives of this present master thesis, the reader is referred to Figure 1.18.

---

[41]Except in Garrod (2013), but this study does not concerns static and temporally constant cloud (with respect to the mean density, temperature, CR-ionisation rate and visual extinction of the radiation field).
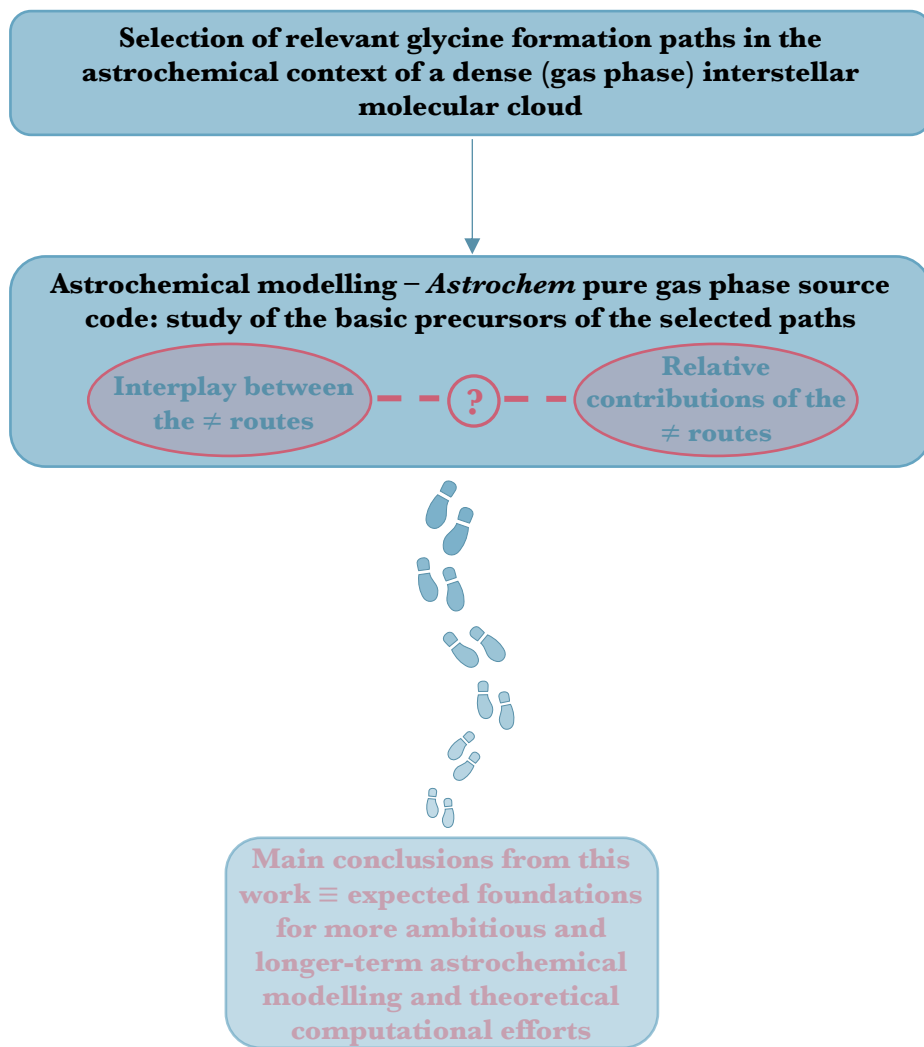
Figure 1.18:   Visual representation of the main objectives followed in this work, with an emphasis on the broader scientific perspectives expected from the main inferred results.

Chapter 2

Astrochemical Modelling

The main objective of this chapter firstly consists in introducing the basic principle behind kinetic astrochemical modelling. Such kind of simulation is needed to achieve a time-dependent monitoring of the abundances of species of interest in an astrophysical context. This step being completed, the astrochemical code used in this work will be introduced.

2.1 Basic principle of Astrochemical Modelling

As discussed in the first chapter, the physical conditions prevailing in the Interstellar Medium (see Table 1.3) are very difficult to reproduce empirically on Earth [1]. Moreover, regarding the very long timescales associated with astrochemical processes, the beforehand discussed interstellar phases cannot reach chemical equilibrium. It then justifies the need of time-dependent chemistry and the subsequent resolution of systems of rate equations. Consequently, we easily understand the use of kinetic modelling to predict and analyse the temporal evolution of the abundance of a chemical entity in a given interstellar phase. Figure 2.1 shows the basic principle behind such astrochemical modelling work in more details, allowing us to discuss it further with a prime emphasis on the interdisciplinary aspect. Basically, each astrochemical model requires two main ingredients: **(i)** the underlying physical parameters & **(ii)** the astrochemical network.

Keeping in mind that the kinetic of a chemical process depends on the number densities and the temperature of the medium, the **physical parameters** ruling astrochemical models consist mainly in the temperature, the mean density, the visual extinction (A_V) of the radiation field, the CR-ionization rate (ξ) and the initial abundances. Such parameters depend on the astrophysical context considered, which will be restricted to dense molecular clouds in our case of study. In addition, the astrochemical timescale taken into account in the modelling computations is also of prime importance and has to be compared with the dynamical time scale of the medium of interest. Actually, assuming an homogeneous medium (same temperature and mean density at all locations)[2], the temperatures and mean density are considered as

- constant with time if the astrochemical timescale ($\tau_{astrochem}$) is smaller than the dynamical timescale (τ_{dyn}). In this case, we consider the situation before any significant change of characteristic physical parameters of the medium;

---

[1] The densities in the ISM are so low that even the lowest reachable ones in terrestrial lab are of several orders of magnitude larger than the typical densities in the densest interstellar phases. Moreover, the low kinetic of such processes lead to reaction timescales which are too long to be monitored and analysed over the timescale of human life.

[2] In the case of dark molecular clouds, this assumption implies neglecting phenomena occurring at the boundaries, where the interactions with photons are completely different from those taking place in the interior.

- changing all along the simulation in the case of a considered $\tau_{astrochem}$ larger than τ_{dyn}. Such modelling work would require upstream shock physics or Magneto-Hydro Dynamics (MHD) simulations, which is totally out of the scope of this present master thesis.
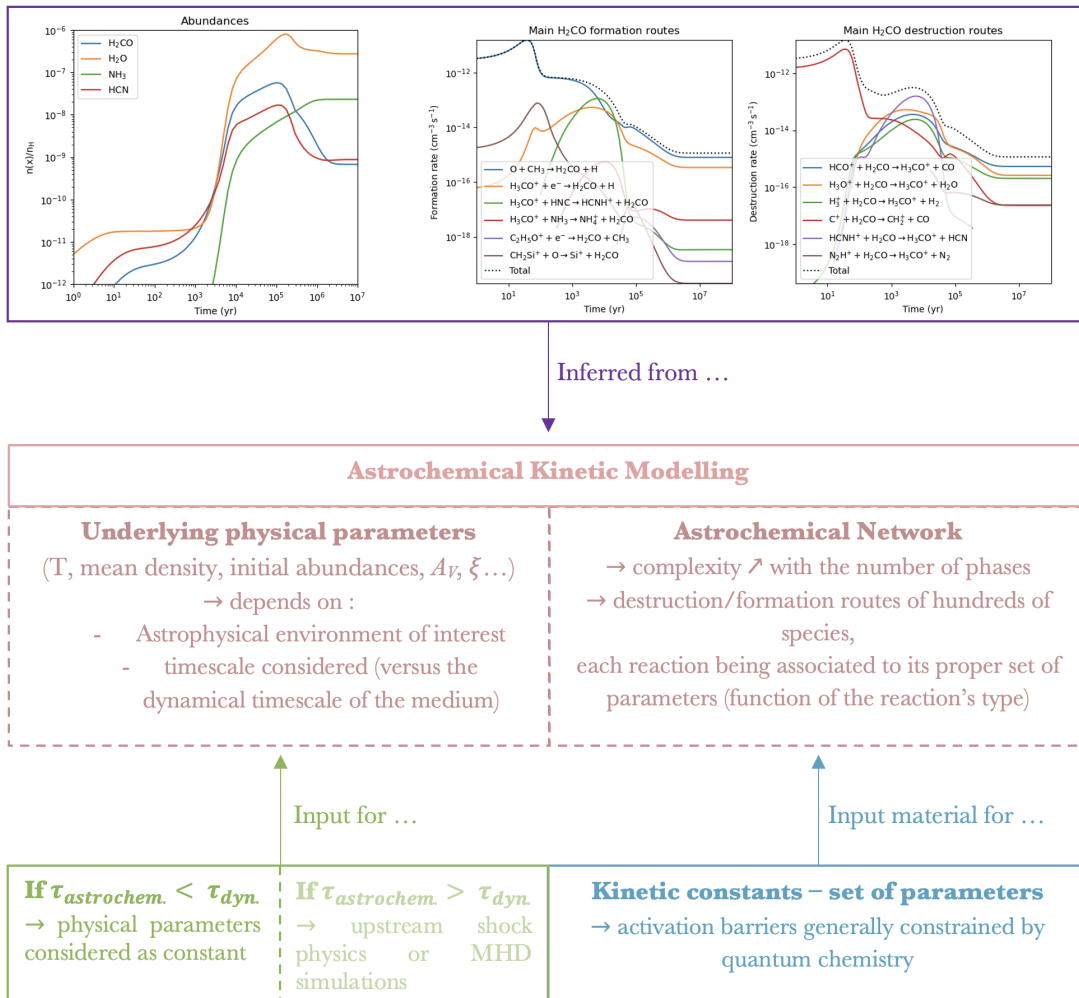
Figure 2.1: Block diagram illustrating the basic principle behind Astrochemical Modelling: (top, in mauve) example of expected results, namely the inferred figures from the model outputs (here, from *Astrochem* analysis), (bottom, green and blue) main inputs needed for the two main ingredients of the model: (i) the physical parameters & (ii) the astrochemical network.

In our case of study, we will therefore restrict ourselves to $\tau_{astrochem}$ smaller than τ_{dyn}. It is worth mentioning that the dynamical timescale of a typical dense molecular cloud is of the order of 10^7 years.

Concerning the second key ingredient of an astrochemical kinetic model, namely the **astro-chemical network**, this concept deserves further explanations. First of all, one has to figure out that the rate equations to be solved become more and more complex by considering systems with an increasing number of interconnected reactions (chemical network). In the context of an astrochemical study, hundred of species are concomitantly [3] taken into account, leading to a very rich expected as-

---

[3] In space, all the species are present and interact, so that we cannot imagine *isolated* reactions without any inter-

trochemical network and requiring the resolution of complex systems of thousands of rate equations. It consequently requests the use of state-of-the-art *stiff Ordinary Differential Equation (ODE) solvers* (robust numerical methods). In practice, an astrochemical network consists of a list of thousands of reactions, together with their respective set of kinetic parameters (needed to characterize the kinetic constants). These sets of parameters depend on the type of reaction (photoreaction, reaction between atoms, ...), as theoretically recalled in Chapter 1 (see examples of expressions of kinetic constants in Tables 1.5 and 1.7, with different parameters depending on the type of process).

Figure 2.2 presents an example of a very simplified schematized astrochemical network, emphasizing on the formaldehyde formation in diffuse and dense clouds (Prasad and Huntress, 1980a).

Figure 2.2: Simplified network gathering the main astrochemical gas phase interconnections implying H_2CO and HCO, from Prasad and Huntress (1980a)
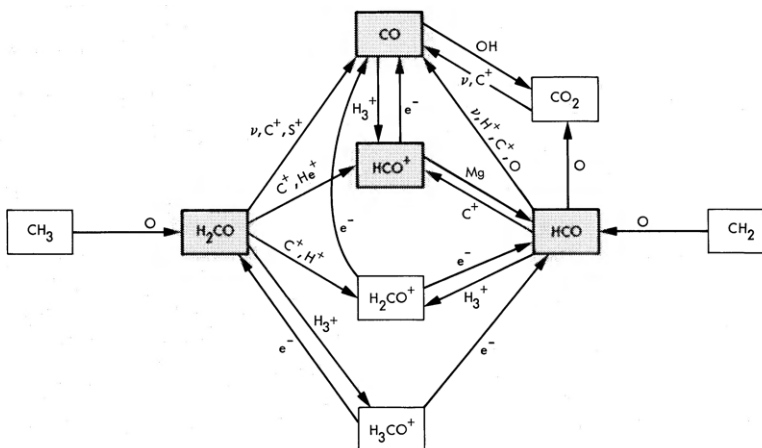
From this simplified network, one can already get a feeling of the complexity behind such grids of astrochemical processes. However, it is worth to keep in mind that astrochemical networks on which kinetic models are based are greatly richer and more ramified. The proper inclusion of all the formation and destruction routes of each intermediate species is indeed of prime importance to infer the temporal evolution of the abundance of a given target. Otherwise, it will lead to bias in the inferred results. For the rest of the discussion, what we will call *the completeness of an (astro)chemical network* will be referred to the level of ramification of the network combined to the comprehensiveness in the inclusion of the formation and destruction routes for each species. Considering a given network owing to a given model, for a fixed molecular complexity, the higher the completeness the higher the veracity of the inferred temporal evolution of the abundances.

Moreover, to completely characterise such a network, another *property* has to be discussed. This will be referred to *the complexity limit of an astrochemical network* for the rest of the discussion. The latter will be defined as the level of molecular complexity reached by the most complex chemical entity incorporated in the model, together with the number of included species reaching such complexity. The higher this complexity limit, the higher the level of molecular complexity potentially analysable.

In addition, the number of phases (gas phase, grain surface heterogeneous catalysis and chemistry occurring in the bulk of interstellar ices) taken into account and the way of implementing the interplay between them have to be considered to discuss the quality of a given astrochemical network. However, most of the available astrochemical networks are only in gas phase. This point will be further commented in section 2.2.

---

connected chemical processes, in contrast to what can be done in terrestrial labs where we can isolate the species of interest.

Henceforth, to characterize a given (astro)chemical network (neglecting the number of phases taken into account), one has to consider both its *completeness* and its *complexity limit*. Figure 2.3 provides insights on the importance of the simultaneous consideration of those properties.

Complexity limit

- Low complexity limit & low completeness → low relevance for the inferred results & poor complexity discutable

- High complexity limit but low completeness → species of relatively high complexity can be analyzed but low relevance for the inferred results

- High completeness but low complexity limit → high relevance for the inferred results but low complexity potential

- High completeness & high complexity limit → species of relatively high complexity can be analyzed, with highly relevant inferred results
  = Ideal (Astro)chemical network

Completeness

Figure 2.3: Visual insights on the importance of the consideration of both the completeness and the complexity limit of a given astrochemical model to discuss the veracity of the inferred results.

As highlighted in this figure, an ideal (astro)chemical network would require both a high completeness as well as a high complexity limit. However, as mentioned before, in practice, an astrochemical network consists in a list of reactions characterized by a set of kinetic parameters. These are generally constrained through quantum chemistry computations. Such computations have to be performed for each reaction steps, which is a very time-expensive process regarding the number of potential reactions to be considered. As a result, the astrochemical networks currently available in the literature are generally showing a quite high completeness, while reaching a quite low complexity limit (yellow circle in Figure 2.3). Indeed, in the absence of current ideal astrochemical network, it is better to progressively rise in the complexity limit, while taking care to always keep a high completeness. With that strategy, inferred results can be discussed with relevance. A great perspective in that field goes therefore hand in hand with progressively constraining rich interconnecting reaction pathways towards networks displaying a higher and higher complexity limit, while keeping the high completeness that is currently reached by up-to-date availaible networks.

To summarize this point, the goal of an astrochemical kinetic study is to infer the temporal evolution of the abundance of species of interest in a given astrophysical environment. Regarding the peculiar conditions prevailing in the ISM, such a study requires the use of theoretical time-dependent kinetic analyses, achieved with astrochemical models. Such models imply two main ingredients:

- (i) the set of physical parameters, mainly including the temperature, the mean density, the visual extinction (A_V) of the radiation field, the CR-ionization rate (ξ) and the initial abundances, as well as the time-scale considered. In this work, only timescale lower than the dynamical one will be studied;

- (ii) the astrochemical network. It can be characterized by its completeness and complexity limit, as well as by the number of phases considered. In this work, we will use a pure gas phase astrochemical model (*Astrochem*), as deeper commented in the following section.

2.2   Kinetic study with *Astrochem*

As seen in section 2.1, the currently available astrochemical networks display quite a satisfactory completeness, but presenting a low complexity limit. The one we will use will therefore not reach glycine, but rather its basic precursors. Moreover, no open source and practicable multi-phase[4] astrochemical code currently exists in the scientific community. Yet, there are two open-source multi-phase codes, namely *Nautilus* and the recent *Chempl* models, but their practical implementation was not possible. Indeed, Nautilus needs a no longer available Fortran compiler, and the Chempl package is too recent, therefore presenting unresolved errors in its source code and leading to the impossibility of using most of its functionalities. Furthermore, these two multi-phase astrochemical codes do not consider the encounter between bulk-ice constituents in a relevant way in the cryogenic context we are studying. Indeed, they only consider thermal migrations, without accounting for any statistical considerations (availability of (a) reaction partner(s) in the surrounding of each bulk-ice chemical entities). This point has been more deeply commented in the introductory chapter. The astrochemical code used in this present work is therefore restricted to the gas-phase source code *Astrochem*, with playable functionalities (Maret and Bergin, 2015).

2.2.1   Astrochem code

Astrochem (Maret and Bergin, 2015) is an open-source code aimed at studying the astrochemistry in various interstellar environments, such as in diffuse and dense clouds, photodissociation regions, prestellar cores, ... This code, written in C, is accompanied by a rich documentation manual on its GitHub page[5]. The following subsections will be focused on the principal bases of Astrochem. The interested reader is referred to the whole documentation manual for supplementary information.

Astrochem - Generalities

The Astrochem code is linked to an easy to read & edit astrochemical network. A huge variety of gas phase processes is included[6], the kinetic parameters coming from the Ohio State University (OSU) astrochemistry database, maintained by Eric Herbst. Moreover, in its code, Astrochem is theoretically able to consider very simple gas-grain interactions, such as freeze-out and desorptions via various mechanisms (thermal, cosmic-ray or photo-desorption). However, in the related network, there is no corresponding reaction. Only electron attachments and ion recombinations on negatively charged grains are considered. In the rest of the discussion, we will therefore consider Astrochem as a pure gas-phase code.

From a practical point of view, Astrochem is used in this work in order to infer the temporal evolution of various astrochemical species in dense molecular cloud conditions. More specifically, the interior of such a cold environment is aimed at being modelled by supposing cryogenic temperatures in an isodense and isothermal medium[7] shielded from the interstellar radiation field (visual extinction A_V equal to 20 magnitudes), allowing us to neglect photo-processes. Such a problem is described in an *input* file and its associated *source* and *network* files, as explained in more details in the following paragraph. The computations are then run from the command line, taking the name of the *input* file as argument.

---

[4]Gas-phase, grain-surface and icy mantle surrounding grains in the densest and coolest parts of the ISM.

[5]`https://astrochem.readthedocs.io/en/latest/usermanual.html#`.

[6]Including most the processes from Table 1.5. Let us notice that the self-shielding of species that dissociate through a line process is neglected. This problem is circumvented in our case of study by considering the interior of dark molecular clouds, with highly extinct radiation fields ($A_V = 20$ mag).

[7]This modelled astrophysical environment is considered as one unique cell.

Input, source files & Astrochemical _network_

```
 1 [files]
 2 source = source_model3a.mdl
 3 chem = osu2009.chm
 4 # Physical parameters
 5 [phys]
 6 chi = 1.0
 7 cosmic = 1.3e-17
 8 # Solver parameters
 9 [solver]
10 ti = 1
11 tf = 1e7
12 # Initial abundances
13 [abundances]
14 H2       = 1
15 He       = 0.14
16 N        = 2.74e-5
17 O        = 3.76e-4
18 C(+)     = 7.30e-5
19 S(+)     = 8.00e-8
20 Si(+)    = 8.00e-9
21 Fe(+)    = 3.00e-9
22 Na(+)    = 2.00e-9
23 Mg(+)    = 7.00e-9
24 P(+)     = 2.00e-10
25 Cl(+)    = 1.00e-9
26 F        = 6.68e-9
27 e(-)     = 7.31012e-5
28 # Output
29 [output]
30 abundances = CO2,H2O,CO,OH,CH2O2,HCN,CH3N,CH4N(+)
31 time_steps = 128
32 trace_routes = 1
33 
```

Figure 2.4: Example of an _input_ file used for Astrochem computations. Lines starting with $\#$ are comments.

As shown in Figure 2.4, the **_input_** file is composed of five sections, namely

  i. **[files]** where the complete name (with the extension) of the files describing the modelled source (keyword _source_, extension mdl) and the astrochemical network (keyword _chem_, extension chm) are given. The format and content of these files will be addressed in further details afterwards;

  ii. **[phys]** where specific physical parameters of the source are defined - _chi_ corresponds to the UV radiation field in Draine units (scaled on the standard interstellar radiation field of Draine (1978)), while the CR-ionization rate (keyword _cosmic_) defines the rate of the direct or indirect ionizations through CR interactions, processes that have already been discussed in Table 1.5. Other parameters may be specified, such as the grain size, or grain to gas mass ratio. However, changing the value of the grain to gas mass ratio has no quantitative influence on the result since no freezing-out or desorption processes are taken into account and the grain size parameter is not relevant in the context of the non inclusion of those grain processes. We will not consider these parameters, letting them to their default values (no grain) and therefore considering a purely gas-phase context without any loss in the solid phase;

  iii. the initial (keyword t_i) and final (keyword t_f) epochs (in years), defining the time interval for which the computations are done, are set in the **[solver]** section. In the latter, the solver

absolute and relative errors on the computed abundances may also be specified. In this work, we have kept the defaults values, 10^{-20} and 10^{-6}, respectively ;

iv. **[abundances]** where the initial abundances are listed (the non listed species are set to a zero initial abundance by default). The values are taken from interstellar standard values corrected from the depletion in the bulk material of dust grains (see Table 1.6 and Figure 1.4);

v. **[output]** where various parameters relative to the output are specified, namely the *abundances* line listing the name of the species for which the abundance has to be computed (the species being separated by a coma), *time_steps* defining the number of time intervals given in the output, and the *trace_routes* keyword enabling the computation of the 12 main formation/destruction routes of the species listed in the *abundances* line (to activate this function, one has to set this parameter to 1).

Regarding the **source file** coding the modelled astrophysical medium more specifically, one unique isodense and isothermal cell will be considered with time independent parameters ($\tau_{astrochem} < \tau_{dyn}$ as discussed in § 2.1). Since each line of such a file describes one cell, one unique line is sufficient for the *source* file in our case of study. An example of *source* file used in this work is given in Figure 2.5.

```
1 # shell number, Av [mag], nH [cm^-3], Tgas [K], Tdust [K]
2 #
3 0       20.0    1e+04   10.0    10.0
```

Figure 2.5: Example of a *source* file used for Astrochem computations. Lines starting with # are comments.

The five columns, separated by a tabulation (or by any number or blank space), respectively define the index of the cell (0 for the first/unique cell), the visual extinction (in magnitudes), the total number density in hydrogen nuclei[8] (n_H, in cm^{-3}) and the gas & dust temperature (in K).

Concerning the **network** (extension .chm), the most up-to-date one (*osu2009.chm*, distributed with Astrochem) has been used. It consists in 6046 processes for 468 species, without considering for e-, grain, UV-photons, CR. It can be very easily read as well as edited. Each line corresponds to one reaction and is composed of two main parts: (a) the chemical equation, and (b) 5 numbers quantifying the rate constant parameters (up to 3, those being different depending on the reaction type), the reaction type (coded by a number between -1 and 23, as further detailed in the Astrochem documentation manual) and the reaction number.

Furthermore, it is worth further discussing the very interesting functionality of computing the 12 main formation/destruction routes of the studied species. One can indeed legitimately wonder on which basis the authors of Astrochem have decided to code the computation of 12 main processes contributing to the computed abundances, rather than computing less/more than 12 processes. In other words, it is justified to further think about this chosen number of 12 main processes: *Has this number been chosen arbitrarily?* Or, *Has it been determined on more stringent considerations?* For the sake of clarity of the discussion, let us consider Figure 2.6 and define X as the number of computed main formation/destruction routes. Moreover, let us suppose a hypothetical chemical network including a sample of species, each of them being characterized by a number (Y) of associated processes included in the network.

---

[8]Note that the term 'hydrogen nuclei' refers, as documented in the Astrochem manual and other astrochemical modelling works (Iglesias, 1977; Prasad and Huntress, 1980a,b), to the assembly of all hydrogen-made species, including mainly H, H$_2$, H$_3^+$, ... species. It has to not be confuse with protons.

In the ideal case of a(n) (astro)chemical network characterized by a high completeness, X is *significantly* lower than Y, and the inferred main formation/destruction processes are expected to be on average[9] representative of the main contributors to the measured abundances, without systematic negligible routes. Yet, let us note that X must not be too small compared to Y, so that we do no miss part of the major contributors. On the other hand, if X is still lower than Y, but tends to Y (δ tends to 0), one can expect the X main processes not to be really relevant in the context of the discussion of the main contributors, almost all of the processes included for the species being retrieved in this list of the main processes. In this case, only the first top processes are expected to be representative to explain the abundance of the studied species. In the last case, X is higher than Y and Astrochem is naturally not able to list X "main" contributors to the computed abundances, but will simply list the Y included routes.
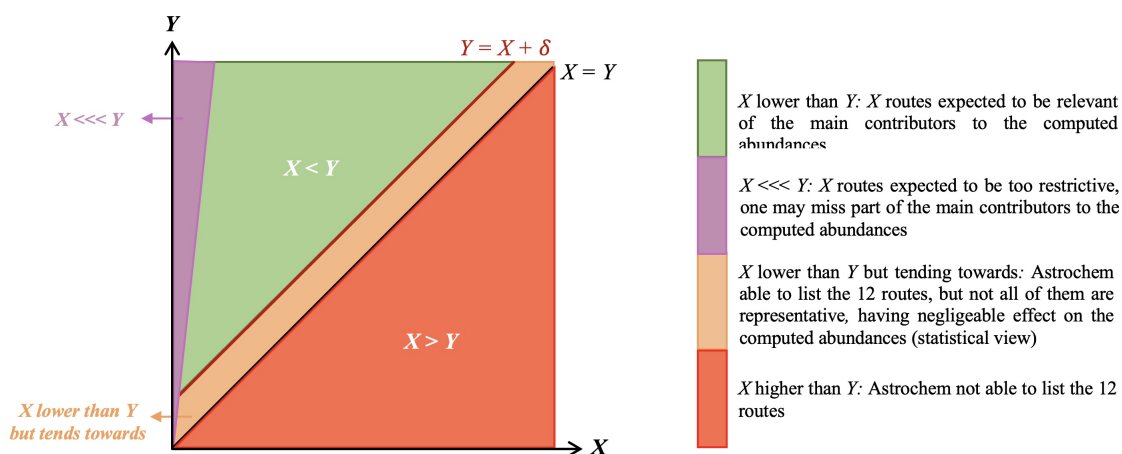
Figure 2.6: Scheme aimed at illustrating visually the discussion on the number of computed main formation/destruction routes as compared to Y, the number of included processes per species.

From these considerations on the chosen number of retained main formation/destruction processes, we can now discuss the used network, from the Astrochem source code. As previously emphasized, the astrochemical network is composed of 468 species for 6048 reactions. From a simple ratio, it leads to ~ 12 reactions per species. However, this value is not really representative of the average number of integrated reaction per species (including formation and destruction), since some species are involved in a huge number of reactions. Going into deeper details, the network file has been checked carefully, listing species in a decreasing order of occurrence, to be able to infer the mean Y and the standard deviation of Y. To perform this counting, a simple python code has been written. From the inferred list of species with their respective occurrence, a general histogram has been built, as shown in the upper biggest plot on Figure 2.7. Additionally, two *zoomed* histograms have been dressed, dividing the x-axis of the biggest histogram into two parts: from 1 to 250, and from 250 to 2360 associated reactions. Finally, a cumulative histogram has been inferred, presented in the lower right panel. Complementary to Figure 2.7, Table 2.1 gathers the most present chemical entities (more than 100 associated processes) in the Astrochem genuine network (osu2009.chm). Naturally, we retrieve the H atom, the most abundant element in the Universe, in first place. Afterwards, we find H_2, the most abundant molecule in the Universe, C and O atoms, the two most abundant elements after H and He,

---

[9]From a statistical point of view, it depends on the Y distribution. If the standard deviation is very small compared to the average Y, this consideration is valid for most species. On the other hand, if the standard deviation is quite high, one must compare each Y to X.

this latter being a bit less represented than C and O due to its noble gas nature. Moreover, species characterized by the lowest Y are also characterized by a higher molecular complexity (e.g. NH_2CH, $HCOOCH_3$ with Y equal to 8, $HCNO^+$ present in two processes, ...). This was expected since more complex species more often display a less *"polyvalent"* reactivity, in the sense that they react with a lower number of potential partners than, for instance, H_3O^+ which may exchange a proton with a large number of neutral species, displaying therefore intrinsically a larger Y.
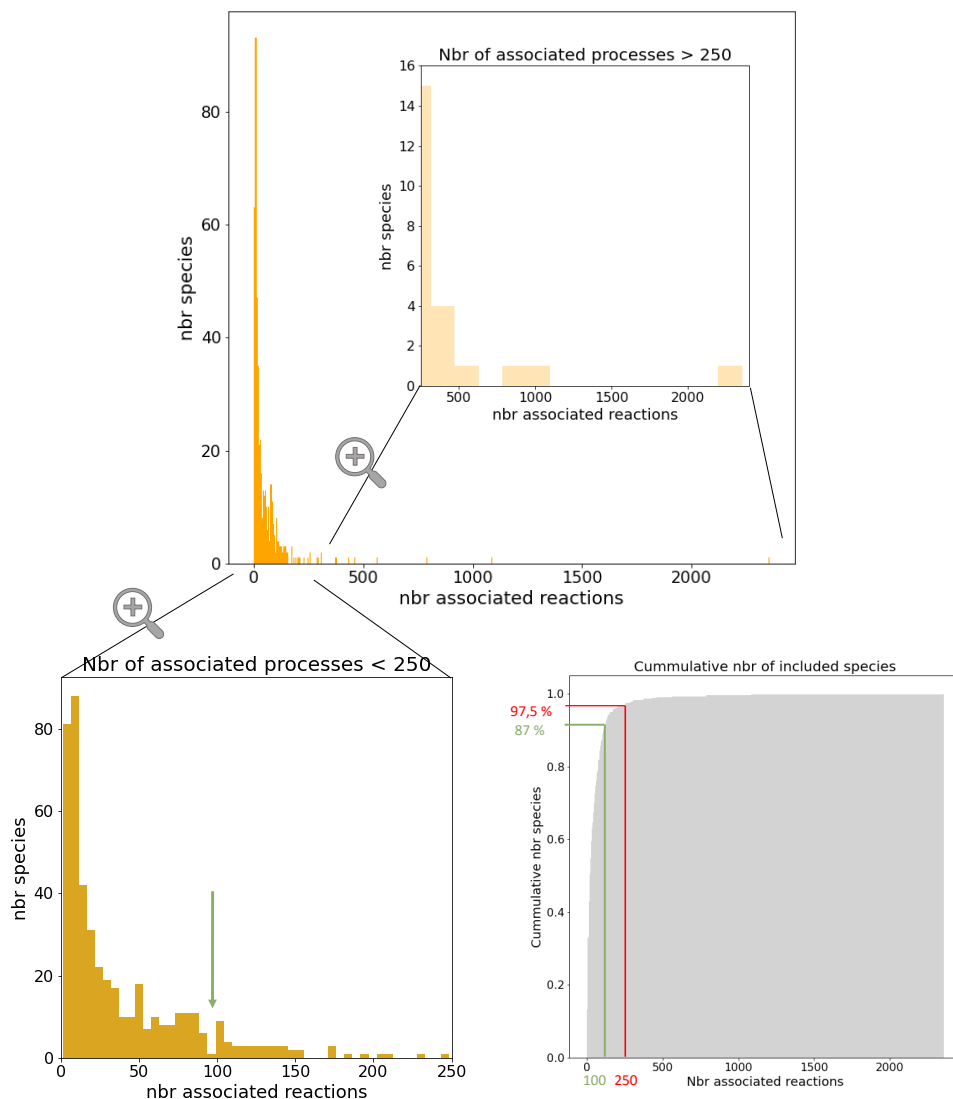
Figure 2.7: Histograms of the Y distribution for the osu2009.chm genuine network.

From theses results, we can apply our reflections linked to Figure 2.6 to our real case. Considering the whole set of species included in the Astrochem genuine network, the average number of corresponding reactions is 54, with a high standard deviation of 138 and a median of 20. As it can be easily visualized on the zoomed histogram, taking into account only the species for which more than 250 processes are included in the network, only a minority of species are present in such a part of the Y distribution, explaining the high discrepancy between the median[10] and the mean Y. Indeed, having a closer look at

---

[10]More robust estimator, less sensitive to extreme values.

Table 2.1: List gathering the most present chemical entities (more than 100 associated processes) in the Astrochem genuine network (osu2009.chm).

Species	Nbr of processes	Species	Nbr of processes	Species	Nbr of processes	Species	Nbr of processes
H	2356	H_2	1087	e(-)	793	C	561
O	465	CO	434	He	377	He(+)	375
CN, HCN(+)	306	N	292	C(+)	290	S	258
H(+)	256	OH	247	H_2O	229	UV	209
CR	205	H_3(+)	194	CH	184	CH_2,C_2	174
C_2H_2	172	H_2CO	153	CH_4	151	CH_3(+), CH_3	147, 146
C_5H	145	C_2H_2(+), HCN	141	C_9H,C_4H, HCO	136	H_3O(+),C_2H_3(+)	134
Si	130	NH_3	129	C_7H, $C_{10}H$,C_6H	126-119	O_2	122
NO	115	C_5, C_6,C_{10},C_8	114-107	C_4H_2,C_5H_2	110	NH	106
S(+), Si(+)	104	C_9, C_7, C_8H	104-102	C_2H_4(+),HCNH(+)	101	N_2	101

the cumulative histogram, for a number of associated reaction of 250, it already represent 97.5% of the total number of included species (472). On the other hand, ignoring these extremes values, considering therefore only species included in less than 250 reactions in the network (zoomed lower left histogram), the mean Y decreases to 38, with a median of 19 and a lower standard deviation of 43. Moreover, as we see on this zoomed histogram (species associated to $Y < 250$), the distribution between 100 and 250 associated reactions is also not really representative of the major part of the included species, with few species characterized by such Y values. Actually, starting from the cumulative histogram and considering the species characterized by a Y of 100 at most, we already account for 87% of the total number of included species. Taking into account only species with Y lower than 100, the standard deviation decreases to 25.7, for mean Y of 27 and a median of 16 (the difference between the median and the mean decreasing due to a lower number of extreme values which are not well represented in the distribution). From this set representing 87% of the Y distribution, the chosen value of X seems justified, although species characterized by Y around and lower of the median value enter the light and more intense zones of Figure 2.6.

Finally, thanks to this deep analysis, we can more quantitatively discuss the completeness of the used network. First of all, a large fraction (87%) of the 472 species taken into account in the used network includes chemical entities associated to a Y lower or equal to 100. These 87% of species are characterized by a median Y of 16, and a standard deviation equal to 25.7, of the order of the mean. The completeness of the network is therefore rather appreciable, even though it seems to decrease a bit when increasing in the molecular complexity. When considering the whole set of included species, this mean increases, and the standard deviation becomes very high, while the median stays approximately constant (slower increase than the mean), pointing out the number of extreme, not many represented Y values in the tail of the distribution. Actually, Y ranging from 100 to 2360 represents only 13% of the 472 species included in the used network. Beside this quite low fraction, this includes species of interest in the present work, such as H_2CO, HCN, CO, OH, ... as listed in Table 2.1. It is therefore worth mentioning that for such well represented species, displaying a high Y compared to X (12), one must stay careful not to fall into the case when X is too low compared to Y, in which case some of the major contributors may be missed. Naturally, let us bear in mind that this beforehand discussion is based on a statistical point of view. It is however possible that species characterized by a very high Y only come from 3 or 4 main formation/destruction pathways. It depends on each species, on the modelled astrophysical medium, and on the nature of the reaction considered. Nevertheless, this reflection is of prime importance to rise our critical mind for the following discussions.

Handling results with *Astrochem* functionalities

The results from Astrochem are stored in a binary file in a HDF5 format. These results may then be analyzed from the Astrochem python module, or directly by using the associated plotting programme of Astrochem, named ***Plabun***. This programme is able to trace the temporal evolution of the abundances of the studied species, as well as their major destruction/formation routes. It will be used throughout this work.

Chapter 3

Preliminary Study with Astrochem

This chapter is dedicated to a preliminary study of the selected pathways towards amino acids using the simple gas-phase kinetic model Astrochem and focusing on the precursors of those routes. All along this first investigation, one has to keep in mind that Astrochem is mainly focusing on gas-phase processes, making abstraction of possible reactions on surfaces or in icy mantles of dust grains (see subsection 2.2 in Chapter 2). The temperatures considered will be typically 10 to 20 K, valid for a dense cold molecular cloud. Moreover, the simulations will be performed over time scales of 10^7 years, the typical dynamical time-scale of such clouds being of the order of $10^7 - 10^8$ years.

From a practical point of view, this preliminary study is firstly meant for a check-up of the primary precursors to our selected glycine formation pathways (see Table 1.8) already included in the genuine Astrochem network (osu2009.chm). In that context, this chapter will be divided into two main parts. The first part will be devoted to the precursors of the Strecker-like routes, while the second part of this chapter will focus on the Woon's radical mechanism and its variants. In both parts, we will comment on the temporal evolution of the abundances of those precursors, and analyse their favoured formation/destruction paths, without jumping into any hasty conclusions. Additionally, a quantitative comparison to previous results (Iglesias, 1977; Prasad and Huntress, 1980a,b) as well as to observational data will be performed. Finally, to end this chapter, a comprehensive summary of the most important results emanating from this preliminary study will be drawn in order to investigate the potential links between these selected pathways and their primary precursors. Furthermore, this summary would pave the way towards discussions about network extensions.

3.1 Precursors for the simple and activated Strecker-like synthesis

3.1.1 Strecker-like synthesis - Neutral pathway

First of all, let us focus on the classical Strecker-like synthesis (Figure 1.10). This pathway invokes four very simple precursors: H_2CO, NH_3, H_2O and HCN. Those are already included in the astrochemical network implemented in Astrochem.

Using the physical parameters (to be mentioned in the source file) describing the **model 1a** given in Table 3.1, a first inference of temporal abundances has been performed, leading to Figure 3.1. From this figure, one can easily notice that, for the time scale considered and the unmodified network from the Astrochem source code, the most abundant precursor to this simple gas-phase Strecker-like synthesis is $\mathbf{H_2O}$ almost all along the simulation (model 1a), except at $\sim 10^3 - 2.10^3$ years. This result could have been anticipated from the stellar nucleosynthesis theory, allowing oxygen and carbon

Table 3.1: Physical parameters describing the modelled cloud considered in chapter 3

	Extinction (mag)	n_H (cm^{-3})	$(n_{H2}/n_H)_{ini}$	$T_{gas}=T_{dust}$ (K)
Model 1a	20	10^4	1	10
Model 2a	20	10^6	1	10
Model 3a	20	10^4	1	20
Model b	20	4.10^5	1	50
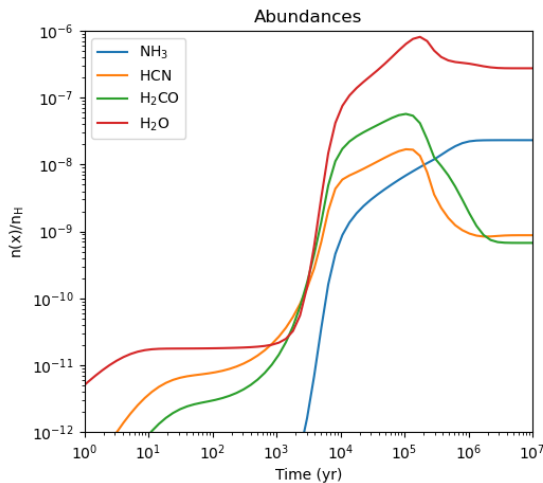
Figure 3.1: Respective abundances as a function of time for H_2CO, HCN, NH_3 and H_2O, the most simple precursors for the classical Strecker-like synthesis, computed with Astrochem (from **model 1a** describing a relatively dense molecular cloud at 10K.)

to be the most abundant elements in the Universe after H and He (Big bang)[1]. Oxygen atoms are therefore likely to be trapped in H_2O molecules in dense medium, even if its most stable molecular reservoir is CO.[2].

Moreover, it is straightforward to retrieve with Astrochem the main formation and destruction routes included in the network for each of the investigated species, as discussed in section 2.2. In this scope, Figure 3.2 lists the 12 main gas-phase formation/destruction routes for H_2O, as computed for model 1a with Astrochem. The main source of H_2O molecules in such interstellar gas-phase is the H_3O^+ ion. Actually, all along the simulated elapsed time of 10^7 years, its dissociative recombination dominates, but only matches the curve of the total formation rate (dotted one) after more than 10^3 years. The other formation paths are mostly presenting negligible contributions compared to the dissociative recombination of H_3O^+, particularly before the elapsing of 10^4 years. Knowing that H_2O is present in 229 processes in the used genuine Astrochem network, the chosen value of X can legitimately be questioned. Coming back to our discussion in Chapter 2, at point 2.2, we are likely in the pastel violet part in Figure 2.6. Moreover, Astrochem is able to list the 6 contributors respectively for the main formation and destruction of each of the studied species, but this set of 6 routes are selected for the whole simulated time interval. In other words, Astrochem is not able to select the 6 main formation routes at each time step, but is only able to select the 6 formation routes that contributed cumulatively the most, all along the 10^7 years. It then retrace the formation (or equivalently destruction) rate profiles for each of these selected routes. Regarding the high difference between the contribution

---

[1]This tendency is taken into account in the initial abundances encoded in the *input* files used for the computations.

[2]As we will see when addressing the Woon's route and its basic precursors, oxygen, when locked in a molecule, is mainly trapped in CO because of the photostability of the latter.
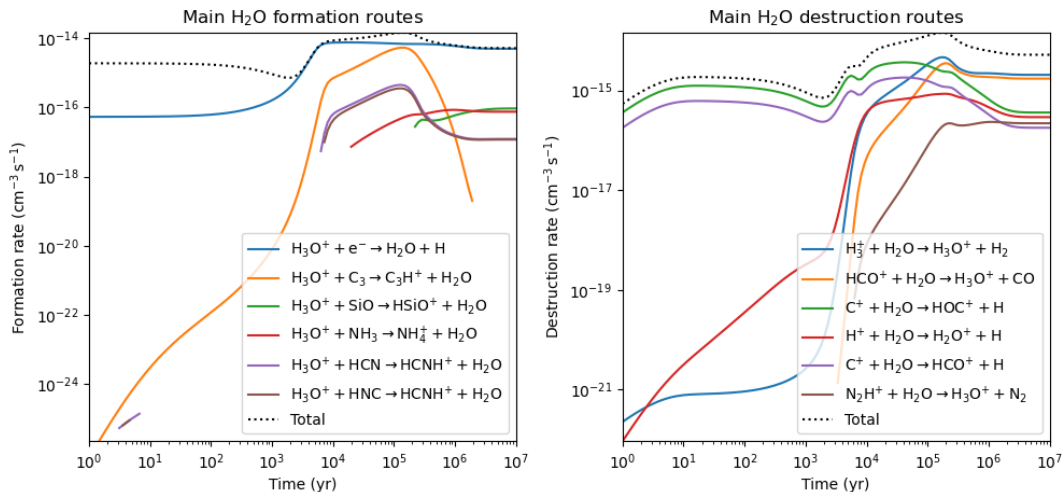
Figure 3.2: Main gas-phase formation/destruction path for H_2O from **model 1a** (Astrochem)

to the main formation path and the total formation rate before $\sim 10^2$ years (quite a small period compared to the whole studied time interval), major contributors to the H_2O formation during that epoch have been missed. This postulate will be checked afterwards in this chapter when perturbing a bit the model parameters (model 2a analysis).

Concerning the main H_2O destruction paths, all of them invoke ion-molecule reactions. Indeed, H_2O is a molecule presenting a permanent dipole. As seen in Chapter 1, paragraph 1.3.3, such processes have a quite high kinetic constant as compared to simple neutral dissociative attachments, most of them presenting a negligible to zero activation barrier. Therefore, their dominance is not surprising. Furthermore, before 10^3 years, the destruction routes implying the C^+ cation dominate. After that epoch, reaction with other abundant cations (predominantly HCO^+ and H_3^{+3}) take part in the quantitative assessment of the H_2O destruction. As it will be discussed further about the formaldehyde profile, the predominance of the destruction path with C^+ before 10^3 years is easily explained through abundance effects, all of the considered reaction paths being of the same nature (ion-molecule reaction, with the implicated molecule being the same) and the modelled clouds staying constant in time in terms of density and temperature. The C^+ cations is indeed very abundant (as compared to other atoms) at early times; actually, as stated by Prasad and Huntress (1980b), the formation of cationic species in dense molecular clouds in all astrochemical models begins with the CR ionization of He, followed by a dissociative charge transfer with the very abundant CO molecule, leading to C^+ production. It is therefore almost the first atomic ion produced in such a dense system, explaining its high abundance at early times. Yet, regarding the highly complex interwoven shape after 10^3 years, the chosen value of X is questionable, as it will be discussed when perturbing the model parameters, as previously mentioned.

In the cases of **HCN** and **H$_2$CO**, their profile is more complex. HCN appears first, dominating the H_2CO profile for the first $\sim 10^3 - 2.10^3$ years. Thereafter, H_2CO profile overhangs the HCN curve, until a kind of stabilisation (towards a chemical equilibrium) of both profiles after 10^6 years at an abundance of $\sim 10^{-9}$ with respect to the hydrogen nuclei abundance. However, one has to keep in

---

[3]H_3^+ is stable in the ISM due to the low temperatures and densities prevailing in it, and takes the form of an equilateral triangle. In dense clouds, such a system with 3 centers and 2 electrons is mainly formed by the reaction of H_2 with H_2^+, and destructed through proton transfers to other species (mostly CO); its destruction is mainly achieved via dissociative recombinations in more diffuse media. The astrochemical role of H_3^+ is of prime importance. Oka (2013)

mind that we have not considered a network characterized by a high complexity limit. Therefore, those results have to be regarded with a great care, without jumping to any premature conclusions. Indeed, HCN and H_2CO are expected to be the starting point of pathways towards more complex species, those pathways themselves being likely interconnected to other astrochemical pathways. As it will be discussed in Chapter 4, the network has to be extended to be able to discuss more and more complex species, approaching progressively the most direct glycine precursors. As a consequence, it would therefore be worthwhile comparing this present discussion with the results from an extended network in order to investigate the model synergy.

Furthermore, one may *deeper insight* into the *formaldehyde* precursor. As shown in Figure 2.2, Prasad and Huntress (1980a) schematized a simplified astrochemical network, gathering the main formation/destruction processes of H_2CO. They based this scheme on their computations performed with their astrochemical code. The latter was fundamentally similar to Astrochem (pure gas-phase), next to their associated astrochemical network, less complete and less constrained in terms of kinetic data. Actually, it consists of 1400 reactions involving 137 species, in contrast to the used network included in the Astrochem source code, consisting in a huge set of 6046 reactions for 472 species. One may therefore wonder about the influence of the extent of the network on the inferred results. Naturally, we can not analyse reactions one by one to compare the complexity limit of the two networks, but the complexity limit of the Astrochem network seems a bit higher, dealing with small organic compounds. Concerning the accuracy of their kinetic parameters, the network of Prasad and Huntress (1980a) seems less rigorous. Indeed, as reported, kinetic constants are tarnished by some uncertainties and assumptions. The Astrochem network is based on more rigorous data, from the Ohio State University (OSU) data base. As mentioned before, this database catalogues a huge set of astrochemical reactions and their kinetic parameters, with an indication whether the indexed quantities have been checked and confirmed or not. Given the huge improvement of our empirical and computational methods since the 1980's, the kinetic parameter determination has become more and more rigorous. In terms of completeness, the difference between the two networks is a bit more difficult to assess by such simple considerations. Indeed, a network may include many more species, and may at the same time display a lower completeness (by focusing on the inclusion of a lot of species, one may forget to keep a high completeness, which is actually a challenging work since one has to think about a lot of possible processes). Therefore, one has to push our comparison further. From a qualitative point of view, the main formation/destruction routes for the H_2CO molecule inferred from both Prasad/Huntress (PH)'s and Astrochem models can be compared. Such a comparison would at least allow to enable us to compare the completeness in the inclusion of the main contributors. In this scope, the results for the 12 main formation/destruction routes for H_2CO for model 1a are given in Figure 3.3, knowing that H_2CO is present in 153 processes in the Astrochem network (Table 2.1).

Comparing these results to the PH's results summarized in Figure 2.2 (from simulations of diffuse and dense molecular clouds), we find a clear global agreement. Regarding the main H_2CO formation routes, our results indicate that the reaction $O + CH_3$ is the main contributor to the formaldehyde formation in a pure gas-phase system (defined by model 1a). The predominance of this route is clearly maintained all along the simulation. Another formation route also displaying an appreciable contribution, especially after 10^5 years, is the dissociative electronic recombination $H_3CO^+ + e^-$. The other formation routes listed in Figure 3.3 do not contribute significantly to the total production of H_2CO, at least for that modelled cloud. Comparatively, Prasad and Huntress (1980a) also reported the reaction of CH_3 with oxygen to be the main formaldehyde formation route in all of their four modelled homogeneous interstellar clouds (diffuse, at 110 K and 22 K, to dark clouds at 50 K). They also reported that the dissociative electronic recombination of H_3CO^+ towards H_2CO is not negligible.
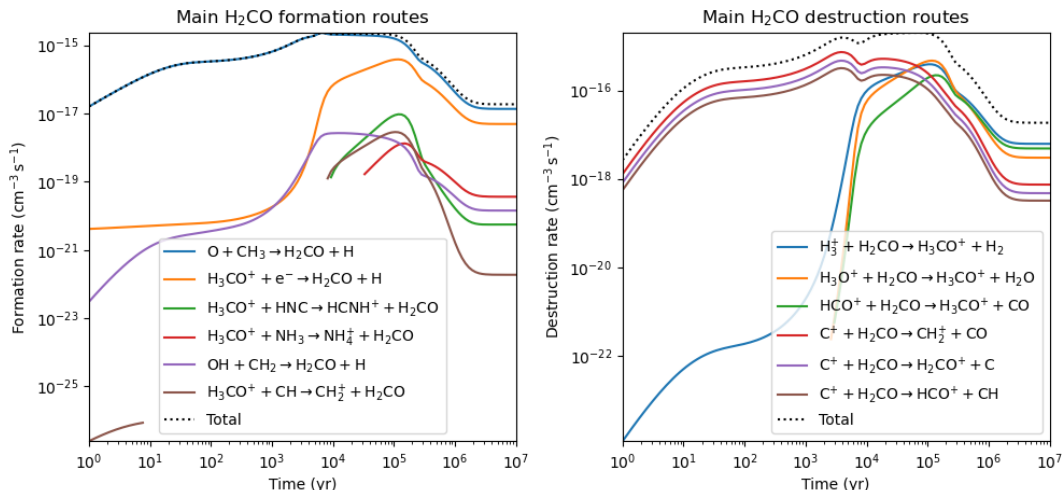
Figure 3.3: Main gas-phase formation/destruction routes for formaldehyde, from **model 1a** (Astrochem computation).

In terms of the main destruction routes, our results (Figure 3.3) are indicating several significant contributors. Before $\sim 10^3$ years, the reactions with the C^+ species dominate the destruction routes of H_2CO. Then, reactions with H_3^+, HCO^+ and H_3O+ ions take over, leading to the production of H_3CO^+ ions. This inversion of dominant mechanisms can be very intuitively explained by simple effects of relative abundances[4], as checked through Astrochem computations (see Figure B.1 in Appendix B for a visual demonstration). Regarding the PH's results from their diffuse and dense molecular clouds simulations, 5 out of the 6 main destruction routes inferred with our 1a model are reported. Actually, the 3 destruction routes invoking C^+ ions are considered as part of the main destruction routes illustrated in Figure 2.2, as well as the reaction with H_3^+. Even if that is not highlighted in their summary scheme (Figure 2.2), they also have identified the reaction of formaldehyde with HCO^+ to take also significantly part to the formaldehyde destruction channels. They however have not reported about the contribution of destruction route involving H_3O^+, which can arguably be due to a difference in the kinetic parameter encoded for this process in Prasad and Huntress (1980a). Indeed, as stated before, the kinetic parameters used by PH are tarnished with more approximations than the ones encoded in Astrochem, which are inferred from more recent predictions. This hypothesis can be checked by accessing the PH's network (see their upstream publication describing their code, Prasad and Huntress (1980b)): once the inclusion of H_3O^+ has been verified, the reaction of interest has been identified in the PH's network. Such reactions displays a kinetic constant well described by the Arrhenius' law, as discussed in Table 1.5. Comparing their α, β and γ parameters to the one encoded in the used Astrochem network, some points are worth discussing:

  i. Concerning the α parameter, Prasad and Huntress (1980a,b) considered a smaller value: 1.1 10^{-9} against 2.60 10^{-9} in the network used in the present work.

 ii. The value of β also differs: Prasad and Huntress (1980a,b) adopted a null β exponent, while a value of -0.5 is assumed in the Astrochem network. The impact on the kinetic constant is easy to grasp - a null value leads to a factor $\left(\dfrac{T}{300} \right)^{\beta}$ equal to unity, whereas a β parameter of

---

[4]The modelled clouds being homogeneous and constant in time in terms of mean density, temperature and radiation field, and the considered reactions being all of the same type, therefore presenting kinetic constants apparently of the same order of magnitude.

-0.5 allows this factor to be greater than unity $\left(\sqrt{\dfrac{300}{T}}\right)$. Indeed, since this work focuses on dense molecular clouds, presenting cryogenic conditions, the temperature is far bellow 300 K. Accounting for a temperature range of 10 to 20 K, the $\left(\dfrac{T}{300}\right)^{\beta}$ term ranges from 3.8 to 5.4.

iii. In both Prasad and Huntress (1980a,b) and Astrochem networks, the γ parameter is null, which is consistent with the fact that we are dealing here with an ion-molecule process for which the molecule involved presents a permanent dipole.

Based on these comments, we note that the kinetic constant used by PH for this process is lower than the one considered for this work, due to a lower α parameter combined to a null β exponent. It may possibly explain why PH did not report on the formaldehyde destruction path involving H_3O^+, and highlights the crucial importance of a rigorous determination of the kinetic parameters included in a given network. The fact that this process is not listed in PH's discussions can also be due to differences in the modelled cloud. However, as we will see in subsequent analyses, when modifying model parameters, the reaction with H_3O^+ stays classified as a major path to formaldehyde destruction. Moreover, it is worth mentioning that Prasad and Huntress (1980a) reported on other destruction routes, including the reaction with H^+, He^+, S+ and the photo-dissociation. Concerning the photo-reaction, in our case of dark molecular clouds, we naturally found no footprint in the main destruction routes, the extinction of the radiation field being too high, therefore preventing photons from entering the cloud's interior. In the case of PH's results, in addition to dense conditions, they also studied diffuse clouds, where the photo-reactions are active. Moreover, one has to keep in mind that Astrochem is only able to list the 6 main destruction and 6 main formation routes for each studied species. Regarding the proximity of the curves in the right graph on Figure 3.3 after an elapsed time of 10^4 years, one can therefore not reject the possibility that H^+, He^+, S+ also give a non negligible contribution, but a bit less important than the listed process due to a lower abundance (kinetic constant assumed to be of the same order, the reaction type being the same). This explanation has been checked and approved through Astrochem computations, showing the abundances of H^+, He^+, S+ lower than the typical values of C^+ before 10^3 years, and H_3^+, HCO^+ and H_3O+ abundances after 10^3 years elapsed (see Figure B.2 in Appendix B for a visual demonstration). Coming back to our previous discussion in chapter 2, for the main contributors to the formaldehyde abundance, characterized by a Y value of 153, the chosen X value of 12 (6 associated to destruction routes) can be a quite low, and one may miss some non-insignificant contributors (pastel violet part in Figure 2.6). This postulate will be checked later on in this chapter when perturbing a bit the model parameters.

From a more quantitative point of view, a direct comparison with the PH's results can not be drawn since model 1a does not correspond to any of the 4 models studied in Prasad and Huntress (1980a). In order to be able to rigorously compare our results to PH's results, subsequent studies with another model (model b,§3.3) has to be performed. We will come back to this point later on.

A similar comparison can be drawn for the *hydrogen cyanide*, also studied in Prasad and Huntress (1980a). Figure 3.4 provides the 12 main destruction/formation routes for HCN from our model 1a. From a qualitative point of view, these results are in complete agreement with the summarizing conclusions of Prasad and Huntress (1980a) after analysis of their four models: they considered the reaction with C^+ as the main sink of HCN, to which they added the contribution of the reactions with H_3^+ and HCO^+, both listed in our 6 main destruction paths. From our results, one may also add the reaction with H_3O as a non-negligible destruction route for HCN, not identified by Prasad and Huntress (1980a) arguably for the same reason discussed beforehand regarding the formaldehyde.

Indeed, the HCN destruction path involving H_3O^+ in the PH's network displays a kinetic constant lower than the one considered for this work, due to a lower α parameter ($1.1 \ 10^{-9}$ versus $8.20 \ 10^{-9}$ in the Astrochem network) combined with a null β exponent (gaianst -0.5 in this work). It is also worth to mention that, as for the formaldehyde main destruction paths, after a 10^4 years elapse, the curves of the 6 main contributions are closely interwoven, with some very similar relative contributions. Further in this chapter, we will come back to this point by perturbing slightly the model parameters to check if other non negligible contributors have been missed (Y being equal to 141 for HCN) because of a too small X value. For the main formation pathways, they concluded that the dissociative electronic recombination of $HCNH^+$ and the reaction of N with CH_2 are the greatest contributors, which completely matches our results (see the blue and red curves coinciding with the dotted one). For a quantitative comparison, I refer the reader to subsequent discussions (model b,§3.3), as justified beforehand for H_2CO.
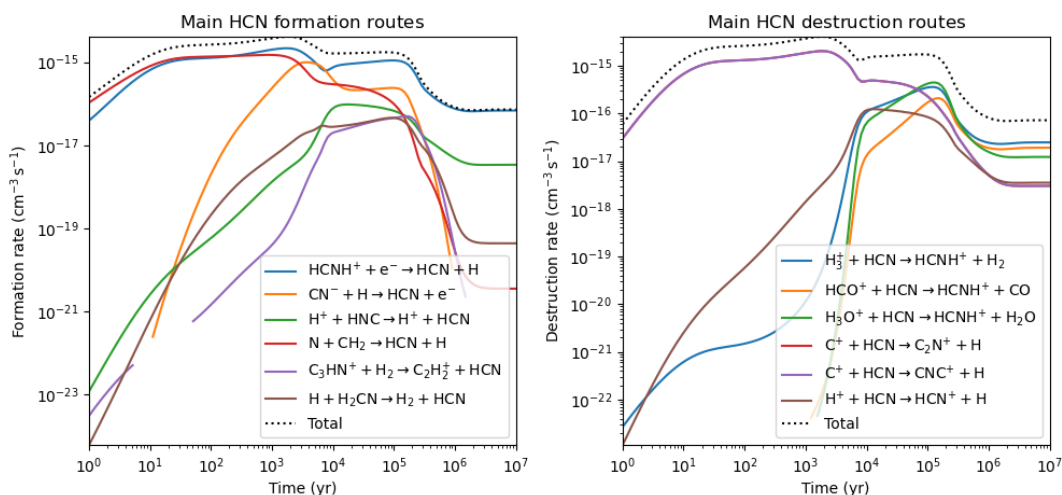
Figure 3.4: Main gas-phase formation/destruction routes for HCN, from **model 1a** (Astrochem computation).

Regarding the **NH$_3$** abundance from model 1a, it quantitatively appears rather late as compared to H_2CO and HCN species. Indeed, we see NH_3 emerging with an abundance of 10^{-12} with respect to the hydrogen nuclei abundance (Figure 3.1) only around $\sim 10^3 - 2.10^3$ years, when HCN and H_2CO are already exceeding 10^{-10} with respect to the hydrogen nuclei abundance. This result is quite interesting and seems to have a potential to be exploited in the context of the discussion of the overall Strecker-like synthesis presented in Figure 1.10. Actually, as stated when discussing this glycine formation mechanism, it can theoretically be archived through two distinct but interconnected pathways (route a and b), depending on the relative abundances of NH_3 and HCN. These are the two candidates for the nucleophilic attack on the formaldehyde in the context of Strecker-like synthesis. From that point and the rather late quantitative appearance of NH_3 as compared to HCN, one can expect the route b to have its own contribution in our modelled cold molecular cloud, provided the activation barriers are not prohibitive at the considered temperature.

From the analysis of the main formation and destruction routes of NH_3 in model 1a (Figure 3.5), the NH_4^+ ion is the main source of ammonia, through a dissociative electronic recombination, ending a cationic chain starting with nitrogen and its cations (as already highlighted by Prasad and Huntress (1980a)). Concerning the main destruction pathway, the reaction with the C^+ ion is dominating

during the first 10^3 years, similarly to HCN and H_2CO. This can easily be explained by the high abundance of this ion during this epoch, as already demonstrated in B.1 in Appendix B. After 10^3 years, reactions with H_3^+, HCO^+ and H_3O+ ions take over, as in the cases of formaldehyde and HCN.
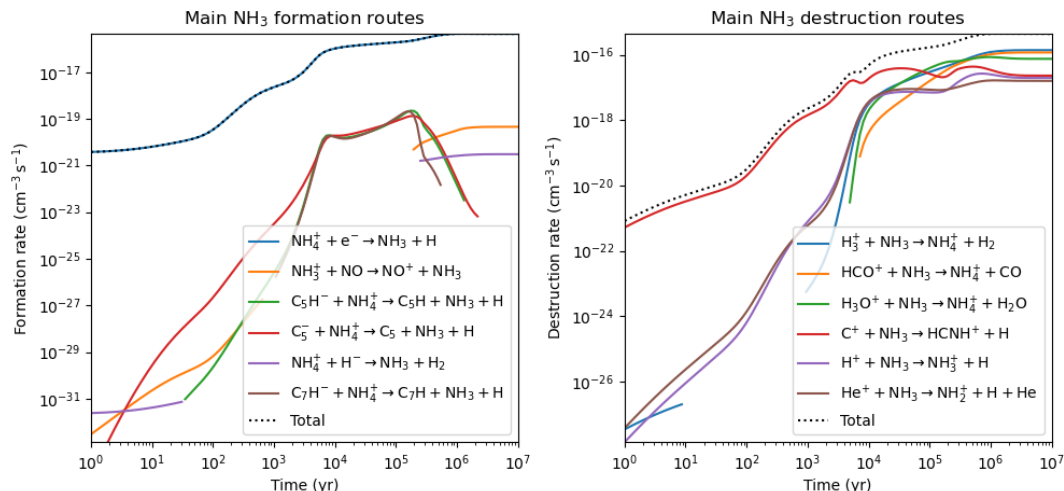
Figure 3.5: Main NH_3 gas-phase formation/destruction paths, from **model 1a** (Astrochem)

To further explain the late appearance of NH_3 with respect to HCN and H_2CO, a comparison of the abundance of their respective main direct source has therefore[5] been performed, as shown in Figure 3.6. As easily seen on this figure, the earlier appearance of H_2CO and HCN compared to ammonia can be rationalized through abundance effects. Actually, NH_4^+ appears quantitatively later than $HCNH^+$, the latter being easily formed not only by a proton capture of HCN with a positively charged proton-bearing ion, but also through the main destruction path of NH_3 itself. Compared to the abundance of HCN, the two formation paths being simple dissociative electronic recombinations, one may therefore expect the HCN abundance to dominate the ammonia profile until the NH_4^+ abundance overcomes the $HCNH^+$ curve, after $\sim 5.10^5$ years. This is exactly what is observed in Figure 3.1. Concerning the comparison between the formaldehyde and ammonia abundances, further considerations have to be taken into account. Indeed, the main formation path towards formaldehyde involves neutral species (O and CH_3), therefore consisting in a neutral-neutral dissociative process. As explained in the introductory chapter, in subsection 1.3.3 (Table 1.5), such neutral-neutral processes are kinetically slow, the only electrostatic interactions involved being Van der Waals forces. On the contrary, dissociative electronic recombinations are barrierless processes associated to larger cross-sections, resulting in greatly higher kinetic constants (several orders of magnitude, see Table 1.5). However, the abundances of O and CH_3 are several orders of magnitude higher than the NH_4^+ abundance for a large time interval, until they become comparable after $\sim 10^5$ years. Such an abundance effect overcomes the lower value of the kinetic constant ruling the main formation route of H_2CO, leading to a higher abundance of H_2CO as compared to NH_3 for a long period of time, until $\sim 10^5$ years, as observed on Figure 3.1. The greater abundance of HCN and H_2CO compared to NH_3 until $\sim 10^5$ years is therefore fully explained by those abundance effects.

---

[5]Actually, as a consequence of the common main destruction agent, we can assume the destruction kinetic constant to be of the same order of magnitude for the reaction of H_2CO, HCN and NH_3 with C^+. These are indeed of the same barrierless nature, the only difference being retrieved in the associated cross-section. This difference should not be large since it implies a common partner, C^+, and H_2CO, HCN and NH_3 are not intrinsically very different in terms of molecular complexity. The difference between the abundance of NH_3 as compared to H_2CO and HCN before 10^3 years can therefore be rationalized as a first approximation by the abundance of their respective main source species.
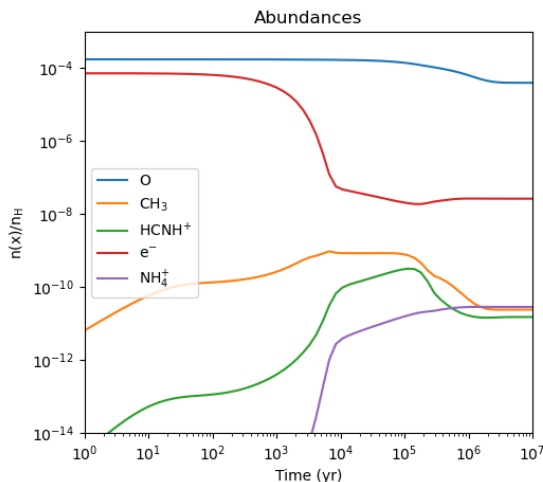
Figure 3.6: Comparison of the abundances of the main source of the precursors of the neutral Strecker-like synthesis: (i) H_2CO, the main source being $O + CH_3$, (ii) HNC, the main contributor being the dissociative electronic recombination of the $HCNH^+$ ion, and (iii) NH_4, for which the main formation path is also given by the dissociative electronic recombination of NH_4^+, ending a cationic chain.

With the aim to deeply explore the potential of route b, the chemical mechanism ruling the reaction between H_2CO and HCN and forming the glyconitrile (equation 1.10) has to be further commented. In that context, results from Woon (2000) indicated an isomerization process during the reaction between H_2CO and HCN or HNC, the reaction with HCN leading to isocyanomethanol ($OHCH_2NC$), while the reaction with HNC yields to the targeted glyconitrile ($OHCH_2CN$). Actually, the activation barrier of the latter is lower (Figure B.3 in Appendix B), thanks to the greater stability of the -CN bound as compared to -NC. Regarding this energetically lower path, one can wonder about the relative abundance of HNC with respect to HCN. Although HCN is more stable than HNC (lower stability of -NC bound), the isomerization towards HCN requires energy, this energy being likely absent at cryogenic temperature (Woon, 2000). In the context of a dense and cold molecular cloud, composed of hundreds of species with their own abundance, we have therefore to take all the possible pathways towards both species into account. Figure 3.7 presents the two profiles inferred from model 1a.
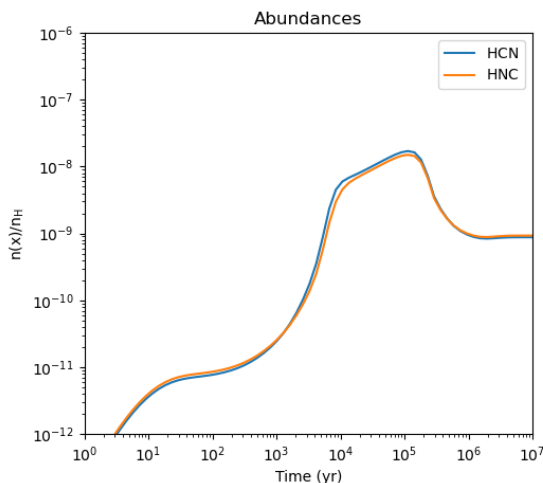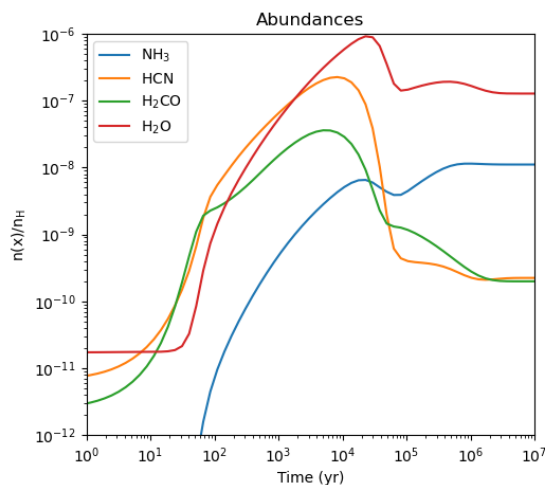
Figure 3.7: Abundances as a function of time for HCN and HNC, computed with Astrochem (from **model 1a** describing a relatively dense molecular cloud at 10K.)

HCN and HNC display very similar abundance profiles, which can be easily understood through their main formation/destruction routes. Actually, comparing Figure 3.4 to Figure 3.8, their main destruction process implies, in both cases, the reaction with the C^+ ion as main contributor (dominating the other contribution until 10^4 years). Such a reaction is a barrierless process (cation-molecule process with HCN/HNC molecules displaying permanent dipole), as described by the null third parameter encoded in the used astrochemical network[6]. The kinetic constant k corresponding to the reactions of HCN/HNC with C^+ are therefore only differentiated by their first encoded parameter, which takes the cross section of each process into account. The main contributions to the destruction of HCN/HNC after an elapsed time of 10^4 years are more complex and intertwinned, with closer contributions. However, among the 6 destruction agents listed as major contributors, 5 are matching when comparing Figure 3.4 and Figure 3.8, with very similar destruction rate profiles for the destruction of both HCN and HNC. All these destruction routes are also barrierless, also invoking the reaction of a cation with a molecule presenting a permanent dipole. Again, the only difference in the kinetic constant between the reaction of each of these cations with respectively HCN and HNC should arise in the cross sections, included in their first encoded parameter. In this context, we have perfomed a check-up of the degree of discrepancy in our network between the first parameter of each couple of reaction with HCN and HNC for each ion listed in the destruction routes in Figures 3.4 and 3.8. From this check-up, it turns out that this discrepancy is very tiny for all couples of reactions between an abundant ion and HCN/HNC[7], which could have been anticipated regarding their similar covalent radii.
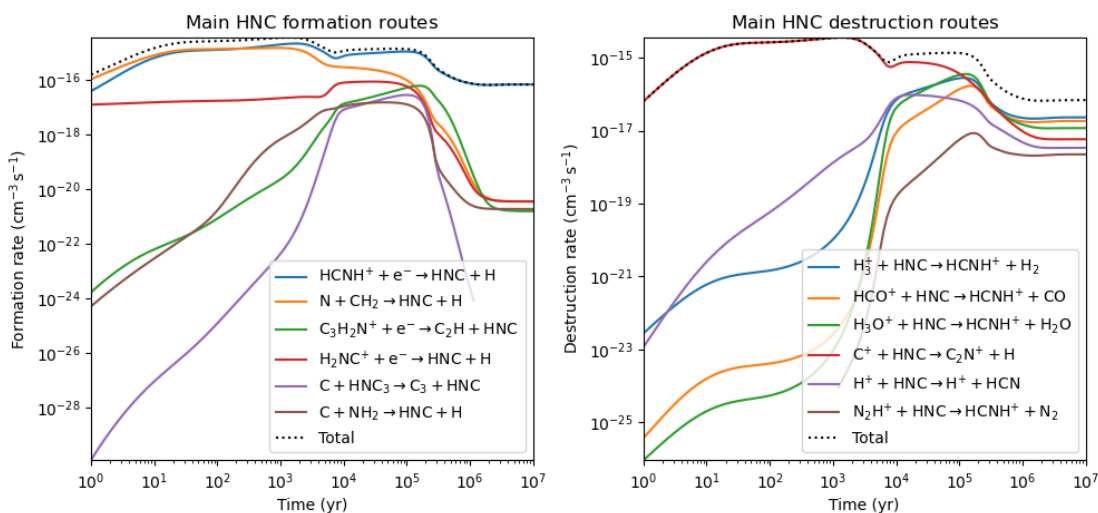
Figure 3.8: Main gas-phase formation/destruction routes for HNC, from **model 1a** (Astrochem).

Regarding the main formation processes, the dissociative electronic recombination of $HCNH^+$ is the main contributor on a large time-scale for both HCN and HNC. Actually, as discussed in the laboratory work performed by Mendes et al. (2012), the dissociative electronic recombination of $HCNH^+$ leads to a production of HNC with a high yield, comparable to HCN production. Indeed, as justified in details in this paper, the internal excitation energy of the HCN/HNC fragment after electronic recombination lies far above the isomerization barrier between HNC and HCN isomers, resulting in an isomeric production ratio near unity.

---

[6]See chapter 2, section 2.2 for the physical meaning of this parameter.

[7]For example, for the reaction with C^+, this parameter is slightly higher for the reaction with HCN ($1.70 10^{-8}$) than for the corresponding process with HNC ($1.50 10^{-8}$).

Additionally, the reaction between N and CH_2 is also listed as a major contributor, as for HCN. Checking the kinetic parameters encoded in the used astrochemical network, we realize that they are exactly the same. One must therefore wonder about the legitimacy of this strict equality in the kinetic parameters used. Searching these reaction in the KIDA data base, we find a difference in the first parameter (alpha parameter, where the cross section is included, as discussed in point 2.2), with an indication that these data have been checked and evaluated as correct. In the KIDA database, we find a first parameter amounting to $5 \ 10^{-11}$ for the reaction towards HCN, while the reaction forming HNC displays an alpha parameter of $3 \ 10^{-11}$. In our used network, it amounts to $3.955 \ 10^{-11}$, therefore between the given value for HCN and HNC from the KIDA database. From our previous discussions, one may expect such approximation not to have any impact on the overall computed abundance profile of HCN and HNC. This has been confirmed when considering these parameters more rigorously via the inclusion of the values from KIDA in our used network, therefore modifying the genuine network from the Astrochem source code. As expected, the computed abundance profiles were very similar, as we got in Figure 3.7 from the genuine, unmodified network.

Finally, for the HNC formation, we need to add the contribution of the dissociative electronic recombination of H_2NC^+ for the first 10^{-2} years, not represented on Figure 3.4.

From this deep comparison of the main formation/destruction processes of HCN/HNC, we can conclude that HCN and HNC have similar abundance profiles in these modelled cloud conditions, after analysing the legitimacy of the proximity of the two profiles. This result is confirmed by the results in Graninger et al. (2014), where they showed that, even taking a gas-grain model, the HCN/HNC ratio is close to unity at cryogenic temperatures.

Assuming a high completeness of the chemical network at this complexity level (which seems reasonable, Y amounting to 51 for HNC)[8], one can therefore expect the reaction HNC + H_2CO to be quantitative, provided the physical conditions of the astrophysical environment are favorable (to overcome the energy barrier). Moreover, the isomerization of $OHCH_2NC$ to $OHCH_2CN$ displays a comparable energy barrier to the HCN/HNC reaction with formaldehyde (see Figure B.3).

Nevertheless, one has to note that, beside the appreciable abundances, these barriers are likely too large to occur at cryogenic temperatures without energy input, despite the enhancement of the kinetics via an icy environment (Woon, 2000). On the other hand, as proposed in Woon (2000), exothermic processes ($\Delta H < 0$) in the medium may generate heat that can drive the beforehand discussed reactions (heat reaction redistribution to the immediate surrounding). However, Woon's considerations are too restrictive, being only valid in cases of processes characterized by an increase of the system entropy. As formerly discussed, all spontaneous chemical processes are not displaying a positive variation of entropy. It is therefore more rigorous to take the free energy variation into account, rather than the limited consideration of the enthalpy variation. In that context, in an exergonic process (ΔG of the reaction < 0), energy is produced at the reaction site, resulting in a energy flow towards the surroundings and affecting the energy budget of the immediate environment. In the scope of cryogenic conditions, the redistribution of the energy stemming from exergonic reactions could thereby provide the missing energy to overcome some activation barriers, prohibitive at such temperature conditions.

In other words, considering the thermodynamics lying behind an astrochemical system

(i) enables more rigorous considerations of the energy budget of the system and its partition;

---

[8]To get rid of the possibility of a lack of some major destruction processes for HNC, leading to a significant decrease of the HNC profile compared to the HCN one.

(ii) in the peculiar context of cryogenic temperatures, this effect is expected to have a non-negligible contribution (the energy budget being quite limited), likely leading to systems with more energy available than without taking this effect into account.

However, this suggestion deserves more comments. Let us bear in mind that Astrochem is only considering gas-phase transformations, without accounting for any grain mantle chemistry or reactions at the icy surface. The Woon' suggestion has been postulated in the context of icy environment chemistry, for which the densities are totally different from the very low densities prevailing in gas-phase. Reaction sites in icy-mantles or at surfaces are therefore much closer on average, and the possibility of reaction heat redistribution is more conceivable than in the gas-phase. Moreover, a point that can not be neglected is the fact that thermodynamical quantities are not taken into account in Astrochem, and more globally in any Astrochemical model aimed at inferring abundances as a function of time. Actually, as described in chapter 2, in section 2.2, Astrochem is based on an astrochemical network, composed of a list of reactions, together with their respective set of kinetic parameters needed to characterize their kinetic constants. No thermodynamic quantities are taken into account, and no equation ruling heat redistribution has been implemented in the code. In any case, this heat redistribution from exothermic reactions can nevertheless not be investigated. In gas phase, at cryogenic temperatures and from a pure neutral pathway, one can therefore anticipate the b route to be insignificant from Astrochem analysis at cryogenic temperatures (the kinetics being inhibited due to the activation barrier and not the abundance of the species of interest).

Notwithstanding, this thorough analysis of the potential of route b brought deep insights into its general feasibility in cryogenic interstellar conditions. These results can be of great interest in the scope of a prospective future astrochemical code, with greatly enhanced capacity to consider the chemistry playing out in icy dust grain mantles in cryogenic conditions, its interplay with the gas phase as well as of the reaction heat redistribution.

> *Deeper comments*: One can indeed imagine the HNC and H_2CO species to be adsorbed on icy surface of dust grains, on the top layer. This layer may be surmounted by additional layers over time if no desorption arises before the formation of this superior layer. In the rest of this reflection, we will assume that the thermal migration is prohibited, except for H atoms, regarding the cryogenic temperatures of the densest interstellar parts. We will therefore consider the icy mantle (surface) chemistry to be only statistical, depending on the potential candidate reaction partner in the surrounding of each species. From those considerations, regarding the quantitatively rather appreciable gas phase HNC/H_2CO abundances, if the accretion of those two species is quantitatively not negligible, one can conceive that the $HNC + H_2CO$ reaction arises in an icy mantle (or at their surface) provided they are in the surrounding of each other, in a place close enough to an exergonic reaction to ensure the climb of the activation barrier.

Finally coming back to ammonia (Figure 3.1), after $\sim 10^5$ years, the ammonia abundance becomes comparable to the HCN content. It then stabilises at an abundance of $\sim 1.10^{-8}$ with respect to the H nuclei abundance. As previously stressed out, one has to be careful not to draw hasty conclusions before having tested the model synergy when facing astrochemical network extensions. In a situation where NH_3 undergoes quick transformations with another compound of similar/higher abundance, this computed abundance is biased if this hypothetical reaction is not genuinely taken into account in the network.

Moreover, one can wonder about the influence of a change in the physical parameters describing the beforehand used model 1a. As seen in Chapter 1, paragraph 1.3.2, the two physical

parameters governing the kinetics of a process are the density of the medium, and its temperature. In this scope, we will modify the temperature and hydrogen number density independently, while staying in the typical range of values for dense interstellar clouds (cf. Table 1.3).

Concerning a change in the density of the considered cloud, keeping the temperature unchanged from model 1a, we have built a second model (Table 3.1), named **model 2a**. The corresponding temporal evolution of the abundance of H_2CO, NH_3, H_2O and HCN is given in Figure 3.9.

Figure 3.9: Respective abundances as a function of time for H_2CO, HCN, NH_3 and H_2O, computed with Astrochem (from **model 2a** describing a dense molecular cloud at 10K.)

As compared to the results from model 1a (Figure 3.1), abundance profiles are impacted by such an enhancement of the H nuclei abundance from an appreciable value of 10^4 cm^{-3} to 10^6 cm^{-3}, the highest values found for interstellar clouds. From pure theoretical considerations, based on the collision theory introduced in chapter 1 (§ 1.3.2), an increase of the overall density of the medium leads to an increase of the collision frequency. Indeed, regarding equation 1.1, defining the rate of disappearance of a reactant A in case of an hypothetical bimolecular transformation[9], the factor Z_{AB} strongly depends on the number densities in reactants. Without any temperature increase, the f factor from the same equation remains unchanged. In other words, the thermally inhibited reactions in model 1a are also inhibited in model 2a, the activation barrier being impenetrable in both cases. From that reflection in our reflection, we know that, for an isolated process, an increase of the overall density of the reaction medium will lead to an increase of the rate of disappearance of the reactants and of the formation of product(s). However, in this present work, we are far from studying isolated reactions, but rather a complex network made of interconnected pathways towards the hundreds of included species. Therefore, a given species is both the reactant and the product of a set of transformations. As highlighted in chapter 2, paragraph 2.2, considering the 472 included species, the average number of reactions is 54 per chemical entity, and the median amounts to 20. For each of the studied species, one consequently has to consider this inter-connectivity as a whole to rationalize the effect of passing from model 1a to model 2a on the computed abundances profiles. It requires a deep analysis of the main formation/destruction paths.

---

[9]This rate of disappearance being easily related to the rate of appearance of products through simple stoechiometric logic.

Before entering such a detailed analysis, when comparing Figures 3.1 and 3.9, one easily notices that all the curves seem to have been broadened to the left when going from model 1a to model 2a. As above-discussed, this can be rationalized very intuitively, an increase of the overall density of the considered medium should lead to an enhancement of the collision frequency, activating the kinetics of the astrochemical system. The abundance profiles are consequently broadened to the left, meaning an earlier quantitative appearance of the species of interest.

Regarding the *tendency* towards a *chemical equilibrium*[10] (horizontal abundance profiles), it seems to be established after a similar elapsed time interval ($\sim 1\,10^6$ years) in both model 1a (Figure 3.1) and 2a (Figure 3.9). In other words, the time-scale needed to reach the *chemical equilibrium* appears to be independent on the hydrogen initial density. This result confirms the discussions found in the early theoretical kinetic study performed by Iglesias (1977). Actually, he drew his conclusions on the general postulate that the main formation/destruction mechanisms for minor species are largely dominated by pathways involving abundant species such as O, N, C, e^-, H_2 etc. Moreover, the formation time of major molecules (e.g. O_2, N_2, CO, ...), before reaching steady state abundances, is roughly equal to the depletion time of their parent atoms, until reaching steady concentrations. The chemical equilibrium time scale is therefore expected to be governed by the time interval needed for these major species to reach steady state abundances. As a consequence, there exists a direct link between the abundance profiles of minor species and the ones for the dominant chemical entities - the abundance profiles of the minor species reach steady behaviour quite simultaneously, in correlation to the tendency towards chemical equilibrium for the most abundant and dominating species[11].

Based on these considerations, Iglesias (1977) actually expressed the chemical equilibrium time-scale as the depletion time of the most abundant parent atoms (H, C, N, O). Considering modelled clouds with the hydrogen initial density ranging from 10^4 to 10^6 cm^{-3} and a negligible molecular condensation on the dust grain surfaces (see their first two simulations)[14], he showed that this equilibrium time scale amounts to $1 - 4\,10^6$ years (depending on the elemental composition of the considered cloud) and is insensitive to the initial hydrogen number density. This theoretical computation has been confirmed by results from their very simple astrochemical model, including 52 species and 150 processes, and is completely matching our results. In addition, the inferred expression of the equilibrium time scale in Iglesias (1977) displays an inverse dependency on the cosmic ray (indirect or direct) ionization rate ξ (see discussion in Chapter 2, § 2.2 for its adopted value). This can be very intuitively understood; the modelled interstellar clouds whether in Iglesias (1977) or in this present study are aimed at mimicking the conditions prevailing in the interior of dense molecular clouds. The extinction of the incident electromagnetic radiation is therefore very high (in our simulations, the visual extinction is equal to 20 mag), preventing any direct photo-chemical processes. Otherwise, CRs are able to penetrate the clouds' interior, leading either to ionisation and dissociation processes, as well as indirect photo-reactions, as discussed in Chapter 1, § 1.3.3. One may therefore intuitively predict that an increase of the cosmic ray (indirect or direct) ionization rate (ξ) will lead to an increase of the ion content of the dense clouds. Since CR-interactions constitute the only cation source in such conditions, the relative increase in cationic abundances will be considerable, leading to an activation of the whole kinetic of the system. One may consequently understand that an increase in ξ parameter will lead

---

[10]Keeping in mind the low complexity limit of the genuine Astrochem network as compared to the precursors studied here (at least for species that can be of interest in the case of the study of the selected glycine pathways). Depending on the kinetics of the added processes in a future network extension, these equilibrium may turn out to be 'pseudo-chemical equilibrium', unstable when facing a network extension.

[11]The interested reader is referred to Figure B.8 in Appendix B, and Figure 1 and 2 in Iglesias (1977) for a visual demonstration.

[14]As a reminder, even if Astrochem is able to consider freeze-out and desorption processes regarding the code, no reaction included in the used network corresponds to such type of processes. The two first simulations performed in Iglesias (1977) are therefore the best to be compared to our results.
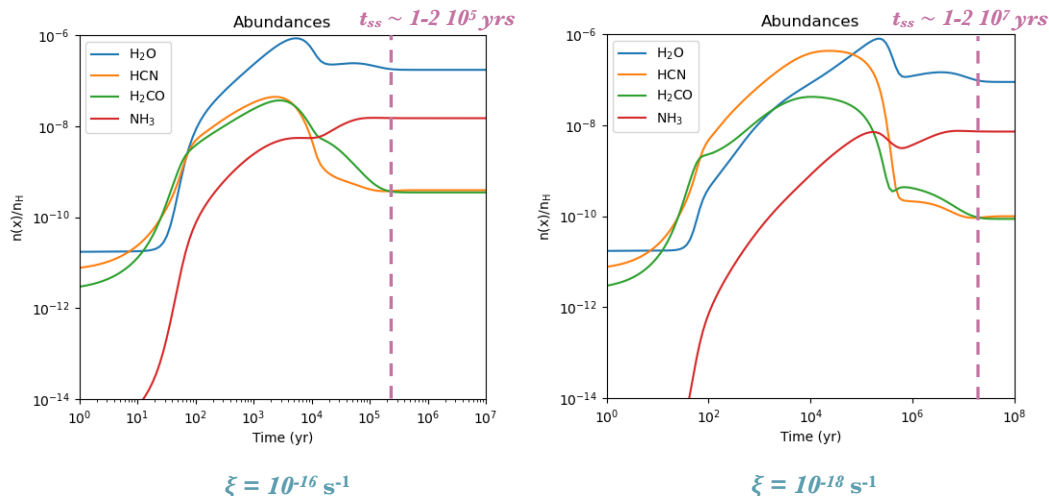
Figure 3.10: Temporal evolution of the abundance profiles for the four precursors of the Strecker-like synthesis, from **model 2a** (Astrochem) - Contrary to the previously studied temporal abundances, the value of ξ [13] has been modified from its commonly adopted value of 1.3×10^{-17} s^{-1} for the study of its influence in the chemical equilibrium time scale (t_{ss}): (*left*) $\xi=10^{-16}$ s^{-1}, arguably reminiscent of fringe regions of dense clouds (Herbst and Klemperer (1973)), (*right*) $\xi=10^{-18}$ s^{-1} , only valid for very dense cloud interiors for which the H$_2$ column density is much greater than 10^{24} cm^{-2} (Herbst and Klemperer (1973)).

to a decrease of the chemical equilibrium time scale (and inversely for a ξ decrease), reached earlier. This effect is illustrated in Figure 3.10 presenting the results of a change in the adopted value of ξ from its commonly adopted value of 1.3×10^{-17} s^{-1} (mentioned in the input file), keeping the same main physical parameters described by model 2a (Table 2.2), mentioned in the source file.

From these points, one may wonder in which conditions the ξ can undergo changes from its standard value. In both studies, one unique cell has been considered for the computations, without accounting for any radial distribution of the initial hydrogen density. However, the density distribution in a real molecular cloud is not constant all along the cloud. As a first approximation, a more realistic case can be defined as a cloud presenting a radial increase of the mean density in molecular content when going from the border towards the center. Moreover, one may expect the ξ value to decrease when going towards the center - the incident flux of CRs should decrease by passing through the cloud since a part of them progressively lose their energy through interactions with species in their trajectory. Combining these considerations, the propositions found in Herbst and Klemperer (1973) can easily be rationalized. Actually, they suggested that a value of ξ higher than 1.3×10^{-17} s^{-1}, for instance 10^{-16} s^{-1}, is arguably reminiscent of the fringe regions of dense clouds. In such border regions, it is worth mentioning that the direct photo-chemistry is still active, leading to an even higher enhancement of the ion content and a clear change in the dominating chemical processes at work. On the other hand, Herbst and Klemperer (1973) discussed that ξ as low as 10^{-18} s^{-1} is only valid for very dense cloud interiors for which the H$_2$ column density is much greater than 10^{24} cm^{-2}.

Furthermore, from a quantitative point of view, the abundances reached at such *chemical equilibrium* are given in Table 3.2.

As one may easily realize, the discrepancy between model 1a and 2a in terms of the computed abundances at chemical equilibrium for the classical Strecker-like synthesis precursors is tiny compared to the enhancement of the initial hydrogen density, of two orders of magnitude (10^2). In fact, based

Table 3.2: Quantitative comparison of the abundances reached at *chemical equilibrium* with model 1a, 2a and for the classical Strecker-like synthesis precursors

	H_2CO	HCN/HNC	NH_3	H_2O
model 1a	$6.3 \ 10^{-10}$	$8.5 \ 10^{-10}$	$2 \ 10^{-8}$	$2.5 \ 10^{-7}$
model 2a	$1.8 \ 10^{-10}$	$2.1 \ 10^{-10}$	$1 \ 10^{-8}$	$1.2 \ 10^{-7}$
model 3a	$5.7 \ 10^{-10}$	$1.13 \ 10^{-9}$	$4.20 \ 10^{-8}$	$3 \ 10^{-7}$

on Table 3.2, for each of the studied molecular entity, the computed abundances in both models 1a and 2a have reached abundances of the same order of magnitude - the discrepancies range from a factor 2 to 4 (compared to a factor 10^2 for the H nuclei density enhancement).

In the first instance, this result can be linked to Herbst and Klemperer (1973)'s considerations in which they discussed the much slower variations of their computed abundances for various molecular species compared to their imposed changes in the H_2 density. Actually, they rationalized their finding through very simple and basic reflections: from a general point of view, species are both created and destroyed by gas-phase transformations. Consequently, they considered that a change in the mean initial density of the simulated cloud is expected to induce a nullification of the changes in the rate of formation and destruction. In other words, following their idea, the abundances are expected to be relatively stable with respect to the initial mean density, provided the ξ value remains unchanged.

However, it is worth mentioning that these very simple considerations in Herbst and Klemperer (1973), even if very convenient to explain our results, are quite restrictive. The reality is more complex, and more advanced principles should be included. From theoretical considerations, let us consider a given species included in the network, characterized by its Y value (number of associated processes, as defined in Chapter 2, § 2.2). One may distinguish 3 cases of study, namely:

a) Species more represented in quantitative destruction paths than in production routes. In other words, this first hypothetical case refers to species that are rather considered as a reactant in their main contributor processes. In such a context, the enhancement of the initial hydrogen density (from model 1a to 2a) should lead to a decrease of its final abundance. Indeed, its disappearance rate should increase due to the increase of the collision frequency.

b) Species for which the number of non-negligible formation paths is greater than the number of quantitative destruction processes. This second hypothetical case therefore refers to chemical entities that are rather considered as a product in its main contributing included processes.

Theses species are expected to be approaching the molecular complexity limit of the network, or at least its boundaries[15]. In such a context, the enhancement of the initial hydrogen density (from model 1a to 2a) should lead to an increase of its final abundance.

c) Species behaving like intermediate of reaction with the respective contribution from quantitative production and destruction paths being similar. In such an intermediate case, an increase of the initial hydrogen density (from model 1a to 2a) should not lead to any significant change in the computed final abundance. The considerations in Herbst and Klemperer (1973) are only valid for this third type of chemical entity.

---

[15]The *boundaries* of a given astrochemical network are considered to be constituted of chemical entities with no quantitative destruction processes included in the network. These boundaries have to be regarded with caution, and one has to deeply evaluate if this lack of quantitative destruction process is simply an omission from the scientist selecting the processes that should be included, or if it is intrinsically due to the reactivity of the considered species. Actually, as rightly stated by Herbst and Klemperer (1973), "The chemistry of dense clouds is complex because of coupling among the many reactions that must be considered. By far the most serious difficulty in the present work is obtaining assurance that all relevant reactions have been included.".

On top of these very simple considerations, the reaction type and the order of each quantitatively contributing reaction may also play a role, since the kinetic influence of densities does not manifest the same way depending on the reaction order.

In principle, this more rigorous approach can be used to investigate the impact of a enhancement in the initial hydrogen density. From a practical point of view, once the main formation/destruction paths are identified, one must refer to equation 1.5 and the discussion related to it. Actually, a chemical equilibrium is defined as a situation where the composition of the system does not change anymore. In other words, the formation and destruction of species at chemical equilibrium occur at the same rate. Knowing the general form of a rate equation (see Table 1.4), the abundance of a given species can be expressed. Let us take ammonia as an example[16],

NH_3 is mainly formed through dissociative electronic recombination [17]. Moreover, the destruction of NH_3 is principally achieved via reaction with C^+, H_3^+, HCO^+ and H_3O+ ions. At chemical equilibrium, one can write that the destruction rate is equal to the production rate, which can be mathematically expressed by:

$$k_{1(+)}.n_{NH_4^+}.n_{e^-} = k_{2(-)}.n_{C^+}.n_{NH_3} + k_{3(-)}.n_{H_3^+}.n_{NH_3} + k_{4(-)}.n_{HCO^+}.n_{NH_3} + k_{5(-)}.n_{H_3O^+}.n_{NH_3}$$

where $k_{1(+)}$ stands for the kinetic constant of the dissociative electronic recombination (the "+" highlights its production role for the studied species), and $k_{2,3,4,5(-)}$ for respectively the ion-molecules reactions implying ammonia and C^+, H_3^+, HCO^+ and H_3O+ ions.

Isolating n_{NH_3}, one gets the following expression for the ammonia abundance at chemical equilibrium:

$$n_{NH_3} = \frac{k_{1(+)}.n_{NH_4^+}.n_{e^-}}{k_{2(-)}.n_{C+} + k_{3(-)}.n_{H_3^+} + k_{4(-)}.n_{HCO+} + k_{5(-)}.n_{H_3O+}}$$

Starting from such an expression, the dependency of each density term on the initial hydrogen density has to be evaluated through the same strategy. It therefore requires a deep analysis of each term in the equation. Such task is not straightforward, and was performed in Iglesias (1977) (under some approximations). For instance, he showed that the gas-phase equilibrium concentration of the H_3^+ roughly behaves as proportional to the inverse of the initial abundance in hydrogen nuclei. This has been validated through Astrochem computations, as demonstrated in Figure B.9 in Appendix B - an increase of two orders of magnitude in the initial hydrogen atom abundance (model 1a to 2a) leads to a decrease of about two orders of magnitude in the equilibrium abundance of H_3^+. Moreover, he proved that the gas-phase ammonia equilibrium abundance is insensitive to variations in the initial hydrogen abundance. Following his considerations, the same is true for the water abundance, and the equilibrium concentrations of H_2CO and HCN behave much more slowly than the initial hydrogen density. These considerations match our results in Table 3.2: the computed abundances are almost insensitive to the enhancement in the initial hydrogen density (factor 10^2), within a factor 2 to 4.

Finally, before addressing the influence of a change in the temperature of the considered cloud, it is interesting to come back to our discussion from model 1a. As mentioned in the analysis of the main formation/destruction processes of the studied precursors, the value of X chosen by the Astrochem authors can be questioned. The analysis of the main formation/destruction routes from model 2a is therefore a great opportunity to discuss this point in details.

---

[16]As we will see in subsequent discussion, the main contributor processes are unchanged from model 1a to 2a for that species. It has been chosen as example for the sake of simplicity and clarity of the present discussion.

[17]That is theoretically a first order process, but is considered as a second order process by some authors such as Iglesias (1977) and Maret and Bergin (2015). We will assume a second order in this discussion.

Starting with **H_2O** (Figure 3.11), it is principally formed via processes involving the H_3O^+ ion. During the first 10^2 years, the early implication of the $O^- + H_2$ reaction is added, which is very interesting when compared to the results obtained for model 1a. Indeed, in model 1a, we discussed the absence of listed main water formation processes for the first 10^2 years, pointing towards a too low X value. This hypothesis is therefore verified. Moreover, let us note that the electronic recombination is not anymore the dominating water formation process over the whole time interval after 10^2 years; the contribution of the reaction with HCN (presenting a permanent dipole) has been added. It highlights the complex influence of an increase of the mean density of the medium, as discussed before. Concerning the main destruction paths, the same processes are listed for both models 1a and 2a.
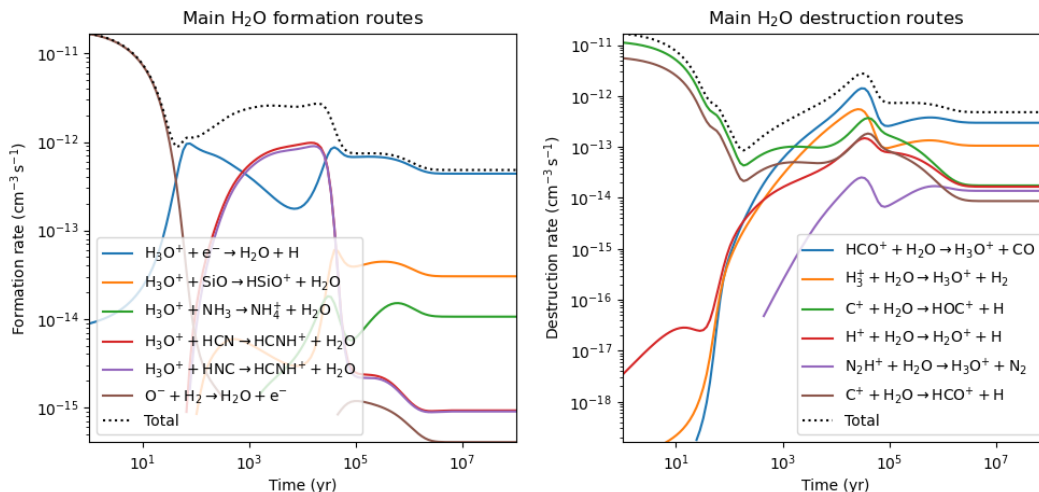
Figure 3.11: Main gas-phase formation/destruction routes for H_2O, from **model 2a** (Astrochem).

Concerning **H_2CO** (Figure 3.12), one can observe differences regarding both the major destruction and formation agents. In model 1a, the total formation rate could be retrieved by just considering the contributions from the $O+CH_3 \rightarrow H_2CO+H$ process combined to the dissociative electronic recombination of H_3O^+ ions. For model 2a, another non-negligible contributor to the formaldehyde formation between 10^2 and 10^4 years has to be taken into account: $H_3CO^++HCN \rightarrow HCNH^++H_2CO$. This process has been listed in the main formation/destruction process of H_2CO in model 1a, but has offered a negligible contribution to the total formation rate. This effect is quite interesting in the context of the discussion of the non-equilibrium chemistry and its non-linear effects, as we will discuss further. Concerning the destruction routes, the reaction with the C^+ ion dominates in both models until 10^3 years. After this time has elapsed, as we have seen in model 1a, reactions with H_3^+, HCO^+ and H_3O+ ions take over, leading to the production of H_3CO^+ ions. In model 2a, after 10^3 years, the same processes dominate, except that an additional transformation of formaldehyde has to be accounted for: $HCNH^++H_2CO \rightarrow H_3CO^++HCN$. This process was not listed in the main destruction paths in Figure 3.3 but is significant, especially between 10^2 and 10^4 years, for model 2a. This result firstly indicates that the X value is rather small for the study of H_2CO. Moreover, coming back to the non-equilibrium chemistry (defined by the time-interval before reaching steady-state abundances), it is worth stressing that the additional non-negligible formation process playing a role in model 2a is exactly the inverse of the H_2CO destruction paths added in model 2a compared to model 1a. It arguably explains the change of dominance of the abundances profiles of H_2CO with respect HCN between 10^3 and 10^4 years: in model 1a, during that epoch, HCN abundance is smaller than the H_2CO one (Figure 3.1). The inverse is true for model 2a (Figure 3.9). Regarding the non-

negligible contribution of $H_3CO^+ + HCN \rightleftharpoons HCNH^+ + H_2CO$ in model 2a, the inverse transformation is apparently of greater influence during that epoch. This is exactly what we see on the right panel on Figure 3.12, where the greatest contributor to the H_2CO destruction is this $HCNH^+ + H_2CO$ process, clearly dominating the other contributions over that time interval[18]. This non-equilibrium effect is expected not to have a quantitative impact on the computed equilibrium H_2CO abundance, the contribution of both the inverse and direct transformations cancelling each other on average.
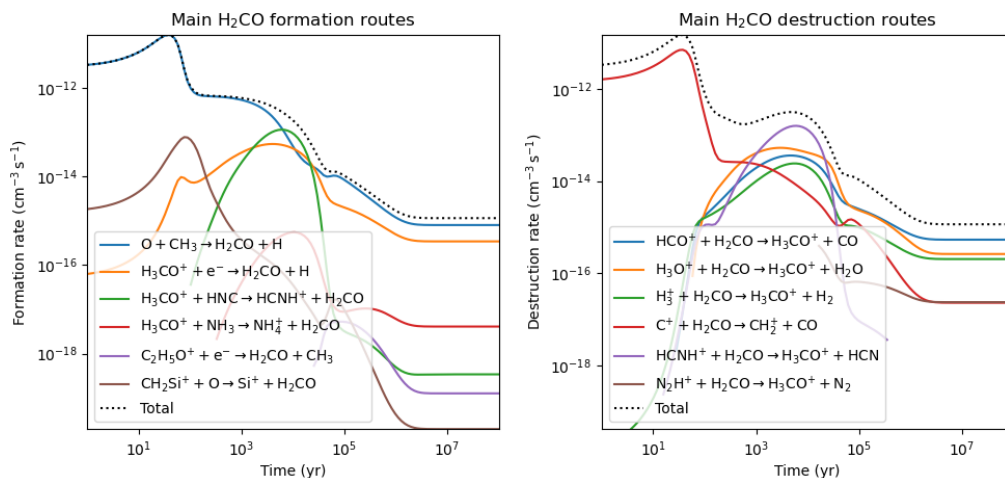
Figure 3.12: Main gas-phase formation/destruction routes for H_2CO, from **model 2a** (Astrochem).

Moreover, regarding the case of **HCN** (Figure 3.13), we retrieve the same main formation/destruction paths in both models. Furthermore, even if the major production routes coincide, there are differences
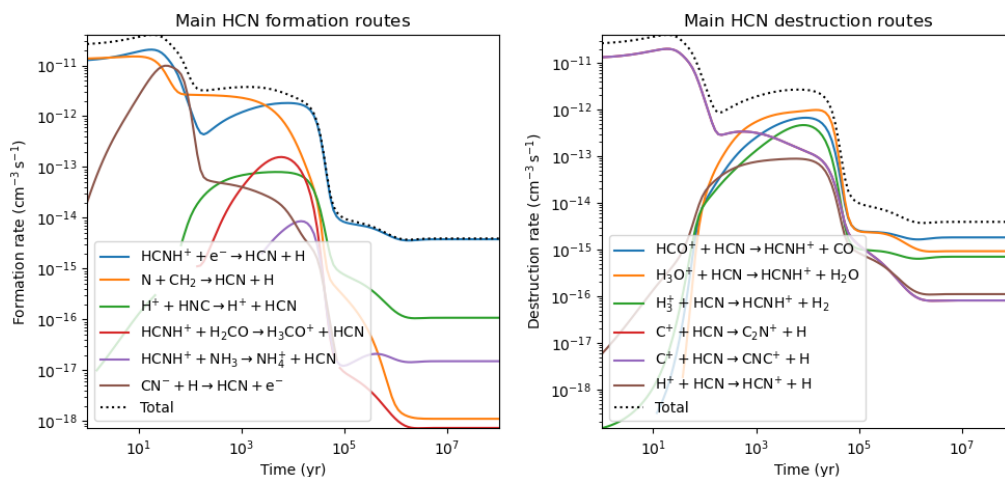
Figure 3.13: Main gas-phase formation/destruction routes for HCN, from **model 2a** (Astrochem).

---

[18]It should be noted that the formation/destruction rates corresponding to $H_3CO^+ + HCN \rightleftharpoons HCNH^+ + H_2CO$ display very similar temporal evolution (Figure 3.12). However, their contribution does not vanish; one has to consider the other contributors and their relative importance with respect to that reversible process. In the case of the H_2CO production rate, the curve corresponding to $H_3CO^+ + HCN$ only dominates the blue and yellow curves during a tiny fraction of time. In the case of the destruction routes, the reaction $HCNH^+ + H_2CO$ dominates over a larger time interval, with a clear predominance on the other contributors. The impact of this reversible reaction in therefore not null, and leads to an increase of the destruction of formaldehyde between 10^3 and 10^4 years.

in the secondary listed main paths towards HCN: the reaction $HCNH^+ + H_2CO \longrightarrow H_3CO^+ + HCN$ is added in model 2a, but has no significant impact on the curve of the total production rate. It seems to indicate that the non-equilibrium effect seen in the change of dominance of the abundances profiles of H_2CO with respect to HCN between 10^3 and 10^4 years is rather linked to an additional H_2CO major destruction path than an additional non-negligible HCN formation route.

Ending with **NH$_3$** (Figure 3.14), the main contributors are the same in both models. Only one of the 6 listed destruction routes differs, but has a negligible contribution to the total destruction rate.
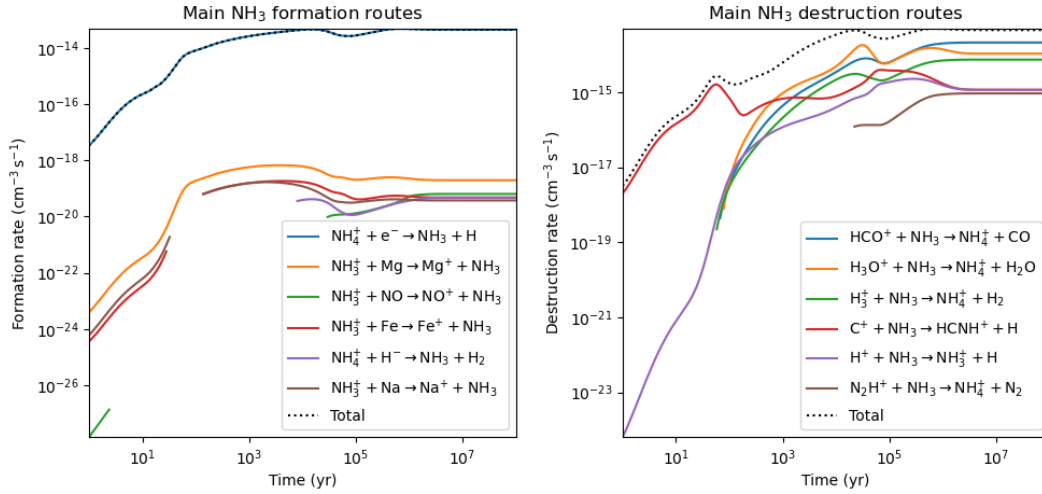
Figure 3.14: Main gas-phase formation/destruction routes for NH_3, from **model 2a** (Astrochem).

Alternatively, keeping the same density as in model 1a but changing the temperature to 20K, a third model (**model 3a**) is defined, as described in Table 3.1.
The corresponding temporal evolution of the abundances of H_2CO, NH_3, H_2O and HCN is given in Figure 3.15.
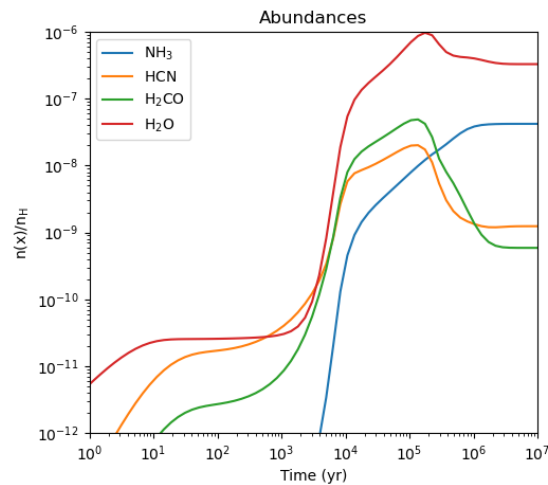
Figure 3.15: Respective abundances as a function of time for H_2CO, HCN, NH_3 and H_2O, computed with Astrochem (from **model 3a** describing a relatively dense molecular cloud at 20K.)

78

Comparatively to Figure 3.1 inferred from model 1a, the results from model 3a are pretty similar[19]. This can be easily and intuitively explained by the too small difference of temperature between the two models (the H density being the same). Indeed, as reflected in the 12 main formation/destruction routes for each of the studied species, equivalent in model 1a and modal 3a[20], mechanisms thermally prohibited in model 1a are also inhibited in models with such small temperature increments of 10 K. The densities being the same, the kintetics of the system is equivalent. More specifically, the kinetics of a system is driven by the temperature, ruling the possibility to cross activation barriers or the diffusion in case of barrierless processes, and the densities. Coming back to equation 1.2, the influence of temperature is expected to be negligible when turning from 10 to 20 K conditions. Indeed, at cryogenic temperatures, only the processes that are characterized by a very small activation barrier, or even null, can take place, the exponential term $e^{-E_a/k_B T}$ in equation 1.2 tending to 0 ($k_B T << E_a$, $e^{-\infty}$) for transformation displaying more considerable activation barrier. When passing from 10 to 20 K temperature conditions, the main contributors stay the same, since processes presenting a too high E_a at 10 K also present a too high barrier for 20 K to be part of the non negligible contributors to the computed abundance. Therefore, only accounting for processes displaying negligible to null E_a ($E_a << k_B$), one may expect the exponential term to tend to unity in both cases of 10 and 20 K temperature conditions, at least for the major routes[21]. Concerning the square root of the temperature present in equation 1.2, it has no major impact on the computed rate values when rising the temperature from 10 to 20 K. In fact, as reflected in this square root, the temperature has an impact on the diffusion, the only mechanism that rules barrierless processes (where the reaction rate is governed by collision frequency rather than by the formation of the activated complex/transition state). Yet, a temperature increment of 10 K at such cryogenic temperatures is intuitively not expected to produce large variations in the rate of encounter between reactants. It eventually explains the slight differences observed in the computed values with respect to model 1a. Taking all these considerations into account, one may therefore expect a temperature increment of 10 K in cryogenic conditions to have no significant quantitative impact on the computed abundances, which is what we observed in this comparison of results from model 1a and 3a.

3.1.2 Strecker-like synthesis - Activated pathways

Henceforth, the basic precursors of the pure neutral Strecker-like mechanism being well studied, we can further push the study by addressing the fate of the precursors of the activated Strecker-like mechanisms. Indeed, as we have seen in the introductory chapter, there are two well distinct ways to activate the kinetics (lowering of the activation barriers) of the classical Strecker-type glycine formation route, as discussed in Walch et al. (2001). Coming back to this paper, they suggested:

i. An activation through ionisation of one of the reactants of reaction 1.7 (**cationic activation**). The principle behind the lowering of the activation barrier relies on physico-chemical principles, and more specifically on the dependency on the distance of the interaction forces which are concerned; as seen in paragraph 1.3.3, when considering neutral-neutral reaction (here, the genuine equation 1.7), the only attractive interactions favoring the encounter of the reactants

---

[19]More precisely, when checking the values of the computed abundances at chemical equilibrium (Table 3.2), they are of the same order of magnitude as the one obtained from model 1a, with very slight discrepencies; the higher difference owns to the H_2CO abundance, with a factor ~ 3 between the computed abundances from model 1a and 3a.

[20]Their profiles perfectly match, as demonstrated when comparing Figures 3.2, 3.3, 3.4, and 3.5, to respectively B.4, B.5, B.6, and B.7. As previously, figures with number beginning by B can be found in Appendix B, gathering supporting visual demonstrations.

[21]This hypothesis is verified by the null value of the gamma factor ($\frac{E_a}{k_B}$) encoded in the used astrochemical network for all the major routes implied for these species.

are Van Der Waals forces, with a steep decrease of their strength with the distance ($\propto 1/r^6$). On the other hand, cation-molecule processes imply polarization induced interactions displaying a less steep dependency on the distance ($\propto 1/r^4$).

This activation type was studied by Walch et al. (2001) in a pure gas-phase context (quantum computations in vacuum). They considered the cationic form of NH_3 rather than that of H_2CO, and they justified this choice by considering the difference in ionization potential (IP) between these two ions ($IP_{NH_3^+} < IP_{H_2CO^+}$). However, it is important to stay critical, and one could wonder if this selection criterion is actually rigorous and scientifically founded. From a purely intuitive point of view, these considerations seem indeed a bit restrictive; one has to keep in mind that the reaction medium considered in this present work, as well as in Walch et al. (2001) in the context of this discussion, is a dense molecular cloud, and more specifically its gas component. Such an astrophysical medium is populated by hundreds of different chemical species presenting their own abundance, each of them being involved in several reactions. Moreover, it is too dense to be permeated by direct ionizing electromagnetic radiations, as highlighted in Chapter 1. Concerning the UV-photon produced through CR interactions, they are generally too low in energy to be able to ionize chemical species given their collisional production mechanism. As a result, the ionizing agents lying in a dense molecular cloud are the CRs and the subsequent charge transfer reactions. This brigns us to the considerations found in Prasad and Huntress (1980a) and aforementioned: the formation of cationic species in dense molecular clouds in all astrochemical models begins with the CR ionization of He, followed by a dissociative charge transfer with the very abundant CO molecules, leading to the C^+ production. Then, charge transfer reactions allow the production of other ions. According to these considerations, the two cations considered in this discussion, H_2CO^+ and NH_3^+, are expected to be mostly produced through charge transfer reactions. This suggestion has been confirmed through Astrochem computation, all of their main formation paths being charge transfer processes (see Figures B.10 and B.11 in Appendix B). Consequently, the abundance profiles of H_2CO^+ and NH_3^+ (Figure 3.16) depend directly on the abundances of their most direct precursors: mostly H_2CO and NH_2^+, respectively [22], according to their major formation routes. In fact, by comparing the

Figure 3.16: Respective abundances as a function of time for H_2CO^+ (not studied by Walch et al. (2001) due to ionisation potential considerations, see text), as compared to NH_3^+, invoked by Walch et al. (2001) for the pure gas-phase cationic activated Strecker-like pathway ; computed with Astrochem (from **model 1a**.)

---
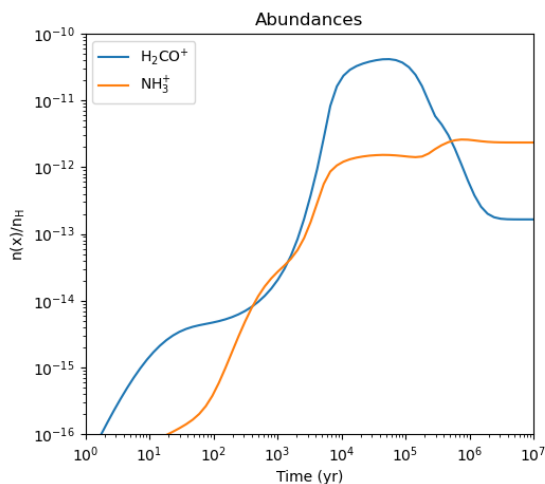
[22]Regarding the main formation routes in Figures B.10 and B.11, the reactions implied are bimolecular reactions (charge transfer reactions). The abundance of the product should therefore be dependent on the two reactants for each of the main formation paths. However, as we can see in these routes, the partners of H_2CO and NH_2^+ are very abundant species, such as H_2, H^+ and C+. The limiting reagents are therefore H_2CO and NH_2^+, consequently governing the abundance profiles of respectively H_2CO^+ and NH_3^+.

profile of H_2CO^+ (Figure 3.16) with the H_2CO profile from the same model 1a (Figure 3.1), one easily visualizes the clear similarity between the two curves in terms of their shape. Concerning the case of NH_3^+, depending mostly on the NH_2^+ abundance, one may also find some likeness to the NH_3 profile. It could have been anticipated since NH_3 is mainly formed via a cationic chain ending with the electronic dissociative recombination of NH_4^+, as discussed by Prasad and Huntress (1980a). Such a cationic chain passes, inter alia, by the NH_2^+. The abundance profile of all nitrogenated species entering this cationic chain are therefore linked.

From this deep analysis of the formation of the H_2CO^+ and NH_3^+ cations and their corresponding abundance profile, the selection criterion used by Walch et al. (2001) actually appears not to be well justified. Indeed, one has to consider complex densities effects, rather than simply comparing the energy barriers needed to remove an electron from the neutral corresponding species. Furthermore, as illustrated in Figure 3.16, at chemical equilibrium, the selection criterion applied in Walch et al. (2001) has no consequence since the NH_3^+ abundance is one order of magnitude higher than the H_2CO^+ one. On the other hand, before reaching the chemical equilibrium, the restrictiveness of the considerations in Walch et al. (2001) is further detrimental to the study. Indeed, the H_2CO^+ concentration is higher than the NH_3^+ abundance in out-of-equilibrium conditions, except between $\sim 2\ 10^2$ and $2\ 10^3$ years. Not studying the cationic version of reaction 1.7 implying H_2CO^+, but only the one invoking NH_3^+, would therefore be a major breach of the non-equilibrium chemistry of the system. In a subsequent work, it would then be interesting to calculate the activation barrier corresponding to both cationic variants of equation 1.7. This will allow the addition of the two reactions in a future extension of the network (which will be discussed in Chapter 4) without neglecting a part of the chemistry occurring in out-of equilibrium conditions.

ii. An activation via **protonation** of the carbonyl group. In this case, the reason for the decrease of the activation barrier compared to the pure neutral nucleophilic attack described by reaction 1.7 is linked to basic organic chemistry principles and the molecular orbital theory.

Walch et al. (2001) studied such a mechanism in the context of the solid-phase chemistry, without calculating energy barriers for the gas-phase. Once more, one could wonder why such protonated mechanism is only designed for the solid phase chemistry of molecular cloud, and if this choice is scientifically well justified. At first glance, the activation through protonation is more difficult to conceive in the gas phase prevailing in dense molecular clouds. In the solid phase, the proton-relay mechanism discussed in the introductory chapter greatly facilitates the proton transfer between species embedded in the ice. This type of mechanism can be easily demonstrated by explicitly taking water molecules in the quantum simulations into account. However, such a proton-relay mechanism is not conceivable in the gas-phase regarding the too low densities prevailing in. The probability to retrieve the reactants at the same place, and close enough to water molecules, is negligible. Nevertheless, in the gas phase of a given dense molecular cloud, we have seen that the formation of H_3^+, HCO^+, H_3O^+ and other H-baring cations is totally plausible. These cations can transfer a proton to formaldehyde, or various dissociative charge transfer reaction may lead to the formation of H_2COH^+ (noted H_3CO^+ in the Astrochem network[23]). The main formation/destruction paths towards H_3CO^+ from model 1a are given in Figure B.12 in Appendix B for the interested reader. The viability of the

---

[23]It should be noted that great care must be taken when searching for a species in the network in order to verify its inclusion, especially when using a network that we did not establish on our own. It is indeed important to check all the possibilities of encoding the chemical formula of a given species. The protonated formaldehyde is a good example to illustrate this point - although one might think it is more intuitive to write it as H_2COH^+, the formula used in the Astrochem network is H_3CO^+. This point was important to underline because, without paying attention, one could

precursors needed for such a protonated version of the classical Strecker-like synthesis in the gas-phase of molecular cloud is consequently imaginable.

Furthermore, coming back to the discussions from paragraph 1.3.3 in the introductory chapter, reactions between chemical entities generally lead to a loss of fragment regarding the absence of energetic exchange with the solvent or stabilizing interactions in the gas phase of the ISM. The following comment is valid either for the discussion of the classical Strecker-like analysis (§3.1.1) and the present discussion on the protonated and cationic Strecker-like synthesis. When reconsidering the Figure 1.10, the cationic version (first step illustrated in Figure 1.17) or the protonated version implying the H_2COH^+ cation and the resulting iminium, no direct fragment loss are considered. However, trying to establish a variant of these mechanisms including fragment losses would be difficult if one wants to keep the chemical principles considered in these paths such as the nucleophilicity of ammonia (except in the cationic path), the step of dehydratation, ... Moreover, it is worth to note that reaction 1.7 (and its protonated and cationic version) is a two-step process, with the second step corresponding to the loss of a water molecule through intramolecular rearrangement. One could see this second step as a loss of a fragment, even if indirect regarding the need of an intramolecular rearrangement in order to occur. Such indirect loss of fragment is intuitively expected to be more energetic; one may eventually imagine that the excess of energy in the NH_2CH_2OH intermediate of reaction could be used for such more energetic loss of fragment. This hypothesis is however quite speculative, and has to be verified.

In any case, the previous discussion from paragraph 3.1.1 and the present discussion of the protonated and cationic version of the classical Strecker-like mechanism are scientifically relevant and have the potential to provide us a rich source of information and results. Indeed, these precursors can potentially be adsorbed on a dust grain, enriching its molecular content and leaving room for these reactions to occur in the solid phase, with all its advantages. On another note, to extend our discussion, let us consider an interstellar shock of moderate amplitude[24] that perturbs the hydrodynamic equilibrium of the cloud in question, leading to an enhancement of its density and temperature (at least in some regions), or even to its collapse; the primary chemical material to be considered for such a dynamic situation is the population of species lying in the parent-cloud just before the perturbation. The computed abundances could therefore be used for more advanced simulations, in which one would simulate the fate of this population of species during the dynamic life of the cloud. Moreover, regarding the increase in temperature and densities resulting from such hypothetical event, in parallel to the rather complex species involved in the Strecker-like mechanisms, one could consider the possibility that the excess of energy is stocked between the ro-vibrationnal energy level, allowing such mechanism to occur regardless any imperative product fragmentation.

Consequently, it seems interesting to analyse the precursors of the protonated Strecker-like synthesis in gas-phase following these deep considerations about the scientific relevance to consider them. In the rest of this paragraph 3.1.2, the analysis of the abundances of the gas-phase precursors for both the cationic and protonated version of the Strecker-like synthesis will thereby be performed.

Henceforth, Figure 3.17 gathers the temporal abundances of all the precursors of both the protonated (H_3CO^+, NH_3, HCN) and cationic (H_2CO^+, NH_3, HCN or H_2CO, NH_3^+, HCN) versions of the classical Strecker-like synthesis precursors, computed from **model 1a**.

---

tend to add a reaction already taken into account in the network, and therefore involving the same reactant. The abundance of the reagents involved would then be skewed, impacting the results of the study.

[24]To not destroy the entire population of molecular species present in the cloud before any perturbation.
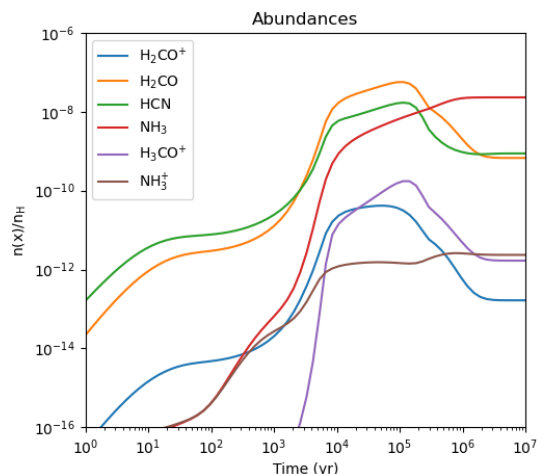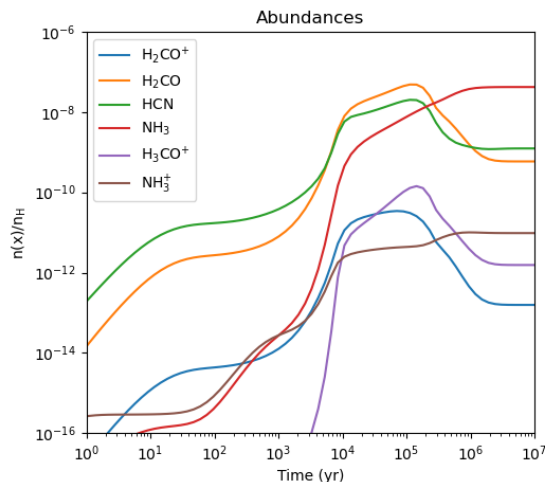
Figure 3.17: Respective abundances as a function of time for the precursors of both the protonated and cationic version of the classical Strecker-like synthesis precursors; in comparison to the pure neutral precursors studied in Figure 3.1, H_3CO^+ (protonated path), as well as H_2CO^+ and NH_3^+ (cationic activation) abundances are added - computed with Astrochem (from **model 1a**.)

First of all, from a general point of view, the abundances of the studied cationic/protonated species are lower than the neutral equivalent in the neutral Strecker-like pathway. However, neutral processes generally display substantial activation barriers, resulting in very slow to prohibited transformations, whether the reactants display a high abundance or do not. On the contrary, as mentioned just before, when considering the activation of the classical Strecker-like synthesis through protonation or the use of cationic species, one actually investigates paths with greatly reduced activation barriers, or even barrierless routes. As a consequence, such a substantial decrease of the activation barriers compared to the neutral path is expected to overcome the quite low abundances of the cation/protonated species studied in Figure 3.17, and one could expect such activated mechanisms to be relevant for the glycine formation in the context of cryogenic conditions, preventing the crossing of some neutral activation barriers.

Moreover, comparing the abundances of H_3CO^+, H_2CO^+ and NH_3^+ at chemical equilibrium, H_3CO^+ and NH_3^+ display abundances of the same order of magnitude ($1.65 \ 10^{-12}$ and $2.13 \ 10^{-12}$ with respect to the total hydrogen nuclei abundance, respectively), and higher than for H_2CO^+ ($1.57 \ 10^{-13}$). If we consequently focus on the activated routes invoking H_3CO^+ and NH_3^+, we know that

- H_3CO^+ is expected to react with NH_3 (activation through protonation), which displays an equilibrium abundance of $2 \ 10^{-8}$ with respect to the total hydrogen nuclei abundance in model 1a (Table 3.2);

- NH_3^+ should react with H_2CO to follow the cationic path proposed by Walch et al. (2001). At equilibrium conditions, the H_2CO abundance amounts to $6.3 \ 10^{-10}$ with respect to the total hydrogen nuclei abundance (Table 3.2) in that pure gas-phase modelled cloud.

From pure density considerations, one may suppose that the first step of the activation of the Strecker-like mechanism through protonation [25] is more efficient at chemical equilibrium, in the pure gas-phase context simulated by model 1a. However, even if this is a good predictive starting point, the reality is more complex, and the activation barriers and cross-sections of these two processes

---

[25]If feasible without direct fragment loss, see previous discussions.

have to be considered to assess the dominance of one of these two routes. Furthermore, considering the out-of-equilibrium chemistry, as discussed previously, the H_2CO^+ abundance is higher than the NH_3^+ profile. Regarding Figure 3.17, one can add that the H_2CO^+ curve overhangs the H_3CO^+ one in such conditions until an elapsed time of $\sim 1\ 10^4$. From pure density considerations, the cationic path involving H_2CO^+ (expected to react with NH_3) is consequently expected to dominate the contributions of the protonated Strecker-like paths during the first $1\ 10^4$ years of the cloud lifetime, at least in the first step. Concerning the higher abundance of H_2CO^+ compared to NH_3^+, it has to be considered together with their respective expected partner, NH_3 and H_2CO respectively. As discussed before, in out of equilibrium conditions, before 10^5 years, the H_2CO is more abundance than NH_3. Once more, these considerations are nevertheless a bit too restrictive and, to further insights in theses results, one has to consider the corresponding activation barriers and cross-sections, especially when the curves of H_2CO^+ and H_3CO^+ become closer and closer.

Henceforward, in order to have deeper insights into this discussion about the two distinct ways of activation of the Strecker-like synthesis, let us analyse the results from **model 2a**, shown in Figure 3.18. In out-of-equilibrium conditions, all the curves seem to have been impacted by a broadening to the left when going from model 1a to model 2a, for the same reason as explained in paragraph 3.1.1 for the discussion of Figure 3.9.
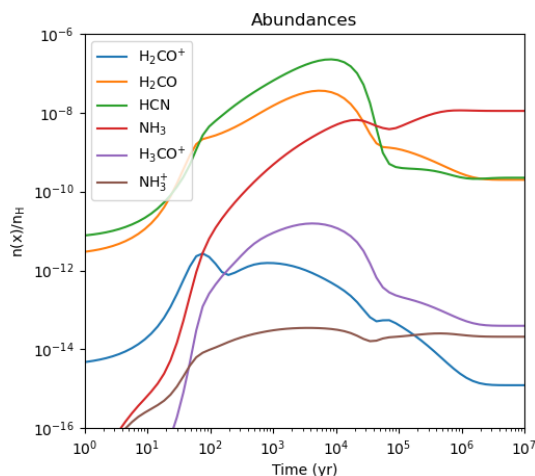
Figure 3.18: Respective abundances as a function of time for the precursors of both the protonated and cationic version of the classical Strecker-like synthesis precursors; in comparison to the pure neutral precursors studied in Figure 3.9, H_3CO^+ (protonated path), as well as H_2CO^+ and NH_3^+ (cationic activation) abundances are added - computed with Astrochem (from **model 2a**.)

Furthermore, concerning the chemical equilibrium reached after $\sim 1\ 10^6$ years (constant value with the hydrogen density if ξ stays unchanged, as justified in the analysis of Figure 3.9), the steady state abundances for the species that have not been analysed yet are given in Table 3.3.

Table 3.3: Quantitative comparison of the abundances reached at *chemical equilibrium* with model 1a, 2a and 3a for the precursors relative to the activation of the Strecker-like synthesis, ignoring the neutral precursors, already analysed in Table 3.2.

	H_3CO^+	H_2CO^+	NH_3^+
model 1a	$1.65\ 10^{-12}$	$1.57\ 10^{-13}$	$2.13\ 10^{-12}$
model 2a	$3.44\ 10^{-14}$	$1.08\ 10^{-15}$	$1.87\ 10^{-14}$
model 3a	$1.49\ 10^{-12}$	$1.31\ 10^{-13}$	$8.13\ 10^{-12}$

Contrary to its influence on the neutral abundances studied in Figure 3.9, the hydrogen density enhancement (model 2a to be compared with model 1a) seems less inconsequential with respect to the computed abundances for the cationic species considered in this discussion. This concrete example illustrates the restrictiveness of the considerations by Herbst and Klemperer (1973), discussed previously when rationalizing the very low sensitivity of the abundances in Table 3.2. Actually, the H_3CO^+, H_2CO^+ and NH_3^+ abundances are roughly inversely proportional to the initial abundance in hydrogen nuclei. This can be understood from our previous discussions: to predict the influence of an enhancement in the initial hydrogen nuclei density on the abundance of a given species, one has to consider the fact that this species can be implied in many formation and destruction routes, each of them presenting its own order and kinetic parameters. To fully develop the expression of the dependency of its abundance with respect to the hydrogen number density, the definition of a chemical equilibrium has to be applied, equalling the rate of disappearance to the rate of appearance of that chemical entity. Each density term in the inferred expression has thereby to be expressed with respect to the hydrogen abundance, which is clearly not straightforward and generally requires the use of approximations, as implemented in Iglesias (1977). He however did not specifically report on the influence of hydrogen density on the abundance of the species that are considered here[26]. Doing the whole proof to determine the abundance of each of these species as a function of hydrogen density would be very time-consuming, and would not bring us new scientifically interesting information in the context of our discussion. Therefore, we will limit ourselves to the impact of the observed inverse proportionality on our previous intermediate concluions from model 1a.

In that context, when considering the relative equilibrium abundances from model 2a (Table 3.3), one must note that H_3CO^+ is slightly more abundant than NH_3^+, both of them presenting a number density (relative to the total hydrogen nuclei density) one order of magnitude higher than H_2CO^+. Compared to our analysis from model 1a, the same conclusions can be drawn, with some subtleties. In model 1a, at chemical equilibrium conditions, H_3CO^+ and NH_3^+ presented similar abundances, the latter being 1 order of magnitude higher than the H_2CO^+. From these results, we have noticed that the abundance of the neutral reaction partner of H_3CO^+, namely NH_3, exceeds the H_2CO (neutral reaction partner of NH_3^+) abundance by a factor higher than 2 orders of magnitude (Table 3.2). Consequently, we have suggested that, from those pure gas-phase calculations, the first step of the protonated Strecker-like synthesis for the glycine formation is arguably more quantitative, even though more comprehensive considerations (activation barriers, cross-section) have to be accounted for. This suggestion seems even more supported by the computed abundances in model 2a; the higher discrepancy between the H_3CO^+ and NH_3^+ abundances compared to model 1a, in favor to H_3CO^+, strengthens the arguable dominance of the protonated activation routes from pure density considerations. The NH_3 abundance is also 2 orders of magnitude higher than the H_2CO one (Table 3.2). Once more, more complex arguments should be considered to ascertain such a hypothesis. Moreover, coming back to the out-of-equilibrium chemistry, the H_2CO^+ profile overhangs the H_3CO^+ curve only during the first 10^2 years, while it dominates over a longer period in model 1a ($1\ 10^4$). The proposal from model 1a, in which the cationic path involving H_2CO^+ is expected to dominate the contributions of the activated Strecker-like paths during the first $1\ 10^4$ is therefore valid, but on a shorter time scale.

Finally, to end this point on the precursors relative to the activation of the Strecker-like synthesis, one may wonder if the findings from the analysis of Figure 3.15 in paragraph 3.1.1 (analysis of the precursors of the neutral Strecker-like synthesis from model 3a as compared to model 1a) are still valid for the positively charged species studied in this point. For that purpose, **model 3a** has been applied, and the results are shown in Figure 3.19.

---

[26]H_3CO^+ and NH_3^+ were considered in his network, but not H_2CO^+.

Figure 3.19: Respective abundances as a function of time for the precursors of both the protonated and cationic version of the classical Strecker-like synthesis precursors; in comparison to the pure neutral precursors studied in Figure 3.15, H_3CO^+ (protonated path), as well as H_2CO^+ and NH_3^+ (cationic activation) abundances are added - computed with Astrochem (from **model 3a**.)

From this plot, several comments can be made. First of all, from a general point of view, the respective shapes of the profiles in Figure 3.19 are pretty similar to the ones in Figure 3.17, especially for the out-of-equilibrium conditions. Furthermore, concerning the steady state abundances reached at chemical equilibrium, they are quantified in Table 3.3. As reflected in this table, the computed abundances at chemical equilibrium for model 3a are of the same order of magnitude as the one obtained from model 1a, with little differences. The highest variation is found in the case of NH_3^+, with a computed value within a factor slightly lower than 4 with respect to model 1a. However, as checked in the main formation/destruction of all of the 3 cations studied here, the main contributors are unchanged from model 1a to 3a, and are keeping a quite similar temporal evolution in terms of the shape[27]. These observations can therefore be justified as the same way it was done for Figure 3.15 (§ 3.1.1).

Before addressing the Woon's mechanism, let us note that the abundances of the three cationic/protonated precursors studied here have also been computed in Prasad and Huntress (1980a,b). A comparison to these results will be discussed in § 3.3, with model b.

3.2 Precursors for Woon's mechanism and its variants

As introduced in details in Chapter 1, the Strecker-like mechanism is not the only interstellar glycine formation path proposed in the literature. Radical-radical pathways have also been suggested, as investigated by Woon (Woon, 2002b) and many subsequent studies. This section will be dedicated to the study of the basic precursors needed for Woon's mechansim (see Figure 1.12) to operate.

Before going into detailed considerations, as highlighted in footnote 39 of the introductory chapter and pointed out several times since then, interstellar glycine formation paths originally thought for the solid-phase (grain) chemistry and studied in the gas-phase for the sake of comparison are generally unmodified from the originally proposed scheme. In other words, the beforehand discussed loss of fragment in gas-phase for small species in the ISM, especially at cryogenic conditions, is neglected. For

---

[27]The interested reader is referred to Figures B.10 to B.18 for a visual proof.

instance, in Woon (2002b), the author proposed a mechanism for the glycine formation in irradiated interstellar ices, and transposed this unmodified mechanism in gas-phase in order to compare the activation barriers. However, regarding the very small species considered in this path (OH, CO, HCN and H, see Figure 1.12) for the first steps, this amounts to making a rather daring and not well justified approximation. It would be wise to think of a variant to this unmodified Woon's mechanism, taking the loss of fragments into account. In that context, intense reflection accounting for the whole body of *a priori* knowledge (abundant species, physical conditions prevailing in a molecular cloud and ruling its astrochemistry, basic physico-chemical principles, ...) has been undertaken, giving rise to the general idea illustrated in Figure 3.20.
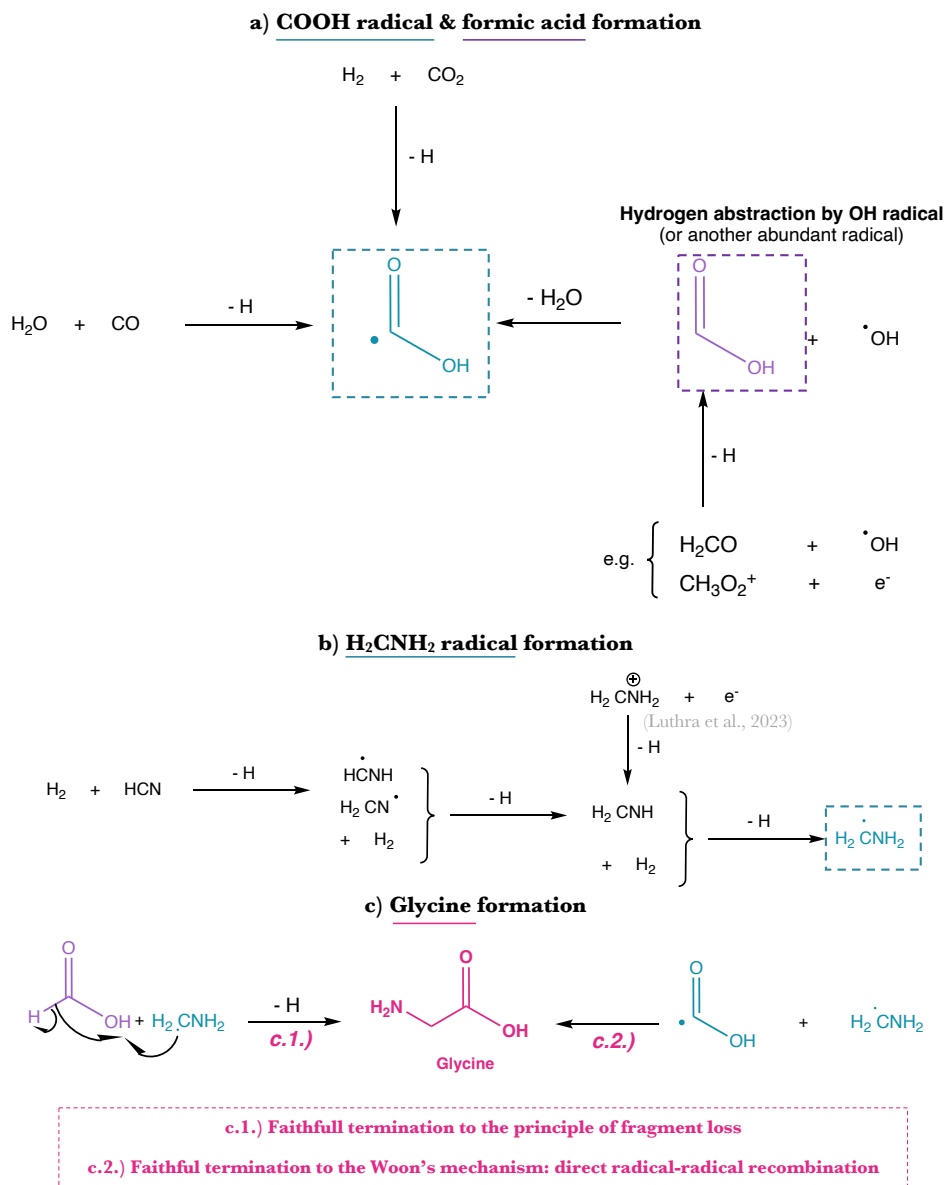
Figure 3.20: Proposed gas-phase glycine formation path, based on the three steps of Woon's mechanism illustrated in Figure 1.12, but revisited to account for the fragment loss occuring in case of reactions at cryogenic temperatures, especially for small species. Two distinct termination paths are proposed (c.1., and c.2, see text for more details) - from personal reasonings.

This scheme is based on the general idea behind the three steps (a, b and c) of Woon's mechanism we described in Figure 1.12 - the proposed a, b and c steps in Figure 3.20 are designed to follow Woon's ideas as closely as possible, while considering the constraint linked to fragment loss. To fully explain the idea behind this revisited Woon's mechanism, let us comment each of the three steps from Figure 3.20:

a) Formation of the COOH radical, and its hydrogenated analogue:

Three distinct sub-routes towards COOH radical have been envisaged. In the first instance, one may discuss both the reaction between CO_2 & H_2 and the reaction involving CO & H_2O, rather similar to the idea of step a of Figure 1.12 (unmodified Woon's mechanism). Actually, from pure density considerations (*kinetics*), H_2 and CO are the two most abundant molecules in molecular clouds. The reason of the predominance of H_2 is obvious, whereas the great abundance of the CO molecules deserves more discussions; in fact, carbon monoxide represents the second most abundant molecules in the Universe, after molecular hydrogen, thanks to its very high photostability (bonding energy of 11.09 eV[28]) and self-shielding capabilities. Continuing on kinetic considerations, such reactions are expected to have a non-zero activation barrier regarding the need of bond breaking and the neutral nature of the reactants. Their feasibility at cryogenic temperatures is therefore quite unlikely, but is not rejected at higher temperature conditions[29]. Moreover, the spontaneity of these transformations is more questionable (*thermodynamics*). Indeed, regarding the two spontaneity criteria discussed in Chapter 1, paragraph 1.3.2,

   i. The probabilistic criterion seems to be favourable ($\mathbf{\Delta S > 0}$) in both cases. Indeed, the molecular order decreases arguably from the reactants (neutral) to the product (a radical).

   ii. The energy criterion, on the contrary, appears intuitively to be more prejudicial ($\mathbf{\Delta H > 0}$) to the spontaneity of the processes. All the reactants (CO_2/H_2 & CO/H_2O) are actually stable species, especially CO. On the other hand, the common product to these proposed sub-routes is COOH, a radical. Such chemical entity is very reactive, and quite unstable. One may therefore expect its energy to be higher than that of the reactants, leading to an enthalpy increase.

These guesses should however be validated more rigorously through thermochemical computations; by rigorously evaluating ΔS and ΔH for both the discussed sub-routes, one should be able to asses their respective contribution at the temperatures of interest through equation 1.4. In other words, once the ΔS and ΔH are computed, the variation in free Gibbs energy can be estimated at relevant temperatures, and the spontaneity of both processes can consequently be assessed in such temperature conditions.

Concerning the third envisioned sub-route for the COOH formation, the underlying physico-chemical principles are totally different. In this case, we no longer rely on density considerations, but rather on the kinetic constant parameter of the rate equation. In such a context, one has to come back to the aforementioned instability conferred to small radicals due to the presence of at least one unpaired valence electron, therefore leading to a violation of the octet rule. This high instability makes free radicals highly reactive, providing them with a shorter life-time. The principle of hydrogen abstraction by a given abundant free radical (e.g. OH) from the

---

[28]The photon of energies higher than 13.09 eV are almost completely absorbed through hydrogen ionization well before reaching the molecular cloud - the only photons left for the CO dissociation are therefore characterized by wavelengths lying in the quite short range [912 - 1118 Å].

[29]At higher temperature conditions, the activation barrier should be passable and the high collision probability between the reactants of interest due to their great abundance could allow these processes to be significant.

formic acid therefore seemed to be a good candidate to counter the uncertainties raised for the previously discussed sub-routes for this step a. Let us emphasize that formic acid will be a key species in the discussion of step c, and more specifically for the sub-route c.1.

In order to find potential gas-phase paths towards HCOOH, a deep reflection has been carried out, and two paths have been theoretically proposed, as shown in Figure 3.20. To have deeper insights into these two propositions, we checked in the Astrochem network if formic acid was included; it turned out to be the case (but not its radical form, COOH). However, its main formation/destruction paths could not be analyzed by the methods provided in Astrochem. Indeed, HCOOH (CH_2O_2 in the Astrochem network) is only included in 11 reactions, with only two formation routes. We are therefore in the intense orange zone ($X > Y$) from Figure 2.6. On the other hand, when checking the guenuine Astrochem network, it is good to notice that the two included HCOOH formation routes correspond to the two routes which have intuitively been thought out and proposed in this revisited Woon path. By taking a closer look at the kinetic parameters associated with these two reactions, the γ parameter is null in both cases, and β is equal to 0 and -0.5 for respectively the reaction between H_2CO & OH, and $CH_2O_2^+$ & a free electron. The highest discrepancy is found in the value of the α parameter, amounting to $1.50 \ 10^{-7}$ for the dissociative electronic recombination of $CH_3O_2^+$, while only to $2.01 \ 10^{-13}$ for the hydrogen abstraction from H_2CO by OH radical (with a great uncertainty on this value, not listed in the current OSU database). From the encoded kinetic parameters, the dissociative electronic recombination of $CH_3O_2^+$ is at least 5 orders of magnitude faster than the hydrogen abstraction from H_2CO by OH radical. On the other hand, before entering into hasty conclusions, one has to analyse the density of the precursors of interest. Their chemical equilibrium abundances (with respect to the total hydrogen nuclei) are given in Table 3.4.

Table 3.4: Quantitative comparison of the equilibrium abundances (model 1a) for the precursors proposed for the formic acid formation.

H_2CO	OH	$CH_3O_2^+$	e_-
$6.3 \ 10^{-10}$	$1.65 \ 10^{-5}$	$1.73 \ 10^{-12}$	$3.17 \ 10^{-8}$

Regarding these numbers, the higher abundance of the H_2CO and OH precursors [30] may arguably balance the huge difference between the kinetic parameters alpha; the two proposed HCOOH formations seem to be plausible.

b) **Formation of the H_2CNH_2 radical**:

As for step a, the radical targeted by this step b (H_2CNH_2) is not included in the Astrochem network. The proposed formation path has been built trying to stick to Woon's idea as closely as possible , starting from HCN and passing by the methanimine. No kinetic or thermodynamic data concerning this proposition are known, are are therefore logically not included in the Astrochem network. It would therefore be interesting to perform quantum computation to better constrain the kinetic and thermodynamical feasibility of this mechanism[31]. On the other hand, gas-phase interstellar imines can be formed in a different way, as proposed in Luthra et

---

[30]Their product amounts to $9.9 \ 10^{-15}$, while the product of the value of the number densities in $CH_3O_2^+$ and free electrons (considered as a second order process by Astrochem, as mentioned previously) is equal to $5.48 \ 10^{-20}$.

[31]It should however be noted that the reaction HCN + $H_2 \rightarrow$ HCNH is quite similar to the HCN + H_3^+/H_3O^+/HCO^+ destruction path towards $HCNH^+$. The physico-chemical interactions taking part of these processes are however totally different (abundance of H_2 used on one side, while the fastness of the charge transfer reaction is used on the other side), and quantum computations are therefore needed to rigorously assess the feasibility (both kinetically and thermodynamically speaking) of the proposed HCN + H_2 transformation.

al. (2023). They actually suggested that the gas-phase abundance of methanimine in a cold core are best reproduced by dissociative recombination of ions, such as the iminium.

Contrary to the targeted H_2CNH_2 radical, the methanimine is included in the network, with only 9 formation/destruction mechanisms suitable in dense conditions (with 3 formation routes). Let us note that it has not been discussed when addressing the Strecker-like precursors since the included formation paths are not matching the Strecker-like route. It is therefore more relevant to discuss this species in this context. The 3 formation paths considered are all dissociative recombinations from ions, including the iminium. This is a direct link with the protonated Strecker-like synthesis, but the formation path is once again totally different.

c) Termination - glycine formation:

Concerning the final glycine formation, two distinct terminations have been designed:

c.1) A termination that is faithful to the principle of fragment loss; this implies the reaction of the methanimine with the H_2CNH_2 radical, leading to the loss of a H atom.

c.2) A faithful termination to Woon's mechanism or, in other words, the direct radical-radical recombination of COOH and H_2CNH_2 radicals. In this subroute, we explicitly postulate higher temperature conditions (during a shock of low to moderate amplitude, for instance) and assume that the formed glycine is at a fairly high level of molecular complexity so that the excess of energy can be shared between its ro-vibrationnal levels. Another scenario relevant for this c.2 subroute is the following: COOH and H_2CNH_2 radicals may be adsorbed[32] on the solid phase, and then recombine, the surface taking the excess of energy.

Henceforward, one can investigate the gas phase behavior of the precursors needed for this mechanism. For the following analyses, the abundance of H_2 is not plotted to focus the vertical axis on the abundance of the non-trivial species. The H_2 abundance is indeed given in Table 3.1. This latter is temporally constant since this is the most abundant molecule in the system; it dominates, with other abundant entities, the formation/destruction of minor species in such a low molecular complexity system. On the other hand, reactions with these minor species have negligible influence on the H_2 abundance, ~ 4 order of magnitude higher than the second most abundant molecule, CO.
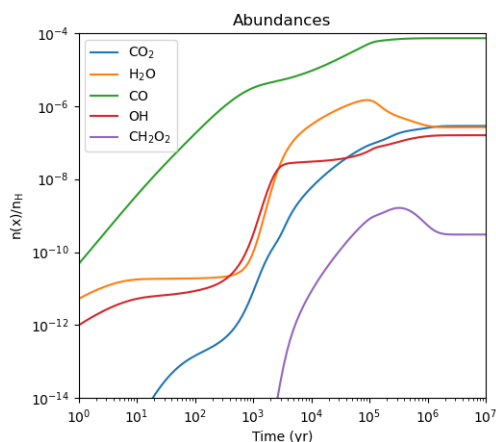
Figure 3.21: Respective abundances as a function of time for the precursors of **step a** of the (revisited) Woon's mechanism - computed with Astrochem (from **model 1a.**)

---

[32]Assuming a passive adsorption, keeping the radical nature of the species to allow the subsequent radical recombination. In other words, one explicitly assume physisorption sites, no chemical bound is considered.

Starting with the results from **model 1a** as previously, Figure 3.21 is presenting the temporal evolution of the abundances for the precursors of **step a** of the revisited Woon's mechanism.
Not surprisingly, the CO molecule dominates the abundances of the analyzed precursors, for the aforementioned reasons. Its high abundance will be discussed in more details in point 3.3. Moreover, as we can see in Figure 3.21, the H_2O and OH profiles present some clear similarities, except between an elapsed time of 1 10^3 and 1 10^5 years. In order to rationalize this likeness, the analysis of the main formation/destruction routes of OH has been performed and is shown in Figure 3.22.
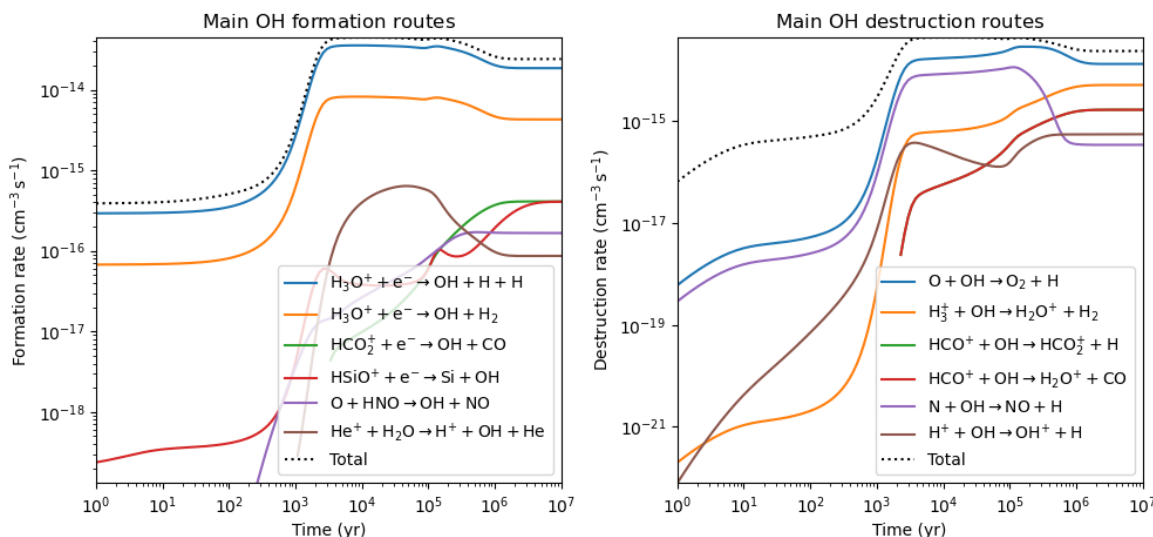
Figure 3.22: Main gas-phase formation/destruction path for OH from **model 1a** (Astrochem)

As mentioned in Table 2.1, OH is present in 247 processes in the used network. It therefore explains why it seems we are missing some of the main contributing routes, especially for the main destruction paths before 10^3 years (several orders of magnitude are separating the total destruction rate and the most quantitative OH destruction routes). As for H_2O and other previously discussed species presenting large Y values, we are in the violet part of Figure 2.6. It should therefore be kept in mind in what follows. Comparing these main OH formation/destruction routes to Figure 3.2 presenting the main routes contributing to the H_2O abundance, the similarity between the temporal evolution of the abundance profiles of H_2O and OH can be explained by their common main formation agent, H_3O^+.
Moreover, these two abundance profiles display their highest discrepancy between 1 10^3 and 1 10^5 years. It may arguably be due to the highest destruction rate of OH at such epoch, with a destruction rate amounting to more than 4.10^{-14} cm^{-3} s^{-1} all along this time interval. Indeed, as shown in Figure 3.2 from the same model, such value of the destruction rate of H_2O is only reached after 10^5 years, following a progressive increase from a value slightly under 10^{-15} cm^{-3} s^{-1} at 10^3 years. Regarding the value of the formation rate for that epoch, the discrepancy is smaller; it amounts to 3.10^{-14} cm^{-3} s^{-1} for OH, and to 10^{-14} cm^{-3} s^{-1} for H_2O. Combining the analysis of the destruction and formation paths, the highest destruction rate of OH during that epoch is expected to dominate the contributions, and the H_2O profile is expected to overhang the OH one, with a dominance decreasing when approaching 1 10^5 years[33]. Such explanation may therefore be a good candidate, even if more complex and complementary considerations might be needed.

---

[33]The H_2O destruction rate becoming comparable to the OH one, and the formation rate of OH being higher during the time interval of interest.

Coming back to Figure 3.21, the profile of the CO_2 species shows a quantitative appearance latter than H_2O and OH, but reaches a similar chemical equilibrium abundance, as we discuss more quantitatively later on.

Before addressing step b, it should also be interesting to note that the formic acid abundance, even if in the smallest amounts on this Figure 3.21, is quite appreciable, with value exceeding 10^{-10} with respect to the hydrogen nuclei abundance after $1\ 10^4$ years. It should be first be kept in mind that, in the used Astrochem network, few formic acid formation paths are taken into account. The completeness of the inclusion of all the quantitative routes towards or from formic acid is therefore more questionable, especially since such molecular specie lies at the top of the molecular complexity of the included compounds. Its pure gas-phase abundance is therefore possibly biased. Additionally, coming back to our previous discussions, even if the formic acid displays lower abundances than CO, CO and H_2O, the feasibility of its reaction with OH towards the COOH radical seems less speculative. This quite appreciable value of the formic acid abundance is therefore an interesting result, and this could have a high potential in subsequent prospective studies of this modified Woon's mechanism.

Concerning **step b** of the revisited (and unmodified) Woon's mechanism, their abundance profiles from model 1a is given in Figure 3.23. As it could have been anticipated, the HCN abundance dominates the studied species regarding its lower molecular complexity and therefore easier reachability in such gas-phase of molecular cloud, braking the climb of the molecular complexity scale.
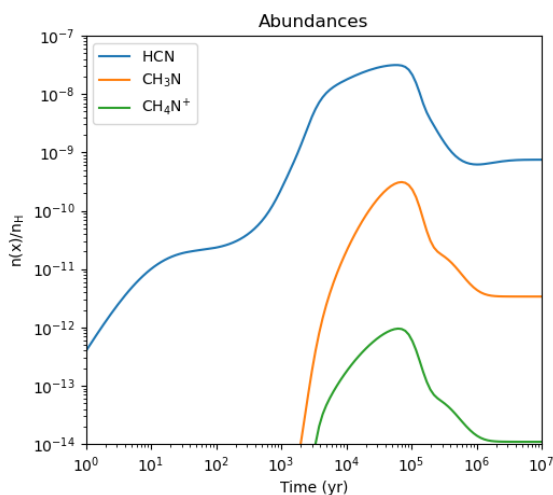
Figure 3.23: Respective abundances as a function of time for the precursors of **step b** of the (revisited) Woon's mechanism - computed with Astrochem (from **model 1a.**)

Moreover, the iminium abundance is well under the abundance of CH_2NH (CH_3N in the Astrochem network), even if the two profiles display similar shape. Such closely related shapes are intuitively expected to come from the fact that $CH_2NH_2^+$ (iminium, CH_4N^+ in the Astrochem network) and CH_2NH are part of the same cationic chain, the latter ending by the dissociative electronic recombination of the iminium. Nevertheless, this result is quite counter intuitive since one would expect a higher abundance of the iminium. This may be arguably due to complementary formation routes, implying other ions, as discussed in Luthra et al. (2023) but not explicitly taken into account in the personal reasoning illustrated in Figure 3.20. Regarding the similarity in the shape of the profiles, these ions are expected to come from a common/interconnected origin to the iminium cation. In the Astrochem network, the other included formation agents are the CH_5N^+ and CH_6N^+ ions (through

dissossiative electronic recombinations towards CH_3N). The kinetic parameters encoded for the three formation routes towards CH_3N (invoking therefore CH_4N^+, CH_5N^+ and CH_6N^+) are considered to be the same: $1.50 \ 10^{-7}$ for the alpha parameter, -0.5 for beta, and a nul gamma parameter. In the context of these Astrochem computations, the different contributions to the CH_3N abundance are therefore only set by the relative abundances of CH_4N^+, CH_5N^+ and CH_6N^+ (given in Figure B.19 in Appendix B). Once more, the species of interest in this discussion are lying near the molecular complexity limit of the used network. Their completeness is therefore questionable, and their computed abundances may be biased if major contributing paths are ignored.

In order to discuss the equilibrium abundances more quantitatively, we have applied the same procedure as in § 3.1 and new Astrochem analysis have been performed with **model 2a**, the results being given in Figure 3.24 and 3.25.
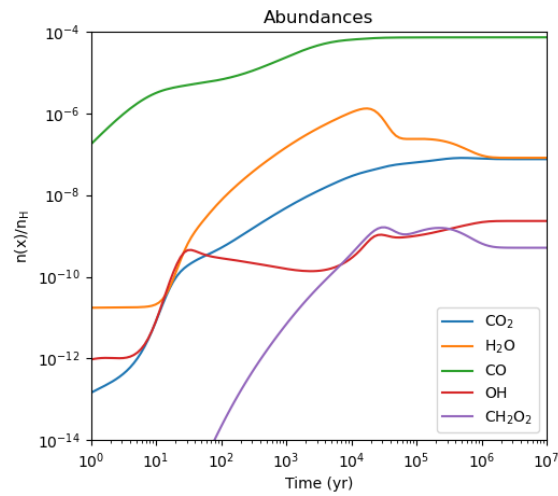
Figure 3.24: Respective abundances as a function of time for the precursors of ***step a*** of the (revisited) Woon's mechanism - computed with Astrochem (from **model 2a**.)
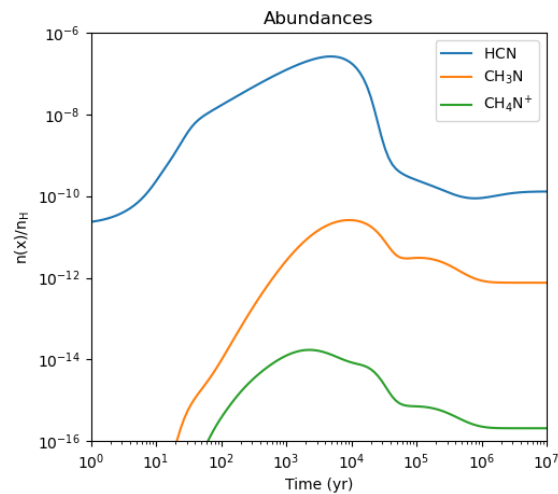
Figure 3.25: Respective abundances as a function of time for the precursors of ***step b*** of the (revisited) Woon's mechanism - computed with Astrochem (from **model 2a**.)

As discussed in paragraph 3.1, due to the hydrogen density enhancement from model 1a to 2a, all the curves are impacted by a broadening to the left in out-of-equilibrium conditions. Moreover, concerning the equilibrium abundances, given in Table 3.5, those are reached after an elapsed time of $\sim 1\ 10^6$ years. Indeed, we have noticed for the analysis of Figure 3.9 (§ 3.1) that this timescale is constant with the hydrogen density if ξ stays unchanged.

Table 3.5: Quantitative comparison of the abundances reached at *chemical equilibrium* with model 1a, 2a and 3a for the precursors relative to the (revisited) Woon mechanism

Step a	CO_2	H_2O	CO	OH	CH_2O_2
model 1a	$2.75\ 10^{-7}$	$2.5\ 10^{-7}$	$6.15\ 10^{-5}$	$1.35\ 10^{-7}$	$2.72\ 10^{-10}$
model 2a	$1.2\ 10^{-7}$	$1.2\ 10^{-7}$	$6.53\ 10^{-5}$	$2.28\ 10^{-9}$	$4.21\ 10^{-10}$
model 3a	$3\ 10^{-7}$	$3\ 10^{-7}$	$6.15\ 10^{-5}$	$1.39\ 10^{-7}$	$2.01\ 10^{-10}$
Steb b	HCN	CH_3N	CH_4N^+	CH_5N^+	CH_6N^+
model 1a	$8.5\ 10^{-10}$	$3.04\ 10^{-12}$	$1.07\ 10^{-14}$	$7.65\ 10^{-16}$	$2.30\ 10^{-14}$
model 2a	$2.1\ 10^{-10}$	$7.10\ 10^{-13}$	$1.81\ 10^{-16}$	$8.09\ 10^{-18}$	$3.71\ 10^{-16}$
model 3a	$1.13\ 10^{-9}$	$4.13\ 10^{-12}$	$1.64\ 10^{-14}$	$8.94\ 10^{-16}$	$3.02\ 1.64\ 10^{-14}$

Results is this table deserve a bit more discussion. Indeed, when comparing the abundances in model 1a and 2a, one may classify the studied species into two main groups:

- Species presenting relative abundances almost independent on the initial hydrogen density (at least in those ranges of temperatures and cloud densities). Among these species, we find H_2O, with a very slight dependency on the initial hydrogen density (within a factor of 2), already discussed in relation with Table 3.2 in the context of the Strecker-like synthesis. CH_2O_2 and CO_2 behave in a similar way as H_2O in the context of an initial hydrogen density enhancement. Concerning CO, it is almost insensitive to such variations in initial conditions.

  Some species are displaying abundances that are more affected by a change in the initial abundance in hydrogen, but still keeping a slow dependency. Indeed, HCN, as already discussed in relation with Table 3.2, and CH_3N see their abundance decrease by a factor ~ 4 when the initial hydrogen density is increased by two orders of magnitude.

- Species for which the relative abundances present a quantitative variation with the initial hydrogen density and, more specifically, behave roughly as inversely proportionally to the initial abundance in hydrogen nuclei. In this category, we retrieve OH, as predicted by Iglesias (1977) and CH_4N^+, CH_5N^+ & CH_6N^+ [34].

Let us notice that the abundances of all these precursors (except for the formic acid, CH_5N^+ & CH_6N^+) have been computed in the already well discussed papers from Prasad and Huntress (1980a,b). A quantitative comparison will be performed in paragraph 3.3 by using model b.

Finally, before closing this discussion of the basic precursors of the Woon-like mechanism, one can check if the findings from the analysis of the Strecker-like synthesis precursors, in both the classical and the activated approach, in paragraph 3.1 are still valid in the context of Woon's mechanism precursors. For that purpose, **model 3a** has been applied, and the results were closely similar to results from model 1a, with very similar shape and steady state abundances of the same

---

[34]This dependency implies that the agents invoked in the destruction paths of CH_3N also see their respective abundance decreases $\sim$ proportionally to the enhancement in hydrogen density, so that it can explain the small effect of a change in the initial hydrogen nuclei density on the CH_3N relative abundance. The Y value associated to the methylamine is too small to infer the main destruction paths, but, from the Astrochem network, the main destruction agents seem to be CR & He^+, C^+, H^+, H_3^+ and HCO^+.

order of magnitude (c.f. Table 3.5). The reason behind this clear correlation is the same as the one deeply discussed in § 3.1. The whole results are illustrated in Figures B.20 and B.21 in Appendix B.

3.3 Quantitative comparison of our results to previous results and observational data

As mentioned several times in the previous discussions, no direct quantitative comparison to other simulated abundances nor to observational data has been performed so far. In this section, new results have been inferred, from a fourth model, namely **model b** (see Table 3.1). The latter is aimed at mimicking the initial conditions set by Prasad and Huntress (1980a,b), therefore allowing the rigorous direct comparison to these quite old results. The authors based their initial physical conditions (density, temperature, visual extinction,CR-ionisation rate) on the peculiar conditions prevailing in the Orion A Molecular Cloud. Moreover, they considered that all the H were in the H_2 form, as in our first 3 models. Indeed, this initial condition seems quite well justified - whether in this present study or in Prasad and Huntress (1980a,b), the simulated clouds are made of one unique homogeneous cell, with constant density, temperature and radiation field conditions with respect to time. In other words, in both cases, one simulates the conditions prevailing in the deep interior of a quiet cloud. In such place, the self-shielding of H_2 is highly efficient, as discussed from Table 1.3 in the introductory chapter. One may consequently consider in good approximation that all the hydrogen nuclei are initially in H_2 molecules. Let us however keep in mind that these considerations are not valid in the outer part of dense molecular clouds, where the physical conditions (i.e. radiation field, density, or even the temperature) are totally different.

Table 3.6 gathers the abundances from model b for species included in the PH's network. Let us note that the results from model 4 of the PH's study are given in fractional abundance with respect to H_2. In our results, we give the abundance with respect to the total H nuclei (noted n_H in the denominator of the vertical axis of all the abundances plot presented in this work). However, as mentioned above, we assumed in our initial conditions that all the hydrogen atoms are in the molecular form H_2. Moreover, we previously discussed that the H_2 abundance is constant over time (as checked through Astrochem computations where the n_{H_2}/n_H ratio is equal to 1 all along the simulation). Our results are therefore normalized by the same quantity as the PH's results, and they can be compared.

From this table, several comments can be made. Focusing first of all on the **neutral species**, the relative abundances computed in this work are of the same order of magnitude as the PH's results within a factor of 3, *except for HCN and CO_2*. More specifically, in the cases of H_2O, H_2CO and CO, our result is the smaller value, contrary to OH and NH_3 for which there is almost a perfect match. The highest discrepancy arises in the case of formaldehyde. This may be arguably partly explained through our previous findings - as discussed in paragraph 3.1.1, the PH's network accounts for the destruction of formaldehyde through charge transfer reactions with the H_3O^+ ion, leading to the protonated formaldehyde. However, the kinetic parameters encoded for this process in the PH's network under-estimate the kinetic constant. Furthermore, H_2O, H_2CO, NH_3 and CO are indeed studied in details in the second publication of Prasad and Huntress, namely Prasad and Huntress (1980a), and the main formation/destruction routes are well studied. As we have seen in our previous discussions, these main contributing paths in general match our results. The network used in Prasad and Huntress (1980a,b) displays an appreciable completeness for these small chemical entities. It may therefore arguably explain the good matching between our results and the PH's ones.

Moreover, when comparing both computed values to the observational data for H_2CO, NH_3 and CO, we find a good match with the observational data, which is not the case for H_2O. The departure from

Table 3.6: Comparison of the abundances of the precursors also studied in Prasad and Huntress (1980a,b) - computed abundances in this work (model b), computed abundance in Prasad and Huntress (1980a,b) (PH 1980), and observational data from observations towards the Orion A Molecular Cloud (Obs. data) when available.

Species	This work	PH 1980	Obs. data [*]
H_2O	$1.11\ 10^{-7}$	$5.04\ 10^{-6}$	$< 7\ 10^{-8}$ [a]
HCN	$7.62\ 10^{-11}$	$8.01\ 10^{-10}$	$\sim 2\ 10^{-10}$ [b]
H_2CO	$3.15\ 10^{-10}$	$9.93\ 10^{-10}$	$4\text{-}8\ 10^{-9}$ [c]
NH_3	$1.03\ 10^{-8}$	$1.25\ 10^{-8}$	$\sim 10^{-8}$ [d], $2\ 10^{-8}$ [e]
CO	$7.11\ 10^{-5}$	$1.44\ 10^{-4}$	$\sim 4\ 10^{-5}$ [f], $8\ 10^{-5}$ [g]
CO_2	$7.92\ 10^{-8}$	$2.09\ 10^{-6}$	-
OH	$5.87\ 10^{-9}$	$6.01\ 10^{-9}$	-
C^+	$2.46\ 10^{-11}$	$2.39\ 10^{-11}$	-
NH_3^+	$4.53\ 10^{-13}$	$8.15\ 10^{-13}$	-
H_2CO^+	$4.59\ 10^{-15}$	$2.23\ 10^{-16}$	-
H_3CO^+	$2.29\ 10^{-13}$	$6.23\ 10^{-16}$	-
CH_4N^+	$9.95\ 10^{-16}$	$1.63\ 10^{-18}$	-

[*] Some of the papers used here were referenced in the Prasad and Huntress (1980b) modelling work.

[a] From the upper limit inferred in Roberts and Herbst (2002), a modelling work aimed to rationalize observational results from the Submillimeter Wave Astronomical Satellite (SWAS). This value does concern the Orion A cloud especially, but rather dark, quiescent clouds from a general point of view.

[b] From the observationnal work performed by Gottlieb et al. (1975), using the 11-m radio telescope of the National Radio Astronomy Observatory (Kitt Peak).

[c] From the observationnal survey perfomed by Evans and Kutner (1976) and reference therein using the 5-m radio telescope at the Texas McDonald Observatory. This study is however not focused on the Orion A Molecular Cloud, but on a set of various dark clouds.

[d] From the observational work performed by Moris et al. (1973), using the 11-m radio telescope of the National Radio Astronomy Observatory (Kitt Peak).

[e] From the observational work of Ohishi and Kaifu (1998), performed with the 45-m mm-wave telescope and a very large acousto-optical radiospectrometer of the Nobeyama Radio Observatory. This study is however not focused on the Orion A Molecular Cloud, but on a set of various dark clouds.

[f] From the observational work performed by Liszt et al. (1974), using the 11-m radio telescope of the National Radio Astronomy Observatory (Kitt Peak).

[g] From the observational work of Ohishi et al. (1992) performed with the 45-m mm-wave telescope and a very large acousto-optical radiospectrometer of the Nobeyama Radio Observatory. This study is however not focused on the Orion A Molecular Cloud, but on a set of various dark clouds.

the observational data to the modelled H_2O pure gas-phase abundances is indeed discussed in Roberts and Herbst (2002). They actually argued that the pure gas-phase models are overestimating the gas-phase abundance of water, especially in cold conditions. They showed that the H_2O abundance is best reproduced with a more comprehensive model, taking the interplay with the solid phase into account, but with still an overestimation during the out-of-equilibrium epoch (arguably due to uncertainties in their desorption time-scale). The solid phase chemistry of H_2O is indeed expected to be important in such temperature conditions, its residence time being quite long, as argued by Roberts and Herbst (2002). Furthermore, the good match between the pure gas-phase modelled abundances of H_2CO, NH_3 and CO with the observational data deserves further attention. Indeed, as discussed all along this work, a pure gas-phase astronomical model in dense and cryogenic conditions is expected to be biased by neglecting the interplay with the dust grain chemistry. We therefore do not necessarily expect a matching between the simulated and observed relative abundances. Assuming an appreciable completeness and accuracy of both networks, one may give different interpretations to this similarity:

i. One may imagine that the number of adsorbed species balance the number of desorbed species. In that context, one has to not forget to account for the potential production of these species in the dust grain mantle or at its surface. Approaching a balance between the number of adosprbed

and desorbed entities for each H_2CO, NH_3 and CO may explain the small difference between the simulated pure gas-phase abundances and the observational ones.

ii. These small species, at least NH_3 and CO, may be rapidly desorbed from dust grain at such densities. Indeed, we are not considering protoplanetary disks, the densities concerned are well lower and the species adsorbed in dust grain are therefore not accumulating over several layers, trapping some chemical species in the bulk of the grain mantle. As a consequence, for NH_3 and CO, the similarity between the pure gas-phase modelled abundances with the observational data may be potentially explained by a grain surface chemistry which is not dominating in such astrophysical conditions. This hypothesis deserves more investigations.

Let us however keep in mind that both networks, especially the PH's network, are tarnished by some uncertainties on the encoded kinetics parameter. The real explanation may be a mixture of the different possibilities.

Concerning the discrepancy between our inferred HCN abundance and the PH's value, it may be partly explained, similarly to the formaldehyde, by the lower kinetic constant associated to the destruction of HCN through charge transfer reactions with H_3O^+ in the PH's network. Moreover, regarding the observational data, it ranges just between the two modelled values. The difference between the modelled and observational results may be partly due to the computed values coming from pure gas phase astrochemical models, not accounting for the solid phase chemistry and its interplay with the gas-phase, as already deeply discussed. To this first source of explanation, one should add the uncertainties on the encoded kinetic parameters. More investigations are needed to further comment this result. The same comment can be made for CO_2.

Focusing now on the **charged species**, the C^+ abundances match perfectly, and the NH_3^+ abundances are on the same order of magnitude, within a factor of two. This may be explained by the very small level of molecular complexity of these species. The network used in this study and the PH's network are therefore displaying a same level of completeness of the main contributing routes concerning these species. The encoded kinetic parameters have been compared and present similar values, with some small discrepancies which arguably come from the improvement of our accuracy in the kinetic parameter determination.

Concerning the more complex cations, namely H_2CO^+, H_3CO^+ and CH_4N^+, the computed values by PH are well under our computed abundances. In both cases, the number of included processes is quite small, but the completeness is largely more appreciable in the more recent network used in this work. Indeed, H_2CO^+ and H_3CO^+ are only involved in two formation routes (against more than 10 in our case) in the PH's network, while CH_4N^+ is only formed through one reaction (3 in the Astrochem network).

Main conclusions from this chapter

Through this chapter, the precursors of the selected glycine formation paths have been studied in details. More specifically, low complexity glycine precursors have been investigated in order to better understand their behaviour in a pure gas-phase cryogenic medium.

Firstly, the precursors of the neutral and activated (cationic or protonated routes) Strecker-like synthesis have been put under the spotlight. Their completeness is expected to be very appreciable regarding their high Y value. In the context of dense molecular cloud conditions, we discussed the main formation/destruction paths of each of these very simple and basic interstellar species, their

relative abundance with respect to the number density in hydrogen nuclei, and the effect of a change in the mean density of the considered modelled cloud on the final steady state abundances[35].

The major results are schematized in Figure 3.26. The description of this scheme is given in the top panel. Notice that the major formation/destruction paths only concern species that have been studied in section 3.1. Visually, they are written in bold text, and are allocated to a given color & surrounding shape depending respectively on their steady state abundance (from model 1a) and their behavior against a change in the mean cloud density (from model 2a versus model 1a). Moreover, it is good to note that the transformation $H_2CO + HCNH^+ \rightleftharpoons HCN + H_3CO^+$, affecting the out-of-equilibrium chemistry of H_2CO and, to a less extent, of H_3CO^+, is not represented on the scheme. Indeed, it has no quantitative consequences on the final steady state abundance.
The grey part illustrates the paths to be investigated for an extension of the network towards more advanced glycine precursors, and will be our starting point to develop our discussion in Chapter 4. Let us notice that the route b has not been represented for the sake of clarity. Indeed, as we have seen, reaction 1.10 seems to be prohibited at cryogenic temperatures, even in an icy matrix lowering the activation barriers. Nevertheless, the possibility of redistribution of reaction heat cannot be ruled out, but no current astrochemical code is able to account for it.

Secondly, the Woon mechanism has been intensively discussed. We noticed that the Woon's genuine unmodified idea concerns very small species without any fragment loss. Indeed, it has been originally thought for the solid-phase chemistry. Contrary to the Strecker-like mechanism for which it is difficult to imagine a glycine formation path with fragments while keeping the basic chemical principle behind the original Strecker-like route, including a kind of a fragment loss through intramolecular rearrangement and subsequent dehydration, the Woon principle may be revisited to account for fragment loss while staying quite similar to the Woon's idea. The proposed revisited Woon-like mecanism is illustrated in Figure 3.20 and its feasibility has been investigated in section 3.2. The implicated species which are not common to the Strecker-like precursors, namely HCOOH, $CH_3O_2^+$, CH_3N, CH_4N^+, CH_5N^+ and CH_6N^+ are included in the Astrochem network, but with a Y under the coded X value of 12. It therefore implies that we were not able to retrace the main contributing paths. We however inferred interesting results, which are represented in Figure 3.27. As for the main conclusion from the Strecker-like precursors analysis, the description of this scheme is highlighted in the top panel of the Figure. The grey array concern the two termination paths proposed in the revisited Woon-like path, and our discussion in Chapter 4 will be built around them. Let us note that the abundances of the methanimine and its iminium form is given in Figure 3.27 contrary to Figure 3.26. Indeed, as previously discussed, the reaction towards these two species in the Astrochem network do not include the paths from the Strecker-like synthesis. It however constitutes a clear similarity between the two main investigated paths (Strecker-like & Woon-like).

Finally, in section 3.3, we performed a quantitative comparison of our steady state results from model b to results earlier inferred in Prasad and Huntress (1980a,b) (PH), with a much simpler astrochemical network, and to observational data. From a general point of view, we observed

- a good match (within a factor of 3) between the PH's results and ours for the neutral species, except for HCN and CO_2 for which the discrepancy is higher (which may be partly explained by the lower kinetic constant associated with the destruction of HCN through charge transfer reaction with H_3O^+ in the PH's network);

---

[35]These being reached after an elapsed time of $\sim 1\,10^6$ years. Indeed, we have seen for the analysis of Figure 3.9 (§ 3.1) that this timescale is constant with the hydrogen density if ξ stays unchanged.
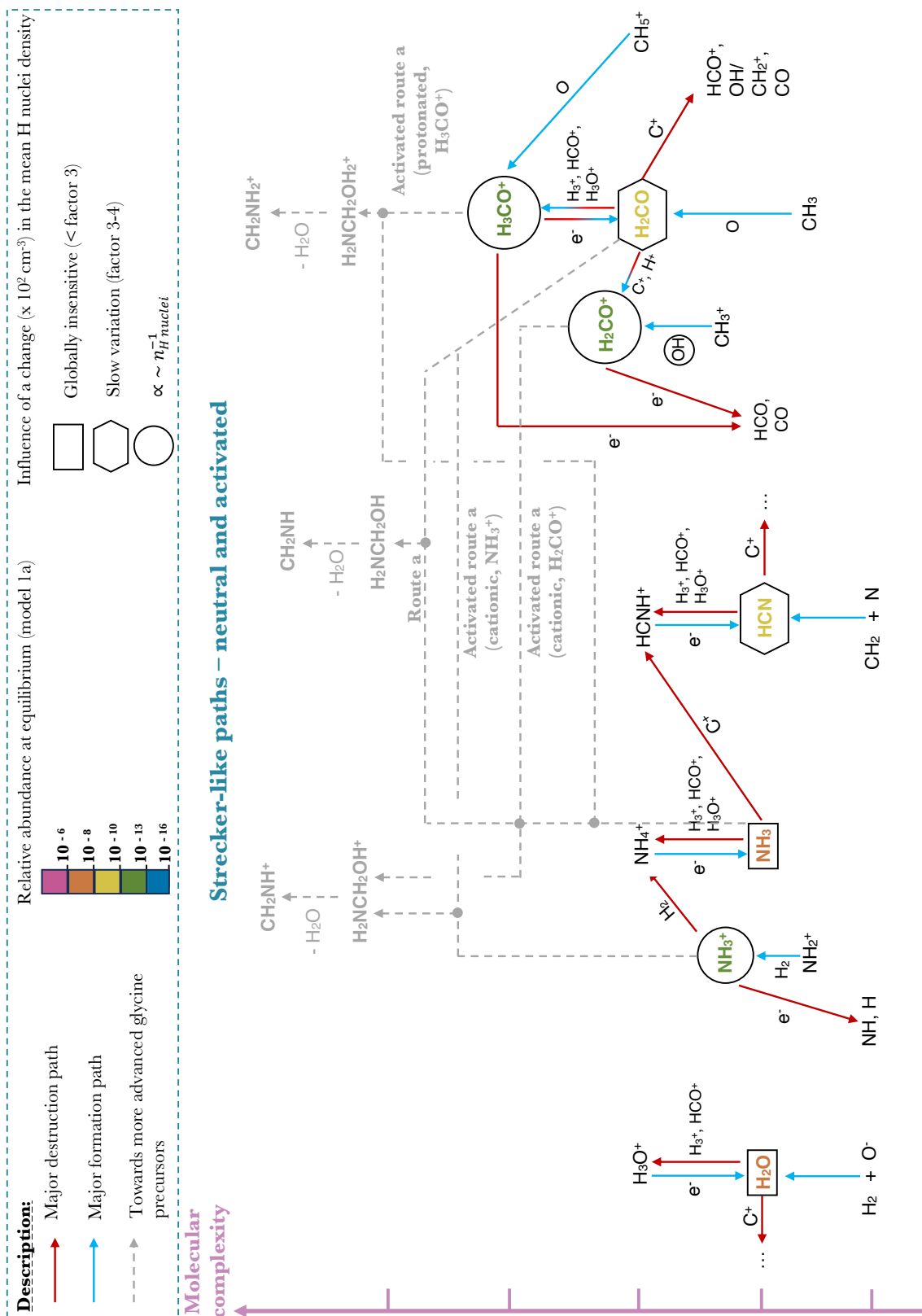
Figure 3.26: Astrochemical network focusing on the main results from section 3.1 (subsections 3.1.1 and 3.1.2) in which the basic precursors to the neutral and activated Strecker-like mechanism have been investigated. The grey arrows stand for the discussed path towards more advanced glycine precursors (neutral & cationic methanimine, and the corresponding iminium, through route a.)
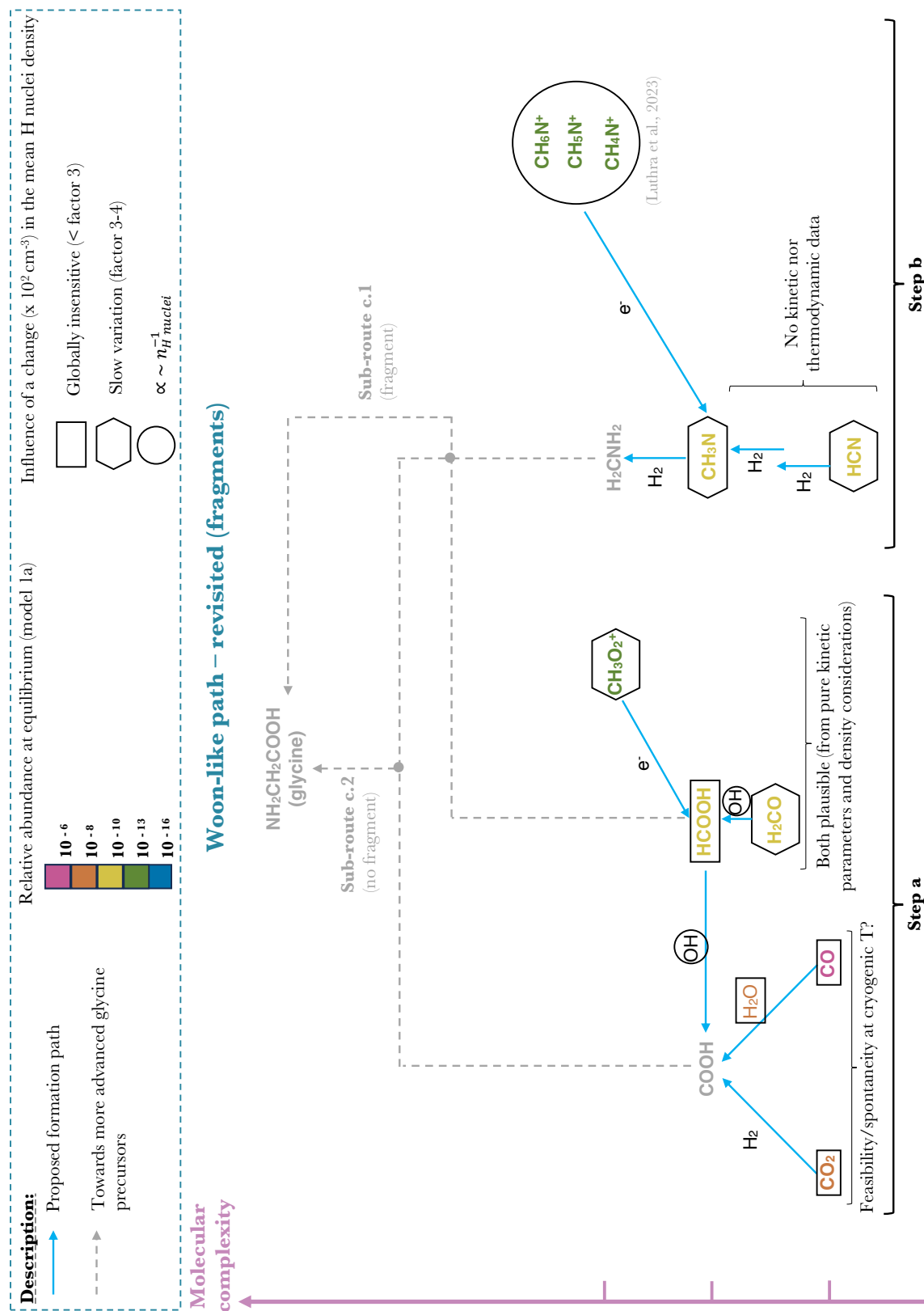
Figure 3.27: Astrochemical network focusing on the main results from section 3.2 in which the basic precursors to the revisited Woon mechanism have been investigated. The grey arrays stand for the two proposed termination paths towards glycine (see Figure 3.20).

- a good match between our results and the observational data for H_2CO, NH_3 and CO. It however fails for the H_2O abundance, which can be explained by the considerations in Roberts and Herbst (2002) where they argued that pure gas-phase models overestimate the gas- phase abundance of water, especially in cold conditions, since its solid-phase chemistry of water is expected to be important. For HCN and CO_2, the observational values just range between the two modelled values;

- a good match between our results and PH's results for the C^+ and NH_3^+ cations;

- a complete disagreement between our computed abundances and the PH's ones for the more complex cations, namely H_2CO^+, H_3CO^+ and CH_4N^+. In each case, the PH's result is well below our computed value. This may be arguably due to a difference in the level of completeness in the inclusion of their main contributing routes; even if it is quite low in the Astrochem network, it is more appreciable than in the PH's network.

This notwithstanding, it is however important to keep in mind that we are considering a purely gas-phase model. The relative abundances computed in this work are therefore ineluctably biased by omitting the interplay between the gas and solid phases coexisting in such astrophysical environments. This remark is worth being nuanced. Indeed, the astrophysical environment modelled here is a dense molecular cloud, with a mean density of 10^6 particles per cm^3 at most (see Table 1.3). Such densities are well below the typical densities that can be reached in the middle plane of a protoplanetary disk. Far enough from the protostar, the interplay between the grain surface and gas-phase chemistry is expected to be very active. Not taking such interplay in these conditions into account would result in a significant departure from the physico-chemistry of the environment. In a molecular cloud, the densities are too low to expect a significant contribution from the surface chemistry, and multiple adsorbed layers are less probable. Mantle chemistry is therefore expected to be not very contributing. Moreover, the very low temperatures prevailing in those regions inhibit most of the migrations on the grain surface, reinforcing the idea that the surface chemistry should not be so impacting. However, these cryogenic temperatures represent a favourable factor to the residence of a given chemical entity on the grain surface (see Table 1.7). For the low molecular complexities studied in this chapter, one may therefore expect the computed abundances to be biased, but to a small extent.

Chapter 4

Towards More and More Advanced Precursors of Glycine

In this Chapter, we will discuss the major paths that have to be investigated from the precursors analyzed in Chapter 3. This discussion will be entirely based on the schemes in Figures 3.26 and 3.27. Let us note that no network extension will be performed since we do not have all the parameters to be encoded in it. Indeed, some of the gas-phase activation barriers are known, as mentioned in Table 1.8, but some of them are missing. Moreover, these activation barriers are generally computed without any mention of the working temperature and pressure (except in some papers, such as in Rimola et al. (2010)). It therefore arguably means that they are inferred at the default values of T and P (T = 298.15 K and P = 1 atm when using Gaussian), which is not scientifically rigorous in the peculiar conditions of the astrochemistry taking place in a cold molecular cloud. Indeed, at such cryogenic temperatures, the vibrational energy levels are not yet activated. The energy of the reactants and transition state are therefore impacted, and the activation barriers are likely modified. Additionally, the alpha, beta and gamma parameters are not constrained for all the reactions that will be discussed here. Therefore, this theoretical discussion will mainly consist of a coming back to our previous considerations, but only focusing on future possible network extensions towards more advanced glycine precursors. It would allow the reader to have a clearer view of the various possibilities, regardless of the other details considered in Chapter 3.

4.1   Focus on the Strecker-like synthesis

First of all, let us address the neutral Strecker-like synthesis. As discussed in the Introductory chapter, the Strecker-like mechansim is sometimes ignored in the literature (e.g. Garrod (2013)) due to some of the activation barriers, even in the solid-phase (e.g. imine formation). It is however important to keep in mind that a molecular cloud has a dynamic life, generally considered after 10^7 years. After such a timescale, a molecular cloud may collapse, leading to an increase of its temperature, pressure and density. The population of chemical entities that should be considered just before this collapse is the population that was present at the end of the non-dynamic life of the cloud. Regarding the quite appreciable equilibrium abundance (reached after 10^6 years) of the precursors considered in this Strecker-like neutral path, one cannot exclude that a part of this population, far enough from the native protostar, may condense on dust grains and follow the Strecker-like mechanism. The preceding study was therefore interesting to evaluate this ending population, at least in a pure gas-phase view.

To further comment on the imine formation (quite high for low temperature conditions, as argued in Rimola et al. (2010) and discussed in the Introductory chapter), our previous hypothesis can be

highlighted: as discussed in Chapter 3, no fragment loss has been considered in the different Strecker-like paths studied in this work. Indeed, as previously justified, it is difficult to find a mechanism that takes fragment loss into account while considering the same chemical principles as in the pure Strecker-like synthesis, originally designed for the solid phase. However, we argued that, contrary to the Woon path, there is a H_2O molecule loss through intramolecular rearrangement. Taking into account that

- such a dehydration presents a non-negligible activation barrier;

- low temperature species are not able to evacuate the excess of energy in their vibrationnal-energy level or through interactions with a solvent/solid matrix after the encounter with a reaction partner;

it should be interesting to wonder if this excess of energy can be sufficient to allow such intramolecular rearrangement and water loss at cryogenic temperatures.

Moreover, it is good to note that the formation of H_2NCH_2OH through route a, according to Rimola et al. (2010), is expected to be feasible in cryogenic conditions, but seems more likely in the solid phase regarding the catalytic effect of the proton relay mechanism. It should therefore be interesting to evaluate the abundance of these precursors in the solid phase, with a more advanced Astrochemical code (not available/practicable while this thesis is being written).

Regarding route b, at the present day, the scientific community is still not able to reckon with the reaction heat redistribution to the direct surrounding in a given chemical system. To go further, little effort has been devoted to this problem, except in Process Safety Strategy in chemical engineering. We will come back on this point in Chapter 6.

Concerning the activated routes, as we have commented in § 3.1.2 of the previous chapter, the considerations in Walch et al. (2001) for the cationic activation seem to be too restrictive, especially in out-of-equilibrium conditions. Indeed, they considered the cationic form of ammonia but not the formaldehyde cation because of an irrelevant selection criterion: the ionization potential. These too simple considerations do not account for the peculiar conditions existing in the gas phase of a dense molecular cloud, that is

- the population of hundreds of species, each of them participating in a number of reactions (this number itself depending on the medium in question), and therefore presenting their own abundance;

- the absence of direct ionizing radiation, the only source of cations therefore being the CR-induced processes and subsequent charge transfers.

In this context, when analyzing the abundance profiles, we noticed that the H_2CO^+ profile overhangs the H_3CO^+ and NH_3^+ ones in out of equilibrium conditions, until an elapsed time of $\sim 1\ 10^4$ years. However, the NH_3 out-of-equilibrium abundance is lower than the H_2CO one until $\sim 10^5$ years. In equilibrium conditions, the H_3CO^+ and NH_3^+ abundances are quite similar, but the NH_3 is more abundant than the formaldehyde. Taking all of these considerations together, it should be interesting to constrain the kinetic parameters of the reaction towards $H_2NCH_2OH^+/CH_2NH^+$ (using NH_3^+/H_2CO and H_2CO^+/NH_3) and towards $H_2NCH_2OH^+/CH_2NH^+$ (see Figure 3.26) in order to be able to assess the potential contribution of each route with higher confidence. Moreover, one has to check if the two-step process towards the activated forms of H_2CNH are feasible at cryogenic temperature.

It is also interesting to note that, for a more ambitious work using a future more comprehensive astrochemical code, theses kinetic parameters should be determined in the different phases constituting the molecular cloud (gas-phase, grain surface and icy mantle).

4.2 Focus on the Woon-like synthesis (& its variants)

In the case of the revisited Woon's mechanism, coming back to Figure 3.27, it should be interesting to test the feasibility and thermodynamical spontaneity of the CO_2/H_2 and CO/H_2O processes at different temperature ranges. Moreover, the reaction between HCN and H_2 may also be thermochemically studied, even if the proposition in Luthra et al. (2023) seems to be a good methanimine supplier.

Additionally, the kinetics parameters of the grey array in Figure 3.27 also have to be constrained.

In a more ambitious work that would use a more comprehensive multi-phase code, it should therefore be interesting to test both the unmodified Woon mechanism (in solid phase) and the revisited one (in pure gas-phase for the steps a and b, and for the c.1 subroute, and in solid phase, after accretion, for the c.2 termination path).

Finally, similarly to Rimola et al. (2012), one may think about an alternative with fragment loss (for the gas-phase context) taking both advantage of cationic and radical species. This may however be more challenging (see Figure 1.14).

Chapter 5

Conclusions

Throughout history, the issue of the origin of living bodies has always fascinated humans. From paleontology to biochemistry, different approaches may be adopted to tackle this question. An interdisciplinary approach is therefore required to gather all the clues towards a clear understanding of this issue. Considering a bottom-up approach, one must firstly wonder what the origin of the primary precursors to terrestrial life are. These precursors are the four families of macromolecules of fundamental biochemical interest: carbohydrates, lipids, nucleic acids, and proteins. The origin of those prebiotic molecules on Earth is however still a matter of debate, with two opposite points of view: the exogeneous (extraterrestrial synthesis and transfer to the terrestrial system via some mechanisms), and the endogenous (in situ formation on Earth) origin.

In that context, this work was to a large extent embedded in the search of the *origin* of *terrestrial amino acids*, building blocks of proteins. Therefore, an **exogeneous** point of view has been adopted. It can be justified through several previous results, such as the identification of amino acids in meteoritic samples (e.g. Murchison meteorite) with isotopic ratios pointing towards a non-terrestrial origin, and the detection of glycine in the coma of comet Churyumov-Gerasimenko as well as of some of its likely precursor in the Interstellar Medium (ISM). Consequently, those results seem to indicate that amino acids may be synthesized in the ISM before any terrestrial processing.

In this scope, we have been focusing our discussions on the possibility of the **formation of glycine in dense molecular clouds**. Several glycine formation pathways in the ISM have been investigated in the literature, but most of those studies were based on quantum chemical computations, focusing on one mechanism at once at a time. In order to reach a more complete view of the problematic and compare the relative contributions of the proposed mechanisms, an astrochemical model has to be used. However, no available network includes the proposed formation/destruction routes of glycine. Moreover, the available and usable Astrochemical models developed in the literature are mostly pure gas-phase models; there exist two open-source multi phases codes, namely *Nautilus* and the recent *Chempl* model, but their practical implementation was not possible[1]. After a deep bibliographic analysis of the many proposed mechanisms and a selection of the most relevant ones to be considered in the Introductory chapter (see Table 1.8), the gas-phase source code Astrochem has been

---

[1]The implementation of *Nautilus* was totally impossible, even with the help of computer technicians, one of the main problems being the need of an old and not anymore available Fortran compiler. Concerning *Chempl*, most of its functionalities were not usable (such as the computation of the major formation/destruction pathways, the use of the python package, ...). Moreover, in both cases, the interplay between the constituents of the bulk of the ice is not appropriately considered: the encounter between bulk species is assumed to be due to thermal diffusion, which is not appropriate for dark molecular clouds characterized by low temperatures inhibiting this motion. A statistical approach would have been more appropriate for that range of temperatures.

used in order to study the temporal evolution of the abundances and major formation/destruction pathways of the most likely precursors of glycine in pure gas-phase. The basic principle of operation of this code has been explained in Chapter 2.

In Chapter 3, we thoroughly discussed the behaviour in a pure gas-phase cryogenic medium of the low complexity glycine precursors for both the Strecker-like synthesis (neutral and activated through cation or protonation) and Woon's mechanism. Intermediate and comprehensive conclusions have been drawn at the end of this third chapter. Figure 3.26 illustrates the main conclusions from our analysis of the precursors for the neutral and activated Strecker-like synthesis. Regarding the high completeness and high Y values associated to theses species, we have been able to infer the main formation/destruction path or each species. On the other hand, concerning the Woon mechanism, a revisited version of the original idea has been proposed, in order to take the fragment loss arising in interstellar gas-phases into account. This proposition is given in Figure 3.20. In that context, apart from the common precursors to the Strecker-like mechanism, the involved species display low Y value, lower than the X value chosen by the Astrochem builders. It therefore implies that the main paths could not be computed through Astrochem tools. We however deeply commented on the question of feasibility of steps a and b, and the results have been gathered in Figure 3.27.

The fourth Chapter is simply an extension of this conclusion, aimed to be separated from the third chapter to only focus on potential network extension.

We can consequently conclude that our results provides a first deep insight into the main proposed glycine precursors, but more complete and rigorous quantum chemical simulations are required to better constrain the rates equations to be used to extend the original network towards glycine. Moreover, a playable three-phase model, allowing the identification of the major formation/destruction routes of species with a rigorous consideration of the interplay between bulk-ice species, would be very welcome.

Chapter 6

Scientific Perspectives

In this last chapter will be addressed the main perspectives emanating from this work. Let us notice that the perspectives of direct extension of the used network have been discussed in details in Chapter 4. We will therefore not come back to these considerations here, but rather focus on more global and long-term scientific perspectives.

6.1 Towards a more comprehensive and appropriate Astrochemical code

As previously discussed, no open source and practicable multi-phase astrochemical code currently exists in the scientific community. However, to better understand the astrochemistry taking place in a given molecular cloud, the interplay between the gas phase and the solid phase (see Figure 1.7) should be taken into account. Indeed, taking the example of H_2O, we commented that the pure gas-phase H_2O abundance is arguably biased following a significant contribution from the solid phase, as argued by Roberts and Herbst (2002). Therefore, it should be welcome to build a new playable Astrochemical code accounting for the interplay between the solid and gas phases (adsorption/desorption) as well as the contribution from the bulk mantle chemistry (chemistry happening within the icy matrix surrounding dust grains in dense and cold medium). In such a prospective three-phase astrochemical approach, the bulk-mantle chemistry and the migration on the solid surface should be considered in a rigorous way. Indeed, as already stated, at cryogenic temperatures, the thermal migration is prohibited; a statistical approach to deal with reaction partner encounters in the solid phase should therefore be more relevant for a cryogenic context (as implemented in Ioppolo et al. (2021) through Monte Carlo methods). When the temperature increases, above $\sim$ 20 K the H may migrate. Most of the other small species constituting such icy mantle are expected to diffuse above $\sim$ 40 K.
Therefore, in order to build a playable astrochemical code that is not restricted to specific cases, both methods should be implemented, as far as possible, in order to be able to change the principle of reagent encounters according to the considered environment.

In that context, after having constrained the missing kinetic parameters (see Chapter 4) in the different phases (some of the processes being relevant only in one or two phases), these should be used as input to feed such a more ambitous multi-phase code.

It should also be interesting to think about a way to reckon with the reaction heat redistribution of exergonic processes to the direct surrounding in the solid phase. Indeed, as justified beforehand, it could be a source of energy in cryogenic ices, allowing to overcome some activation barriers. In other

words, the energy present in such a solid cryogenic phase is maybe more appreciable than what one would expect by neglecting such an energy redistribution (as discussed in the scope of the potential of route b). Let us however notice that the ΔH and ΔS associated to a given chemical transformation vary with the temperature. They have therefore to be evaluated in different temperature ranges. Such considerations are however not easy to practically implement in an astrochemical code. Whether in the field of astrochemistry or pure chemistry, the efforts are not focused on it. This heat redistribution is only considered for chemical engineering in order to avoid any thermal runaway reactions (Process Safety Strategy in the jargon of chemical engineers) (Hungerbühler et al, 2021). Such an assessment of the thermal process safety is generally illustrated by what they called *Semenov Diagrams*, as shown in Figure 6.1. Such a diagram represents the heat produced by the reaction and the heat removed by the cooling system against reaction temperature.
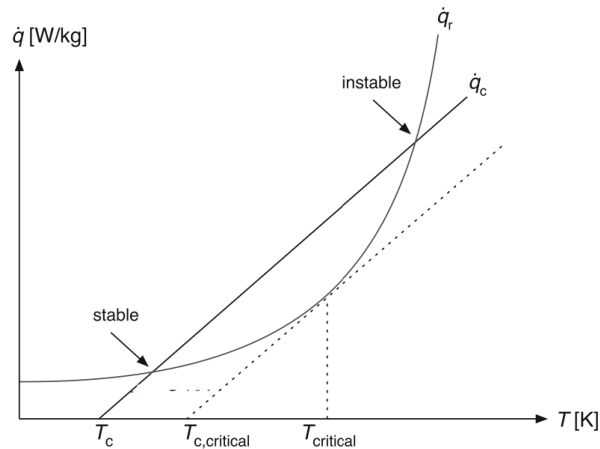
Figure 6.1: Semenov Diagram representing the heat balance of a batch reaction; T_c stands for the coolant temperature, $T_{c,critical}$ for critical temperature of the coolant and $T_{critical}$ for the critical temperature (defined as the position on the x-axis where the slope of the heat produced is equal to the slope of the heat removed - above this temperature, a thermal run-away will begin). Concerning $\dot{q}_r$ and $\dot{q}_c$, they are respectively defined as the heat produced by the reaction and the heat removed by the cooling system, from Hungerbühler et al (2021)

.

Indeed, exothermic reactions in a volume-confined system (constant volume) may act as a positive feedback loop since they are themselves accelerated by a temperature rise, increasing heat produced by the reactions by unit time. As a consequence, if the heat in such a medium is not removed through an efficient mechanism, it may enhance the kinetics through a rise in the medium temperature from reaction heat.

These considerations are however only restricted to the variation of enthalpy (ΔH). As argued previously, it is nevertheless more rigorous to consider exergonic process and the associated release of reaction energy. In addition, such diagrams concern system with a linear external heat removal with respect to the temperature. In the case of a molecular cloud, the potential heat removal may arise from endothermic/endergonic reactions for instance, which is an internal cooling source, not necessarily evolving linearly with the temperature. Moreover, it concerns a constant volume, which can be considered as valid in a dust grain mantle. If one finds a method to consider this reaction heat transfer to the surrounding medium, and the balance with the cooling due to endergonic processes, one may potentially reconsider the proposition from Woon (2000) (heat reaction redistribution to the immediate surrounding) or, more rigorously, the reaction energy redistribution.

6.2   Towards more rigorous kinetic parameters

In most of the analyzed quantum studies dealing with glycine formation paths, the results are generally inferred through DFT computations using the hybrid functional B3LYP. Even if the most used, this functional is however not always so accurate; it systematically underestimates reaction barrier heights, and suffers of inaccuracy in the computation of interactions dominated by medium-range correlation energy, such as van der Waals attraction (dominating the encounter between neutral species) (Zhao and Truhlar, 2008). A benchmark through high-level wavefunction methods could be used to select appropriate exchange-correlation functionals.

6.3   What about the real distribution of the chemical entities in a molecular cloud? And what about its dynamic life?

In this present work, we have only considered molecular clouds modelled with a unique cell, homogeneous and temporally constant with respect to temperature, mean density, CR-ionisation rate and mean radiation field. However, the reality is more complex; one may for instance assume from a more realistic point of view a power-law or exponential decrease of the mean density, temperature, and visual extinction A_V from the center of the cloud, associated with a constant CR-ionisation rate. Considering different cells and computing their temporal evolution in terms of chemical population, as allowed in the functionalities of Astrochem, would lead to a more global view of an interstellar dense cloud, rather than the rather limited consideration of the cloud interior.

Coming back to our previous discussions, it would allow us to consider the totally different chemistry existing in the deep cloud, compared to what is happening at the outer edges, where the interaction with direct ionizing/exiting radiation field is no longer negligible.

Additionally, as mentioned before, the dynamic time-scale of a given molecular cloud amounts to few 10^6 up to 10^8 years. The simulations in this work have therefore been restricted to this time interval in order to neglect change in the physical conditions defining the modelled clouds.

To further insight into the fate of a molecular cloud after its quiet life in a temporary hydrostatic equilibrium, one may wonder about what is the quantitative consequence of an encounter with a shock-front (of a supernova remnant for instance) on the astrochemistry taking place in a molecular cloud. In a long-term and cooperative work, the perturbation of the hydrostatic equilibrium of the cloud may be modelled through (magneto)hydrodynamic simulations. These can be theoretically coupled with the Astrochem code, as stated in their documentation Maret and Bergin (2015), by using time-dependant multiple-cells physical parameters (source file). It could therefore be interesting to perform such simulations from abundances after an elapsed time of:

- 10^6 years;

- 10^8 years.

6.4   And beyond glycine?

In a longer term, such more realistic proposals of scientific perspectives and improvements of the current available astrochemical codes are expected to be extended to other amino acids, and if possible, to sugars and various important prebiotic chemical species.

Bibliography

Abplanalp et al. Low-temperature synthesis of polycyclic aromatic hydrocarbons in Titan's surface ices and on airless bodies, Science Advances. 5: 11p, 2019.

Altwegg et al. Prebiotic chemicals—amino acid and phosphorus—in the coma of comet 67P/Churyumov-Gerasimenko, Science Advances. 2: 5p, 2016.

Aléon et al. Multiple Origins of Nitrogen Isotopic Anomalies in Meteorites and Comets, The Astrophysical Journal. 772: 1342–1351, 2010.

Asplund et al. The chemical composition of the Sun, Annual Review of Astronomy & Astrophysics. 47: 481–522, 2009.

Atkins and de Paula. *Physical Chemistry, 11th Edition, Oxford University Press.* 2017.

Becker. From Langmuir to Ertl: The "Nobel" History of the Surface Science Approach to Heterogeneous Catalysis, Encyclopedia of Interfacial Chemistry. 46: 99–106, 2018.

Belloche et al. Detection of amino acetonitrile in Sgr B2(N), Astronomy & Astrophysics. 482: 179–196, 2008.

Belloche et al. Increased complexity in interstellar chemistry: detection and chemical modeling of ethyl formate and n-propyl cyanide in Sagittarius B2(N), Astronomy & Astrophysics. 499: 215–232, 2009.

Bernstein et al. Racemic amino acids from the ultraviolet photolysis of interstellar ice analogues, Nature. 416: 401–403, 2002.

Blagojevic et al. Gas-phase syntheses for interstellar carboxylic and amino acids, Monthly Notices of the Royal Astronomical Society. 339: L7–L11, 2003.

Bohme. PAH [Polycyclic Aromatic Hydrocarbons] and fullerene ions and ion/molecule reactions in interstellar and circumstellar chemistry, Chemical Reviews. 92: 1487–1508, 1992.

Busemann et al. Interstellar chemistry recorded in organic matter from primitive meteorites, Science. 312: 727–730, 2006.

Campisi and Candian. Do defects in PAHs promote catalytic activity in space? Stone–Wales pyrene as a test case, ACS Earth and Space Chemistry. 22: 6738–6748, 2020.

Cheung et al. Detection of NH_3 Molecules in the Interstellar Medium by Their Microwave Emission, Physical Review Letters . 21: 1701–1705, 1968.

Colzi et al. Carbon isotopic fractionation in molecular clouds, Astronomy & Astrophysics. 640: 20p, 2020.

Courmier et al. A computational study of the water-catalyzed formation of NH_2CH_2OH, Chemical Physics Letters. 405: 357–363, 2005.

Cronin and Moore. Amino Acid Analyses of the Murchison, Murray, and Allende Carbonaceous Chondrites, Science . 172: 1327–1329, 1971.

Cronin and Pizzarello. Enantiomeric Excesses in Meteoritic Amino Acids, Nature. 275: 951–955, 1997.

De Becker. Astrochemistry: The issue of Molecular Complexity in Astrophysical Environment, Bulletin de la Société Royale des Sciences de Liège. 82: 33–94, 2013.

De Becker. *Astrochemistry, SPAT0020-2, lecture notes.* 2021-2022.

Draine. Photoelectric heating of interstellar gas, Astrophysical Journal Supplement Series . 36: 595–619, 1978.

Draine. *Physics of the Interstellar and Intergalactic medium, Princeton series in Astrophysics.* 2011.

Du et al. Chempl: a playable package for modeling interstellar chemistry, Research in Astronomy and Astrophysics. 21: 11p, 2021.

Elsila et al. Mechanisms of Amino Acid Formation in Interstellar Ice Analogs, The Astrophysical Journal. 660: 911–918, 2007.

Elsila et al. Cometary glycine detected in samples returned by Stardust, Meteoritics and Planetary Science. 44: 1323–1330, 2009.

ESA. ESA's webpage of the Rosetta mission. URL `https://www.esa.int/Space_in_Member_States/France/Rosetta`.

Evans and Kutner. H_2CO emission at 2 millimeters in dark clouds, Astrophysical Journal . 204: L131–L134, 1976.

Garrod. A Tree-Phase Chemical Model of Hot Cores: the Formation of Glycine, The Astrophysical Journal. 765: 29p, 2013.

Garrod and Herbst. Formation of methyl formate and other organic species in the warm-up phase of hot molecular cores, Astronomy & Astrophysics. 457: 927–936, 2006.

Garrod and Pauly. On the Formation of CO_2 and Other Interstellar Ices, The Astrophysical Journal. 735: 18p, 2011.

Garrod et al. A Tree-Phase Chemical Model of Hot Cores: the Formation of Glycine, The Astrophysical Journal. 682: 283–302, 2008.

Garvie and Buseck. Prebiotic carbon in clays from Orgueil and Ivuna (CI), and Tagish Lake (C2 ungrouped) meteorites, Meteoritics and Planetary Science. 42: 2111–2117, 2007.

Glavin et al. Amino acid analyses of Antarctic CM2 meteorites using liquid chromatography-time of flight-mass spectrometry, Meteoritics and Planetary Science. 41: 889–902, 2006.

Gottlieb et al. Observations of millimeter-wave HCN in four prototype clouds, Astrophysical Journal. 202: 655–672, 1975.

Graninger et al. The HNC/HCN ratio in star-forming regions, The Astrophysical Journal Letters. 787: 11p, 2014.

Hadraoui et al. Distributed glycine in comet 67P/Churyumov-Gerasimenko, Astronomy & Astrophysics (Special issue) . 630: A32, 8p, 2019.

Herbst and Klemperer. The Formation and Depletion of Molecules in Dense Interstellar Clouds, The Astrophysical Journal . 185: 505–533, 1973.

Hollis et al. Interstellar Glycoaldehyde: the First Sugar, the Astrophysical Journal . 540: 107–110, 2000.

Holtom et al. A Combined Experimental and Theoretical Study on the Formation of the Amino Acid Glycine (NH_2CH_2COOH) and Its Isomer ($CH_3NHCOOH$) in Extraterrestrial Ices, The Astrophysical Journal. 626: 940–952, 2005.

Hungerbühler et al. *Chemical Products and Processes Foundations of Environmentally Oriented Design (Chapter 8: Thermal Process Safety), Springer.* 2021.

IAS Orsay. Paris-Sarclay University, Faculty of Sciences of Orsay: Institut d'Astrophysique Spatiale (IAS). URL `https://www.ias.u-psud.fr/en/research-activities/astrochemistry-and-origins`.

Iglesias. The Chemical Evolution of Molecular Clouds, The Astrophysical Journal . 218: 697–715, 1977.

Ioppolo et al. A non-energetic mechanism for glycine formation in the interstellar medium, Nature Astronomy. 5: 197–205, 2021.

Japan Aerospace Exploration Agency (JAXA). JAXA, In Search of Origins, Asteroid Explorer "Hayabusa2". URL `https://global.jaxa.jp/projects/sas/hayabusa2/`.

Jenkins. A Unified Representation of Gas-Phase Element Depletions in the Interstellar Medium, The Astrophysical Journal. 700: 1299–1348, 2009.

Jones. Dust evolution, a global view I. Nanoparticles, nascence, nitrogen and natural selection ... joining the dots, Royal Society Open Science (The Royal Society Publishing). 3: 17p, 2016.

Kalvans and Shmeld. Subsurface chemistry of mantles of interstellar dust grains in dark molecular cores, Astronomy & Astrophysics. 521: 11p, 2010.

Kayanuma et al. A theoretical study of the formation of glycine via hydantoin intermediate in outer space environment, Chemical Physics Letters. 687: 178–183, 2017.

Kippenhahn and Weigert. *Stellar Structure and Evolution, Astronomy and Astrophysics Library, Springer-Verlag.* 1994.

Koch et al. Concerted Proton-Transfer Mechanism and Solvation Effects in the HNC/HCN Isomerization on the Surface of Icy Grain Mantles in the Interstellar Medium, Journal of Physical Chemistry C (ACS). 111: 15026–15033, 2007.

Koch et al. A Theoretical Study of the Formation of the Aminoacetonitrile Precursor of Glycine on Icy Grain Mantles in the Interstellar Medium, Journal of Physical Chemistry C (ACS). 112: 2972–2980, 2008.

Koga and Naraoka. A new family of extraterrestrial amino acids in the Murchison meteorite, Scientific Reports. 7:636, 2017.

Kuan et al. Interstellar Glycine, the Astrophysical Journal . 593: 848–867, 2003.

Kwenvolden et al. Evidence for Extraterrestrial Amino-acids and Hydrocarbons in the Murchison Meteorite, Nature . 228: 923–926, 1970.

Kwenvolden et al. Nonprotein Amino Acids in the Murchison Meteorite, Proceedings of the National Academy of Sciences of the United States of America . 268: 486–490, 1971.

Lawless. Amino acids in the Murchison meteorite, Geochimica et Cosmochimica Acta . 9: 2207–2212, 1973.

Lawless et al. Amino Acids Indigenous to the Murray Meteorite, Science. 173: 626–627, 1971.

Le Guillou et al. Evolution of organic matter in Orgueil, Murchison and Renazzo during parent body aqueous alteration: In situ investigations, Geochimica et Cosmochimica Acta. 131: 368–392, 2014.

Lerner et al. Influence of Murchison or Allende minerals on hydrogen-dueterium exchange of amino acids, Geochimica et Cosmochimica Acta. 59: 1623–1631, 1995.

Lerner et al. Influence of Allende minerals on deuterium retention of products of the Strecker synthesis, Geochimica et Cosmochimica Acta. 61: 4885 – 4893, 1997.

Linnartz et al. Atom addition reactions in interstellar ice analogues, International Reviews in Physical Chemistry. 34: 205–237, 2015.

Liszt et al. CO and CS in the Orion Nebula, Astrophysical Journal . 190: 557–564, 1974.

Lunar and Planetary Institute. webpage of the Lunar and Planetary Institute. URL `https://www.lpi.usra.edu/science/`.

Luthra et al. Predictions of gas-phase methanimine (CH_2NH) abundance in cold cores, Monthly Notices of the Royal Astronomical Society . 521: 2181–2186, 2023.

Maret and Bergin. Astrochem: Abundances of chemical species in the interstellar medium, Astrophysics Source Code Library. 2015.

Meierhenrich et al. Identification of diamino acids in the Murchison meteorite, Proceedings of the National Academy of Sciences of the United States of America . 101: 9182–9186, 2004.

Mendes et al. Cold Electron Reactions Producing the Energetic Isomer of Hydrogen Cyanide in Interstellar Clouds, The Astrophysical Journal Letters. 746: L8, 2012.

Miller. A Production of Amino Acids Under Possible Primitive Earth Conditions, Science. 117: 528–529, 1953.

Mil'man. A Complexity Mesure for Chemical Compounds, Journal of Structural Chemistry. 29: 957–960, 1989.

Miura et al. The Asteroid 162173 Ryugu: a Cometary Origin, The Astrophysical Journal Letters. 925: L15, 2022.

Moris et al. Interstellar Ammonia, Astrophysical Journal . 186: 501–528, 1973.

Munoz Caro et al. Amino acids from ultraviolet irradiation of interstellar ice analogues, Nature. 416: 403–406, 2002.

Nakamura et al. Formation and evolution of carbonaceous asteroid Ryugu: Direct evidence from returned samples., Science. 379: 14p, 2023.

Naraoka et al. Soluble organic molecules in samples of the carbonaceous asteroid (162173) Ryugu, Science. 379: 10p, 2023.

NASA. NASA's webpage of the Stardust mission. URL `https://www.jpl.nasa.gov/missions/stardust`.

NASA Ames Research Center. NASA Ames Research Center: The Astrophysics and Astrochemistry Lab. URL `https://www.astrochem.org/sci/Master_Residues.php`.

Oberg et al. . THE SPITZER ICE LEGACY: ICE EVOLUTION FROM CORES TO PROTOSTARS, The Astrophysical Journal. 740: 16p, 2011.

Ohishi and Kaifu. Chemical and physical evolution of dark clouds Molecular spectral line survey toward TMC-1, Faraday Discussions . 109, 1998.

Ohishi et al. Molecular Abundance Variations among and Within Cold, Dark Molecular Clouds, Astrochemistry of Cosmic Phenomena. 150: 171–177, 1992.

Oka. Interstellar H_3^+, Chemical Reviews. 113: 8738–8761, 2013.

Pagani et al. . The ubiquity of micrometer-sized dust grains in the dense interstellar medium, Science. 329: 1622–1624, 2010.

Potiszil et al. Insights into the formation and evolution of extraterrestrial amino acids from the asteroid Ryugu, Nature Communications . 14: 7p, 2023.

Prasad and Huntress. A model for gas phase chemisty in interstellar clouds. II. Nonequilibrium effects and effects of temperature and activation energies, The Astrophysical Journal. 239: 151–165, 1980a.

Prasad and Huntress. A model for gas phase chemistry in interstellar clouds: I. The basic model, library of chemical reactions, and chemistry among C, N, and O compounds., The Astrophysical Journal Supplement Series . 43: 1–35, 1980b.

Qasim et al. An experimental study of the surface formation of methane in interstellar molecular clouds, Nature Astronomy. 4: 781–785, 2020.

Randic and Plavsic. A Complexity Mesure for Chemical Compounds, Croatica Chemica Acta. 75: 107–116, 2002.

Rimola et al. Deep-space glycine formation via Strecker-type reaction activated by ice water dust mantles. A computational approach, Physical Chemistry Chemical Physics. 12: 5285–5294, 2010.

Rimola et al. Computational Study of Interstellar Glycine Formation Occurring at Radical Surfaces of Water-ice Dust Particles, The Astrophysical Journal. 754: 10p, 2012.

Roberts and Herbst. The abundance of gaseous H_2O and O_2 in cores of dense interstellar clouds, Astronomy & Astrophysics . 395: 233–242, 2002.

Roueff et al. Isotopic fractionation of carbon, deuterium, and nitrogen: a full chemical study, Astronomy & Astrophysics. 576: 18p, 2015.

Sandford et al. Organics Captured from Comet81P/Wild 2 by the Stardust Spacecraft, Science. 314: 1720–1724, 2006.

Sato et al. First-principles study of the formation of glycine-producing radicals from common interstellar species, Molecular Astrophysics. 10: 11–19, 2018.

Snyder and Buhl. Microwave Detection of Interstellar Formaldehyde, Physical Review Letters . 22: 679–681, 1969.

Snyder et al. A Rigourous Attempt to Verify Interstellar Glycine, the Astrophysical Journal . 619: 914–930, 2005.

Sofia and Parvathi. Carbon Abundances in Interstellar Gas and Dust, Cosmic Dust - Near and Far. 414: 236–242, 2010.

Tielens. Interstellar Polycyclic Aromatic Hydrocarbon Molecules, Annual Review of Astronomy & Astrophysics. 46: 289–337, 2008.

Trixler. Quantum Tunnelling to the Origin and Evolution of Life, Trixler. 17: 1758 – 1770, 2013.

Walch and Bakes. On the reaction $CH_2NH_2^+$ + HCN/HCN $\rightarrow$ $NH_2CH_2CNH^+$, Chemical Physics Letters. 346: 267–273, 2001.

Walch et al. On the reaction CH_2O + NH_3 $\rightarrow$ CH_2NH + H_2O, Chemical Physics Letters. 333: 6, 2001.

Woodall et al. UMIST database for astrochemistry, 2007. URL `http://udfa.ajmarkwick.net`.

Woon. Ab Initio Quantum Chemical Studies of Reactions in Astrophysical Ices, 2. Reactions in H_2CO/HCN/HNC/H_2O, Icarus. 149: 277–284, 2000.

Woon. Ab initio quantum chemical studies of reactions in astrophysical ices. 4. Reactions in ices involving HCOOH, CH_2NH, HCN, HNC, NH_3, and H_2O, International Journal of Quantum Chemistry. 88: 226–235, 2002a.

Woon. Pathways to Glycine and Other Amino Acids in Ultraviolet-irradiated Astrophysical Ices Determined via Quantum Chemical Modeling, The Astrophysical Journal. 571: L177–L180, 2002b.

Wouters. *Concentré de Chimie, 2e édition, Presse Universitaire de Namur.* 2015.

Zamirri et al. Quantum Mechanical Investigations on the Formation of Complex Organic Molecules on Interstellar Ice Mantles. Review and Perspectives, ACS Earth and Space Chemistry. 3: 1499–1523, 2019.

Zhao and Truhlar. Density functionals with broad applicability in chemistry, Accounts of Chemical Research. 41: 157–167, 2008.

Ziurys and Turner. Detection of interstellar vibrationally excited HCN, Astrophysical Journal Letters. 300: L19–21, 1986.

Appendix A

Thermodynamics: a short review of the first and second laws

First of all, let us recall the first law of thermodynamics. The latter has close links with the energy conservation principle and stipulates that, in an isolated system (i.e. without mass and energy exchange), the internal energy variation ΔU is equal to zero. In other words, the **internal energy** U (equal to the sum of potential and kinetic energies of the system constituents) is constant in such a system. As a consequence, this first principle can be generalized to any system by stating that the internal energy U of a given system is constant except if a work is done or if heat is provided (not possible in an isolated system). The expression of ΔU is given in equation A.1, this variation being the result of two main types of energy transfers: **heat**[1], Q, and **work**[2] provided by the system, W. A schematic representation of the fundamental difference existing between those two energy transfer types is given in Figure A.1. It is worth noticing that the internal energy is a state function, meaning that $\Delta U = U_{final,product(s)} - U_{initial,reactants}$ is valid independently on the way the system goes to the initial to the final state.
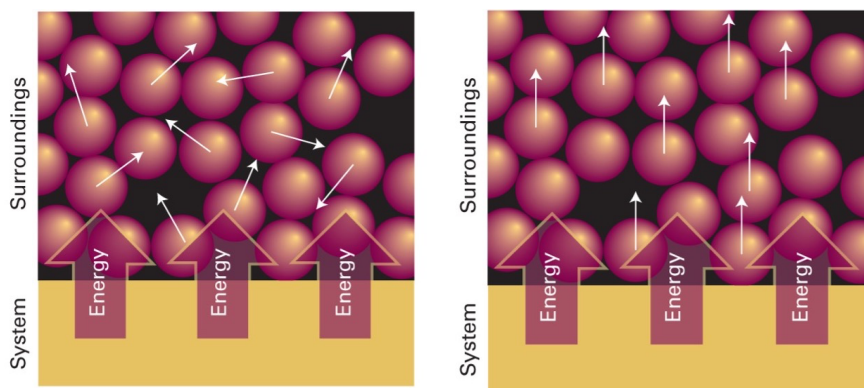
Figure A.1: Right: "When energy is transferred to the surroundings as heat, the transfer stimulates random motion of the atoms in the surroundings. Transfer of energy from the surrounding to the system makes use of random motion (thermal agitation) in the surroundings"; Left: "When a system does a work, it stimulates orderly motion in the surroundings. For instance, the atoms shown here may be part of a weight that is being raised. The ordered motion in a falling weight does work on the system", from (Atkins and de Paula, 2017)
.

---

[1]The heat corresponds to the energy transfer (from or towards the system) coming from disordered and random motion of particles from the environment. This disordered displacement is the so-called thermal agitation.

[2]Contrary to the energy transfer through heat, the work corresponds to the energy transfer (from or towards the system) coming from the ordered motion of particles from the environment (such as electron in a current).

$$\Delta U = Q + W + (\Delta E_{chemical} + ...) \tag{A.1}$$

Where $\Delta U = 0$ for an isolated system (units: J/mol for the intensive quantity, namely the molar internal energy; however, by definition, U is an extensive quantity with J as units.),
$Q = m.c.\Delta T$, with m the mass (in g usually), c is the mass specific heat (in J/g.K) [3],
$W = -P\Delta V$ with P the pressure and ΔV the volume variation,
$\Delta E_{chemical}$ is the variation of chemical energy.
Finally, "..." stands for other minor energy transfer forms that will not be taken into account in this development.

However, this first principle can not explain the direction in which a system will evolve. It is nevertheless highly justified, in order to further characterize a given system, to raise the question of its spontaneous evolution without any input of external work. In that context, the second principle of thermodynamics is of great importance. This second principle provides the spontaneity criteria of a given chemical transformation. One can define those criteria as:

i. **A probabilistic criterion**: during an irreversible transformation, a system always evolves towards its most likely state, corresponding to the state where the disorder is maximal. Indeed, energy and matter tend to scatter spontaneously in a disordered way. This randomness is quantified through the **entropy**, noted S (state function, (units: J/K.mol for the intensive quantity, or simply J/K for the extensive quantity)). Under the statistical thermodynamical view, this quantity can also be considered as the movements (translation, rotation, vibration) animating matter. Indeed, it comes from the idea that a change in the randomness of a system is the result of an energy transfer through heat. Moreover, the variation of entropy $\Delta S = S_{final,product(s)} - S_{initial,reactants}$ during a given chemical transformation (ΔS - entropy of reaction) is proportional to the heat transferred normalized by the temperature at which the transformation is occurring. It translate the fact that a fixed heat quantity provided at low temperature leads to a greater increase in entropy than the same transfer at larger temperature.

   However, even if an irreversible transformation leads to a positive ΔS, there exist spontaneous chemical processes with $\Delta S < 0$ (simply such as the spontaneous freezing of H_2O under 0°C). One therefore needs a second spontaneity criterion to completely characterize the spontaneity of a given chemical transformation.

ii. **An energetic criterion**: a system tends to evolve naturally towards the minimal energy. To analyze this criterion more deeply, one has to introduce the **enthalpy**, noted H (units: in J/mol if the intensive quantity is used, or simply J for the extensive quantity). As in the case of the entropy and the internal energy, H is a state function. From a physical point of view, the enthalpy H quantifies the internal energy to which the product of the pressure and volume is added. Figure 1.2 provides a graphic view of this variation of enthalpy during a given chemical transformation. On the left part of this figure, a hypothetical one-step exothermic elementary process is presented, with an enthalpy of reaction $\Delta H < 0$. In constast, the right part refers to a hypothetical one-step endothermic elementary process, characterized by a $\Delta H > 0$.

---

[3]Often confused with the heat capacity. However, there is a fundamental difference in the definition of those two terms. The heat capacity is an extensive quantity, with units being J/K. In contrast, the specific heat is the corresponding intensive quantity (in J/g.K), therefore characteristics to each body.

Moreover, the variation of enthalpy corresponds to the heat exchanged at constant pressure, Q_p. If we only consider Q and W as in equation A.1, we therefore get the expression A.2.

$$\Delta H = Q_p = \Delta U + P\Delta V \tag{A.2}$$

According to the minimal energy principle, it suggests that for a spontaneous transformation, the process has to be exothermic ($\Delta H < 0$). However, there exist numerous spontaneous endothermic reactions. In conclusion, the energy release is not the only requirement to characterize the spontaneity of a chemical process.

It is worth mentioning that the temperature also influences the spontaneity of a reaction. At ambient temperature, an ice block will spontaneously melt even if the process is endothermic. However, below the melting temperature, there is no spontaneous melting.

Based on the above findings, we take notice that the energetic and probabilistic criteria cannot explain the spontaneity of any given reactions individually. Conceptually, it can be explained by the fact that only a part of the total energy exchanged during a chemical reaction (ΔH) is available for effective work. Only a fraction of this energy is usable to perform such efficient work, and this energy fraction can be defined by the variation of **(Gibbs) free energy**, noted ΔG (G being also a state function, with units generally given in the intensive form kJ/mol). The remaining fraction of ΔH, corresponding to exchanged but unusable energy, is lost in form of thermal energy ($T.\Delta S$).

As a consequence, the variation in free energy allows to define a requirement for a spontaneous chemical process by combining the two criteria seen above in a single one, being: at constant pressure and temperature (and composition), a given process is spontaneous if it is characterised by a decrease in free energy, G. For a process at thermodynamical equilibrium, the ΔG is equal to zero. Mathematically, this spontaneity criterion can therefore be translated by the equation A.3, with the hypothesis that $\Delta P = \Delta T = 0$. Let us note that a spontaneous reaction, therefore with a $\Delta G < O$, is called an exergonic reaction:

$$\Delta G = \Delta H - T.\Delta S < 0 \tag{A.3}$$

where ΔG is the energy available for an effective work during a given transformation (< 0 for a spontaneous/exergonic transformation, and is equal to 0 for a process at thermodynamical equilibrium), ΔH is the total energy exchanged during the transformation, $T.\Delta S$ is the energy fraction which is unusable for efficient work and dissipated as thermal energy.

Appendix B

Visual supporting information

This appendix aims at providing additional visual information to support some parts the discussion. Theses figures have only been inferred for some check-up of intuitive explanations, or for the sake of completeness of the analysis. They are not discussed in more details than in the peculiar point for which they are referred to in the text.
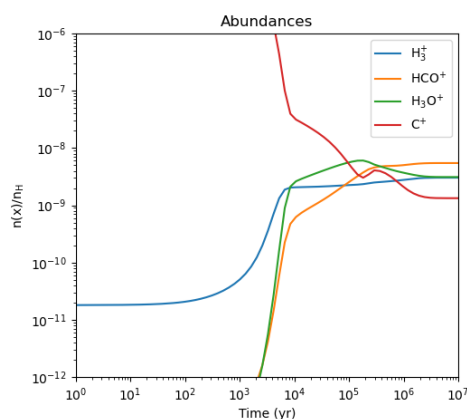
Figure B.1: Abundance as a function of time for the main contributors to the formaldehyde destruction from model 1a (Astrochem). A clear change of trend arises at $\sim 10^3$ years.
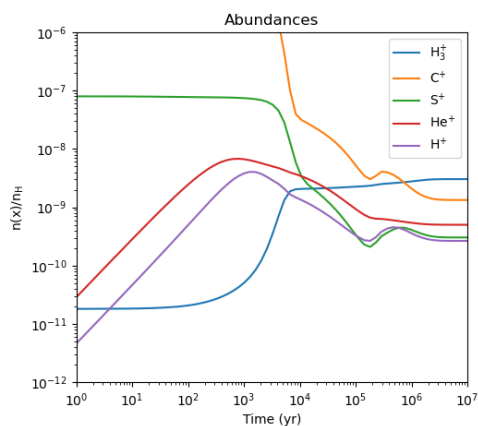
Figure B.2: Abundance as a function of time for H^+, He^+, S^+, to be compared with the abundance of C^+, H_3^+, HCO^+ and H_3O^+ (model 1a, Astrochem)
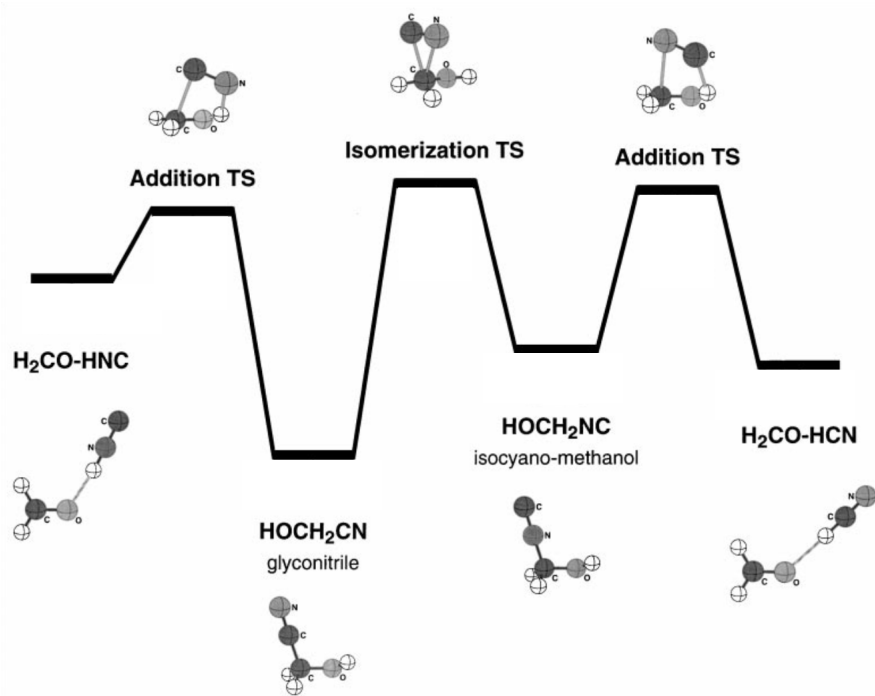
Figure B.3: United reaction surface and structure for the reaction of HCN and HNC with formaldehyde, linked through the product isomerization. The activation barriers are described in terms of relative height (gas phase activation barriers have not been computed in Woon (2000) and are not given in the KIDA data base), allowing us to illustrate the discussion, modified from Woon (2000)
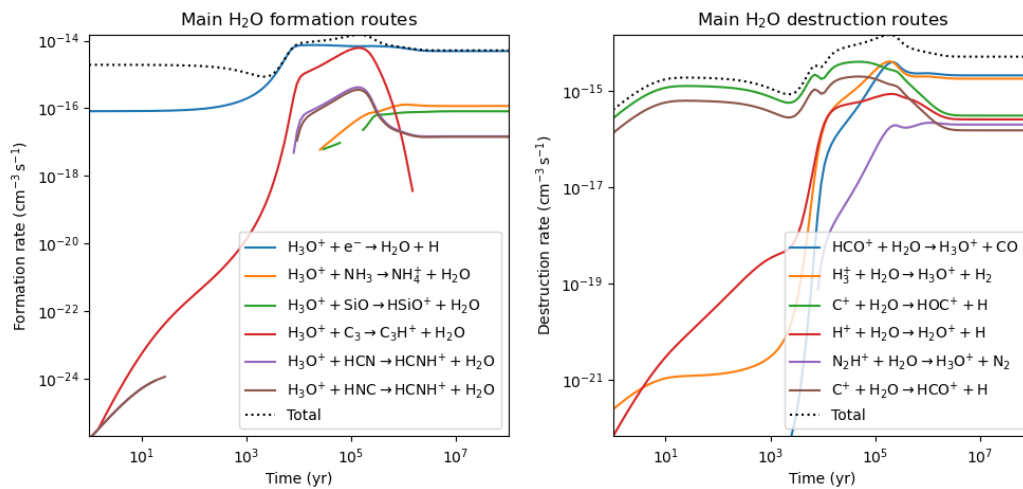
Figure B.4: Main gas-phase formation/destruction path for H_2O from **model 3a** (Astrochem)
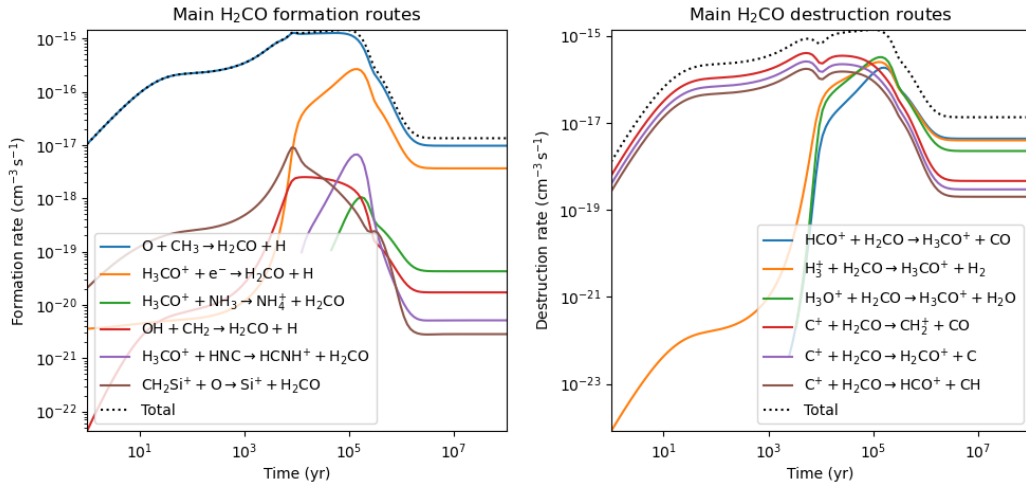
Figure B.5: Main gas-phase formation/destruction path for H₂CO from **model 3a** (Astrochem)
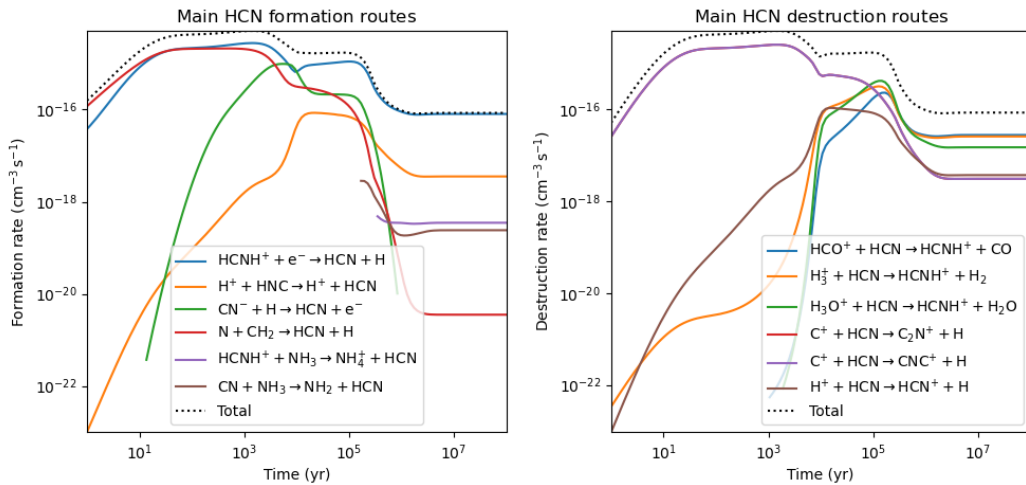
Figure B.6: Main gas-phase formation/destruction path for HCN from **model 3a** (Astrochem)
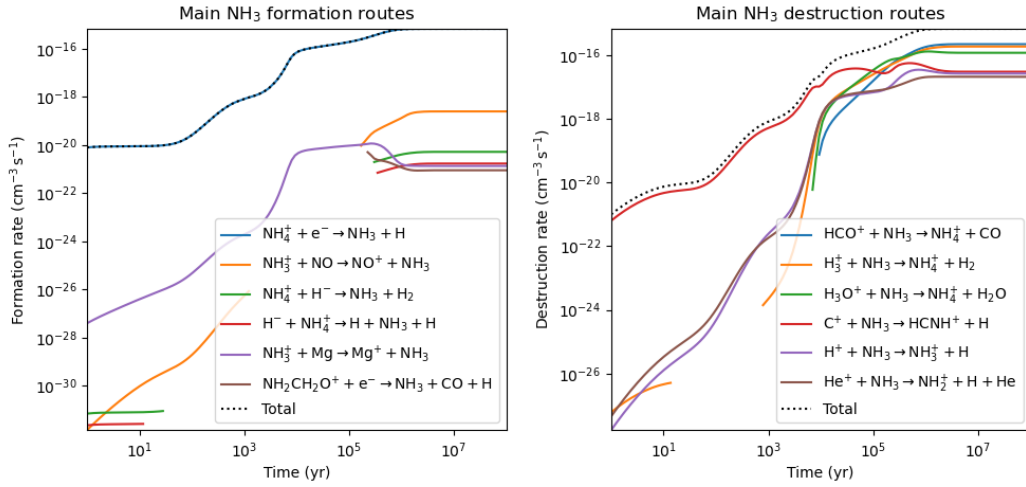
Figure B.7: Main gas-phase formation/destruction path for NH$_3$ from **model 3a** (Astrochem)
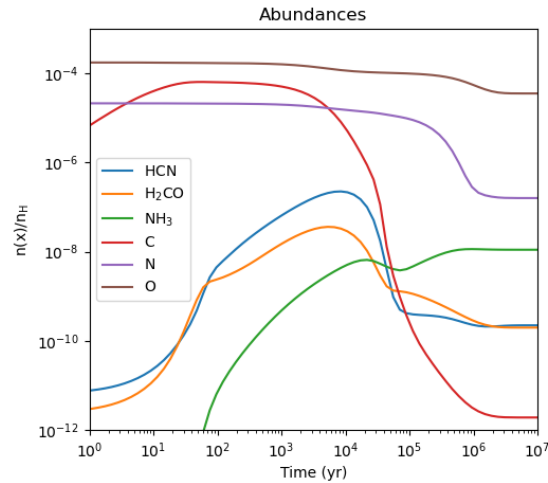
Figure B.8: abundance profiles of minor species,NH$_3$, H$_2$CO and HCN , reaching steady behavior quite simultaneously, in correlation to the tendency toward chemical equilibrium for the most abundant and dominating species (C, N and O), from **model 2a** (Astrochem).
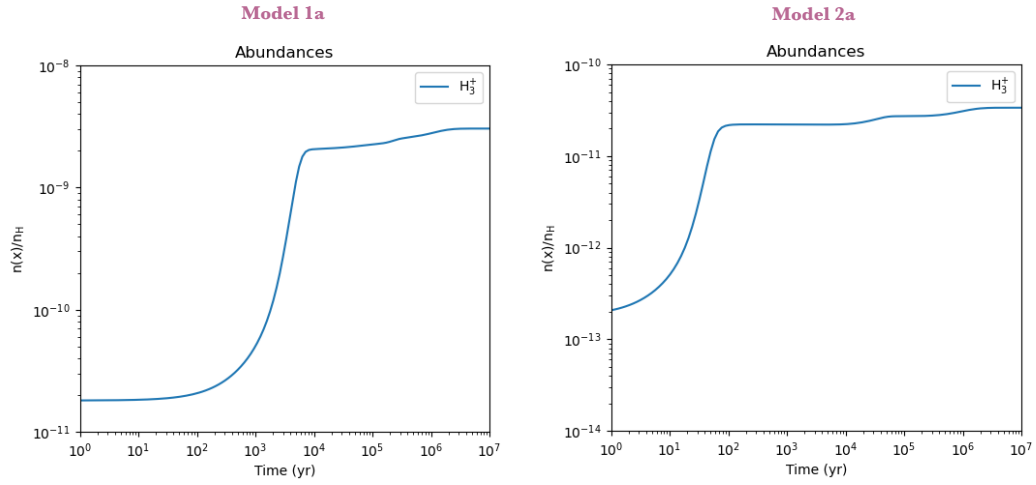
Figure B.9: Gas-phase equilibrium concentration of the $H_3^+ \sim$ proportional to the inverse of the initial abundance in hydrogen nuclei, with (Left) $n_H = 10^4$; (Right) $n_H = 10^6$ (Astrochem)
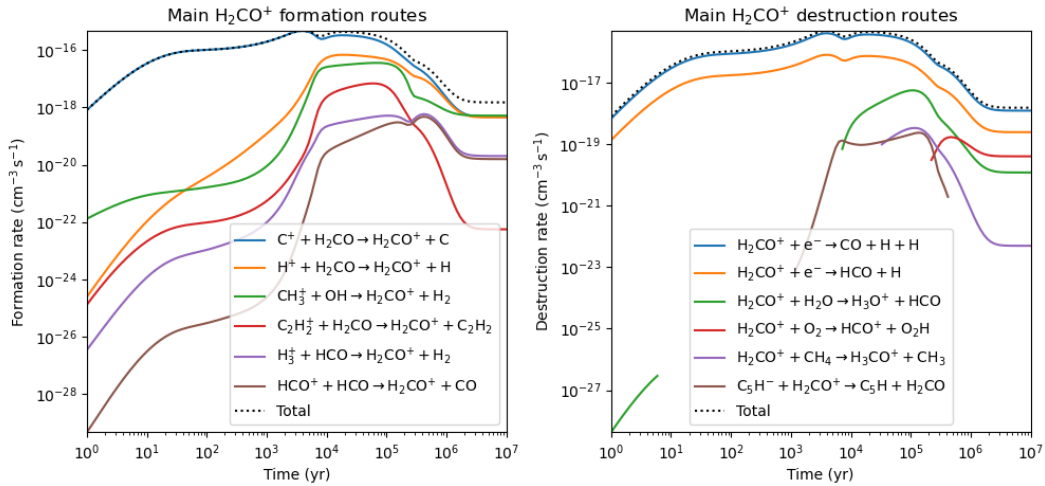
Figure B.10: Main gas-phase formation/destruction routes for H_2CO^+, from **model 1a** (Astrochem).
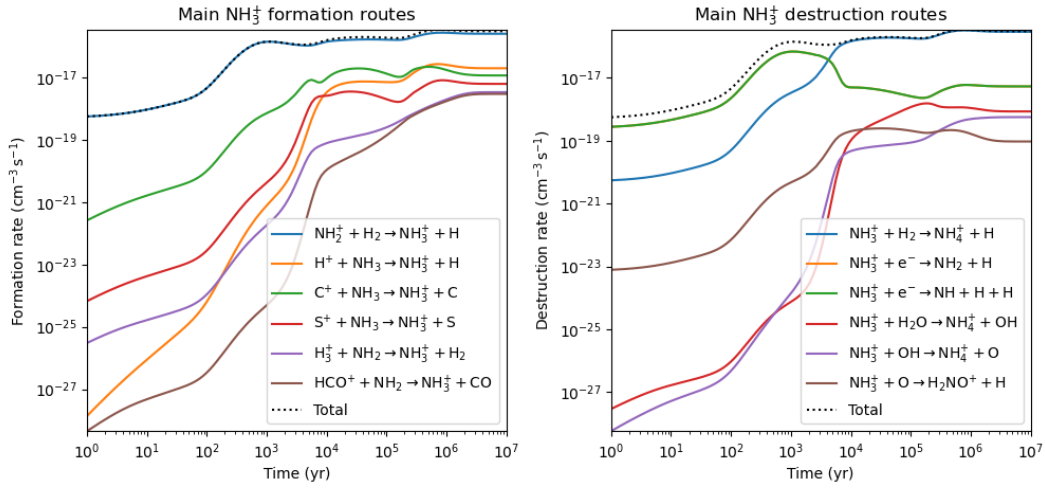
Figure B.11: Main gas-phase formation/destruction routes for NH_3^+, from **model 1a** (Astrochem).
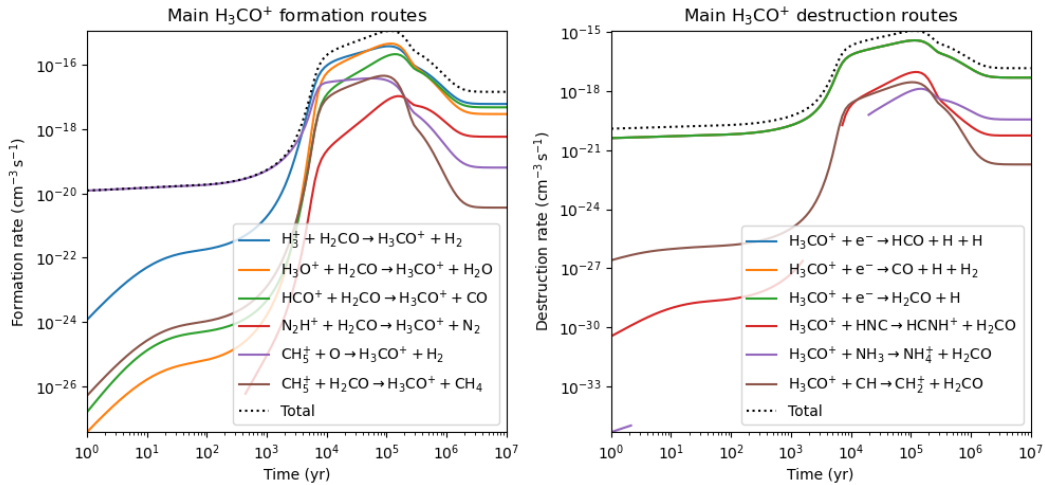
Figure B.12: Main gas-phase formation/destruction routes for H_3CO^+, from **model 1a** (Astrochem).
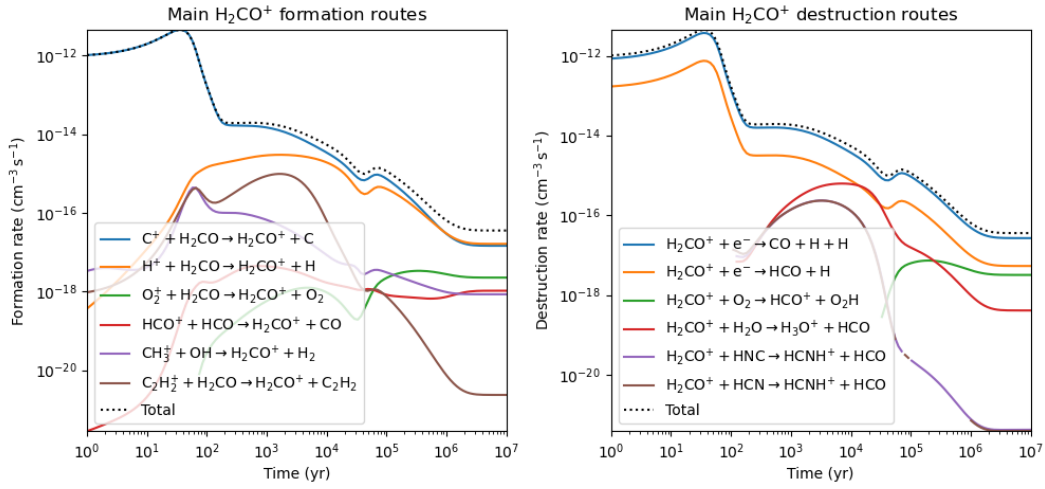
Figure B.13: Main gas-phase formation/destruction routes for H_2CO^+, from **model 2a** (Astrochem).
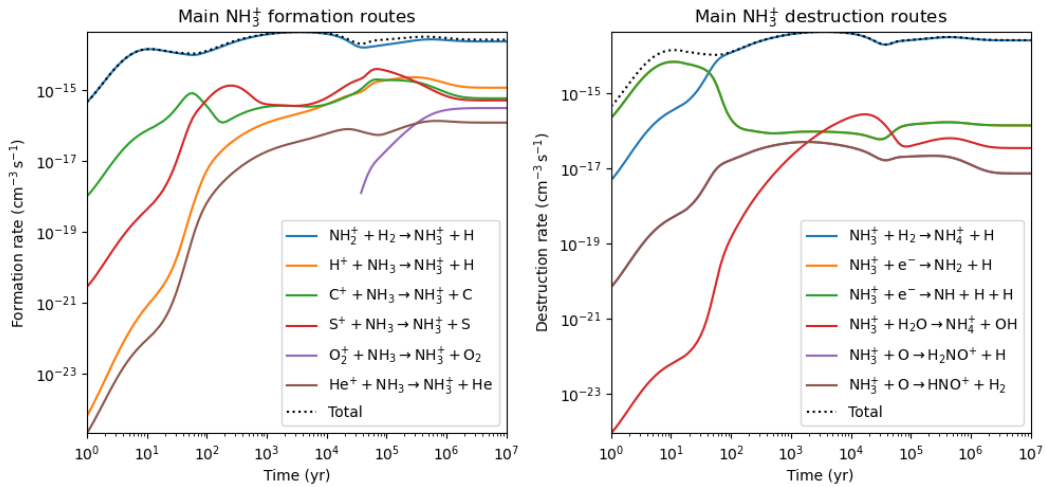
Figure B.14: Main gas-phase formation/destruction routes for NH_3^+, from **model 2a** (Astrochem).
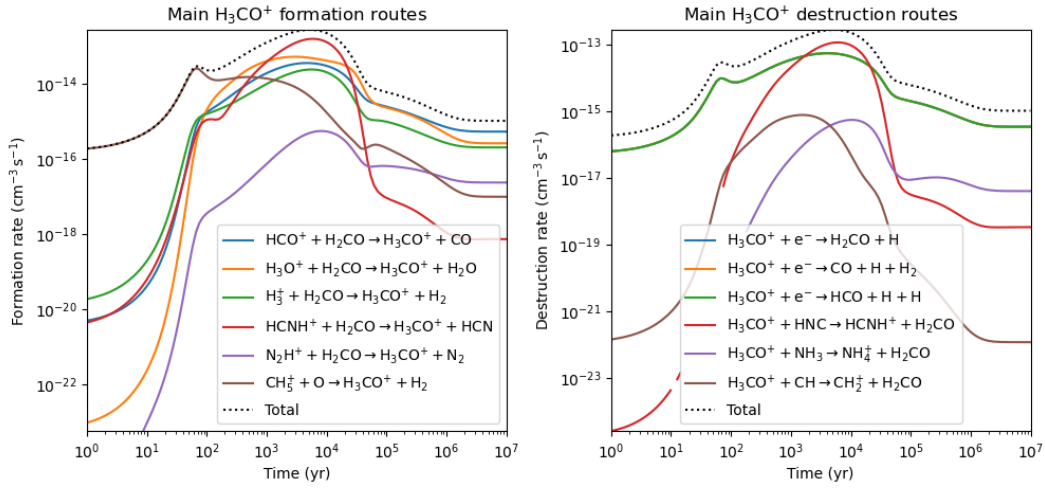
Figure B.15: Main gas-phase formation/destruction routes for H_3CO^+, from **model 2a** (Astrochem).
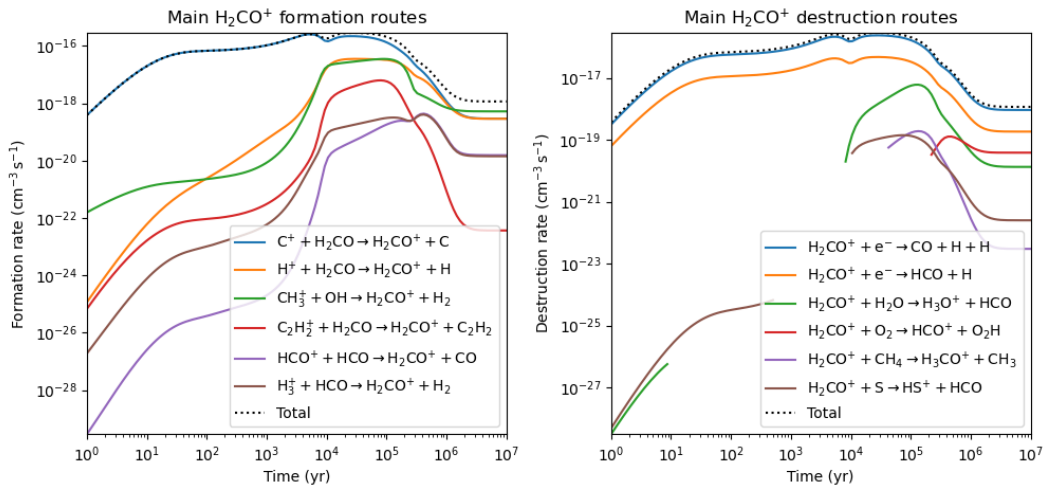
Figure B.16: Main gas-phase formation/destruction routes for H_2CO^+, from **model 3a** (Astrochem).
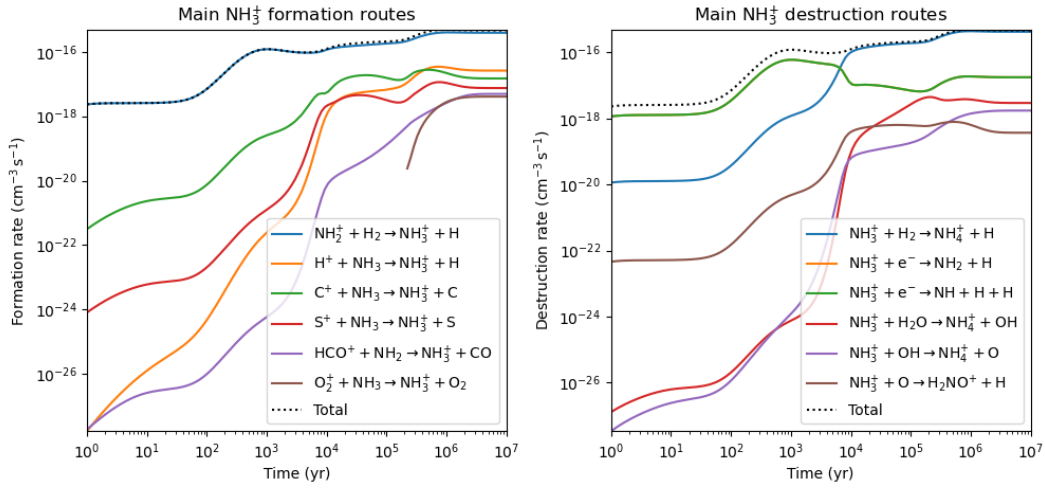
Figure B.17: Main gas-phase formation/destruction routes for NH_3^+, from **model 3a** (Astrochem).
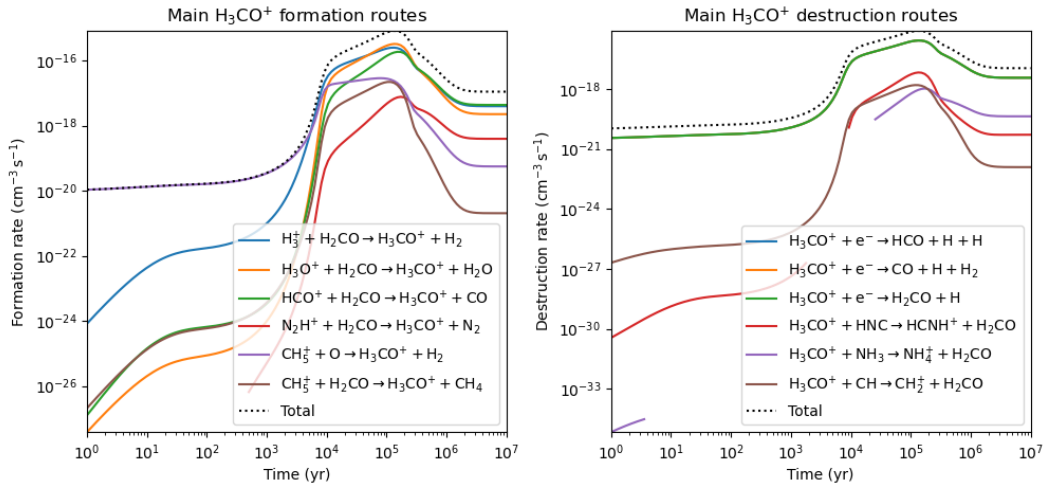
Figure B.18: Main gas-phase formation/destruction routes for H_3CO^+, from **model 3a** (Astrochem).
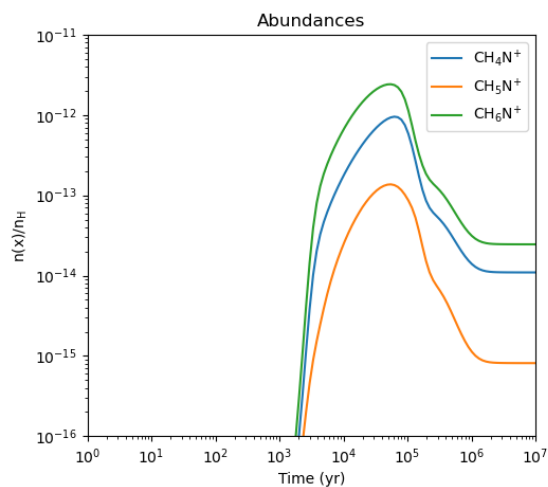
Figure B.19: Temporal evolution of the gas phase abundances of CH_4N^+, CH_5N^+ and CH_6N^+ from **model 1a**.
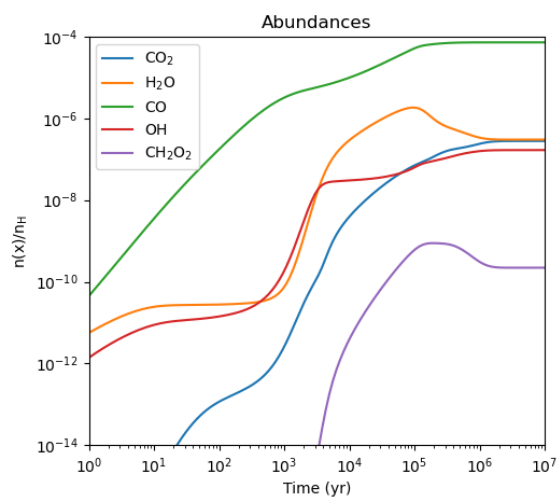
Figure B.20: Respective abundances as a function of time for the precursors of the ***step a*** of the (revisited) Woon's mechanism - computed with Astrochem (from **model 3a**.)
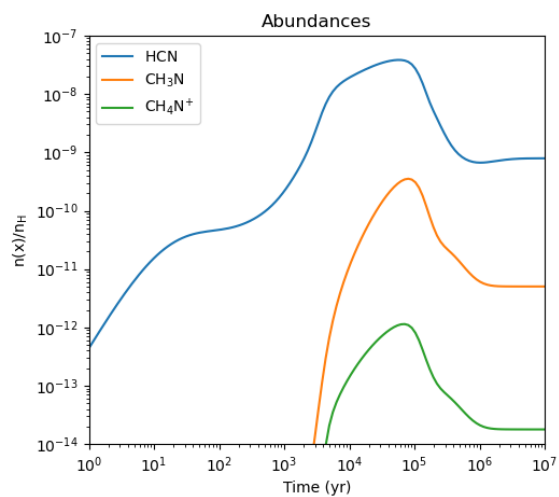
Figure B.21:   Respective abundances as a function of time for the precursors of the ***step b*** of the (revisited) Woon's mechanism - computed with Astrochem (from **model 3a**.)

List of Abbreviations

CR Cosmic Rays. 3, 7, 15, 16, 18, 19, 24, 25, 36, 37, 41, 46, 48, 51, 53, 61, 72, 73, 80, 103, 109

DFT Density Functional Theory. 34, 109

ISM Interstellar Medium. iv, 2–4, 6–8, 11, 12, 15–21, 24–26, 28–30, 32–34, 36, 43, 48, 51, 61, 82, 86, 105, 136

PAHs Polycyclic Aromatic Hydrocarbons. 21, 24, 25, 29

TS Transition State. 41, 43

List of Figures

List of Tables